CHARGE TRANSPORT PROCESSES IN CONDUCTING POLYPYRROLE AND POLYANILINE BLENDS AND COMPOSITES

A THESIS

SUBMITTED TO THE

UNIVERSITY OF PUNE

FOR THE DEGREE OF

DOCTOR OF PHILOSOPHY

In

CHEMISTRY

BY

SWATI G. UNDE

DIVISION OF POLYMER SCIENCE & ENGINEERING

NATIONAL CHEMICAL LABORATORY

PUNE - 411008

OCTOBER 2000

DEDICATED TO

MY PARENTS

FOR THEIR LOVE AND ENCOURAGEMENT

THROUGHOUT MY LIFE

CERTIFICATE

Certified that the work incorporated in the Thesis entitled **" Charge Transport Processes in Conducting Polypyrrole and Polyaniline Blends and Composites"** submitted by **Ms. Swati G. Unde,** was carried out by her under my supervision at the Polymer Science and Engineering Group, Chemical Engineering Division, National Chemical Laboratory, Pune-8. Such material as has been obtained from other sources has been duly acknowledged in the thesis.

October 2000

Dr.S. Radhakrishnan
Research Guide

AKNOWLEDGEMENTS

I express deep gratitude and respects to my guide Dr.S.Radhakrishnan for his keen interest and valuable guidance, strong motivation and constant encouragement during the course of the work. I thank him from the bottom of my heart for introducing me to the physics of conducting polymers. The fruitful discussions, valuable suggestions and criticism lead to the quest of perfection in all respects that gave me a true perspective of analysing scientific problems.

I would like to thank the Director, National Chemical Laboratory, Pune for permitting me to submit this work in the form of a Ph.D thesis.

Financial assistance from the Council of Scientific and Industrial Research, New Delhi is gratefully acknowledged.

I wish to thank my colleagues Mr. S.D. Deshpande, Dr. Saujanya and Arindam for their willing co-operation during the difficult stages of work.

I owe sincere thanks to Sandhya and Yogesh Phatak for providing a timely help.

Last but not the least, I would like to thank Rahul and Pranit for their moral support that kept my spirits up during the endeavour.

National Chemical Laboratory
Pune 411008

Swati Unde

CONTENTS

List of symbols:

A - Richardson- Schottky constant

C - molar concentration of the dopant

d-values - inter-planer spacing

d - interdomain distance

D - particle size

D - diffusion constant

E_f - fermi energy

E_d - energy levels for donors

E_t - energy levels for trapping centers

ΔE - activation energy

E - activation energy

e - electronic energy

F - the electric field

f - exponent of the critical volume fraction

g - gravitational acceleration

I - current

J - current density

k - Boltzmann constant

k* - high frequency dielectric constant

K - rate parameter

n - integer having values 0,1,2, etc.

n_e - number of electrons

N - density of states

N_d - the density of donor states

N_t - density of trapping states

r - ionic radius

R - resistance

R_g - gas constant

S - chemical sensitivity σ_{max}/σ

t - time

t_r - response time

t_d - decay time

T - temperature

T_o - initial temperature

T_g - glass transition temperature

V - applied voltage

x - distance along the thickness of the film

z - number of charges on the ion

α - absorption constant

β - Poole-Frenkel parameter

β_{PF} - Poole- Frenkel parameter

β_{SE} - Schottky parameter

ε - dielectric constant of the material

ϕ - the volume fraction

Φ - work-function

Φ_o - potential energy og the barrier in Schottky effect

η - viscosity

φ - volume fraction of the conductive filler

φ_c - volume fraction of the conductive filler at critical concentration

Λ - equivalent molar conductivity

λ - mean free path

μ - carrier mobility

θ - volume fraction of the insulating material

ρ - resistivity

σ - conductivity

σ_o - initial conductivity

$\Delta\sigma$ - change in conductivity

τ - tunneling factor

List of acronyms:

A	acceptor
B E	binding energy
CdS	cadmium sulfide
CPC	conducting polymer composites
CuPc	copper phthalocyanine
CVD	chemical vapour deposition
D	donor
EM	electromagnetic
ESCA	electron spectroscopy for chemical analysis
FWHM	full width at half maxima
HOMO	highest occupied molecular orbital
ICP	intrinsically conducting polymer
IR	infrared
ITO	indium tin oxide
I_L/I_D	light sensitivity
I-V	current Vs voltage
J-V	current density Vs voltage
LED	light emitting diode
Log $I/V^{1/2}$	log current Vs square root voltage
Log I/ 1/T	log I Vs reciprocal temperature
LUMO	lowest unoccupied molecular orbital
M-I-M	metal-insulator-metal
MO	molecular orbital
PA	polyacetylene
PANI	polyaniline
PANI-(H)	polyaniline with high dopant concentration
PANI-(L)	polyaniline with low dopant concentration
PC	polycarbonate
PE	polyethylene
PEO	polyethylene oxide
PF	Poole-Frenkel

PMMA	polymethyl methacrylate
PP	polypropylene
PPy	polypyrrole
PS	polystyrene
PVAc	polyvinyl acetate
PVC	polyvinyl chloride
Py	pyrrole
RF	radio frequency
SCLC	space-charge-limited-conduction
SE	Schottky emission
SCE	saturated calomel electrode
SPE	solid polymer electrolyte
THF	tertrahyrofuran
UV	ultra-violet
V_{TFL}	voltage at trap filled limit
VRH	variable range hopping
WAXD	wide angle x-ray diffraction
XPS	x-ray photoelectron spectroscopy
XRD	x-ray diffraction

Chapter 1 - Introduction

1.1 Conducting Polymers:

Conducting polymers are the subject of considerable current research interest due to their fundamental opto-electronic physics and their potential applications in photodiodes, light emitting diodes, thin film transistors, etc. The use of conjugated polymers as an electroactive material in microelectronic devices is a rapidly growing area. Burroughes et al[1], reported the first examples of high performance Schottky diodes, metal-insulator-semiconductor (MIS) diodes and the MIS-field effect transistors (MISFET) structure involving conjugated polymers. The all-organic high mobility transient reported by Garnier et al [2] is an excellent example of how new organic materials can be exploited to produce components with superior characteristics such as flexibility, high volume to weight ratio over inorganic semiconductor material.

1.2 Types of conducting polymers:

The conducting polymers can be broadly classified as:

1. Inherently conducting polymers
2. Conducting polymer composites
3. Ionically conducting polymers

1.3 Inherently conducting polymers:

The research on inherently conducting polymers began nearly a quarter of a century ago, when films of polyacetylene were found to exhibit dramatic increase in electrical conductivity when exposed to iodine vapours. The procedure for synthesizing polyacetylene was based upon a route discovered in 1974 by Shirikawa and coworkers through addition of 1000 times the normal amount of catalyst during the polymerization of acetylene [3]. These films were also semi conductive and had an energy band gap of 1.4eV. Leading on from this breakthrough, many other small conjugated molecules were found to polymerize, producing conjugated polymers, which were either insulating or semiconductive but becoming conductive upon oxidation or reduction.

The **Fig.1.1** shows some of the conjugated polymers, which have been studied as intrinsically conducting polymers. Their chemical structures are also shown in the figure. The unique electronic properties of the conjugated polymers are derived from the presence of Π-electrons, the wave functions of which are delocalized over long portion of polymer chain when the molecular structure of the backbone is planar. It is therefore necessary that there are no large torsion angles at the bonds, which would decrease the delocalization of the pi-electron system [4,5].

The essential properties of the delocalized Π-electron system, which differentiate a typical conjugated polymer from a conventional polymer with o-bonds are as follows: (a) the electronic (Π-) band gap (Eg) is relatively small (~1 to 3.5eV), with corresponding low excitations and semiconducting behavior; (b) the polymer molecules can be rather easily oxidized or reduced, usually through charge transfer with atomic or molecular dopant species, to produce conducting polymers; (c) net charge carrier mobilities in the conducting state are large enough so that high electrical conductivities are realised, and (d) quasi-particles, which, under certain conditions, may move relatively freely through the materials [6,7].

The electrical and optical properties of these materials depend on the electronic structure and basically on the chemical nature of the repeat unit. The general requirements of the electronic structure in these polymers were recognized and described many years ago. The electronic conductivity is proportional to both the density and the drift mobility of the carriers. The carrier drift mobility is defined as the ratio of the drift velocity to the electric field and reflects the ease with which carriers are propagated. Enhancing the electrical conductivity of polymer then requires an increase in the carrier mobility and the density of charge carriers.

1.3.1 Commonly used conducting polymers:

Polypyrrole (PPy) and polyaniline (PANI) are the most commonly used due to more stability in air as compared to the other polymers. A brief discussion is presented below.

(I) Polypyrrole :

Polypyrrole is most frequently used in commercial applications due to the long-term stability of its conductivity and the possibility of forming homopolymers or composites with optimal

mechanical properties. It was first synthesized in 1916 as pyrrole black by oxidation of

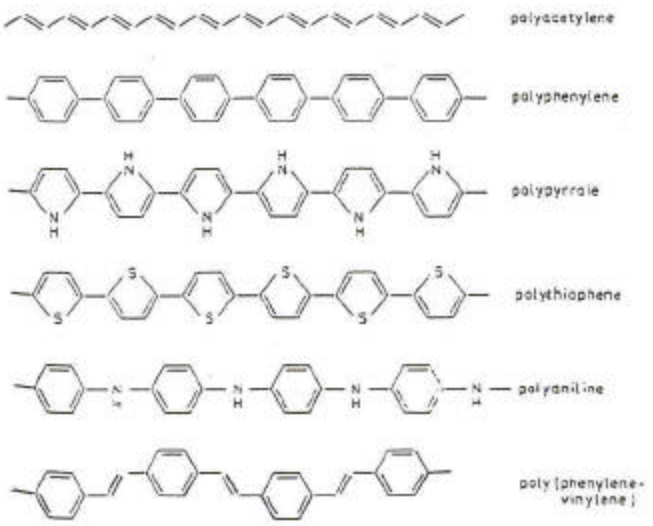

Fig. 1.1 Examples of inherently conducting polymers

pyrrole. The electrochemical synthesis of PPy was first carried out by Dall'Ollio [8] who obtained poly pyrrole blacks by oxidation of pyrrole in aqueous sulfuric acid on Pt electrode.

Methods of synthesis:

The two main processes for the synthesis of PPy are by chemical and electrochemical polymerization method. Chemical methods are used for mass production of the polymer at low cost while electrochemical polymerization is applied for materials with better conducting properties and for applications such as the construction of electronic devices.

(a) Chemical polymerization:

Polypyrrole has been prepared in the presence of various oxidizing agents like sulfuric acid, nitrous acid, quinones or ozone. The material obtained was in the insulating range 10^{-10} to 10^{-11} S/cm [9]. This could be then doped with halogenic electron accepters such as bromine and iodine to achieve a stable conductivity of 10^{-5} S/cm [10].

In recent times, polypyrrole is synthesized chemically in conducting state, because the polymer oxidation occurs with oxidant salts acting as dopant agents. Several metallic salts such as $FeCl_3$, $Fe(NO_3)_3$, $K_3[Fe(CN)_6]$, $CuCl_2$, $CuBr_2$, etc. have been employed for the polymerization of pyrrole [11]. Ferric salts are the most commonly used oxidants for the chemical synthesis of highly conductive polymer complexes. The polymerization process using $FeCl_3$ as an initiator can be summarized as

$$3mPy + FeCl_3 \longrightarrow m(Py_3Cl) + nFeCl_2 \qquad \text{Eq. 1.1}$$

The mechanism is similar to that proposed by Hsing et al [12]. The reaction would be initiated by the cationic radical $C_4NH_5^{\bullet+}$, which coordinates with other pyrrole units. The transition metal ion being the electron acceptor, probably forms a donor-acceptor complex with the Π-system of pyrrole at the chain initiation step as well as the polymer intermediate at the final rearomatization step.

XPS studies of the chemically obtained PPy using Fe(III) oxidants reveal a reaction stoichiometry that accounts for the 25% oxidized pyrrole units being favoured. In general polymer conductivity is a function of the monomer and the oxidant agent concentration,

solvent, time of reaction and temperature of synthesis. Conductivities as high as 190 S/cm have been reported for PPy synthesized from methanol solution of $FeCl_3$ [13].

(b) Electrochemical synthesis:

The electrochemical synthesis of PPy has been reported by Diaz et al. According to Diaz and Kanazawa [14] the electrosynthesis of this film proceeds via the oxidation of pyrrole at the platinum electrode to produce an unstable Π-radical cation which then reacts with the neighbouring pyrrole species. The cyclic voltammograms of these solutions show an irreversible peak for the oxidation of pyrrole at +1.2 V (E_{pa}) versus the saturated calomel reference electrode (SSCE) [15]. The mechanism of the overall reaction for the formation of fully aromatized product is very complicated and involves series of oxidation and deprotonation steps.

In practice PPy films are prepared by the electro-oxidation of pyrrole in one-compartment cell equipped with platinum working electrode, gold wire counter electrode and a saturated calomel reference electrode. A wide variety of solvents and electrolytes can be used as the electrical resistance of the solution is high and the nucleophilicity does not interfere with the polymerization reaction. These conditions can be accomplished by selecting solutions where the electrolyte is highly dissociated and which are slightly acidic. As already mentioned, physical properties of the resulting films are sensitive to the changes in the reaction conditions. Films of various thicknesses can be prepared by changing the current density. Many other authors have investigated the process of electrochemical deposition of conducting PPy [16].

(c) Vapour phase deposition:

This technique, although known for depositing PPy films since about a decade ago [17]. The gas phase preparation of PPy has been described by Mohammadi et al [18]. Conducting polymer films were prepared in a similar manner to the chemical vapour deposition method. The PPy films were prepared in two ways i.e. by vapour phase polymerization using H_2O_2 or HCl, or by chemical vapour deposition of PPy doped with $FeCl_3$. Some workers have also reported the preparation of PPy-polymer composites using vapour phase deposition. Yosomiya et al [19] have used PVC-cupric chloride complex film as base polymer and PPy

was vapour phase polymerized on this. Radhakrishnan et al [20] have also made PPy films by this method. They used PEO and $FeCl_3$, which were first dissolved in a suitable solvent, from which, films were cast on glass slides. These were dried and exposed then exposed to pyrrole vapors. The sample showed in-situ growth of PPy films, which also developed crystalline order.

(II) Polyaniline:

Polyaniline is a typical phenylene based polymer having a chemically flexible –NH- group in a polymer chain flanked on either side by a phenylene ring. The protonation, deprotonation and various physico–chemical properties of polyaniline can be said to be due to the presence of –NH- group. There are four stable insulating oxidation states [21], leucomeraldine base (LEB) emeraldine (EB) and pernigraniline (PNB) shown schematically in the **Fig. 1.2**.

1. Leucomeraldine base (LEB)
2. Emeraldine (EB)
3. Pernigraniline (PNB
4. Emeraldine salt.

Oxidative doping of the leucomeraldine base or protonic acid doping of the emeraldine base material produces the conductivity from emeraldine salt whose conductivity varies between 0.5 S/cm and 400 S/cm depending on the means of preparation. Extensive studies of these emeraldine salt (ES) materials have shown that the metallic state is governed by inhomogeneous disorder. That is in the conducting state there are regions that are three dimensionally ordered in which the conducting electrons are three dimensionally delocalized and the regions either where the polymer is strongly disordered, in which the conduction electrons diffuse through one dimensional polymer chains that are nearly electrochemically isolated. One – dimensional localization in these nearly isolated chains lead to decrease in conductivity with decreasing temperature.

Among all the conducting polymers polyaniline has a special representation due to easy synthesis, chemical flexibility and ease of derivatization, its environmental stability and

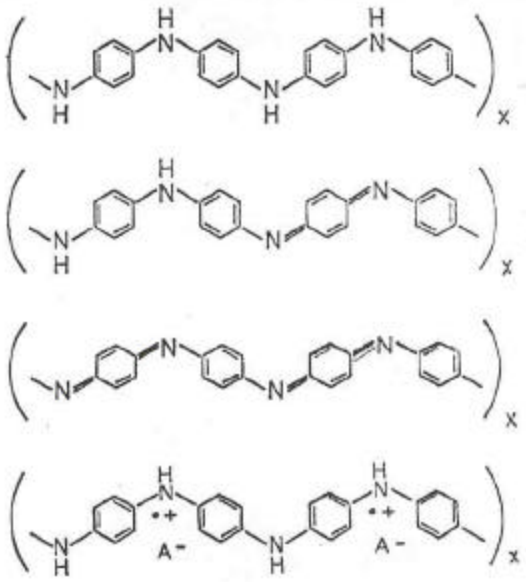

(a) Leucoemeraldine base (LEB), (b) emeraldine base (EB), (c) pernigraniline base PNB), (d) emeraldine salt (ES).

Fig. 1.2 Various oxidation states of Pani

processability into fibers, films and various composites and above all simple non redox doping by protonic acids is an important aspect where a number of electrons in a polymer chain remain unchanged during doping process. During doping all the hetero-atoms in the polymer namely nitrogen becomes protonated.

PANI is prepared either by chemical or electrochemical oxidation of aniline under acidic conditions. The method of synthesis depends on the intended application of the polymer. Whenever thin films and better patterns are required, an electrochemical method is preferred.

(a) Chemical synthesis of emeraldine salt:

The most preferred method is to use hydrochloric acid with ammonium persulphate as an oxidant [22]. Oxidative polymerization is a two-electron chain reaction and hence the 1:1 quantity of the oxidant is required but lesser amounts are required to prevent overoxidation. The aniline salt of protonic acid with the protonic acid was mixed with ammonium persulfate containing the protonic acid with continuous stirring for two hours. The precipitate obtained was then filtered and washed with distilled water/methanol so as to obtain emeraldine salt.

The principal function of the oxidant is to withdraw a proton from an aniline solution. The polymerization reaction is summarized as follows:

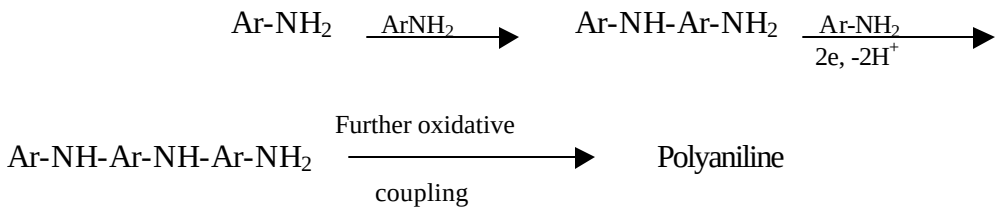

The factors affecting the polymerization process are the pH of the solution, type of the acid used, its concentration, effect of the size, solvation and electronegativity of a conjugated base associated with a given acid.

(b) Electrochemical synthesis:

Electrochemical polymerization is a radical combination reaction and is diffusion controlled. The anodic oxidative polymerization is the preferable method to obtain a clean and better ordered polymer as a thin film. Electrochemical synthesis is achieved by

1. Galvanostatic method
2. Potentiostatic method-keeping potential constant 8-0.7-1.1 V Vs SCE
3. Potential sweep method-between two potentials limits-0.2 to +1.0 V versus SCE

Electrochemical reaction is carried out by dissolving 0.1 mole of protonic acid in distilled water at the platinum electrode. The polymerization reaction is depicted in the **Fig.1.3.** The first step in the oxidation of aniline is the formation of a radical cation, which is independent of the pH. Mohilner [23] suggested the oxidation of aniline as an ECE reaction (a succession of rapid electrochemical-chemical-electrochemical reactions). The radical coupling is predominantly through para (1:4 coupling) monomer coupling. The colour changes observed with polyaniline are –0.2 V yellow, 0.0 blue and 0.65 V green which are associated with different oxidation states (doping levels).

1.3.2 Charge transport in inherently conducting polymers:

It is well known that polymers with conjugate bonding system, i.e. an uninterrupted sequence of single and double bonds running through the whole molecule are usually electrically conductive.

According to Rehwald and Keiss [24] such a system cannot exist as a one dimensional metal with a half filled band, but rather as an insulator with a gap forming at the Fermi level, the reason being either Perierls instability, or electron correlation, or a combination of both. With a energy gap of 1 – rev, polymers seem to resemble inorganic crystalline semiconductors. The quasi one dimensional structure of this material gives rise to strong electron phonon interaction, leading to new quasi particles upon doping: these are solitons, polarons and bipolarons. Disorder within the chain and within its environment plays an important role in such polymers.

(1) Electronic Ground State:

Conjugated polymers are treated theoretically as one-dimensional systems. i.e. each lattice point is coupled to two neighboring points only. In their review the authors use two

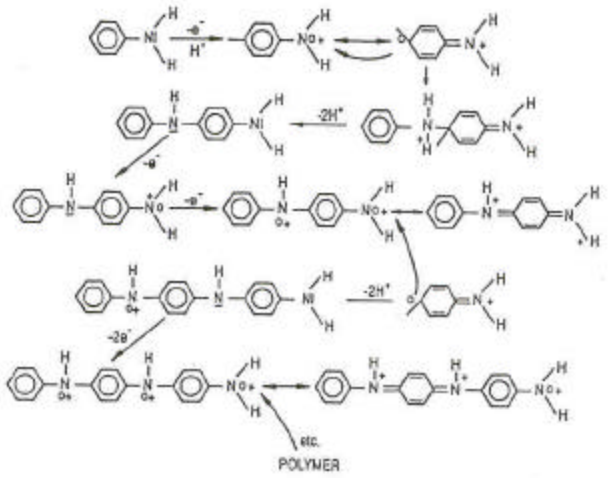

Fig. 1.3 Schematic diagram for the chemical polymerization of aniline

theoretical approaches to explain the formation of bandgap. They take either electron – phonon interaction or electron correlation as the dominant mechanism. Accordingly if the gap is result of electron phonon interaction Peierls' argument [25] can be used to give a physical reason for why a chain of unsaturated carbon atoms with one conduction electron (π electron) per atom does not exhibit metallic properties. It seems that Peierls' argument indicates quite fundamentally that a one-dimensional chain of unsaturated carbon atoms leads necessarily to a semiconducting state. However, as has been shown by Froehlich [26], the Peirel's state is only semiconducting if the periodic lattice distortion is commensurate with the lattice. If it is incommensurate, the phase of the periodic lattice distortion can move through the lattice carrying a charge density wave. In this case the Peirels state is conducting. A more detailed investigation of the question of lattice distortion and of bond alternation in polymeric chain has been made within the frame-work of the Huckel theory. The Peirels model neglects completely the Coulomb repulsion for an electron that is transferred to a state already occupied. In the simple Hubbard model [27] electron correlation is taken into account, but electron-phonon interaction is assumed to be negligible.

This model yields a gap also in the absence of a Peirels distortion. The question arises therefore, whether the on-site Coulomb interaction or the electron phonon interaction is the dominant mechanism. It has been shown that both interactions are of similar order of magnitude and that indeed Coulomb interaction enhances bond alternation.

(2) The Nature of the Charge Carriers:

Conducting polymers are different from conventional semiconductors. In conducting polymers the defects are the distortions in the long chain molecules which in turn are due to transfer of charges.

The continuum model developed by Brazovskii and Kirov [28] and by Fesser *et al* [29] gives a coherent description of these defects whose extension is usually several monomer units. The simplest of the defects is created by adding an electron or hole to the ground state and following the lattice to relax. In fact, this thought experiment simulates the doping process of a polymer chain, assuming that no mixing of the wave functions between dopant molecule and polymer occurs. The defects generated in this way are called radical anion or radical cation in chemistry, in physics positively or negatively charged polaron. A polaron

represents a combination of two defects, namely of a charge and a neutral defect or, in chemical terms, of an ion and a radical.

For the purpose of discussing the carrier transport it is important to know the energy of formation of the various quasiparticles; this decides which species is created. Polaron can be envisaged as a combination of charge and neutral defects in close proximity. When these effects are separated, the energy of formation increases to about 0.8 eV. So the first charge is added to a chain will lead to the formation of polaron. Solitons can be created only in pairs from topological reasons. When a second charge is added, the two polarons disintegrate into two charged solitons.

At low doping concentration, when an average only one charge per chain is found. Polarons are expected; if more than one charge is transferred to the chain, correlated pairs of charge defects bipolarons are usually favored due to their lower energy of formation. Bipolarons are called in chemical parlance carbodication or carbodinion.

In the band structure picture the Polaron form two states in the energy gap in positions symmetrical to the center of the gap. The lowest level of a hole polaron is singly occupied, the higher level empty. In the electron polaron the lower level is doubly occupied by electrons with antiparallel spin, whereas the upper level is singly occupied. Both states carry an unpaired spin and give rise to Para magnetism. The length of the deformed chain section is of the order of several repeat distances, e.g. about four rings in polythiophene. The solitons, on the other hand, forms an energy level at the center of the gap (as long as electron-hole symmetry is fulfilled). This level singly occupied if the soliton is neutral, resulting in an unpaired spin and paramagnetism. By doping with donor or acceptors the soliton can become negatively or positively charged. Both types of charged solitons are characterized by zero spin. **Fig. 1.4** gives a schematic view of the energetic positions of these excitations.

Taking electron-electron interaction into account, the soliton level is no longer located at the center of the gap and differences occur whether its level is occupied or not. The effective mass of a carrier is of particular interest to the charge transport along a polymer chain. For electrons or holes it is determined by the curvature of the respective band at the band edge. For Polarons, soliton and bipolarons it is calculated from the kinetic energy. The

effective masses for these quasiparticles, estimated on this basis are of the order of 1-6

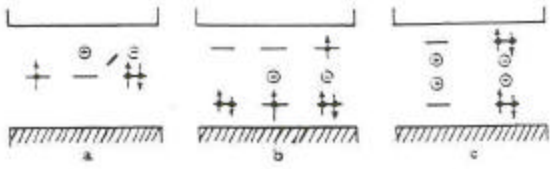

Fig. 1.4 Positions of energy levels of (a) a soliton in neutral (S^o), positively (S^+) and negatively (S^-) states; (b) a polaron in the neutral (P^o), positively (P^+)n and negatively charged state (P^-), (c) a bipolaron charged (B^{++}) and negatively (B^{--})

electron masses. Since these defects are also charged and not localized within a unit cell, there motion will be coherent along a chain and their mobility is accepted to be high.

(3) Disorder along the chains:

So far the discussion of the one-dimensional model has been based on the assumption of an ideal, infinitely long chain in a homogeneous environment. In fact, the chains have a finite length, and their lengths vary randomly in polyacetylene the structure may change between trans and cis, resulting in bends, folds, kinks, gogs and similar geometric defects. In poly (p-phenylene) torsion of monomer units out of their ideal planar position represent another type of geometric disorder. Apart from that, chemical defects are possible, such as crosslinks between chains sp3 defects in polyacetylene and β linkage of heterocycles in a chain of α – linked monomer units. Chemical modifications at discrete points of the chain, such as oxidation, also belong to this category.

A third type of disorder results from the changes in the environment of the chain, the so called secondary structure, being described by the limiting cases of crystalline and amorphous regions. Disorder may also come from doping. At least at low dopant concentrations, the dopant molecule occupy random positions between the chains. They affect the electronic properties by their Coulomb potential and by hybridization with polymer π orbital.

(4) Low and intermediate doping:

Doping with acceptor or donor molecules causes a particle oxidation or reduction of the polymer molecule. Positively or negatively charged quasiparticles are created, presumably Polarons in the first steps of doping. When doping proceeds, reactions among polarons take place, leading to energetically more favourable quasiparticles, i. e. a pair of charged solitons in materials with a degenerate ground state and a bipolaron with polymers with single ground state. Applying statistical mechanics allows calculation of the density of Polarons, bipolarons and solitons, and the density of electrons and holes in band states at any temperature. The basis of this calculation is the neutrality condition and the Fermi distribution function. Furthermore it has to be assumed that the life-time of the electrons (holes) and polarons is sufficiently long to treat them as quasiparticles. On this basis Conwell [30] has given an estimate of the density of free electrons at a doping level of 5 % and

found a value for free charge density of about 3 x 10^{24} m^{-3} or less at 300 K. this is about a fraction of 1/1000 of the total dopant concentration. If the charge carriers in the band states have mobility comparable to that in inorganic semiconductors, the contribution alone would already the measured conductivity values. The other quasi particles (polarons, bipolarons and solitons) exist in a much higher concentration, but have presumably a significantly lower mobility. In view of this, the contributions of various particles to the conductivity are uncleared. Recent theoretical treatments of three dimensional interactions in trans $(CH)_n$ have suggested soliton order in a adjacent chains, solitons confinement and the absence of polarons and bipolarons. These findings shed additional light upon these questions and might explain the importance of free carriers in conduction band. Although only outlined for $(CH)_n$, these consideration are relevant for other conducting polymers with only polarons, electrons and holes in the bands as carriers for the electrical transport.

(5) Conduction in localized states:

Carriers in localized states can move into adjacent empty states by thermally assisted tunneling, called hopping. The hopping probability depends on the mutual overlap of the wave functions, determined by the ratio of intersite distance R_{ij} to the localized length r_0 (decay length of the wavefunction). It depends in addition on the occupation of the initial and final state and, if the jump takes place to a site j with higher energy Ej – Ei an approximation proposed by Ambegaonkar et *al* [31] is often used for the hopping rate.

$$\Gamma_{ij} = \gamma_0 \exp\left[\frac{-2R_{ij}}{r_0} - \frac{|E_i - E_f| + E_j - E_f| + E_i - E_j|}{2kT}\right] \qquad \text{Eq. 1.2}$$

The prefactor γ_0 denotes a kind of attempt frequency of the order of a molecular vibration frequency, i.e. 10^{12} – 10^{13} s^{-1}. In equilibrium the hopping rates Γij and Γji in both direction are equal. An applied electric field changes the energies Ei and Ej and a net current is the result.

At sufficiently high temperatures and in diluted systems the hopping rate is determined by the overlap. Therefore, only hops between nearest neighbours contribute to the conductivity. The mobility is determined by an activated process.

If the temperature is low and if hopping takes place near the Fermi level, Mott [31] has shown that the hopping probability reaches a maximum at an optimum combination of hopping distance Rij and the energy difference Ei – Ej if the hop goes over a large distance, more sites are available to which the carrier can hop, and as a consequence the carrier has a higher probability to find a site with lower energy than in a short hop. Therefore such a process is preferred at low temperatures. For a constant density of states at the Fermi level Mott's famous variable – range hopping law results,

$$\mathbf{s} = \mathbf{s}_0 \exp(-\mathbf{T}_o / \mathbf{T})^{1/4} \qquad \text{Eq. 1.3}$$

with

$$T_0 = 24 (\pi r^3_0 k N(E_F)) \qquad \text{and}$$

$$\mathbf{s}_0 = \frac{\mathbf{9}}{\mathbf{4}} - \sqrt{\frac{\mathbf{3}}{\mathbf{2p}}} \mathbf{e}^2 \mathbf{g}_0 \sqrt{\frac{\mathbf{roN(EF)}}{\mathbf{kT}}}$$

A similar formula can be derived from a percolation treatment of the hopping conductivity [32], but only asymptotically in the low – temperature limit, as long as $T_0 / T > 100000$. Amorphous inorganic materials, typical values of To, as derived from experiments, are of the order of 10^8 K. when the density of states near the Fermi level is not constant but varies quadratically, the temperature exponent changes from ¼ to ½ . On the other hand, density – of – states functions also lead to an exponent ¼ and the same variable range hopping law. A $T^{1/4}$ law is by no means a unique characteristic of variable range hopping. Taking into consideration multi – phonon process (instead of one photon process only, as in most treatments) hopping leads to a similar $T^{1/4}$ law, and Emin [33] has calculated. In addition, if Columb correlation's are taken into account exponents vary between ¼ and 1 have been omitted.

Although many experimental data on the conductivity of disordered systems (polymers, amorphous inorganic semiconductors, impurity – band conduction) we interpreted in terms of variable range hopping, there was always the problem of obtaining a reasonable numerical value of the prefactor. According to Eq.1.3 T_0 and the prefactor have the variables N (E_F) and r_0 in common with r_0 and N (E_F) fixed, unrealistic values result for

y_0 . Wurtz and Thomas [34] could give a remedy for curing this discrepancy by including hopping between π - like electronic states. Averaging overall directions introduces a factor $(T_0/T)^{m/4}$ with m between 2 and 10 into the prefactor that can easily account for the values of $\sigma_0$determined from the experiment.

(6) Transport by Quasi – Particles:

In conjugated polymer, as long as one-dimensional model is valid, the addition of charge leads to the formation of polarons, bipolarons or charges silicon. These quasiparticles are expected to be quiet mobile along intact segments of the polymer chain. For electrical transport through the macroscopic samples, however these quasi-particles have to move finally from on chain to a neighbouring one.

For inter- chain transitions of polarons, bipolarons or solitons are difficult to assess, because not only the charge but also the molecular distortion has to be transferred. Electrons can tunnel, but the question is how the deformations can be transmitted to neighbouring chain.

Chance et *al* [35] calculated the transfer rate of a bipolaron. It is determined by combined probability for finding a bipolaron on one chain and sufficiently long segment free of any excitation on the neighbouring chain, and by the appropriate Frank – Condon factor f. denoting the length of a bipolaron by l (expressed in monomer units) and the molar fractions of dopant molecule by y, the probability for interchain transfer is given by

$$Pb = (y/2)\,(1 - iy/2)^{1+2} \qquad \text{Eq. 1.4}$$

as long as the interactions between polarons can be neglected. The transition rate, and hence the conductivity, peak at y = 0.05 – 0.07, assuming a bipolaron length I = 4-5. More sophisticated treatments are required if Columb interaction between bipolaron play an important role at high dopant concentrations.

The same authors also consider interchain transfer of solitons by a similar mechanism. Two charged solitons on a chain approach each other, being separated by a distance l, and

perform an transition to an adjacent chain in the same way as described for a bipolaron. Taking exp (-βl) for the Frank – Condon factor, the total transfer rate is obtained as

$$P_s = y \sum P(I) = \text{const} \{y^2 (1-y)\} / \{1-(1-y) \exp(-\beta l)\} \qquad \text{Eq. 1.5}$$

The transition probability and hence the conductivity as a function of y are s – shaped; leveling off at higher doping concentrations.

The above calculations implies that a hop of two solitons on an adjacent chains is only highly probable if the region of "wrong" bond arrangement between them is small, and a relative small molecular distortion has to be transferred with the charge carrier. This mechanism for a transition is no longer possible in the doping ranges, at which doping proceeds via conversion of neutral solitons into charged ones, and at which the soliton gas is so diluted that only single, charged solitons may be found on the chains. Single solitons are unlikely to hop due to the high energy required for structural reorganization Kivelson [36] envisaged for this doping range a mechanism for the transition, involving the charged soliton generally pinned to a doping molecule, and a neutral soliton can tunnel it to the positively charged soliton, if the electronic of both excitations nearly coincide. This require that the neutral soliton is also closed to an ionized impurity, otherwise an energy equal to the binding energy of the charged soliton would have to be overcome. Under such conditions the charge can tunnel without the need to transfer a large amount of molecular deformation. The resulting formula

$$\mathbf{s(T) = 0.45 \frac{e2}{kT} x_0 (1 - x_0) \frac{(T)ro}{NR0R0} \exp(-2.78 R_0 / r_0)} \qquad \text{Eq.1.6}$$

depends on the fraction of neutral (x) and charged solitons ($1-x_0$), the average chain length N, the ration of average localization length r_0 to the average acceptor distance R_0 and on a frequency factor γ(T), which is assumed to vary with temperature like T^n, with

n = 10 – 12, a rather unphysical dependence. This formula predicts, firstly, a strong exponential increase of the conductivity with doping, provided that the fraction of neutral solitons remain constant and, secondly, a power dependence of σ on temperature. Considering three-dimensional effects [37,38] , this process unlikely, since solitons on adjacent chains are bound to one another forming a soliton molecule.

1.3.3 Applications of conducting polymers:

Conducting polymer represent materials with wide area of potential applications. Apart from bulk use in static charge dissipation and RF shielding [39], some of them find use in corrosion protection [40], various types of sensors [41], batteries [42], electrochromic cells [43], controlled release applications [44]. Other applications include third-order non-linear optical polymers and LEDs [45].

Functionalized conducting polymers, which are made by incorporation of functional molecules or by structural control are being investigated for possible applications in the field of photochromism, photoelectric conversions, chemical sensors, etc. Conducting polymers have already been demonstrated for the fabrication of electronic devices such as diodes, light emitting diodes, resistors, capacitors and field effect transistors.

1.4 |Inherently conducting polymer blends and composites:

The first requirement of the successful application of a conducting polymer is convenient processibility. However, the conducting polymers synthesized via the chemical route as well as the electrochemical route are obtained as insoluble and infusible powders or films which have poor mechanical properties. The processing of the conducting polymers has been limited due to low solubility and high temperature stability of conducting polymers in their doped form [46]. Some efforts have been made to overcome this problem by making blends of conducting polymers with conventional thermoplastics.

Mixtures of materials can be both homogenous and heterogeneous. In case of polymers the homogenous mixtures are called as blends while the heterogeneous are called composites. Interpenetrating network (IPN) or semi – IPN is another class of polymer mixtures. Blends can be miscible partially miscible or compatible while composites are mixture of two immiscible materials. Conducting composite systems are obtained by mixing various polymers with conducting particles such carbon black, metal powder or flakes, metal coated particles or fibers. It has been shown that the conductivity of these heterogeneous materials depends on the concentration of the conducting filler and their shape. Usually the percolation threshold is high (above 25 V %).

Recently, fully organic, heterogeneous conducting systems have been obtained from mixtures of conducting organic materials e.g. conducting crystals (organic metals) with inert polymers. These have been classified by Kryszewski into four groups [47]:

(a) Films cast from conducting solutions with other film – forming inert polymers.
(b) Blends of processible conducting polymers with inert polymers.
(c) Reticulate doped polymers (RDPs) consisting of conducting crystal network and
(d) charge-transfer complexes formed in situ of an inert polymer.

1.4.1 Methods of synthesis:

The blends and composites have been synthesized by using different techniques including mechanical blending, dispersion swelling emulsion technique and diffusion. Broadly they can be classified as prepared by electrochemical methods and those prepared by chemical synthesis of the conductive polymers. Electrochemical methods are generally used for small-scale preparations and production of different kinds of devices. Chemical preparation allows large-scale production of the conductive polymer blends and composites.

(a)Blends prepared by electrochemical methods :

Conductive polymer films can be electrochemically deposited on the surface of metallic or semiconducting electrodes. The area of the film depends on the dimension of the electrodes while the thickness depends on the charge density used.

To obtain blends, the working electrode is coated with film of insulating polymer prior to the anodic deposition of the conducting film. The coated electrode is immersed in electrolyte solution containing the desired monomer and swells over a period of time. When the swelling process is complete, a potential is applied to oxidize the monomer. Polymerization starts at the electrode/film interface and proceeds to fill the bulk of the insulating film until reaching the film/electrolyte interface. Thus a blend is formed depending upon the miscibility of the conductive and insulating polymer.

Blends can also be prepared by co-deposition methods. In this case, the insulating polymer host is dissolved in electrolyte solution, which also contains the monomer. As the conducting polymer film is anodically deposited on the surface of the electrode, it becomes soaked with insulating polymer solution. After accumulating the required charge density, the film formed on the electrode thus contains a combination of conducting as well as insulating phase. Soluble polyelectrolytes can also be used in this method, eliminating the need to use an electrolyte salt. The polyelectrolye itself acts as a counter ion or dopant.

(b) Blends prepared by chemical synthesis of conductive polymers:

A blend can be prepared by mechanical mixture of conductive and insulating polymer using a counter ion rotating mixer or a double screw extruder. In this case the resulting conductivity will strongly depend on the miscibility and rheological properties of the components of the blend. The conductive polymer used for blending is normally synthesized by chemical polymerization. Blends of polyaniline and poly vinyl chloride have been prepared using this procedure [48].

The percolation threshold for instance is strongly affected by the miscibility of the blend components.

Another method is co dissolution of the blend components in common solvent, followed by evaporation of the solvent. Here, phase segregation may occur during solvent evaporation because of the different solubility of the polymer in the common solvent. Miscibility is also important. In polyaniline, the polymer can be reduced in a basic solution (dedoped) in order to increase its solubility in common organic solvents. After preparation of the blend it can be doped again.

Polymerization can be achieved by addition of the heterocyclic monomer to a solution of the insulating polymer containing an oxidising agent. Films of the blend can then be obtained by evaporating the solvent in aqueous suspension of latex covered by PPy or collidal dispersion of polypyrrole / poly (2-vinyl pyridine). Films can be obtained by casting, spin coating or spraying [49].

Interfacial polymerization of conductive polymers producing a material with different superficial properties is an alternative method. A two-phase system is necessary: one solution containing an insulating polymer and a heterocyclic monomer (organic phase) an another containing an oxidising agent (aqueous phase). The monomer diffuses to the

interphase where oxidative polymerization occurs. Blends were obtained by this method combining polypyrrole with nafion or PMMA [50].

Polymers can also be swollen with a solution of an oxidant, then drained and dried retaining the oxidants a filler in its bulk. Blend is then obtained by exposing the polymer containing the oxidant to vapor of heterocyclic monomer in closed chamber. Polypyrrole was combined with cellulose, with poly (ethylene terephthalate) or nylon [51].

The solid inorganic oxidant can be introduced into the insulating polymer as a filler. Thus blends can also be prepared by exposure of such solid polymer matrices containing the oxidant to vapors of heterocyclic monomers.

The mechanical mixture of oxidant and the polymer is also an interesting method to incorporate oxidant in the polymer matrix. Blends of polypyrrole and EPDM rubber were obtained using EPDM matrix impregnated with $CuCl_2$ by calendaring [52].

Blends or composites are prepared by combination of two conducting polymers also. A sandwich like composite with layers of polypyrrole adhered to poltyacytelene was synthesized electrochemically. Graft co-polymerization of pyrrole with pyrrole derivative polystyrene was used to improve the mechanical properties of polypyrrole. Electrochemical deposition of polyaniline onto the surface of n – type of porous silicon layers has been studied. Polypyrrole and polyaniline were encapsulated in zeolites, FeOCl, porous PVC, or V_2O_5 [53].

However the conducting-insulating polymer blends obtained by these methods often have low conductivities, typically of the order of 10^{-3}S/cm and that is achieved at a high concentration of the conducting polymer content. For example, a blend of PPy/PEO exhibited a conductivity of 10^{-3}S/cm at 22.5% PPy content while the PPy/PVC blend showed a conductivity of 10^{-5}S/cm by adding 37% PPy to the PVC matrix [54]. In another case, PPy coated nylon 66 and PE spheres exhibited a similar conductivity at much a lower percolation threshold of 10-20% [55], however the ultimate value of conductivity reached was still low i.e. 10^{-3}S/cm in spite of adding 60% PPy coated polymer. Furthermore, the flexibility and hence the processibility of the blends deteriorate as the concentration of the conducting constituent increases. Hence a higher conductivity may be achieved only at the cost of the mechanical properties. These drawbacks could be partly overcome by electrochemical preparation of the blends. In this case, the deposition of conducting polymers was carried out in insulating porous substrates coated on electrodes or matrices that are soaked in the solvent prior to the

deposition of the conducting polymer [56]. Relatively, interpenetrating networks with higher conductivities were obtained. Niwa et al [57] also used the same method to obtain semi-transparent free standing films of PVC/PPy with a conductivity of 15 S/cm also retaining the flexibility of the polymer. Unfortunately, this method was not popularly used to synthesize the blends of conducting polymer-insulating polymer due to limitations of small-scale production. Hence dispersion technique was still favoured so as to obtain blends on a larger scale.

1.4.2 Charge transport in blends and composites:

The charge transport behaviour in blends and composites is dominated by the morphology that consists of an insulating matrix and conductive filler. The composite changes from an insulator to a conductor over a very narrow range of filler concentration. A typical curve of resistivity Vs volume fraction of filler is shown in the **Fig. 1.5.** At lower filler concentrations the composite remains an insulator. At a critical volume fraction, the resistivity of the composites falls sharply to a level at which the composite can readily conduct electricity. The transition of a blend/composite from the insulating material to the conducting material is called the percolation phenomenon. The critical concentration at which the blend/composite behaves as a conductor is called the percolation threshold.

The transition from the insulating to the non-insulating behaviour is generally observed when the volume fraction of the conductive filler in the mixture reaches a threshold of about 25%. Increase in the filler content above the percolation threshold above the critical loading does not appreciably reduce the resistively of the blend/composite but results in the reduction of mechanical properties.

The addition of a conductor to an insulator affects the electrical properties according to the degree of filling and proximity of the conducting particles. Three situations are possible:

1. No contact between the conductive particles
2. Close proximity
3. Physical contact

When the conductive particles are isolated, the conductivity of the blend/composite is changed only slightly. The blend/composite may remain an insulator although its dielectric properties may change significantly.

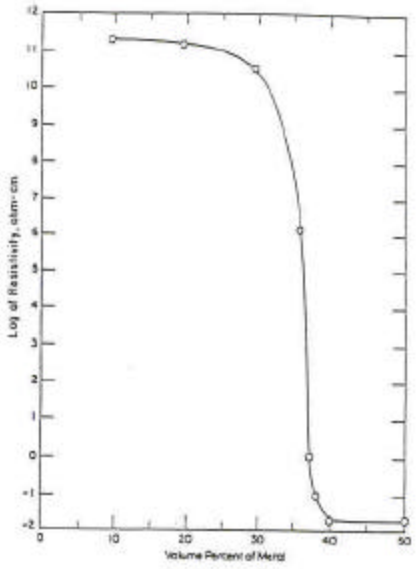

Fig. 1.5 Typical curve of resistivity Vs volume fraction of filler concentration

When the conductive particles are in close proximity, the electrons can jump the gap between the particles, creating current flow. The ability of an electron to jump a gap under a given voltage field, increases exponentially with decreasing gap size. Gaps as large as 10nm can be jumped. The process of electron transport across an insulator gap is referred to as 'hopping or tunneling'. Tunneling consists of jumping or tunneling of electrons from the valence band of ions or molecules on one side of the gap to the conduction band on other side without an energy exchange. The equation for the probability that an electron will tunnel from one energy state to another through the insulator is of then form,

$$P = a\, e^{-\tau \Delta E/kT} + e^{\Delta Ep/kT} \qquad \text{Eq. 1.7}$$

where

a is a constant

E is the activation energy to travel the energy gap

T is the sample temperature

Ep is the local polarization across the barrier

τ is the tunneling factor

The tunneling factor can be expressed as

$$\tau = e^{-\alpha r}$$

where α is a constant

r is the spatial distance through which the electron must tunnel

The exponential form of the tunneling factor shows the importance of maintaining close proximity between the adjacent conductive particles.

The third condition, which is possible when conductive filler is introduced in to an insulating matrix, is that the conductive particles will physically contact each other to form a continuous network throughout the blend/composite. Under this condition the composite conducts through the particle network by conduction mechanism of the particles. In highly loaded composites actual touching does occur and such composites have shown a linear current-voltage characteristics, but in some cases a non-ohmic (non-linear) behaviour was also observed.

Gurland [58] has also shown that the sharp transition from insulator to conductor is due to the formation of a network among the conductive fillers. As mentioned earlier, this does not imply a physical contact.

The network formation has been most frequently treated as a percolation process. The percolation model simply refers to a means of continuous network formation through a lattice, taking into account relative concentration of the two materials comprising network.

As discussed earlier a considerable amount of filler loading is necessary to achieve the percolation threshold even as high as 25% of volume. This high loading leads to a sharp increase in viscosity and a reduction in the mechanical properties.

(a) Sharp increase in viscosity:

From the processing point of view, viscosity is one of the important parameters. Einstein was the first to postulate an expression for viscosity of filled systems, given as follows;

$$\eta / \eta_o = 1 + 2.5\,\phi \qquad \text{Eq.1.8}$$

where

ϕ the volume fraction of the filler

η viscosity of the suspension

η_o viscosity of suspension medium

Hence it is clear that the viscosity rises sharply with the filler loading.

(b) Reduction in the mechanical properties:

The mechanical properties of the conducing polymer blends/composites drop considerably by the addition of the fillers. A continuous and drastic reduction in the fracture energy is found resulting in a brittle, weak product. The crucial parameters influencing the fracture energy were found to be the volume fraction of the filler, and their interfacial adhesion.

1.5 Conducting polymer composites:

1.5.1 Synthesis and applications:

These are also referred to as metal-filled polymers and are the most widely used. Conducting polymers composites (CPCs) are mixtures/blends of conductive particles and polymers. Various conductors have been used in different forms. Initially aluminium flakes

were used to load polypropylene (PP) to make conductive compounds. These could be injection moulded in to desire shapes. The lengths of aluminum flakes range from 1 to 1.4 mm and thickness form 25 to 40 microns. Typically 18-22% volume loading was used. The resistance of the compound suddenly drops at a certain percentage of filler at the percolation threshold. The various polymers which have been used as major matrix are ABS, PP, PC< PE< HDPE< PVC etc. and the different fillers used for loading are typically carbon black, graphite, metal particles, fibers, platelets etc.

Although the conducting polymer composites are quite suitable for some applications such as anti-static materials, EMI/RF shielding etc. their mechanical properties may not always be satisfactory. In fact high amount of filler loading might make the material brittle. As the conductivity is decided by volume of concentration, a low-density resin like PP would need 46% filler by weight. This might cause film to crack under its own weight. Also the compounding time has to be kept minimum to avoid degradation of fillers.

The processes involved in making these composites are different for different polymers. The basic procedure is to take the appropriate volume fraction of polymer and conductor and mix them thoroughly so as to form a uniform distribution of tiller particles in the polymer. If both, the polymer and filler are in powder form, they can be dry mixed and then pressed into desired shapes under high pressure and appropriate temperature. In certain cases the polymer is first dissolved in a suitable solvent is then allowed to evaporate to obtain a film. Another method used in meltmixing where the polymer is heated to melt it and to the free flowing polymer the desired filler is added and mixed thoroughly. This melt can be pressed into dies to get the desired shapes. In all these cases, care has to be taken to avoid degradation of filler particles. For example in the case of aluminum flakes compounding with the polymer melt, shear must be kept as low as possible. Also the compounding time must be kept minimum.

ABS/PC with 40% weight load of aluminum flakes as reported to give 40-50 dB attenuation over a frequency range of 2 .6 to 3.9 GHz [59]. Various grades of carbon blacks too are available and are used extensively for packaging in the fields of electronics, photography, watch industry etc. Antistatic pipes have been manufactured for transporting combustible liquids. For this carbon black is added to a resin to make the glass reinforced epoxy pipe.

The resistivities of these composites range from 10^7 to 10 ohm-cm. In certain applications conductivity of 10^7 ohm-cm is quite sufficient, as in the case of anti-static pipes where lower resistance would be desirable for EM shielding.

1.5.2 Charge transport in conducting polymer composites:

The addition of conducting material drastically changes the electrical properties of the original polymer and the resistivity drops down by a large value, sometimes by as 12 orders of magnitude. The electrical conduction mechanism in such conductor-filled systems vary one from system to another system depending on the insulating polymer and the type of conductive filler used.

Jean-Pierre Reboul [60] while discussing the dc conduction in carbon-polymer composites has mentioned that the transition from insulating to non-insulating takes place when volume fraction of conductive filler is about 25%. The exact percentage depends upon the aspect ratio of the conducting particles. The conduction behaviour is explained by percolation. The author has also carried out the contact resistance measurements and has found that the contact resistance is not constant but changes as a function of applied voltage.

The conduction mechanisms in such systems have been discussed by various workers. Sherman *et al* [61] have proposed that three distinct physical processes govern electron transport through a conductor filled polymer- Percolation, Quantum mechanical tunneling and thermal expansion. According to them the key feature of percolative transport, suggesting its relevance to conductor- filled polymer is the existence of a density threshold. In crossing this threshold, the mediums transport coefficient (such as resistivity) changes sharply from non-conducting to conducting (or vice-versa). They suggest that it is at point that a macroscopic-length chain appears. For example, in systems where two dry powders, one a conductor and the other an insulator, are mixed in various proportions it is observed that, as the volume fraction of conductive material increases, at a certain critical volume the overall resistance of the mixing drops sharply from insulating value to a value nearer to that of conductive filler. This has been shown to be similar to a liquid percolating through a material e. g. soil.

Quantum mechanical tunneling has been also used to explain the conduction through the insulating materials. According to this theory, two conductors whose separation is large

(> 100 Angstrom) compared to atomic dimensions see each other through a resistance controlled by the bulk resistivity of the polymer itself. However when this distance is small (< 100 angstroms) electrons may tunnel quantum mechanically between the conductive elements, leading to a lower resistance than would be expected from the insulator alone. Thermal expansion of polymers has been used to explain the importance of critical volume fraction in such materials. Due to the difference in the thermal expansion coefficient of polymers (which are quite high) and fillers, with increase in temperature the distance between the adjacent filler particles increases. If the initial volume fraction is just greater than the critical volume fraction and therefore the resistance is low), then the increase in temperature will cause the filler particles to move apart. Due to this distance between the filler particles may increase beyond the critical value, thus causing a large increase in the resistance value.

Jean-Pierre Reboul[60], in a review, has discussed the conduction in carbon black- filled polymers and also the effect of electrode material on the conduction process. In such systems non-linear current-voltage characteristics have been observed and different conduction mechanisms such as tunneling between carbon black particles and hopping conduction have been proposed. According to Reboul the resistance of such samples is influenced by many parameters such as length, orientation, voltage, temperature etc. Therefore no significant value for the conductivity of the material can be deduced from a single measurement of current and voltage. It is therefore necessary to distinguish between properties of the medium and properties of a particular sample with given shape, length, and the electrode material.

Jachym [62] mentions that for polymers conducting powders at high concentration, the mechanism of conduction is characteristic of the doping agent alone. At concentrations close to critical there is a large change in resistance with change in temperature, resulting from the different linear expansion coefficients of the polymer and filling material. Frequently, tunneling effects take place, which induce corresponding temperature dependencies have been observed. At low concentrations, the temperature dependence of the composite is comparable to that of the pure resin. The dependence of conductivity sigma on temperature takes the form:

$$\mathbf{s} = \mathbf{s}_0 \exp\left(- \frac{\mathbf{W}}{\mathbf{k}_B \mathbf{T}} \right) \qquad \text{Eq. 1.9}$$

Where σ_0 is a constant and *W* is the activation energy.
The activation energy can be defined by the equation

$$\mathbf{W} = -\mathbf{k}_{\mathbf{B}} \frac{\partial (\ln \mathbf{s})}{\partial (\mathbf{1}/\mathbf{T})} \qquad \text{Eq.1.10}$$

Various values of activation energy are observed for different cross-linking agents and for their variable concentrations. It is also observed that above the glass transition temperature T_g of the resin, the activation energy decreases with temperature for example in case of polyesters and in low-conductivity composites.

For increase in carbon black content, above some critical value, there is an abrupt increase in the conductivity of the composite. In this highly conducting region, the conductivity varies according to the following relation:

$$\mathbf{s} = \mathbf{s}_{\mathbf{0}} \frac{\mathbf{1}}{\mathbf{T}} \qquad \text{Eq. 1.12}$$

which is valid for the composite with polyester resin cross-linked with styrene, whereas for the same composite but cross-linked with methyl methacrylate the variation in conductivity is as follow:

$$\mathbf{s} = \mathbf{s}_{\mathbf{0}} \left(\frac{\mathbf{1}}{\mathbf{T}} \right)^{\mathbf{1/2}} \qquad \text{Eq.1.13}$$

The variation in the temperature dependence of conductivity is said to be dependent on the scattering centers. Such as in case of methyl methacrylate, because of presence of C=0 bond, can be considered as effective scattering centers. Because of these scattering centers the magnitude of N i.e. density of scattering centers increases in resins cross-linked by methyl methacrylate. It can be further assumed that the concentration of charge carriers, n, generated from the particles of carbon black do not influence the temperature dependence of

the conductivity as the conductivity of carbon black is virtually temperature dependent. In general the temperature dependence of such systems can be expressed as follows:

$$\sigma \propto \frac{n}{N}\left(\frac{1}{T}\right)^{1/2} \qquad \text{Eq.1.14}$$

In case of carbon black – polyester resin composites the current – voltage characteristics were found to be non-linear and according to Jachym these can be explained by the theory of space-charge –limited currents (SCLC).

The current voltage characteristics in polyester resins containing carbon black satisfies the equation $I = AU^3$ where U is applied voltage. Non-linear characteristics have been observed in certain composites, at carbon black contend of 0.4 to 1.0 g per 100 g of resin. Exponent 5 in between 1.07 and 1.85 depending on the carbon black concentration. According to Jachym these non-linear effects can be expanded by the theory of space-charge limited currents (SCLC). Further in agreement of SCLC theory, the current density depends on voltage in the following way:

$$j \propto U^{L+1}$$

where $L = T_c/T > 1$ & T_c is a parameter defining distribution of traps [63].

The effects of pressure on the electrical conductivity of composites have been found to be useful to distinguish between ionic and electronic conduction in such systems. While an increase in pressure causes increase in conductivity for electronic conduction, in case of ionic conduction, conductivity decreases with increase in pressure.

1.6 Fillers:

Fillers are used in order to make blends and composites for incorporating special properties of photoconductivity, chemical sensitivity, etc. Fillers like phthalocyanines (Pc) and cadmium sulfide (CdS) can be used for this purpose.

1.6.1 Phthalocyanines:

(a) As chemical sensors :

The effect of oxygen on phthalocyanine was discovered in 1948. This effect was studied quantitatively by Heilmerier and Harrison [64] using CuPc single crystal in vacuum, air, oxygen and hydrogen atmosphere. Admission of oxygen was found to increase conductivity and lower the activation energy. This was recognized to be a bulk rather than a surface effect. Admission of hydrogen reversed the oxygen effect to yield a lower conductivity and higher activation energy, which remained constant in subsequent evacuation. The effect of oxygen, nitric oxide, nitrogen dioxide and ammonia on sublimed films of metal free, Fe - , Co - , Ni – 1 Cu- and Zn – Phthalocyanine were studied by Kaufhold and Hauffo [65]. The nitrogen dioxide NO and NO_2 resulted in large increases in conductivity and reduction in activation energies. Also charge transfer interactions were evident in the visible spectra of these films.

A surface accoustic waves (SAW) device responds to changes in the coatings mass, conductivity and mechanical properties. A SAW device was constructed using lead phthalocyanine coated 110 MHz lithium niobate SAW sensor responding to 10 ppm nitrogen dioxide.

(b) Photoconductors:

Almost 90 % of the photoconductors in the charge generation (copiers, lasers, printers) are organic semiconductors (especially titanium phthalocyanines) have been observed in phthalocyanines thin film devices. The contact of the solid molecular semiconductor like a phthalocyanine with a material of a different electrochemical potential of electrons (Fermi levels) of metals and semiconductors redox potential of an electrolyte) may result in :

a) Rectification in the dark under an applied potential / electrical field.
b) Photovoltaic effect and a photo potential under illumination.

Different cell configuration are Schottky cells, n/p double layer cells three / multi layer cells, photoelectrochemical cells. All these cells use phthalocyanines in the form of thin layers on electrically conducting carriers such as 1T0, Nesa glass, Ag, An, Al. etc or inorganic semiconductors like P-Si, CdS .

Under illumination, a Schottky contact can exhibit a photovoltaic effect. If the metallic electrode is thin enough to be semitransparent in the contact of a metal low work function and an organic p- conductors then excited holes can cross the barrier into the semiconductor. But this contribution is small due to low transmittance of the metal electrode. Excited states in the depletion region of the semiconductors can be separated into electrons and holes by

the built-in electrical field. In addition, excitons from excited states obtained by light absorbed in the bulk of the p-conductor may diffuse to the depletion region for separation contributing to the photocurrent. Under illumination, the concentration of minority charge carriers is increased more efficiently than that of majority carriers therefore though junctions that lead to depletion layers (high surface concentration of minority carriers) are most interesting for photoelectrochemical cells and studies.

1.6.2 Cadmium sulfide (CdS):

CdS has interesting semiconducting properties and is an n-type semiconductor. It is widely used as a thin-film cell for solar energy conversion and is a photoconductor and electroluminescent [66]. These properties have found use in phosphors, photomultipliers, radiation detectors, thin-film transistors, diodes and rectifiers, etc [67]. It is found in cubic and hexagonal crystal lattices. The photoconducting properties of this material are utilized by forming Schottky barriers or p-n junctions.

Photovoltaic effect in CdS is associated by the use of non-ohmic contacts. CdS rectifiers have been made by including a crystal of conducting CdS:Cl or CdS:In between a non-ohmic contact such as Ag or Cu [68]. Such a rectifier biased in reverse direction can be also used as a photorectifier [69], where light falling on the rectifying junction causes an increase in conduction by a factor of 10^6. Crystals of CdS show appreciable photosensitivity on account of the presence of imperfections e.g. a Cu^+ center in place of Cd^{2+} or a cation vacancy. These sensitizing centers may be categorized as compensated acceptors. If sensitizing centers are absent these other imperfections dominate and an insensitive material results. Sensitivities of several typical forms of CdS are reported [70]. In case of a polycrystalline system associated with a CdS dispersed in an insulating binder, it is likely that a tunneling between photoconducting particles through a thin film of binder plays an important role in the conductivity at low applied electric fields [71].

Heterojunctions using CdS were also of interest in which light can be directly incident on the junction if directed through the large band gap materials [72]. Typically, the Cu_2S-CdS heterojunction, can be conveniently made by a dipping process in an aqueous solution of Cu^{2+}, by which a layer of Cu_2S is topoaxially formed. The diffusion of Cu into the CdS leads to a high-resistivity compensated layer in the CdS, the properties of which are extremely important.

1.7 Special properties:

Various types of materials can be used along with conducting polymers in order to tailor the application of the polymer blends. Criteria of the filler selection entirely depends on the property desired. For example a photoconducting material like CuPc or CdS can be introduced to form a composite of conducting polymer. Chemical sensitivity of the conducting polymers can also be enhanced in a similar manner. A brief account of the properties is presented below.

1.7.1 Photosensitivity:

A broad definition of photoconductivity would be increased conductivity produced in a material when it is irradiated with and absorbs radiation in the ultra-violet-visible region of the electromagnetic radiation.

Photoconduction studies in polymers have been initiated by the report on a photoconducting polymer (N-vinyl carbazole) [73]. The polymeric photoconductors are based on two types of systems :

(a) The activity is built into the polymer structure itself.

(b) The binder polymers containing high concentration of active chromophores or charge transport molecules.

Considering the above principles, the polymeric photoconductors are classified into five categories :

(A) Polymer with pendant group :

(B) Molecularly doped polymers :

(C) Backbone conjugated polymers :

(D) Liquid crystalline systems :

(E) Nanoclusters/ polymer composites :

The process of photoconduction can be separated into the following steps

:

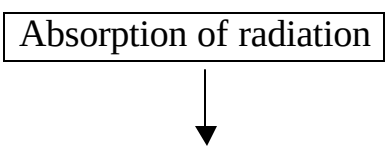

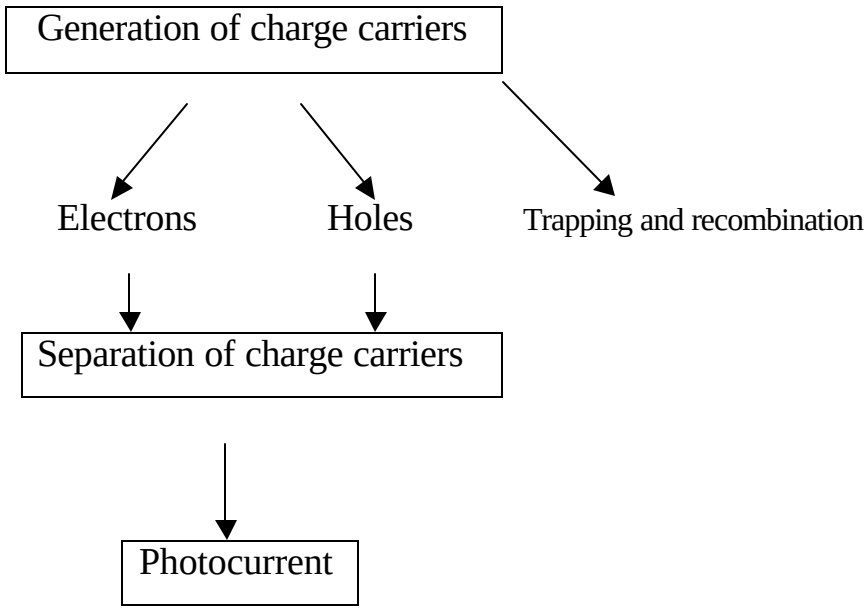

Photoconductivity is the result of two processes [74]:

(a) one utilizes photophysical processes at semiconductor (SC) junctions such as pn & Schottky.

(b) the other is based on photochemical processes between sensitizer (photoexcitation center) and acceptor/donor

For both the process, separation of photo-produced charges (electron & holes) is most important.

This separation of charges occurs at the junctions in photo-physical devices. A pn junction is formed when a p type semiconductors is contacted with the n-type semiconductor resulting in an electron flow from n-type to p-type semiconductor making the Fermi level come to the same height. This induces band bending of the valence band and the conduction band. Illumination of the junction causes electron transition from the valence band to the conduction band, giving rise to a hole in the valence band. The holes and electrons thus produced by irradiation diffuse in different directions because of the band bending at the p-n interface. The photoseparated charges flow in the external circuit giving a photocurrent.

The second type of junction giving photoconductivity is the Schottky junction formed between a p-type semiconductor and a metal with a proper Fermi level similar to the pn junction.

The photochemical process comprises exchange of electron & holes at separate electrodes by the photochemical reaction products. For example, electron donor (D), sensitizer (photoexcitation center P) and electron acceptor (A) produce photochemically oxidized D and reduced A via photoexcitation of P as shown

$D+P+A+nv$ ----------$D+P^{*}+A$

----------$D+P^{+}+A^{-}$

oxidative quenching

----------$D^{+}+P+A^{-}$

$D+P+A+hv$ ----------$D+P^{*}+A$

----------$D^{+}+P^{-}+A$

reductive quenching

----------$D^{+}+P+A^{-}$

If the three components are arranged in a multilayered structure it is possible to obtain an electrical output. It is very important to suppress the charge recombination in a photochemical process.

Photoconduction in polymers is of two types: intrinsic e.g. PVK exposed to UV radiation or extrinsic, as in pigment particles dispersed in PVK.

The existence of intrinsic photogeneration of carrier has been doubted for energies lower than 4.6 eV (~260 nm). Due to UV irradiation, photo-oxidation products of PVK are formed which act as acceptor like impurities and form charge – transfer complexes with unoxidised PVK. These charge transfer complexes act as charge carrier generators.

The second type of photogeneration is due to sensitization. Sensitization effect is brought about by adding molecular species such as dyes, electron acceptors and electron donors to the host polymer. For example, PVK was sensitized with crystal violet (CV), a benzopyritium salt B-20) and a carbonium salt [75]. PA was sensitized with dyes such as pinacyanol, methylene blue, chlorophyll a, hematin, phthalocyanine, etc. A hetero p-n junction device was also built using PA. PA n-type was formed by doping with a donor such as alkali metals & p-type PA was formed by doping with an acceptor such as halogens (Cl_2, Br_2, I_2, etc) [76].

1.7. 2 Chemical sensing properties:

There are various types of chemical sensors based on the chemical interaction and the sensor configuration used. Recently, thin layers of molecular, supra molecular and polymeric compounds gain interest as sensitive, selective and stable coatings for transducers for

chemical sensors [77]. Gases such as oxygen, chlorine, nitrogen dioxide and carbon dioxide and volatile compounds can be easily detected. The materials have been applied in the form of coatings on the substrates. Polypyrrole has been used to detect toxic gases in air films were deposited electrochemically on interdigited electrode patterns from an aqueous solution of 0.1 molar $LiBF_4$ [78]. The films thus prepared were sensitive to electron donating gases such as ammonia. It was found that a past fabrication treatment enabled the sensors to respond to additional gases.

Results also show that polypyrrole also behave as a p-type material. The conductivity hence decreases in the presence of a reducing gas (ammonia) and conductivity decreases in the presence of an oxidizing gas (nitrogen dioxide). The mechanism is similar to that occurring on tin dioxide in which the gas molecules cause changes in the near surface charge carrier (electron and holes) density by reacting with surface adsorbed oxygen ions. The response of to 0.1 % ammonia in air showed an increase in background resistance by around 20 % of its initial value after 8 exposure cycles. In case of hydrogen di sulfide there was an evidence of an irreversible surface reaction due to the gas retention by the testing apparatus [79].

Yoneyama et al [80] have shown that electropolymerized PPy films exhibit noticeable gas sensitivities to electron acceptor gases such as PCl_3, SO_2 and NO_2 at room temperature. The authors also investigated the gas sensing properties of PTh films (16 d) but they found a more irreversible behaviour in the conductivity change after exposure to ammonia and H_2S.

Field effect transistor (FET) devices have been fabricated using ECP based chemical sensors [81]. SGFCTs operating in solid state have been developed by Janata et al which respond to lower aliphatic alcohols at room temperature and with a time response of seconds [82]. PPy/3-nitro toluene exhibit selective sensitivity to alcohols and aromatics and is explained on the basis of M – H or M – N interactions.

PANI coated on four-probed electrode device shows sensitivity towards methanol, ethanol acetone and acetonitrile vapours in the nitrogen carrier gas [83]. PANI based micro-electrochemical transistors can operate in the solid state by using a PVA / Phosphoric acid solid-state electrolyte, in this way water vapours can be detected [84].

Ion detectors have been fabricated using ECP conducting polymers. PPy films prevented the permeability of anions of larger size than the cut off size, which was decided by the size of the anion used for ECP of pyrrole. Thus specificity to the ions may be obtained

by functionalization of the ECP by species offering specific interaction with the ion to be analyzed. PPy coated by the carbothiotate ligand showed on uptake of Cu2+ ion from the solution, with a detection limit of 1ppm [85]. Thus it can be observed that the gas sensitive devices based on conducting polymers are straightforward to fabricate robust and simple to use. The selectivity and sensitivity to a particular type of gas can be altered by tailoring the matrix/substrate used. Several other types of sensors have been made using conducting polymers like radiation detectors, electrochemical bio-sensors, etc.

Irrespective of the configuration of the sensors, the action of chemical species is detected as changes in parametric values such as resistance, current or electrochemical potential, or the work function of the polymer the mechanism of the interaction which occur on PPy and p–poly phenylene films during their exposure to various organic vapours was investigated by UV–vis spectroscopy and by the Kelvin probe technique. The spectroscopic method follows the changes in polaron and bipolaron concentration, which are sensitive to any charge transfer that moves into / out of the films, while the Kelvin probe monitors directly any changes that occurred in the work function of the polymer. The results indicated a mechanism consisting of the following steps : interaction of the vapour molecules with a polymer, partial charge transfer to form a mid gap state in the film and lateral dispersion of the charge between all the absorbed molecules.

1.8 Ionically conducting polymers:

1.8.1 Types of ionically conducting polymers:

Ion conducting polymers are effectively solutions of ionic salts in heteropolymers such as polyethylene oxide (PEO). Ionic conducting polymers can be classified into two groups. The distinction is based on the temperature at which the polymer shows appreciable conductivity relative to its glass transition temperature T_g. This distinction is found to be directly related to the ionic transport mechanism. The first group is composed of polymers that show appreciable ionic conduction only at temperatures above their glass transition. This group includes all the ionic conductors based on complexes of polyethers and alkali metal salts such as the classic ionic conducting polymers developed by Wright et al. [86] and Armand et al [87]. Also included in the group are the polyphosphazene backbone polymers to which ion-solvating groups have been grafted, such as the polymer MEEP, and analogues of

PEO complexes such as poly(ethyleneimine) complexed with alkali metal salts. In this group of polymers the ionic conduction process involves a cooperative interaction between the mobile ionic species and the polymer matrix. The second group consists of polymers that have appreciable ionic conductivity at temperatures (typically, room temperature) below their glass transition temperatures. Nafion and blends of poly (vinyl alcohol) and H_3PO_4 (PVA/ H_3PO_4 are examples of polymers in this group.

1.8.2 Charge transport mechanism ionically conducting polymers:

In these systems, the conduction mechanism can be described by a percolation model in which a highly conductive phase is embedded in a poorer conducting phase (or insulator). Significant conduction does not occur until a critical volume of the highly conductive phase is reached, at which point the highly conductive phase forms a continuous network throughout the polymer matrix. If the ionic conductivity in a polymer were governed by single jump diffusion mechanism the ionic conductivity can be obtained by the Stokes-Einstein equation [88]:

$$D = kI / 6\Pi r\eta \qquad \text{Eq.1.15}$$

Where D is the diffusion constant, r is the ionic radius, k is Boltzmann's constant, T is temperature, and η is viscosity) with the Nernst-Einstein equation,

$$\sigma = z^2F^2c(D_+ + D_-) / RT$$

(where c is the concentration of mobile ions, z is the charge of the ion, F is Faraday's constant, and D^+ and D^- are the diffusion coefficients of the two mobile species that are present, an anion and a cation). For a situation in which only one mobile species is present, the combination of the above equations predicts that the conductivity is inversely proportional to the viscosity and is given by

$$\sigma = z^2 F^2 c / N_A 6\Pi r\eta \qquad \text{Eq.1.16}$$

where N_A is the Avogadro's number.

An alternative expression that is often used to describe the ionic conductivity in an amorphous polymer system is based on free volume theory and is given by the Vogel-Tamman-Fulcher(VTF) equation

$$C(T) = A \exp (B/T-T_0) \qquad \text{Eq.1.17}$$

Where C(T) can be any reduced –transport parameter. If C(T) is $DT^{-1/2}$, or $\sigma T^{-1/2}$, the following expression for ionic conductivity results:

$$\sigma = AT^{-1/2} \exp (B / T\text{-}T_o) \qquad \text{Eq.1.18}$$

1.9 Solid polymer electrolytes:

The insulating-conducting blends suffered from a major drawback of possessing lower conductivity. Hence these cannot be used in applications such as batteries, electrochromic display devices, etc wherein the internal resistance is required to be low. A novel way to overcome this problem was to replace the insulating polymers with semiconducting materials/polymers in the blends. These semiconducting polymers belonged to the class of ionically conducting polymers. viz. the solid polymer electrolytes.

Ionic conduction is associated with liquids, solvents with either high dielectric constants or molten salts. However solids can function as electrolytes also known as solid ionic conductors. Fast ion conducting electrolytes (typical conductivity $10^{-6} \leq \sigma \leq 10^{-1}$ S/cm) are exciting because of their wide ranging applications such as gas sensors, electrochemical display devices, intercalation electrodes, power sources, solid state high density batteries, etc.

The poly(ethylene – oxide) based chemically conducting polymer as the solid electrolyte was reported by Armand et al. Since then polymer electrolytes based on complexes formed between PEO and alkali metal salts have become materials of considerable interest due to their desirable conductivity, mechanical properties and compatibility. SPEs were made by complexing a polymer like polyethylene oxide, poly vinyl alcohol, poly vinyl pyridine etc with inorganic salts such as lithium perchlorate, sodium or potassium iodide etc.

The solid polymer electrolytes can be classified as:

(1) conventional polymer electrolytes

(2) non-conventional polymer electrolytes

The conventional polymer electrolytes are alkali metal salt complexes of high molecular weight polymers containing optimally spaced electron donor atoms or groups, which coordinately bond with the metal ion in the salt. The well-known example is PEO-$(LiX)_n$ in which the LiX is a Li salt e.g. $LiSO_3CF_3$, and n in this case is the mole ratio of Li salt to ethylene oxide (EO) monomer unit in the polymer host, n is also the mole ratio of Li^+ to O.

For a given concentration of the salt, the concentration of the ionic charge carriers in the electrolyte is determined by the dielectric constant of the polymer and the lattice energy of the salt. Polymers with high dielectric constants and salts having low lattice energies are generally expected to promote greater dissociation of the salt thereby providing higher concentrations of the ions. Larger anions as in the case of the complex ions, promote substantial delocalization of the negative charge, that occurs with the reduction of ion-ion interactions consequently yielding high conductivity. The motion of the ions (i.e. conductivity) in polymer electrolytes appears to occur by a liquid-like mechanism in which the movement of ions through the polymer matrix is assisted by a large amplitude segmental motion of the polymer backbone. Ionic conductivity primarily occurs in the amorphous regions of the polymer [89]. The conductivity behaviour is dependent on the crystallinity of the polymer, the complex formed and the salt. The ratio of different phases depends on the PEO : dopant ratio, and the time interval and temperature of the measurement as well as the polymer characterization such as molecular weight, molecular weight distribution, completeness of crystallization and the kinetics of crystallization. Different techniques including DSC , XRD , optical microscopy and electron microscopy, NMR and IR have been used to determine the phase diagrams and structural characteristics of the polymer salt complexes [90].

The temperature dependence of conductivity is best related by the Vogel-Tamman-Fulcher (VTF) equation

$$\sigma = AT^{-1/2}\exp(-B/T-T_o) \qquad \text{Eq.1.19}$$

where σ is the conductivity, A is a constant proportional to the number of carrier ions, B is a constant and T_o is the temperature at which the configurational entropy of the polymer becomes zero and is close to the glass transition temperature (T_g). The thermal transitions are the glass-transition temperature (T_g) and the melting point (T_m) for the crystalline fraction of the polymer. The influence of these properties on the conductivities of the electrolytes can be derived from the temperature dependence of conductivity. An abrupt increase in the conductivity at 60^oC is associated with PEO-based electrolytes because PEO is partially crystalline whereas a steady rise in the conductivity is observed in case of complexes of poly(propylene oxide) (PPO) and poly[bis-(methoxyethoxy) phosphazene] (MEEP) that are fully amorphous. As regards dimensional stability, it generally exhibits an inverse

relationship, the higher the conductivity of the electrolyte, the lower is its dimensional stability.

Comparatively, the non-conventional solid polymer electrolytes with ionic conductivities approaching those of their liquid counterparts (i.e. $\sigma \approx 10^{-3}$S/cm) have been reported. This can be possible by adding plasticizers to the polymer electrolyte. For example Kelly et al [91] showed that the conductivity of PEO-($LiSO_3CF_3$) could be increased to ~ 10^{-4}S/cm at 40°C with the addition of 20 mole percent poly(ethylene glycol) dimethyl ether (PEGDME).

Poly(ethylene oxide)(PEO) and other polyethers were blended with polypyrrole by chemical polymerization using $FeCl_3$ as oxidant [92]. In another case solutions of the polymers and oxidant-$FeCl_3$ were mixed and cast on glass substrates producing highly viscous films. These films were then exposed to pyrrole vapours. The PPy thus deposited produced a material with conductivities of 2-3 x 10^{-3} S/cm. Highly cross-linked PEO gels incorporated with $CuCl_2$ were also used to make blends with PPy [93]. Hence it was observed that blends with higher conductivity and processibility could be obtained

Solid polymer electrolytes have been used as thin films on the conducting polymer substrates and sandwich cell type devices fabricated in the past, some of which were reported to be more efficient than others. The devices reported in the past make use of the conducting polymer film in liquid electrolyte (mostly non-aqueous), which may spill during handling or evaporate during long term storage. To overcome these limitations, attempts have been made for replacing the liquid electrolyte with solid polymer electrolytes (SPEs). Thus the devices were safe and also provided low volume and weight. The processing and fabrication of the SPEs in the thin film configuration are relatively simple as these can be routinely fabricated in the form of thin films with thickness of less than 1μm.

Some of the applications of solid polymer electrolytes in conjunction with the conducting polymers are discussed briefly.

(1) Lithium-polymer batteries:

The use of conducting polymers as battery electrodes relies on their redox(doping) processes being driven electrochemically. For example the p-doping process of for PPy has been extensively exploited in cathode material for batteries with a lithium anode and a suitable electrolyte, e.g. a $LiClO_4$-PC solution. The electrochemical charge-discharge process of this battery can be written as ,

$$(Py)_n + nyLiClO_4 \text{ charge / discharge } [(Py)^{y+} (ClO_4^-)_y]_n + nyLi \quad \text{Eq.1.20}$$

The lithium-PANI system was exploited by Japan's Bridgestone Company in the large-scale production of high-cycle-life, button-type, three-volt battery [94]. A PEO–SEU–$LiCiO_4$ polymer having interpenetrating network was used in combination with poly(N–oxyalkylpyrrole) electrodes designed to form a mixed ionic electronic conducting matrix[95,96].

(2) Polymer supercapacitors:

These can be defined as high-power, energy-storage devices wherein the conducting polymers are used as electrode-active materials. Conducting polymers are useful due to the fast doping-undoping processes with suitable morphology, the charge is stored throughout the volume of the material and they can be generally produced at lower manufacturing costs[97].

(3) Electrochromic devices:

An electrochromic material is one whose colour changes in a persistent yet reversible manner through an electrochemical reaction. Accordingly, conducting polymers can be repeatedly switched electrochemically from the doped to the undoped states with high contrast in colour have emerged as an extremely versatile class of electrochromic materials [98].

The colour changes elicited are due to the modification of the polymer's band electronic structure. To take advantage of the electrochromic effect to form a display, a method of reversibly injecting electrons and ions into an electrochromic film must be devised. This is achieved by using an ionic conducting electrolyte to separate the electrochromic material from an electrode which is a source of ions fabricated as a multilayered structure. For example, Poly (3-methyl thiophene) was used in conjugation with lithium intercalated nickel oxide on IT0 as an electrochromic device [99-103].

1.10 Charge transport:

The blends and composites of the conducting polymers as discussed in the above section actually represent a heterogeneous mixture of two or more components. Hence the different materials are in intimate contact in a polymer matrix and are dispersed uniformly throughout the matrix. The contact of the materials at the interface will strongly affect the electrical properties of the blends and composites on a macroscopic level. The dissimilarities in work-function of the materials gives rise to the formation of a potential barrier at the

interface [104]. Various such junctions were fabricated in the past in the view of their potential use in electronic devices. The conducting polymers are p-type organic semiconductors. Hence the junctions formed at the interface of conducting polymers and inorganic materials in contact were termed as heterojunctions. Electronic devices based on conducting polymers have been reported in the past. The first example of transistors was reported in 1988 by Burroughes et al. using PA and Assadi et al using poly(alkyl thiophene) [105]. The Schottky diodes using polymers as an active material has been reported by several groups [106]. These new devices provided means of adding and removing charges to the polymer by injection and depletion that avoids chemical doping of the polymer and possible side reactions. These devices revealed novel physics that the characteristics of polymeric devices are similar to the inorganic semiconductor devices. Thus the polymer films are amorphous and the devices have acceptable characteristics.

The electrical properties of the blends and composites are exclusively governed by the charge transport across the potential barrier formed at the interface of the materials. As discussed earlier, similarities can be drawn between the conducting polymer composites and the blends and composites of inherently conducting polymers due to the fact that both represent filling of conducting material in the insulating counterpart. Hence the charge transport in the conducting polymer composites is reviewed in the following section.

In general, such composites may be considered to be metal – insulators – metal type of materiel (M-I-M) and therefore the conduction processes at metal insulator interfaces should also be reviewed here

According to Simmons [107] the conductivity in insulator is often due to extrinsically rather than intrinsically bulk generated carriers. The intrinsic current carried by an insulator is given by.

$$\mathbf{I = e\mu N_C F}.\exp\left[-\frac{\mathbf{Eg}}{\mathbf{2kT}}\right] \qquad \text{Eq.1.21}$$

where *e* is electronic charge, μ is charge mobility, F is field in the insulator, N_C the effective density of states in insulator, E_g the insulator energy gap, K the Boltzman constant, T is the absolute temperature. This value of current density turns out to be 10^{-18} A/cm^2 which is many orders of magnitude small.

When an electric field is applied across an insulator, if sufficient number of carriers are available to enter the insulator so as to replenish those which are drawn out, then the I-V characteristics of sample will be dependent on the bulk properties of insulator and we say that the conduction process is bulk limited. At high fields, or if the contact is blocking type then the current supplied through the electrodes to the insulator will be less than that capable of being carried in the insulator.

Under these conditions the I-V characteristics of the sample will be controlled primarily by conditions existing at the cathode-insulator interface, this conduction process is referred to as being emission-limited or contact-limited.

1.10. 1 Types of contacts

The types of contacts that can exit at a metal-insulator interface fall into three categories : (i) ohmic contact, (ii) neutral contact, and (iii) blocking contact.

(i)Ohmic Contact – Mott-Gurney contact:

In this case the electrode work function ψ_m is smaller than the insulator work function ψ_i as shown in the **Fig. 1.6 (a)** and the electrode can readily supply electrons to the insulator as needed. Under these conditions, in order to satisfy thermal-equilibrium requirements, electrons are injected from the electrode into the conduction band of the insulator, thus giving rise to a space-charge region in the insulator. This space-charge region is shown in **Fig. 1.6 (b)** to extend a distance λ_o into the insulator, and is termed the accumulation region.

(ii)Neutral contact:

In this case $\psi_m = \psi_i$, which means that the conduction band is flat right up to the interface, that is, no band bending is present, as shown in **Fig. 1.6 (d).**

(iii) Blocking contact- Schottky barrier:

A blocking contact occurs when $\psi_m > \psi_i$, and in this case electrons flow from the insulator into the metal to establish thermal- equilibrium conditions. A space-charge region of positive charge, the depletion region, is thus created in the insulator and an equal negative charge resides on the metal electrode. As a result of the electrostatic interaction between the

oppositely charged regions, a local field exists within the surface of the insulator. This

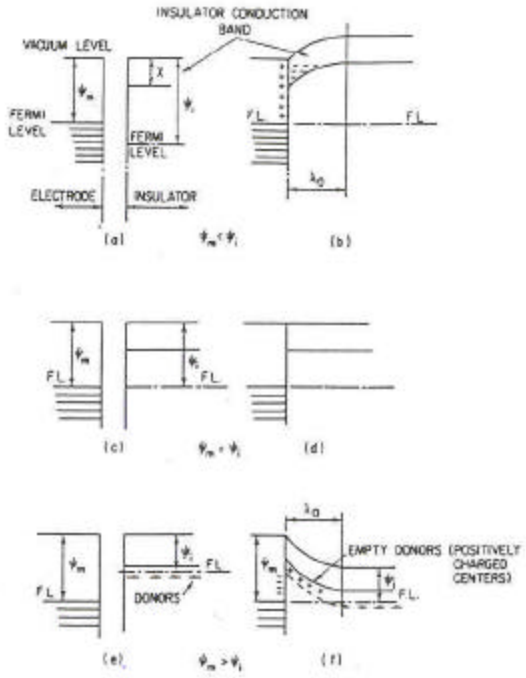

Fig. 1.6 Energy diagrams showing various types of contacts at metal-insulator interface: (a,b) ohmic contacts, (c,d) neutral contacts, (e,f) blocking contacts

causes the bottom of the conduction band to band downward until the Fermi level within the bulk of the insulator lies ψ_i below the vacuum level.

Various workers in this field of electrically conducting polymers have suggested different conduction processes as already mentioned. A detailed review of the physical processes involved in the mechanisms such as Tunnel effect, Poole-Frankel effect and Space Charge Limited conduction is given here.

1.10.2 Tunnel effect:

If the energy of an electron is less than the interfacial potential barrier in a metal-insulator-metal junction upon which it is incident, the quantum- mechanical wave function $\psi_{(x)}$ of the electron has a finite values within the barrier (see **Fig. 1.7**), and since $\psi_{(x)}\,\psi_{(x)}\,dx$ is the probability of finding the electron within the incremental range x to x + dx, this means that the electron can penetrate the forbidden region of the barrier. The wave function decays rapidly with depth of penetration of the barrier from the electrode-insulator interface and, for barrier of macroscopic thickness, is essentially zero [Fig. 1.7(a)] at the opposite interface, indicating zero probability of finding the electron there. However, if the barrier is very thin (< 50 A^o), the wave function has a nonzero value at the opposite interface. For this case, then. There is a finite probability that the electron can pass from one electrode to the other by penetrating the barrier, as shown in Fig. 1.7 (b). When the electron passes from one electrode to the other by this process, one speaks of the electron as having tunneled through the barrier.

The generalized formula gives the relationship connecting the tunnel current density with the applied voltage for a barrier of arbitrary shape as

$$\mathbf{I} = \mathbf{I_0}\left\{\overline{\Phi}\exp\left(-\mathbf{A}\overline{\Phi}^{1/2}\right) - \left(\overline{\Phi} + \mathbf{eV}\right)\exp\left[-\mathbf{A}\left(\overline{\Phi} + \mathbf{eV}\right)^{1/2}\right]\right\} \qquad \text{Eq. 1.22}$$

$$\text{where } \mathbf{I_0} = \frac{\mathbf{e}}{\mathbf{2ph}(\mathbf{b}\Delta\mathbf{s})^2} \text{ and } \mathbf{A} = \frac{\mathbf{4pb}\Delta\mathbf{s}}{\mathbf{h}}(\mathbf{2m})^{1/2}$$

Δs = width of the barrier at the Fermi level of the negatively biased electrode

$\bar{\mathbf{f}}$ = mean barrier height above the Fermi level of the negatively biased electrode

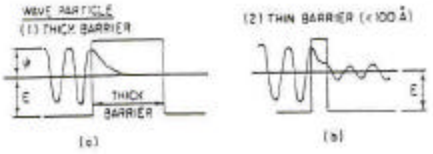

Fig. 1.7 Quantum mechanical tunneling of an electron at metal-insulator-metal junction (a) at a thick barrier (b) at a thin barrier

h = Planck's constant

m = mass of the electrons

e = unit of electronic charge

β = a function of barrier shape and is usually approximately equal to unity, a condition we will assume throughout

Expressed in conventional units, except for Δs, which is expressed in angstroms, above equation 1.3.7 a becomes

$$\mathbf{I} = \frac{\mathbf{6.2 \times 10^{10}}}{(\Delta \mathbf{s})^2} \left\{ \overline{\Phi} \exp\left(-\mathbf{1.025} \Delta \mathbf{s} \overline{\Phi}^{1/2}\right) - \left(\overline{\Phi} + \mathbf{V}\right) \exp\left[-\mathbf{1.025} \Delta \mathbf{s} \left(\overline{\Phi} + \mathbf{V}\right)^{1/2}\right] \right\} \qquad \text{Eq. 1.22 b}$$

1.10.3 Poole-Frenkel effect:

The Poole-frenkel effect (field-assisted thermal ionization) is lowering of a Coulombic potential barrier when it interacts with an electric field, as shown in **Fig.1.8.** This process is the bulk analog of the Schottky effect at an interfacial barrier. Since the potential energy of an electron in a Coulombic field $-e^2/4\pi\in^0 kx$ is four times that due to image-force effects, the Poole-Frenkel attenuation of a Coulombic barrier $\Delta\phi_{PF}$ in a uniform electronic field is twice that due to the Schottky effect at a neutral barrier.

$$\Delta \mathbf{f}_{\mathbf{PF}} = \left(\frac{\mathbf{e}^3}{\mathbf{p} \in_{\mathbf{0}} \mathbf{K}^*} \right)^{1/2} \mathbf{F}^{1/2} = \mathbf{b}_{\mathbf{PF}} \mathbf{F}^{1/2} \qquad \text{Eq. 1.23}$$

This result was first applied by Frenkel [108] to the host atoms in bulk semiconductors and insulators. He argued that the ionization potential E_o of the atoms in a solid are lowered an amount given by equation 1.23 in the presence of a uniform field-dependent conductivity of the form

$$\sigma = \sigma_0 \exp\left(\frac{\beta_{PF} F^{1/2}}{2kT} \right) \qquad \text{Eq.1.24}$$

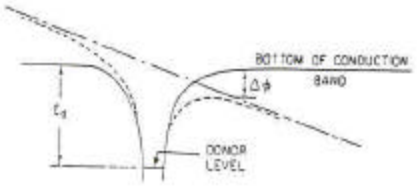

Fig. 1.8 Lowering of Coulombic potential barrier in Poole-Frenkel effect

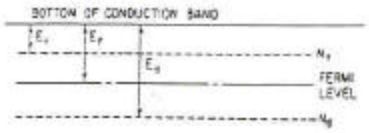

Fig. 1.9 Energy band diagram in deriving Eq. 1.21

where σ_0 [= $e\mu N_c \exp(-E_0/2kT)$] is the low-field conductivity. Equation 1.24 may be written in the form

$$J = J_0 \exp\left(\frac{b_{PF} F^{1/2}}{2kT}\right) \qquad \text{Eq. 1.25}$$

where J_0 ($= \sigma_0 F$) is the low-field current density.

It is interesting to note that although $\Delta\phi_{PF} = 2\Delta\phi_S$, the coefficient of $F^{1/2}$ in the exponential is the same for both the Richardson-Schottky and Poole-Frenkel J-F characteristics (i.e., $\beta_{PF}/2 = \beta_S$), Mead [109] has suggested, however, that since traps around in an insulator and that a trap having a coulombic-type barrier would experience the Poole-Frenkel effect at high fields, thereby increasing the probability of escape of an electron immobilized therein, the current density in thin film insulators containing shallow traps is given by

$$J = J_0 \exp\left(\frac{b_{PF} F^{1/2}}{kT}\right) \qquad \text{Eq. 1.26}$$

Note in this case that the coefficient of $F^{1/2}$ is twice that in Eq.1.25 and for this reason Eq.1.26 is usually the form of Poole-Frenkel equation associated with thin film insulators rather than that given by Eq.1.25.

From what has been said it follows that it should be possible to differentiate between the Schottky and Poole Frankel effects in thin-film insulator from their different rates of conductivity with field strength; viz., a plot of In J vs. $F^{1/2}/kT$ results in a straight line of slope β_s or β_{PF} depending upon whether the conduction process is Richardson-Schottky or Poole-Frankel. These experimentally determined slopes can be compared with the theoretical β_s and β_{PF} , which can be calculate quite accurately provided the high frequency dielectric constant K^* should satisfy the equation $K^* = n^2$, where n is the refractive index for the material.

Furthermore, if it is assumed that the insulator contains donor centers which he know the Fermi level this assumption is supported by the fact that the conductivity of the films continues to increase with increasing temperature above room temperature and shallow neutral traps (see **Fig.1.9**), the bulk J – V characteristic of the film is given by

$$J = J_0 \exp\left(\frac{b_{PF} F^{1/2}}{2kT}\right) \qquad \text{Eq. 1.27}$$

where $J_0 = emN_c \left(\frac{N_d}{N_t}\right)^{1/2} F \exp\left(-\frac{E_d + E_t}{2kT}\right)$

Thus in this case the coefficient of $F^{1/2}/kt$ is $\beta_{PF}/2$ (= β_s) even though the conductivity is not electrode-limited, which explains the anomalous experimental results.

1.10.4 Space - Charge – Limited (SCLC) Currents in insulators:

An insulator which does not contain donors and which is sufficiently thick to inhibit tunneling will not normally conduct significant current. However, if an ohmic contact is made to the insulator, the space charge injected into the conduction band of the insulator is capable of carrying current, this process is termed SCL conduction.

The results of the applied bias to an insulator having two ohmic contacts on its surface is to add positive charge to the anode and negative charge to the cathode, as would be the case with any such capacitive system. Thus, as the voltage bias increases, the net positive charge on the anode increases and that on the cathode decreases. Calling the charge on the cathode Q_1, that on the anode Q_2 and the negative space-charge density p(x), the condition of electrical neutrality demands that

$$\int_0^s p(c)dc = Q_1 + Q_2 \qquad \text{Eq.1.28}$$

Equation 1.28 may be rewritten as

$$\int_0^{l_m} p(c)dc + \int_{l_m}^{L} p(c)dc = Q_1 + Q_2$$

where λ_m is chosen such that

$$\int_{0}^{l_m} \rho(c)\,dc = Q_1 \qquad \text{Eq.1.29}$$

and

$$\int_{l_m}^{s} \rho(c)\,dc = Q_2 \qquad \text{Eq.1.30}$$

The insulator has thus been divided into two portions with λ_m as the boundary separating the two.

The significance of Eq 1.29 and Eq.1.30 is that the positive charge on wither contact is neutralized by an equal amount of negative charge contained between the contact and the plane at $x = \lambda_m$. Thus, the field in the insulator due to Q_1 and Q_2 is zero at $x = \lambda_m$, the net field there must be zero, as shown in **Fig. 1.10**, and for this reason the plane at $x = \lambda_m$ is termed as the virtual cathode. The region $0 \leq x \leq \lambda_m$ is designated the cathode region, and the region $\lambda_m \geq x \geq s$ the anode region.

From consideration of Eq 1.29 and Eq.1.30 and the fact that Q_1 decreases and Q_2 increases with increasing voltage, it will be clear that the virtual cathode region decreases and the anode region increases. Eventually, when $Q_1 = 0$, the virtual cathode coincides with the physical cathode-insulator interface. Under this condition, then, the anode region extends throughout the whole of the insulator, and an ohmic contact no longer exists at the cathode-insulator interface. Thus, for further increasing voltage bias, the conduction process is no longer space-charge limited, but rather it is emission –limited.

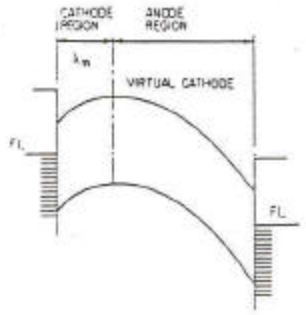

Fig. 1.10 Energy band diagram illustrating virtual cathode, cathode region under space -charge-limited condition

1.10.5 Matrix Of Uniformly Dispersed Particles - Various conduction equations

The effect of fillers on the electrical conductivity of polymers has been discussed using a model by Radhakrishnan [104]. A polymer containing uniformly dispersed filler particles is considered as a matrix of particles with average dimension D separated from each other by an average distance d. The electrical equivalent of this system is a net work of resistors R_p and R_f (where R_p and R_f are effective resistances of the interparticle junction and the particle itself respectively). The net work is considered to be a linear array of a umber (N_s) of R_p and R_a alternatively placed in series and N_p such arrays placed in parallel. These number of series elements (N_s) and parallel arrays (N_p) depend on the filler concentration through the interparticle distance as

$$N_s = (L - d) / (D + d)$$
$$N_p = (B - d)^2 / (D + d)^2 \qquad \text{Eq.1.31}$$

where L is the length and B^2 the cross section of the filled polymer sample. The interparticle distance and filler concentration θ (volume fraction) are related as

$$\theta^{1/3} = D(L - d) / (D + d).L \qquad \text{Eq. 1.32}$$

The externally measured resistance R_x is given as

$$\mathbf{R_x} = \left[\frac{(\mathbf{B}-\mathbf{d})^2}{(\mathbf{D}+\mathbf{d})^2}\right]^{-1} \frac{(\mathbf{L}-\mathbf{d})}{(\mathbf{D}+\mathbf{d})} \left(\mathbf{R_p} + \mathbf{R_f}\right) \qquad \text{Eq.1.33}$$

the resistance R_p depends upon the type of conduction process taking place in the polymeric material as well as type of contact. In case of ohmic conduction R_x is related to θ as

$$\mathbf{R_x(OH)} = \frac{\mathbf{1}}{\mathbf{2}}\mathbf{r_p}\frac{\left(\mathbf{1}-\mathbf{q}^{1/3}\right)}{\mathbf{q}^{1/3}\left(\mathbf{1}+\frac{\mathbf{L}}{\mathbf{D}}\mathbf{q}^{1/3}\right)} + \frac{\mathbf{1}}{\mathbf{L}}\mathbf{r_f}\mathbf{q}^{1/3} \qquad \text{Eq.1.34}$$

Where ρ_p and ρ_f are bulk resistivities of polymer and filler particles respectively.

The charge transport characteristics in polymers, however, are mostly non ohmic, especially at high fields. Therefore Radhakrishnan has considered the non ohmic processes involved in such polymers. The relation of R_p have also been derived.

For Schottky emission (SE) the current voltage characteristics are given by :

$$\mathbf{J = AT^2}\ \exp(-\Delta/\mathbf{kT})\exp\left[\frac{\mathbf{bV^{1/2}}}{\mathbf{kTd^{1/2}}}\right] \qquad \text{Eq.1.35}$$

Where J is the current density, A the Richardson – Schottky constant (120 A / cm2), T the temperature, k the Boltzmann constant Δ the barrier height, β the RS exponent, V the voltage and d the thickness of the layer.

$$I_p = D^2\ AT^2 \exp(-\Delta/kT)\exp(\beta Vp^{1/2}/d^{1/2}kT) \qquad \text{Eq.1.36}$$

The effective resistance R_p is given by

$$\mathbf{R_p = \frac{V_p}{I_p} = \frac{V_x}{LDAT^2}(1+d/D)e^{\frac{\Delta}{kT}}\exp\left[\frac{V_x^{1/2}b}{d^{1/2}}\left(1+\frac{D}{d}\right)^{1/2}\right]} \qquad \text{Eq.1.37}$$

From the above equations Rx (SE) can be put in terms of filler concentration θ as.

$$\mathbf{R_x(SE) = \frac{V_x}{LADT^2}e^{\Delta/kT}\frac{\left(1-q^{1/3}\right)}{q^{2/3}}\exp\left[-\frac{bV_x^{1/2}}{kTLq^{1/6}}\frac{\left(1+\frac{L}{D}q^{1/3}\right)^{1/2}}{1-q^{1/3}}\right]} \qquad \text{Eq 1.38}$$

In case of Poole - Frenkel effect the current voltage characteristics are similar to that of Schottky emission and hence the final R_x - θ is similar to the above equation except for β.

In case of space charge limited conduction process, there are various types current – voltage relationships possible, depending upon various types of trap distributions and their concentration. The Mott – Gurney type relation which is related to polymer is:

$$J = \frac{8}{9}\mu f e \frac{V^2}{d^3} \qquad \text{Eq.1.39}$$

and I_p will be

$$I_p = \frac{8}{9}\mu f e \frac{V_p^2}{d^3} \qquad \text{Eq. 1.40}$$

where μ is the mobility of the charge carriers, ϕ the trap parameter and e the dielectric constant of the medium. R_p is then given by

$$R_p = \frac{8}{9}\,\frac{1}{\mu f e}\,\frac{(L-d)d^3}{Vx(D+d)D^2} \qquad \text{Eq.1.41}$$

The expression for R_x in terms of θ in this case is

$$R_x(SL) = \frac{8}{9}\frac{10^{13}}{V_x \mu f e}\frac{L^2}{q}\frac{\left(1-q^{1/3}\right)^3}{\left(1+\frac{L}{D}q^{1/3}\right)^2} \qquad \text{Eq.1.42}$$

The tunneling of charge carriers which takes place in metal – polymer – metal systems through mechanical processes directly in thin films or via traps in comparatively thicker films. The current voltage characteristics at high enough fields are governed by Fowler – Nordheim equations namely:

$$J = \frac{3.38\times10^{10}E^2}{\Delta}\exp\left(-\frac{0.69\Delta^{3/2}}{E}\right) \qquad \text{Eq.1.43}$$

Where E is the field (volts / A) across the rectangular barrier of height Δ (eV). The current Ip is given as

$$\mathbf{I_p} = \frac{\mathbf{3.38\times10^{10} D^2 V_p^2}}{\mathbf{\Delta d^2}} \exp \frac{\mathbf{-0.69\Delta^{3/2} d(L-d)}}{\mathbf{V_x(D+d)}} \qquad \text{Eq.1.44}$$

and the resistance R_p is given as

$$\mathbf{R_p} = \frac{\mathbf{(L-d)\Delta d^2}}{\mathbf{3.38\times10^{10} V_x D^2 (D+d)}} \exp \frac{\mathbf{0.69\Delta^{3/2} d(L-d)}}{\mathbf{V_x(D+d)}} \qquad \text{Eq.1.45}$$

The Rx - θ relation in this case becomes:

$$\mathbf{R_x(TN)} = \frac{\mathbf{LD\Delta}}{\mathbf{3.38\times10^{10} V_x q^{1/3}\left(1+\frac{L}{D}q^{1/3}\right)^2}} \left(1-q^{1/3}\right)^2 \exp\left[\frac{\mathbf{0.69\Delta^{3/2} L q^{1/3}\left(1-q^{1/3}\right)}}{\mathbf{V_x\left(1+\frac{L}{D}q^{1/3}\right)}}\right]$$

Eq.1.46

Thus it has been shown that externally measured resistance of filled polymer system depends on the filler concentration in a complex manner and the exact relationship depends on the internal conduction mechanism governing the carrier transport across the interparticle sites.

1.11 Aim and scope:

It is observed from the above discussion that processibility can be achieved by synthesis of blends and composites of conducting polymers. Moreover dispersion is the most convenient way of making blends and composites. The lower conductivities can be enhanced by the replacement of insulating polymer by solid polymer electrolytes, which makes them prospective materials for various applications. The dissimilarities in the work-function of the constituents gives rise to the formation of junctions in blends and composites. However the charge transport studies across the conducting polymer/insulating polymer interface have not

been investigated in the detail in the past. Properties exhibited by a blend are by the virtue of the junction formation between the two component polymers. The understanding of the charge transport processes at the interface of the materials can lead to better devices, configuration and characteristics.

Hence, it is proposed in the present work to investigate the charge transport across the junctions formed as a result of the blending of different polymers. The blends reported in the past are mostly synthesized by mechanical dispersion method. However, these blends represent junction formation on a rather macroscopic scale effectively yielding less number of junctions. It also exhibits a percolation threshold at a higher composition of the conducting polymer. On the other hand, the blends prepared by electrochemical method of synthesis yield blends on a smaller scale. Therefore polypyrrole blends are synthesized using vapour phase method of polymerization of PPy in the present case. This method allows the deposition of the conducting polymer in the semiconducting matrix of the solid polymer electrolyte. Consequently, the outcome is reflected as an interpenetrating network of the conducting polymer in the matrix. Thus blending may be achieved at a sub-micron level and ensure a better mixing of the polymers and hence lower percolation thresholds. Solid polymer electrolytes was used as the major matrix in all the blends and composites as the conductivity of these materials is in the semiconducting range that reduces the internal resistance that makes it suitable for various applications.

The properties of the junctions can also be enhanced by addition of fillers to the solid polymer electrolytes by dispersion method. Fillers such as CuPc and CdS can be used in order to induce photoconductivity to the blend. The junction formation across the conducting polymer/filler interface is studied as a function of the compositional variation and the other parameters involved.

The type and magnitude of potential barrier formed are investigated by recording the current-voltage characteristics. Furthermore, the modulation of the barriers when subjected to external changes such as the chemical environment is also deliberated. The effect of various parameters such as the method of synthesis of the blend, doping level and composition of the conducting polymer on the barrier formation are studied. The role of barriers in determining the properties of the blends and composites are investigated. In other words the properties of the blends and composites can be tailored by proper selection of the materials and optimized by appropriate compositional range.

1.12 References:

1. Burroughes J H, Jones C A, Friend R H, Nature 335 (1988) 137

2. Garnier F, Florowitz G, Peng X, Fichou D, Adv Mater 2 (1990) 592

3. Shirakawa H, Louis E J, MacDiarmid A G, Chaing C K, Heeger A J, J Chem Soc Chem Commun (1977) 578

4. Bredas J L, Silbey R, Conjugated Polymers (Kluwer Dodrecht, 1991)

5. Salaneck W R, Conjugated Polymer Surfaces and Interfaces, Stafstrom S and Bredas J L, Cambridge University Press, 1996, Chapt 4

6. Heeger A J, Kivelson S, Schrieffer and Su W P, Rev Mod Phys 60 (1988) 781

7. Salaneck W R and Bredas J L, Solid State Communications, special Issue on Highlights in Condensed Matter Physics and Material Science 92 (1994) 31

8. Dall'Ollio A, Dascola Y, Varacca V, Bocchi V, Comptes Rendus C267 (1968) 433

9. (a) Gardini G P, Adv Heterocycl Chem 15 (1973) 67
   (b) Salmon M, Kanazawa K K, Diaz A F, Krounbi M, J Polym Sci Polym Lett Ed 20 (1982) 187
   (c) Nalwa H S, Dalton L R, Schmidt W F, Rabe J G, Polym Commun 27 (1980) 240

10. (a) Nalwa H S, Rabe J G Schmidt W F, Dalton L R, Makromol Chem Rapid Commun 7 (1986) 533
    (b) Nalwa H S, J Mater Sci 27 (1992) 210

11. (a)Rapi S, Bocchi V, Gardini G P, Synth Metals 24 (1988) 217
    (b)Machida S, Miyata S, Techagumpuch T, Synth Metals, 31 (1989) 311
    (c)Chao J H, March J, J Polym Sci Polym Chem Ed 26 (1988) 743
    (d)Armes S P, Synth Metals, 20 (1987) 365
    (e)Kang E T, Neoh K G, Kong Y, Tan K L, Tan BTG, Macromolecules 24 (1991) 2822

12. Hsing C F, Kovacic P, Khoury I A, J Polym Sci Polym Chem Ed 21 (1983) 457

13. Pron A, Kucharski Z, Budrowski C, Zagorska M, Kirchene S, Suwalski J, Dehe G, Lefrant S, J Chem Phys 83 (1985) 5923

14. Diaz A F, Kanazawa K K, Gardini G P, J Chem Soc Chem Commun (1979) 635

15. Diaz A F, Martinez A, Kanazawa K K, Salmon M, J Electroanal Chem 130 (1981) 181

16. Street G B, Handbook of Conducting Polymers, Ed Skotheim T J, Marcel Dekker, New York 1986, p673

17. Otero T F, de Larreta E, Synth Metals 26 (1988) 79

18. Mohammadi A, Lundstorm I, Salaneck W R, Inganaes O, Chemtronics, 3(4) (1988) 219

19. Yosomiya R, Hirata M, Haga Y, An H, Seki M, 7(11) (1986) 697

20. Radhakrishnan S, Saini D R, Synth Metals 58 (1993) 243

21. (a)Green A G, Woodhead A E, J Chem Soc (1910) 1117
(b) Green A G, Woodhead A E, J Chem Soc (1910) 2388

22. (a)MacDiarmid A G, Chiang J C, Halpern M, Huang W S, Mu S L, Somasiri N L, Wu W, Yangier S I, Mol Cryst Liq Cryst 121 (1985) 173
(b) Chiang J C, MacDiarmid A G, Synth Metals 13 (1986) 193
(c) Armes S P, Miller J F, Synth Metals, 22 (1985) 385
(d) Austrias G E, MacDiarmid A G, Epstein A J, Synth Metals 29 (1989) E157

23. Mohilner D M, Adams R N, Angersinger W J, J Am Soc 84 (1962) 3618

24. Rehwald W, Kiess H G, Conjugated Conducting Polymers Ed. Kiess H, Springer, Berlin, 1992, Chapt 3

25. Peierls R E, Quantum Theory of Solids, Clarendron, Oxford, 1955 p.108

26. Froehlich H, Proc Roy Soc (London) Ser 223 (1954) 296

27. Hubbard J, Proc Roy Soc A276 (1963) 238

28. Brazowski S A, Kirova N N, Pis'ma Zh Eksp Tear Fiz 33 (1981) 4

29. Fesser K, Bishop A R, Campbell D K, Phys Rev B27 (1983) 4804

30. Conwell E M, Phys Rev B33 (1986) 2465

31. Ambegaonkar V, Halperin B I, Langer J S, Phys Rev B4 (1971) 2612

32. Mott N F, Phil Mag 19 (1965) 835)

33. Emin D Phys Rev Lett 32 (1974) 303

34. Wurtz D, Thomas P Phys Stat Solidi, B88 (1978) K73

35. Chance R R, Bredas J L, Silbey R Phys Rev B29 (1984) 4491

36. Kivelson S, Phys Rev B25 (1982) 3798 ; Phys Rev Lett 46 (1981) 1344

37. Baeriswyl D, Maki K, Synth Metals 28 (1989) D513

38. Vogl P, Campbell D K, Sankey O F, Synth Metals 28 (1989) D513

39. (a)Shacklette L W, Colaneri N F, IEEE Trans Instrumentation and Measurement 41 (1992) 291
(b)Aldissi M, EMC Technology 1992 Sept/Dec, 33

40. (a)Akelah A, J Mater Sci 21(9) (1986) 29778
(b)May P, Phys World 8(3) (1995) 52
(c)MacDiarmid A G, Short Course on Electrically Conductive Polymers, New Paltz New York, (1985)

41. Panero S, Prosperi P, Bonino F, Scrosati B, Corradini A, Mastragostino M, Electrochim Acta, 32 (1987) 1007

42. (a)Guiseppi-Elie A, Wilson A M, Am Chem Soc PMSE Prep, 71 (1994) 651
(b)Collins G J, Buckley L J, Synth Metals, 78 (1993) 93
(c) Pearce T C, Gardner J W, Friel S, Barlett P N, Blair N, Analyst 118 (1993) 371
(d) Baughmann R H, Shacklette L W,in Science and Applications of Conducting Polymers Ed W R Salaneck et al IOP (1990) 47
(e)Otero T F, Angulo E, Rodriguez J, Santamaria J C, J Electroanal Chem 341 (1992) 369

43. (a)Cogan S F, Plante T D, McFadden R S, Rauh R D, Solar Energy Mater 16(5) (1987) 371
(b) Scrosati B, Mol Cryst Liq Cryst , 190 (1990) 161
(c) Andrei M, Polymer 35 (17) (1994) 3592
(d) Mastagostino M, Synth Metals 68 (2) (1995) 157

44. Clark L C Jr, Lyons C, Ann L Y, Acad Sci 102 (1962) 29

45. (a)Cao Y, Smith P, Heeger A J, Synth Metals 48 (1992) 91
(b)Braun D, Heeger A J, Appl Phys Lett 58 (1991) 1982
(c)Gustafsson G, Cao Y, Treacy G M, Klavetter F, Colaneri N, Heeger A J, Nature 357 (1992) 477

46. (a) Frommer J E, Chance R R, Encyclopedia of Polym Science and Engineering, Vol 5, Wiley New York (1985) 462
(b)Ruckenstein E, Park J S, J Appl Polym Sci 42 (1991) 925

47. Kryszewski M, Synth Metals 45 (1991) 289

48. Subramanium C K, Kaiser A B, Gilberd P W, Wessling B, J Polym Sci Polym Ed

31 (1993) 1425

49. (a)Yassar A, Roncali J, Garnier f, Polymer Commun 28 (1987) 103
(b)Armes S P, Aldissi M, Polymer 31 (1990) 569

50. Nakata M, Kise H, Polym J 25 (1993) 91

51. (a) Bocchi V, Gardini G P, Rapi S, J Mater Sci Lett 6 (1987) 1283
(b)Li C, Song Z, Synth Metals, 41 (1991) 1013
(c)Chen Y, Qian R, Li G, Li Y, Polymer Commun 32 (1991) 189

52. (a)Zoppi R A, Felisberti M I, De Paoli M A, J Polym Sci: Polm Chem 32 (1994) 1001
(b)Enzel P, Bein T, J Phys Chem J Phys Chem 93 (1989) 6270
(c)Kanatzidis M G, Touge L M, Marks T J, J Am Chem Soc 109 (1987) 3797

53. Vosaki K, Okazaki K, Kita H, J Polym Sci A: Polym Chem 28 (1990) 399

54. Ezquerra T A, Kremer F, Mohhamadi M, Ruhe J, Wegner G, Synth Metals, 28 (1989) C83

55. Yin X H , Yoshino K, Yamamoto H, Watanuki T, Isa I, Nakagawa S, Adachi M, Jpn J Appl Phys Vol 35 (1996) 4692

56. De Paoli M A, Waltman R, Diaz A, Bargon J, J Chem Soc Chem. Commun (1984) 1015

57. Niwa O, Tamamura T, J Chem Soc, Chem Commun (1984) 817

58. Gurland J, Trans Met Soc AMIE, 236 (1966)

59. Sternfield A, Modern Plastics International, July 1982

60. Reboul J P, Carbon Black Polymer Composites, Ed. E K Sichel, Marcel Dekker Inc, New York, 1982 Chapt 3.

61. Sherman R D, Middleman L M, Jacobs S m, Polymer Science and Engineering, Vol 23, No.1,Jan 1983

62. Jachym B, Carbon Black Polymer Composites, Ed E K Sichel, Marcel Dekke5r inc, New York , 1982 Chapt 3

63. Sodolski H, Zielinski R, Slupkowski T, Jachym Phys. Status Solidi-A 32: 603 (1975)

64. Heilmerier G H, Harrison S E, Phys Rev 132 (1963) 2010

65. Kaufhold J, Hauffe K, Ber Bunsenges, Phys Chem 69 (1965) 168

66. Ray B, II-VI Compounds, Pergamon Press, Oxford U K 1969

67. Radtke S F, Proceedings of the Ist Internationaal Conference, Metal Bulletin Ltd. London ,p.41

68. Smith R W, Phys Rev 97 (1955) 1525

69. Reynolds, Greene, Antes, J Chem Phys 25 (1956) 1177

70. (a)Bube R H, RCA Engr 5 (4) (1960) 28
(b)Kanev S K, Fahrenbruch A C, Bube R H, J Appl Phys, 45 (1974) 1264

71. Bube R H, J Appl Phys 31 (1960) 2239

72. Milner A G, Feucht D L, Heterojunctions and Semiconductor junctions, Academic Press, New York 1972

73. Ikeda M, Morimoto, Murakami Y, Sato H, Jap J Appl Phy 8 (1969) 759

74. Kaneko M, Handbook of Organic Conductive Molecules and Polymers: Vol 4 Edt.H S Nalwa (1997) John Wiley and Sons

75. Hoegl H, J Phys Chem 69 (1965) 755

76. Shirakawa H, Loius E J, MacDiarmid A G, Chiang C K, Heeger A J, J Chem Soc Chem Commun 1977 (1977) 578

77. Gopel W, Sensors and Actuators B 18 (1994) 1

78. Maisik J J, Hooper A, Tofield B C, J Chem Soc Faraday Trans 1, 82 (1986) 1117

79. Maisik J J, Hooper A, Moseley P T, Tofield B C, (L Alcacer Ed) Conducting Polymers 189 (1987) D Reidel Publishing Co

80. Hanawa T, Huwabata S, Hashimoto H, Yoneyama H, Synth Metals 30 (1989) 173

81. Tsumura A, Koezuka H, Tsunoda S, Ando T, Chem Lett (1986) 863

82. Josowicz M, Janata J, Anal Chem 58 (1986) 514

83. Boyle A, Genies E, Lapkowski M, Synth Metals, 28 (1989) C769

84. Chao S, Wrighton M, J Am Chem Soc 109 (1987) 6627

85. O'Riordan, Wallace G, Anal Chem 58 (1986) 128

86 (a)Fenton B E, Parker J M, Wright P V Polymer 14 (1973) 589
(b)Wright P V, Brit Polym J 7 (1975) 319

87. (a)Armand M B, Chabagne J M, Duclot M J, Second International Conference on Solid Electrolytes, St Andrews (1978) paper 6.5
(b)Armand M B, Chabagne J M, Duclot M J, In Fast Ion Transport in Solids (Eds. P Vashishta, J N Mundy and G K Shenoy) (1979) North-Holland, New York p.131

88. Ratner M A (1990) Paper presented at the DOE/EPRI Worshop on Polymer Electrolytes, Kirkland, Washington, October 1990

89. (a)Cheradame H, Niddam-Mercier P, Faraday Disscuss. Chem Soc 88 (1989) 77
(b)Ratner M A, Shriver D F, Materials Research Society Bulletin Sept, 39

90. Sircar A, Weissman P T, Binod K, Marsh R A, Thermochim Acta, 226 (1993) 281

91. Kelly I E, Owen J R, Steel BCH, J Power Sources 14 (1985) 13

92. Rabek J F, Kucki J, Kereszti H, Krische B, Qu B J, Shi W F, Synth Metals, 45 (1991) 335

93. Radhakrishnan S, Badiger M V, Graham N B, Polymer 36 (1995) 707

94. Nakajima T, Kawagoe T, Synth Metals 28 (1989) C269

95. Minnet M G, Owen J R, Solid State Ionics, 28-30 (1988) 1192

96. Hamaide T, Synth Commun 20 (1990) 2913

97. Rudge A, J Davey, Raistick I, Gottesfield S, Ferraris J P, J Power Sources 47 (1994) 89

98. Mastragostino M, Applications of Electroactive Polymer (Ed. B.Scrosati), Chapman and Hall ,1993

99. Saoka T A, Tokabayashi T, Abe T, Yoshida T, 40th ISE Meeting, Kyoto, 17-22 Sept 1989 Ext Abstr Vol 1, p. 245

100. Jelle B P, Hagen G, Odegard R, Electrochim Acta 37 (1992) 1377

101. Rocco A M, De Paoli M A, Mastragostino M, Electrochim Acta (submitted)

102. Rocco A M, De Paoli M A, Zanelli A, Mastragostino M, Electrochim Acta, 41 (1996) 2805

103. Arbizzani C, Mastragostino M, Meneghello L, Morseli M, Zanelli A, J Appl Electrochem 26 (1996) 121

104. Radhakrishnan S, Polym Commun 26 (1986) 153

105. (a)Assadi A, Svensson C, Willander M, Inganas O, J Appl Phys 72 (1992) 2900
(b)Assadi A, Svensson C, Willander M, Inganas O, Appl Phys Lett 53 (1988) 195

106. (a) Tomozawa H, Braun D, Phillipson S, Heeger A J, Synth Metals 28 (1989) 687
(b) Gustafsson G, Inganas O, Svensson C, Synth Metals 41-43 (1991) 1095
(c) Ohmori Y, Manda Y, Takahashi H, Kawai T, Yoshino K, Jpn J Appl Phys 29 (1991) L837

107. Simmons J G, Handbook of Thin Film Technology, Ed. Maissel L I, Glang R, McGraw-Hill, New York, 1976, Chapt 14

108. Frenkel J, Phys Rev 54 (1938) 647

109. Mead C A, Phys Rev 128 (1962) 2088

Chapter 2 - Experimental

2.1 Introduction :

Amongst the various ways of synthesis of blends and composites, which have been discussed in the earlier chapter, mechanical dispersion and vapour phase polymerization techniques were selected in the present studies so as to obtain ex-situ and in-situ blends and composites. The present chapter elaborates the methods of synthesis, characterization and measurement of properties of conducting polymer blends and composites. Polypyrrole and polyaniline were chosen for the purpose due to their better stability in ambient conditions than other ICPs. Blends were prepared with solid polymer electrolytes such as PEO-$CuCl_2$, PVC-$CuCl_2$, PVAc-$CuCl_2$ while the composites were synthesized using fillers such as copper phthalocyanine (CuPc) and cadmium sulfide (CdS). The various methods of sample preparation along with characterization by techniques viz., FI-IR , UV-vis, spectroscopy, ESCA and X-ray diffraction studies, TGA/DTG studies are described herein. The measurement of properties by various techniques such as chemical sensitivity, light sensitivity & cyclic voltammetry are also discussed. The techniques for investigating charge transport mechanisms like I-V characterization, conductivity-temperature studies are also presented.

2.2 Chemicals used:

The various chemicals used alongwith the sources are presented in the table 2.1. The chemicals used were of AR grade. The solvents used were distilled water, methanol and tetrahydrofuran.

Table 2.1: Chemicals used and their sources

Chemical	Acronym	Source
Pyrrole	Py	Aldrich Chemical Co
Aniline	Ani	S.D Fine, India
Polyethylene oxide	PEO	BDH Chemical UK
Polyvinyl chloride	PVC	Reliance Ind
Polyvinyl acetate	PVAc	
Copper phthalocyanine	CuPc	Color Chem/Hoechst(India)
Cadmium sulfide	CdS	Loba Chemie, India
Ferric chloride, ferric nitrate, ferric sulfate, ferric ammonium sulfate, ferric perchlorate, cupric chloride, cadmium chloride	$FeCl_3$, $Fe(NO_3)_3$, $NH_4[Fe(SO_4)_2]$, $FeClO_4$, $CuCl_2$, $CdCl_2$	Loba Chemie, India
Toluene sulfonic acid, naphthalene disulfonic acid	p-TSA, NDSA	Loba Chemie
Ammonium persulfate	$(NH_4)_2S_2O_8$	Loba Chemie
Potassium chloride, sodium sulfate, potassium sulfate	KCl, Na_2SO_4, K_2SO_4	S D Fine, India
Lithium perchlorate	$LiClO_4$	Aldrich Chemical Co

2.3 Methods of synthesis :

2.3.1 Synthesis of conducting of polymers :

(a) Chemical synthesis :

A general method of synthesis of conducting polymer involves the oxidation reaction of monomer pyrrole and aniline in aqueous medium in the presence of oxidizing agents such as ammonium persulphate or $CuCl_2$ in an acidic medium. For example, the polymerization of pyrrole was carried out by using 1:1 mole $FeCl_3$ / monomer pyrrole. 3.26 gms of $FeCl_3$ were dropped in 200ml distilled water to which was added 1.4 ml of pyrrole by continuous stirring. The reaction was carried out mainly at room temperature for 24 hours. The type of oxidizing agents and the extent of doping were varied to yield polymers of different properties. The variations of stoichiometry are discussed in detail in each chapter separately in the respective experimental sections.

(b) Electrochemical polymerization :

Gold coated glass or PET substrates were used as electrodes for the electrochemical deposition of PPy and PANI. Gold deposition was carried out in a Hind Vac Vacuum coating unit (model 12 A4D) using thermal evaporation method on clean glass substrates or PET films. Electrodes were made by cutting the gold coated substrate into 3 cm x 2 cm size. Air drying silver paste was then applied on one end to achieve electrical contact.

The electrochemical deposition was carried out in a single compartment cell with three electrodes system. The set-up is as shown in the **Fig.2.1**. The working electrode was the gold substrate while the counter electrode was a platinum foil. Reference electrode used was saturated calomel electrode (S C E) connected through he salt bridge containing agar-agar/ KCl mixture. Under normal conditions, the electrolyte was a monomer along with an oxidizing agent in appropriate concentrations. The electrolyte medium in all cases was distilled water. Electrochemical deposition was carried out by chronoamperometric technique at constant applied voltage against SCE. A potential of 700 mV was applied in the case of PPy polymerization process while 900 mV was applied in the case of PANI. The duration of deposition was 120 sec - 180 sec.

(c) Vapour phase polymerization :

This technique was employed for the polymerization of pyrrole because of the low boiling point so that it vaporizes easily at room temperature. Substrate electrodes were dip coated with solutions of solid polymer electrolytes i.e. PEO-$CuCl_2$ and PVC-$CuCl_2$ in methanol and tetrahydrofuran respectively and dried in a dry chamber. A desiccator was then saturated with pyrrole vapours for 20 hours and the substrates were then exposed to these pyrrole vapours for varying durations ranging from .25 min to 600 min depending on the type of studies carried out on the same.

Electrochemical cell

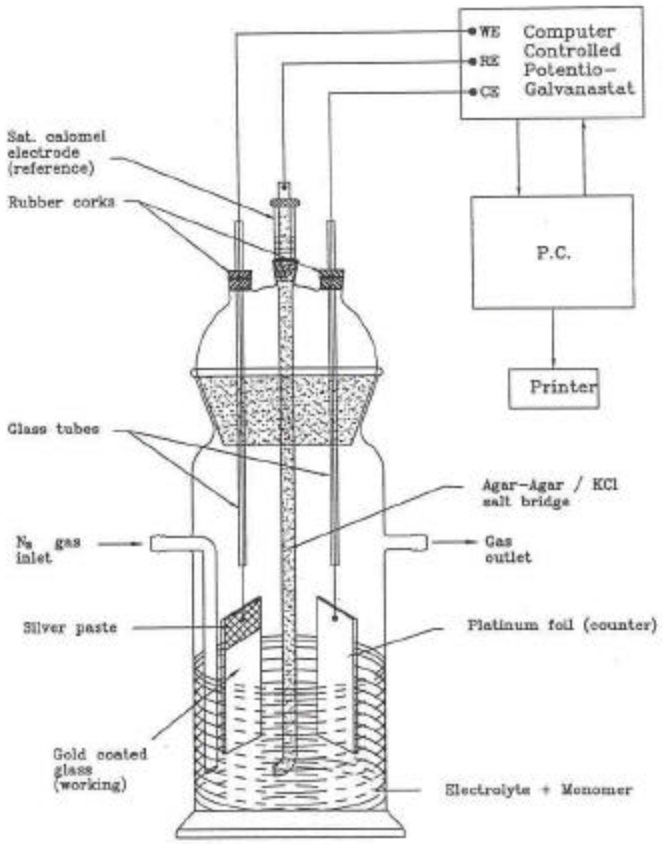

Fig. 2.1 Electrochemical cell for the polymerization of PPy and PANI

2.3.2 Synthesis of blends :

Blends were synthesized by two methods: ex-situ and in-situ techniques.

(a) Ex-situ blends:

The ex-situ blends were prepared by external addition of the conducting polymer to a solid polymer electrolyte solution i.e. PEO-$CuCl_2$, PVC-$CuCl_2$, PVAc-$CuCl_2$. The viscosity of the solid polymer electrolyte, time of stirring was strictly controlled. Compositional variation was carried out in case of all the blends.

(b) In-situ blend :

This type of blending technique was carried out in the preparation of PPy blends. Vapour phase polymerization technique was used for polymerization of PPy into the matrix of the solid polymer electrolyte giving a blend having fine dispersion level (sub-micron level) of conducting polymer in major matrix.

2.3.3 Synthesis of composites:

The composites of conducting polymers were made by physical dispersion method. Generally in the case of ex-situ composites, the fillers like CuPc and CdS were added to the solid polymer electrolyte under constant stirring and then the conducting polymer was also added to the same. On the other hand, in the case of in-situ composites, the fillers were added to the solid polymer electrolyte solution and stirred to make a paste. This was then coated on the electrodes deposited on glass/PET substrates. It was then dried and then exposed to and exposed to the pyrrole vapours for depositing PPy. The viscosity was retained same by controlling the polymer content and stirring time whereas composition was varied.

2.4. Electrode configuration :

The electrodes were prepared by vacuum deposition of gold on various substrates as discussed in section 2.3.1 (b). Two types of configurations were made.

(a)Surface cell :

Surface cells were made using gold coated glass and PET substrates. An inter digited electrode pattern was made as presented in the **Fig. 2.2 (a)**. The electrode gap was 1 mm. Electrical connection were made to the two electrodes using silver paste.

(b)Sandwich cell :

In a sandwich cell, [see **Fig.2.2 (b)**] the conducting polymer blend / composite was in the form a film. One of the electrodes; Au coated glass or ITO was dip-coated with the blend or composite. These were then dried thoroughly. The other electrode Au / 1T0 was placed on top of the film so as to form a sandwich structure.

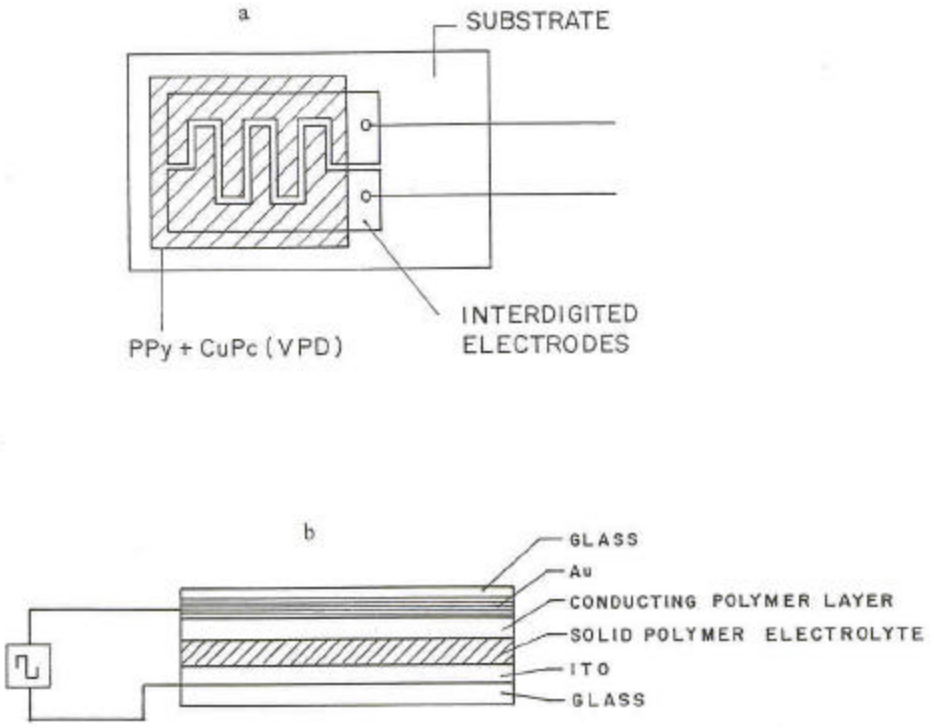

Fig. 2.2 Electrode configurations used for the resistivity measurement and I-V characteristics of blends and composites, (a) Surface cell (interdigited electrode pattern) and (b) Sandwich cell

2.5 Sample preparation :

The polymers synthesized by chemical polymerization route were obtained in a powder form. In order to prepare test samples, 200 mg polymer powder was pressed in a single ended compaction die held at 5-ton pressure for 60 seconds so as to form pellets/discs (1.1 cm diameter, 0.1 cm thick). These were used for conductivity measurements.

The blends and composites were made in a thick paste form. This slurry was then applied on the inter-digited electrodes to produce samples for testing. The thickness of the film formed was on an average 30 um.

Single junctions were created in the form of sandwich cells. Multi layered structures were prepared by using electrochemically deposited polymer films. The other electrodes (counter electrodes) carried the film solid of polymer electrolyte casted on to it or vacuum deposition of Cds or CuPc. This top electrode was then overlapped on the conducting polymer film to form of multi layered sandwiched cell device.

2.6 Characterization :

2.6.1 Infrared (IR) Spectroscopy :

Infrared (IR) studies were carried out to analyze the effect of doping on the conductivity of the polymer using IR spectrometer.

The powdered samples of the polymer were mulled with dry potassium bromide or nujol and the IR spectra was recorded using Perkin Elmer model 1600. The absorption bands were compared with the known literature.

2.6.2. UV-VIS Spectroscopy :

The creation of mid-gap states in a conducting polymer due to charge transfer complex formation can be judged by UV-vis spectroscopy. Also the complex formation between the polymer and the added salt in case of solid-polymer electrolytes such as PEO-$CuCl_2$ PVAc-$CuCl_2$ can be studied with the help of the above technique. Conducting polymer in the form of electrochemically deposited films was used for the purpose while films of solid polymer electrolytes were solution cast on cleaned glass substrate.

2.7 Structural and compositional characterization :

2.7.1 X-ray diffraction studies :

The conducting polymers synthesized by chemical route offered an amorphous structure. The dopant size often played an important role in arrangement of the polymer chains. Hence the conducting polymer powder obtained by using a variety of dopant ions were characterized by wide angle X-ray diffraction (WAXD) technique. A powder X-ray Diffrractometer (Phillips PW 1730 model) using CuKα source and βNi filter. The scans were recorded in the 2θ region of 5-40^0 at a scan rate of 4^0/min. From the 2θ values for the reflections, 'd' values were calculated using the well-known Bragg's equation,

$$2d \sin \theta = n\lambda$$

2.7.2 X-ray Photoelectron Spectroscopy (XPS) / ESCA studies :

X-ray photoelectron spectroscopy deals with a special form of photoemission, namely the ejection of an electron form a core level by X-ray photons of energy hν. The energy of these emitted photoelectrons is then analyzed by an electron spectrometer and the data are presented as a graph of intensity (counts per second) versus the electron energy (eV). The binding energy of the photoelectron peak defines not only the energy level within the atom from which it emerged but also the chemical environment. Hence it is also called electron spectroscopy for chemical analysis (E S C A).

The intensity of electrons 'I', emitted from a depth 'd' is given by Beer- Lamberts equation,

$$I = Io \exp (-d / \lambda \sin O)$$

where Io = the intensity from clean substrate

λ = inelastic mean free path (the value is a function of kinetic energy of emitted electrons.

θ = Angle subtended by the sample surface.

The technique has been used presently to determine the contribution of the charged / uncharged species. The XPS were recorded using V.G. scientific ESCA–3 MK II spectrometer Al-Kα (1486.6 eV) and Mg – Kα (1253.6 eV) radiation was used for excitation

and photoelectron Kinetic energy was measured with respect to the Fermi level. All the spectra were recorded under identical conditions at 50 eV pass energy, 4 mm slit and vacuum better than 10^{-9} Torr. The instrumental resolution obtained for the Au $4f_{7/2}$ levels under this condition is 1.6eV (Full width at half maximum – FWHM). The binding energy values were normalized by taking internal carbon standard (285 eV) in all cases.

2.7.3. Thermo Gravimetric Analysis (TGA):

Thermo gravimetric analysis was carried out for various polymers to determine the weight loss at different temperatures. All the measurements were carried out using TG / DTA (Seiko II SSC 5100 Japan model). The samples used were in the form of powder and tested under nitrogen atmosphere at the rate of 10^0/min from room temperature to 500^0C. The thermal analysis of pure conducting polymer was recorded for comparison as original standard in any given system. The weight loss recorded for the blends and composites was then compared with that of the pure one in order to estimate the fractional component of the polymer that was vapour phase deposited at a fixed temperature and composition.

2.8 Measurement of properties :

2.8.1 Conductivity measurements :

The conductivity measurements were carried out by a two-probe technique recorded by a Keithley electrometer 614 model. Samples were tested in a surface cell as well as in a sandwich cell form. Pellets were also used in the case of pure conducting polymers. The specific resistivity was calculated as,

$$\rho = R\,A/l$$

Hence $$\sigma = 1/\rho$$

where ρ is its resistivity, A the cross sectional area, l is the thickness, R is the sample resistance and σ is the conductivity.

2.8.2 I-V characterization :

The I-V characteristics were recorded for the polymer blends and composites using a constant DC power supply and the Keithley electrometer. The current was recorded as a function of the changing applied potential across the two terminals.

2.8.3 Temperature conductivity studies:

The interdigited electrodes were placed in the sample holders as shown in the **Fig.2.3.** The apparatus consists of a sample holder that was enclosed in an electromagnetic shielded cell, which in turn was mounted inside a glass jacket, which could be sealed and connected to a rotary pump. A small heater was mounted close to the film or pellet and using a suitable control device controlled the rise in the temperature to 4^0/ min. The temperature was varied from room temperature to 120^0 C while in the case of some samples it was varied from –100 to 120^0C using liquid nitrogen. The change in conductivity was noted with respect to the temperature. The activation energy was determined using Arrhenius formula.

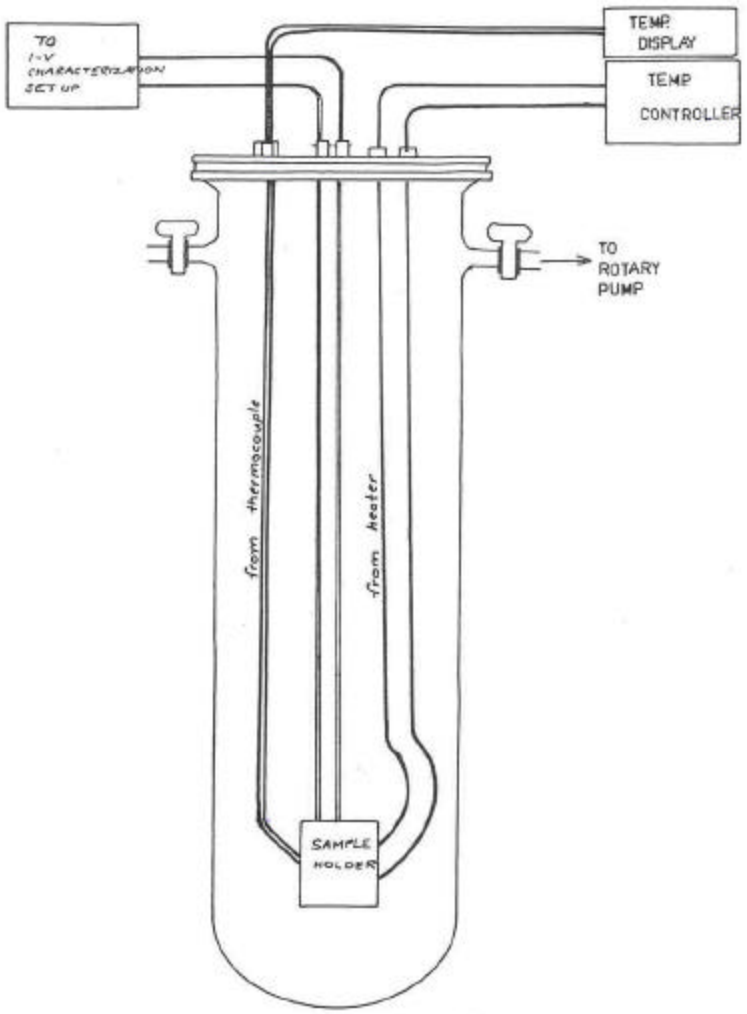

Fig. 2.3 Apparatus used for studying the temperature dependence of conductivity of polymer films. Films deposited on glass slides were held in the electromagnetically shielded sample holder which also enclosed a small temperature controlled heater and a thermocouple. These studies were carried out in vacuum (about 10^{-3} Torr).

2.8.4 Chemical sensitivity measurements:

The blends and composites were tested for chemical sensitivity towards gases like methanol, NO_2, etc. A closed chamber as illustrated by the **Fig.2.4** was used for the purpose that could be connected to a rotary. The change in the resistivity of the sample on injecting the gas was recorded by a fast x-y-t recorder (Lienses, Germany). The sensitivity factor was then calculated using the formula,

$$S = R_{max} / R_{min}.$$

Where Rmax and Rmin are the resistance after the exposure to chemical vapours and initial resistance respectively.

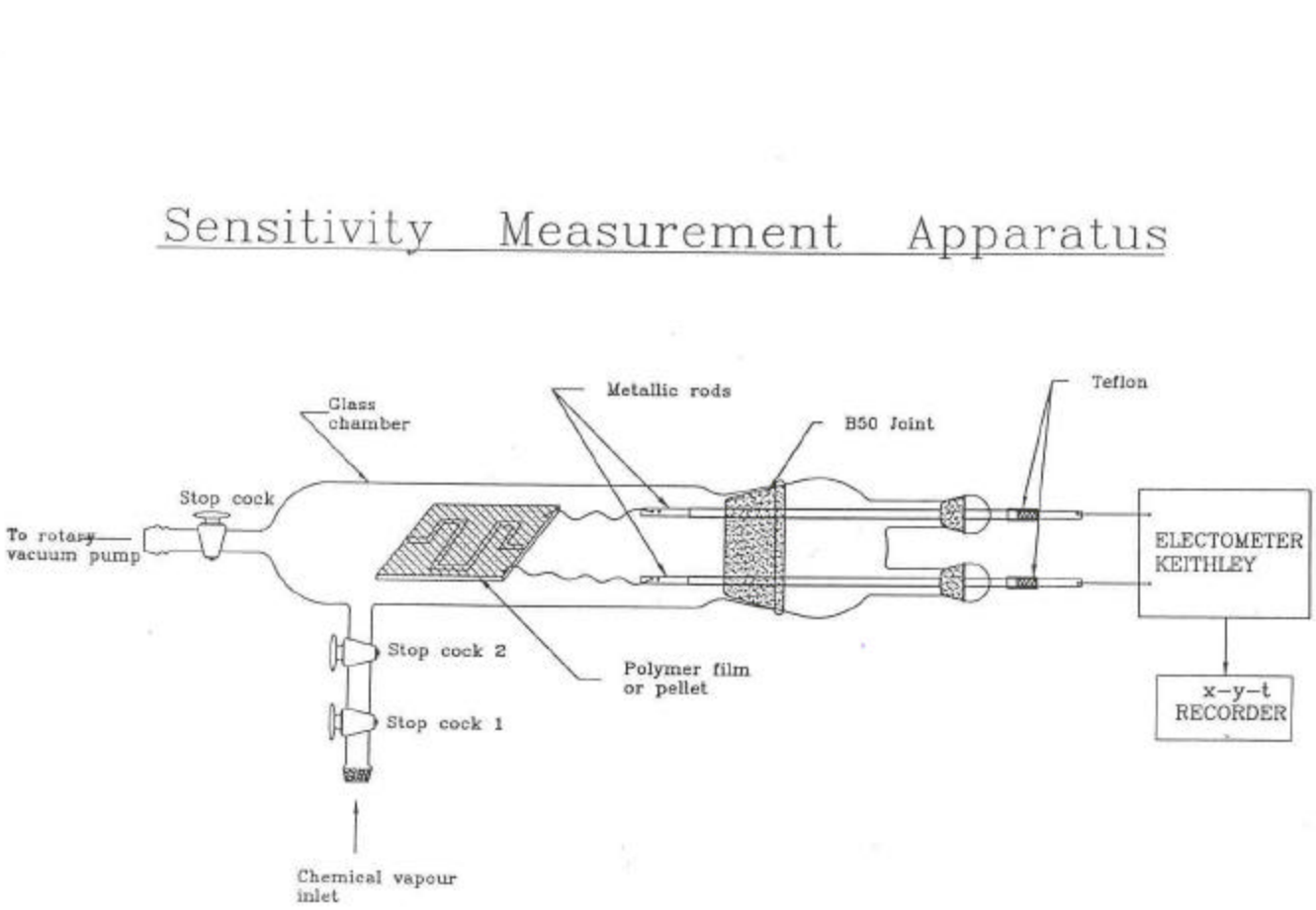

Fig. 2.4 Apparatus for studying the sensitivity of polymer films towards various gases. Various parameters such as the response time, decay time and the sensitivity factor were determined as a function of resistivity.

2.8.5 Cyclic Voltammetry:

Cyclic voltammetry studies were carried out to obtain information of the charge transport in and out of the polymer film that reflected the redox behaviour of the polymer. These studies were carried out using various aqueous electrolytes such as $LiClO_4$, K_2SO_4, KCl, etc.

Chapter 3 - PPy/PEO-$CuCl_2$ based blends and composites

3.1 Introduction:

The method of synthesis, dopant type, dopant concentration, etc, are important factors which govern the conductivity of the polymer which in turn depend on the internal charge transport processes. In order to investigate the effects of these various parameters, PPy was synthesized using different dopant ions. Also the PPy blends with PEO-$CuCl_2$ were made by different techniques such as (i) powder blending, (ii) in-situ blending by vapour phase deposition. Similarly, the composites were also synthesized by various routes. Since the charge transport processes are controlled by interfacial contacts, multilayered films were also deposited from each component materials so as to form sandwich cells. Different configurations were used for such samples. The preparation, characterization and investigations of electrical properties of these various PPy blends and composites are described in this chapter.

3.2 Experimental:

3.2.1. Synthesis of PPy:

PPy was synthesized by three methods viz., chemical polymerization, electrochemical polymerization and vapour phase polymerization technique, so as to obtain PPy powders for powder blending, PPy films (for sandwich cell having multilayers) and in-situ PPy blend respectively.

(a) Chemical polymerization technique:

Dopants like $FeCl_3$, $Fe(NO_3)_3$, $FeClO_4$, $Fe_2(SO_4)_3$, $NH_4\{Fe(SO_4)_2\}$ and $CuCl_2$ were used for the polymerization reaction. 0.1 M aqueous solutions of these salts with 1:1 M pyrrole monomer (except $CuCl_2$ wherein methanolic solutions were used) were digested for 20 hours with constant stirring. The resulting powder was washed with water and dried thoroughly. Samples were made in a pellet form by pressing the powder at 3.0 tons, 25°C.

(b) Electrochemical polymerization technique:

PPy was potentiostatically deposited on gold-coated glass substrates from an aqueous electrolyte containing 0.1M pyrrole in 0.1 M H_2SO_4 at an applied potential of 700mV with respect to SCE. The duration of deposition was 120 seconds. The films were then rinsed with water and then stored in a desiccator.

(c) Vapour phase polymerization technique:

Solutions of PEO-$CuCl_2$ were prepared by dissolving PEO and $CuCl_2$ in methanol in various ratios ranging from 1:1, 2:1, 4:1, 6:1, 8:1, to 12:1 monomer/ mole of $CuCl_2$. The electrodes-interdigited, vacuum deposited Au or ITO were dip coated in these solutions and the films were dried. These were then exposed to dry pyrrole vapours in a desiccator for various time intervals when PPy was formed in the PEO-$CuCl_2$ films the quantity of which depended on the exposure time.

3.2.2. Synthesis of blends:

PPy/PEO-$CuCl_2$ blends were prepared in two ways viz.: external addition of PPy in PEO-$CuCl_2$ and vapour phase deposition of PPy in the PEO-$CuCl_2$ matrix while the composite was prepared by dispersion of CuPc in the PEO-$CuCl_2$ prior to vapour deposition of PPy. These were categorized accordingly as follows:

(a) Ex-situ blend:

Chemically synthesized PPy was added in various percentage compositions of 5,10, 20, 30 and 40% containing to PEO that contained 10% $CuCl_2$ by weight. The slurry was made in methanol and applied on interdigited electrode pattern.

(b) In-situ blend:

The PEO-$CuCl_2$ (4:1) was applied on interdigited electrodes and exposed to pyrrole as mentioned in the earlier section. Samples were also prepared in a sandwich configuration by coating the ITO electrode with PEO-$CuCl_2$ followed by vapour phase polymerization of PPy with the vacuum deposition of a thin layer of Au as the top counter electrode.

3.2.3. Synthesis of the PPy-CuPc in-situ composite:

Commercially available CuPc powder was dispersed in various compositions ranging from 2 % to 45% by weight in PEO-$CuCl_2$ (4:1) solution in methanol. The slurry was made homogeneous by constant stirring and then applied on interdigited electrodes, dried and then exposed to pyrrole vapours. The exposure time was varied from 1min to 24 hours so as to obtain different concentrations of PPy in the composite.

3.2.4. Fabrication of single junctions:

(a) PPy/SPE:

ITO electrodes coated with SPEs that were prepared by complexation of PEO with different alkali metal salts, such as KCl, KI, $LiClO_4$, $NaClO_4$, $CuCl_2$, etc., in a 4:1 molar ratio in methanolic solution. These were then dried and contacted with the PPy films electrochemically deposited on Au coated glass plates. Thus sandwich structure of Au/PPy/SPE/ITO were obtained.

(b) PPy/CuPc:

The samples were made in a sandwich cell configuration by first depositing PPy on glass substrates precoated with gold films. The gold films were coated on plain glass slides as well as pretreated glass substrates by vacuum deposition technique. The glass substrates were precoated with polyvinyl butyral (PVB) by dip-coating process using 1% solution in methanol and their thickness was the same in all cases in the range of 2-2.5 μm. The thickness of the gold film was 200-250 nm. The thickness of PPy was in the range of 1-1.5 μm. The CuPc films were vacuum (10^{-6} mbar) deposited on the PPy films at the substrate temperature of 27°C using a mask and the thickness ranging from 10 nm to 500 nm (confirmed by optical absorption spectra at the open areas surrounding the junctions). The top electrodes were aluminium films that were also vacuum deposited so as to form the Au/PPy/CuPc/Al type sandwich cells.

3.3 Results and discussion:

3.3.1 Characterization of PPy:

The yield, nature of the deposit and the value of conductivity obtained in PPy synthesized under the same condition of temperature, solvent and concentration were found to be highly dependent on the dopant ion used during the reaction. The PPy powders obtained from sulfuric acid and toluene sulfonic acid were brownish flaky while that obtained from naphthalene disulfonic was dark green/black in colour. The comparison of the conductivities obtained for the PPy containing dopant ions is made in **Table-3.1 (a) and (b)**. It is seen that the conductivity is maximum when $FeCl_3$ is used while it is lower for the sulfate/sulfonic groups. A large variety of doping agents have been used in the past such as Cl^-, I_3^-, Br^-, ClO_4^-, SO_4^{--}, etc.[1-3]. The value of conductivity was found to be dependent not

Table 3.1 (a) Conductivities of PPy obtained by using different dopant ions from Fe^{3+} salts

Sample	Conductivity (S/cm)
PPy-$Fe(NO_3)_3$	4.0
PPy-$FeCl_3$	2.0
PPy-$FeClO_4$	0.116
PPy-$NH_4\{Fe(SO_4)_2\}$	0.0298
PPy-$Fe_2(SO_4)_3$	0.018
PPy-$CuCl_2$	0.003

(b) Conductivities of PPy using dopant ions from sulfate/sulfonic acid groups

Sample	Conductivity(S/cm)
PPy-SO_4	3.17×10^{-9}
PPy-PTSA	4.74×10^{-7}
PPy-NDSA	1.89×10^{-7}

only on the dopant ion introduced but also on the synthesis route used for making PPy and the compound from which it is derived. The conductivity was found to be the lowest in the

case of PPy synthesized from $CuCl_2$. This normally may not be expected as $CuCl_2$ is equally a strong oxidizing agent as $FeCl_3$. Polymerization of PPy by chemical route in various solvent mediums has been reported by Machida and Miyata [4]. The conductivity is found to be the highest in methanol (σ = 190 S/cm), closely followed by water, ethanol, etc. The pyrrole/$FeCl_3$ ratio used in this case was 1:3.5 $FeCl_3$ concentration /mole % while the reaction temperature was maintained at 0°C. Thus the solvents possessing an –OH group such as water, alcohols that are protic solvents are reported to be favourable for the synthesis of highly conducting PPy. The present reaction using $CuCl_2$ was carried out at room temperature with 1:1 molar of the monomer to oxidant ratio in methanol that is less polar than the aqueous medium. Another paper by Rapi, Bocchi describes the chemical polymerization of PPy in aqueous medium using selected transition metal complexes [5]. PPy synthesized from $CuCl_2$ with a molar ratio of oxidant to pyrrole as 12:1 showed a conductivity as high as 8 S/cm. However, the yield is very poor i.e. 14%. On the contrary, a low value of conductivity, $6x10^{-5}$S/cm has been reported by Budimir et. al.[6]. This has been attributed to the presence of copper that has been confirmed by cyclic voltammetry from the oxidation-reduction reaction of Cu^{+}/Cu^{++} system incorporated in PPy. Moreover, a new method of chemical synthesis of doped PPy initiated by $CuCl_2$-C_2H_5OH system is reported wherein polymers with different yield and conductivities were obtained by varying the initial concentration of Cu^{2+} [7]. Hence the low conductivity of PPy can be attributed to the less protic, methanolic reaction medium and low concentration of $CuCl_2$ used.

The temperature variation of conductivity showed distinct differences depending on the type of dopant ion present in the PPy. **Fig 3.1** shows the plot of log σ vs. 1/T for PPy containing different dopants from ferric salts all being prepared under the same concentration of 0.1 mole/mole Py. It is seen that whereas the conductivity shows little change with temperature for PPy with $FeCl_3$ that for nitrate and sulfate as dopants there is a sharp variation in log σ - 1/T plot especially at 360K. In order to examine this sharp change in conductivity PPy containing different sulfate, sulfonic groups were studied. **Fig. 3.2** shows that log σ vs 1/T graphs for PPy containing SO_4^{--}(curve A), TSA (curve B) and NDS (curve C). It is evident from this figure that temperature dependence of conductivity is not only different from that observed for PPy but also shows distinct transition peak at about 360K. This transition appears to become increasingly sharp as one goes from SO_4^{--} to TSA

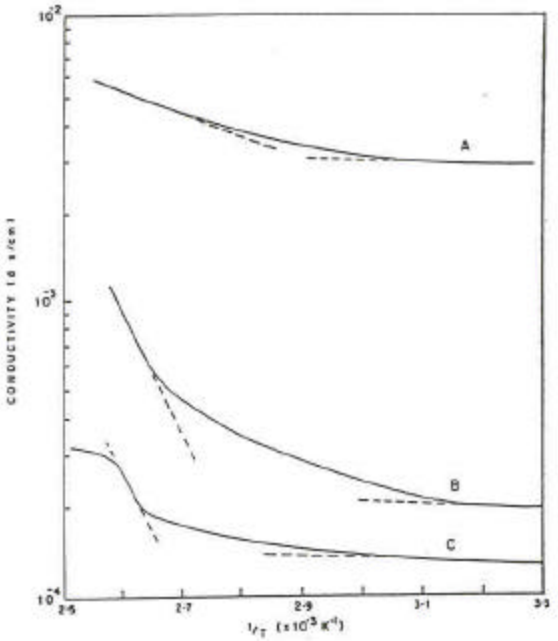

Fig. 3.1 Temperature dependence of conductivity in PPy containing various dopants from ferric salts at 0.1 mole/mole concentration (A) $FeCl_3$ (B) $Fe(NO_3)_3$, (C) $Fe_2(SO_4)_3$

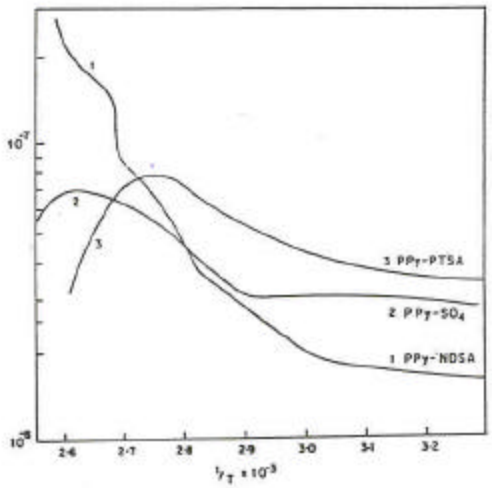

Fig. 3.2 Temperature dependence of conductivity in PPy containing sulfate/sulfonated ions Dopant ions used : (1) NDSA (2) H_2SO_4 (3) TSA

to NDS ions as dopants. The activation energy (ΔE) for charge transport was evaluated in the two regions of the graphs, viz., low temperature and high temperature using the conventional

Arrhenius equation. The values of (ΔE) derived are indicated in **Table 3.2**. The comparison of these values suggests that the charge transport may be similar in all the cases at low temperatures but distinctly different and/or affected by the ions present especially at high temperatures.

Table 3.2 Activation energies for PPy containing different dopant ions

Sample	(ΔE) eV
PPy-$FeCl_3$	0.038 (0.13)
PPy-$Fe(NO_3)_3$	0.068 (0.15)
PPy-$Fe(SO_4)_3$	0.063 (0.31)
PPy-SO_4	0.044 (0.33)
PPy-PTSA	0.046 (0.19)
PPy-NDSA	0.057

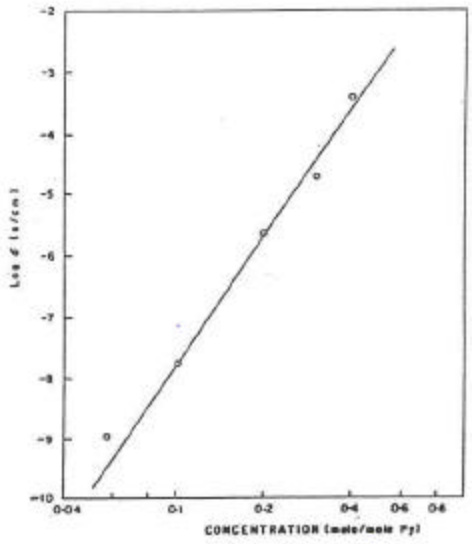

Fig. 3.3 Conductivity in PPy-NDSA samples (at 28°C) as a function of dopant ion concentration on a log-log scale

Since the PPy-NDS complex exhibited sharp changes in conductivity, the electrical

properties of these were studied in more detail with respect to concentration. **Fig.3.3** shows the room temperature conductivity for PPy as a function of concentration of NDS. It may be observed that there is a large increase in conductivity- by almost 6 orders of magnitude- when the dopant concentration is increased from 0.06 to 0.6 mole/mole PPy. This change in conductivity may be approximated as a power law of the type $\sigma \propto C^n$ where n = 7 with C being the concentration of the dopant. Such dependence of conductivity on concentration is typical for many conducting polymers including PPy and has been noted for other dopants as well [8,9]. There have been a few mechanisms suggested in the past for the rapid rise in conductivity of the dopant concentration, which consider the increase in the number of carriers as well as the decrease of distance between the hopping sites. However these do not take into account the exact nature of the dopant ion such as its size, distribution or aggregation in the polymer matrix. Further, there can be other charge transport processes different from hopping mechanism especially at high temperature. These various aspects are discussed later.

The temperature dependence of conductivity in PPy-NDS was carefully monitored by recording the sample resistance at constant potential and fixed heating rate (3.5°/min) in order to minimize the side effects that may cause shifts in the transition peak. **Fig 3.4** shows the σ-T plots for PPy samples containing three different concentrations of NDS, curves A to C corresponding to 0.05 mol, 0.3 mol and 0.5 mol of NDS respectively. It is interesting to note that in all cases the conductivity exhibits a broad peak centered at about 330 K followed a sharp transition above 360 K. The sharpness of the latter transition decreases with increasing dopant concentration. In order to understand these results, one has to first look into the nature of the experiment. Since the conductivity (directly proportional to the current) was noted at constant potential and fixed heating rate, these conditions are essentially equivalent to thermally stimulated current (TSC) measurements [10-12]. Hence one may draw similarities between the present data and the TSC curves. It is important to note that the dynamic mechanical relaxation curves for PPy doped with toluene sulfonic acid salt have been reported in literature [13], which also exhibit broad relaxation peaks in their tan δ value at 230 K, 335 K and 423 K respectively. The peaks above room temperature in their data correlate well with the present data clearly suggesting that there is a close similarity in the two and one can understand these peaks on the basis of TSC relaxation. The various peaks in the TSC originate from different mechanisms such as trapping and detrapping of charge

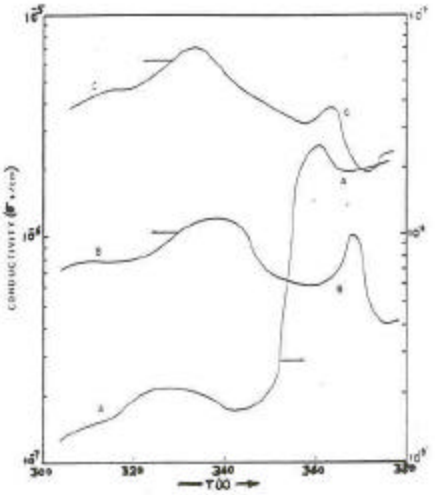

Fig. 3.4 Variation of conductivity in PPy-NDSA samples with respect to temperature recorded at constant applied field and heating rate of 3.5 ^{0}/min. Curves (A) to (C) correspond to NDSA concentration of 0.05, 0.3 and 0.5 mole/ mole Py

Table 3.3 (a) XRD results for PPy containing dopant ions from Fe^{3+} salts

Sample	2θ max	Peak width (radian)	R (°A)
PPy-$FeCl_3$	24.7	0.147	4.50
PPy-$Fe(NO_3)_3$	23.2	0.167	4.79
PPy-$FeClO_4$	22.6	0.199	4.92
PPy-$Fe_2(SO_4)_3$	23.0	0.180	4.83
PPy-$NH_4\{Fe(SO_4)_2\}$	24.9	0.122	4.47

(b) XRD results for PPy containing different sulfate /sulfonic acid dopants

Sample	2θ (deg)	Peak Width (radian)	R (°A)
PPy-H_2SO_4	21	0.19	5.29
PPy-Fe_2SO_4	23	0.18	4.83
PPy-TSA	20	0.20	5.55
PPy-NDS	22	0.21	5.05

carriers, segmental motion of the polymeric chain, dipolar relaxation, etc. Since both the dynamical relaxation curves as reported earlier and the present conductivity data show

similar peaks occurring in the same temperature range, these are no doubt associated with motion of polymer chain segments. This movement of the chain segment can affect the mobility of the charge carrier, interaction between the dopant and the polymer molecules or the distance between the sites. These various factors cause the changes in the conductivity value with temperature in the manner observed here.

The wide angle x-ray diffraction of the PPy doped with sulfate/sulfonate ions exhibited only an amorphous halo with possibly a weak reflection occurring at 2θ of about 25°. However, the position of the maximum intensity of the amorphous halo changes considerably with the dopant ion. One can estimate the average interchain separation from these maxima using the relation [14],

$$R = 5/8 [\lambda / \sin \theta] \qquad \text{Eq. 3.1}$$

where λ is the CuK_α x-ray wavelength and θ the diffraction angle at the maximum intensity in the amorphous halo. The full width at half maximum of this diffuse halo is also indicative of average distance between the chains [15]. These parameters are compared for PPy containing different dopants in **Table 3.3**. It is evident that the charge separation is the largest for PPy-NDS samples. On the other hand the charge transfer interaction between the dopant and PPy can be adjudged from the x-ray photoelectron spectroscopy (XPS). The core level spectra for C_{1s} and N_{1s} for the NDS doped PPy are indicated in **Fig 3.5.** These were further deconvoluted in the usual way [16,17] and it is evident that there are at least two additional charged species other than the neutral ones. The binding energy values and their relative contributions for these different parts of the XPS spectra for PPy containing sulfate/sulfonic and ferric salts are indicated in the **Table 3.4 (a)** and **(b)** respectively. The comparison of these values shows that although both NDS and TSA dopant ions give rise to similar charge transfer interaction with PPy, the actual distribution of the charge over different carbon or nitrogen atoms differ between the two types of dopants. This is evidenced from the different contributions to XPS from the charged carbon or nitrogen species. These differences can arise from change in placement of the dopant ions with respect to PPy chain as well as their separation.

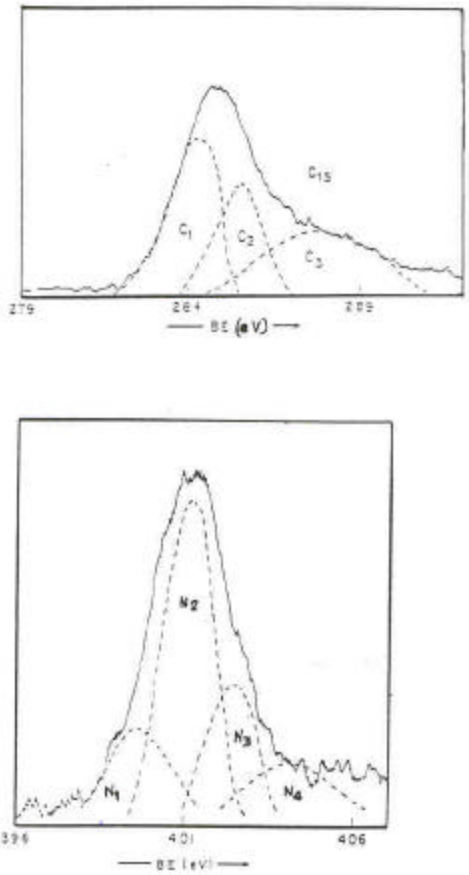

Fig. 3.5 XPS core-level spectra for PPy-NDSA samples (A) C_{1s} and (B) N_{1S} spectra with deconvoluted components indicated by the dotted lines

Table 3.4 (a) XPS results for PPy containing different sulfate/sulfonic acid dopants

Species (BE eV)	PPy-H_2SO_4	PPy-TSA	PPy-NDS
C(I) (284.3)	34%	27%	40%
C(II) (285.6)	51%	58%	27%
C(III) (287.8)	15%	15%	33%
N(I) (399.6)	31%	25%	16%
N(II) (400.9)	37%	32%	52%
N(III) (402.5)	32%	27%	20%
N(IV) (404.0)	0%	16%	12%

(b) XPS results for PPy containing dopant ions from Fe^{3+} salts

Species Binding Energy (eV)	PPy-$FeCl_3$	PPy-$Fe(NO_3)_3$	PPy-$Fe_2(SO_4)$
C(I)	68.9	70.8	58.49
C(II)	17.7	18.51	27.32
C(III)	13.4	10.69	14.18
N(I)	49.86	67.9	39.61
N(II)	28.65	21.17	36.59
N(III)	21.49	10.93	23.78

The above results on the WAX and XPS characterization of PPy doped with sulfate and sulfonic groups show that the dopant polymer interaction does not change very much but the

interchain distance gets affected by the size and the type of the dopant molecule. This in turn affects the movement of the polymer chains giving rise to peaks in the conductivity-temperature curves.

Due to the variations observed in the conductivity behaviour of PPy during the studies carried out with different dopant ions, the same dopant ion was used for all the further experiments. $CuCl_2$ was selected as a dopant in spite of the low conductivity exhibited by PPy synthesized using $CuCl_2$ as the major advantage was the complex formation with PEO to form a solid polymer electrolyte that could be used for the vapour phase polymerization of PPy. In addition, the Cu^{+}/Cu^{++} redox matches with the work function of PPy facilitating efficient charge transport between PPy and the SPE.

3.3.2 Charge transport in PPy /PEO-$CuCl_2$ ex-situ blend:

(a) Compositional dependence of conductivity(s):

The **Fig.3.6** indicates the change in conductivity of the blend with respect to the composition of PPy. The conductivity of the system is observed to increase with higher PPy concentration. Moreover, it rises continuously from the conductivity of the matrix (PEO-$CuCl_2$) at one end to the conductivity of the additive, pure PPy at the other. This transition from 10^{-8} S/cm to a value of 10^{-3} S/cm occurs gradually and saturates at 15% PPy content. It can also be noticed that pure PPy (100% composition) exhibits a conductivity value of 1.3 x 10^{-3} S/cm, which is quite low. The type of dopant ion, its concentration and the reaction medium are some of the important factors in controlling the conductivity of the polymer as discussed in the earlier section.

The plot also shows a sharp rise in conductivity that exhibits similarities with the classical percolation behaviour [18,19]. In case of the conducting polymer composites, the percolation threshold indicates the percentage of filler particles in the insulating matrix at which the conductivity increases sharply. According to the theory, the conductivity σ, depends on the volume fraction of the conductive component. The equation can be given as,

$$\sigma \propto (\varphi - \varphi_c)^{f} \qquad \text{Eq. 3.2}$$

Hence, $$\log \sigma = \log A + f \log (\varphi - \varphi_c) \qquad \text{Eq. 3.3}$$

where φ is the volume fraction and φ_c is the volume fraction at the critical concentration and f an exponent.

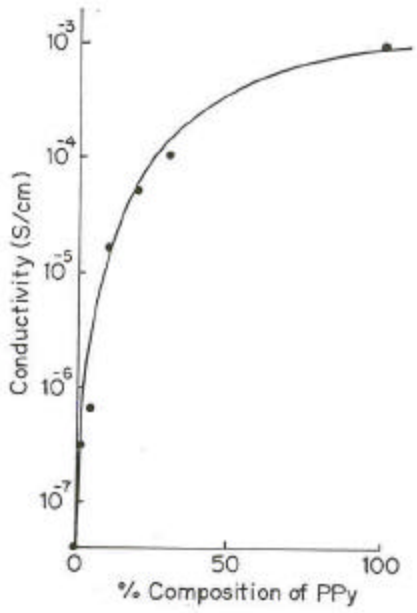

Fig. 3.6 Variation of conductivity with the composition of PPy in the ex-situ PPy/PEO -$CuCl_2$ blends

A plot of log σ vs weight fraction of PPy was made and is illustrated by the **Fig. 3.7**.

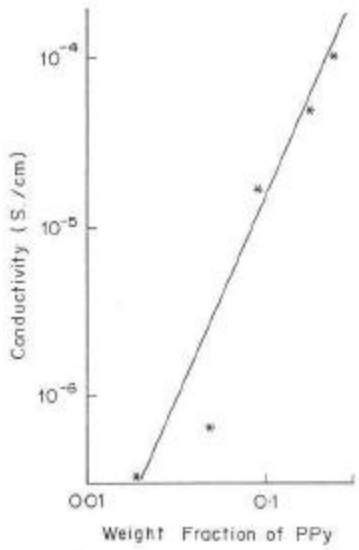

Fig. 3.7 Dependence of conductivity on the weight fraction of PPy for the PPy/PEO-$CuCl_2$ ex-situ blend

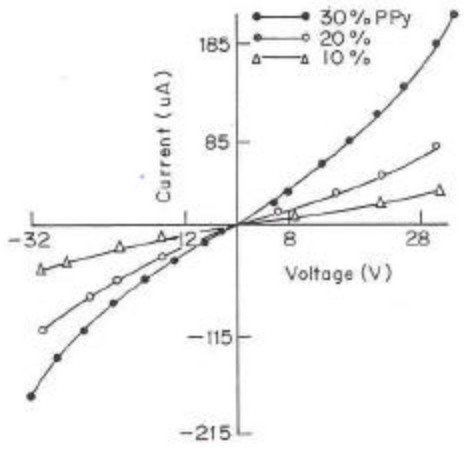

Fig. 3.8 I-V characteristics for PPy/PEO-$CuCl_2$ ex-situ blends containing 10, 20 and 30% PPy

It can be noticed that the plot is a straight line thus following the percolation model of conduction. This behaviour exhibited by the system can be understood as follows. The blend

consists of conducting PPy particles (10^{-3} S/cm) embedded in a semi-conducting matrix of PEO-$CuCl_2$ (10^{-9} S/cm). Schematically, it may be considered to form an M-I-M structure wherein the conducting regions are well separated by the insulating material. Incorporation of more PPy in the insulating matrix reduces the distance between the two conducting sites. At a critical concentration, the PPy particles contact each other, forming a network [20,21]. This effect is pronounced at higher PPy concentrations whereafter the conductivity reaches saturation.

Wegner has reported the electrical properties of composites based on PPy externally added to PEO [22]. The properties were studied as a function of the size of PPy particles. However, the conductivity even at 20% volume fraction was not very high (10^{-4} S/cm) similar to that obtained in the present case.

(b) I-V characteristics of PPy/PEO-$CuCl_2$ ex-situ blend:

The I-V characteristics were observed to be non-linear in nature as indicated by the **Fig.3.8**. Moreover, the degree of non-linearity was found to rise with the increase in PPy concentration. In order to find the charge transport mechanism, i.e. the exact dependence of current on the voltage, one has to fit the data in the mathematical expressions governing each mechanism. For example, in Space-Charge-Limited-Conduction, SCLC,

$$I_p = \frac{8}{9}\mu f \varepsilon \frac{V_p^2}{d^3} \qquad \text{Eq. 3.4}$$

or $$I \alpha V^n \quad \text{where } n \geq 2 \qquad \text{Eq. 3.5}$$

relationship is followed. A plot of log I versus log V was made to verify this equation and was observed to give a linear dependence but with a slope of <2 (1.3 to 1.5) (see **Fig 3.9**). Hence one cannot justify the conduction process using the SCLC mechanism in these blends.

In the case of Poole-Frenkel or Schottky effect, an I-V dependence of the type,

$$I = \sigma_o \exp\ (\beta V^{1/2} / kTd^{1/2}) \qquad \text{Eq. 3.6}$$

is expected to be followed. Hence the plot of log I versus $V^{1/2}$ would represent a straight line and the slope (S) would correspond to,

$$S \ \alpha \ \beta / kT\, d^{1/2} \qquad \text{Eq. 3.7}$$

where β is the Poole Frenkel parameter.

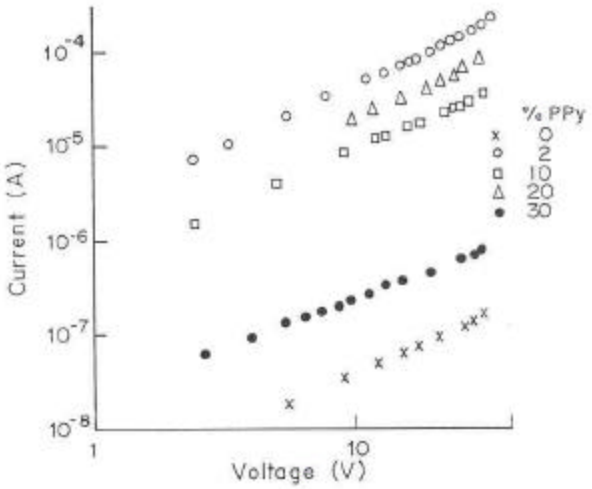

Fig. 3.9 I-V characteristics for the PPy/PEO-$CuCl_2$ ex-situ blends containing 0,2, 10, 20 and 30 % PPy plotted on a log-log scale.

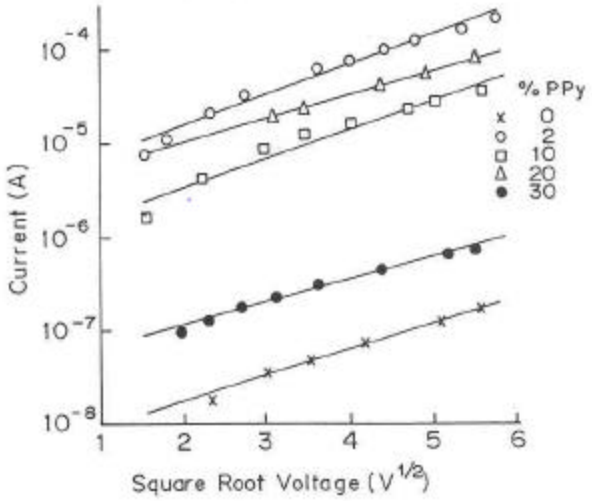

Fig. 3.10 Dependence of conductivity on the square root voltage for the PPy/PEO-$CuCl_2$ ex-situ blends containing 0,2, 10, 20 and 30% PPy

Applying this equation to the present blends, the data was plotted as log I Vs $V^{1/2}$ for varying PPy content as shown in the **Fig.3.10**. Further, the slopes of these graphs were determined and are shown in Fig **3.11** as a function of the PPy concentration in the blend. It can be clearly noticed that the slopes rise sharply beyond the 20% PPy. Considering the Schottky emission type of conduction, it always depends on the nature of electrode used i.e. Φ, the work function of the metal. A Schottky type of barrier formation is reported at the In/PPy/Au junction wherein the PPy contained a small quantity of PEO [23]. However, in the present case the I-V characteristics were studied on interdigited electrodes of gold (on both sides), which, has a high work function and forms an ohmic contact with p-type PPy. Hence the Schottky effect can be ruled out. The abrupt increase of the slope from 0.24 to 0.44 can be explained by considering its dependence on 'd', the interparticle distance between the PPy particles (see eq 1.7). As the PPy composition increases, the concentration of the conducting sites is increased, the particles come closer thus reducing the interparticular distance and in turn increase the slope S. Thus the charge transport process in the ex-situ blends is predominantly of Poole-Frenkel type.

(c) Temperature dependence of conductivity (s -T):

Arrhenius plots are normally presented as the dependence of log (σ) against 1/T, which are represented by **Fig.3.12** for the PPy/PEO-$CuCl_2$ ex-situ blend. The changes in conductivity are observed to be entirely dominated by a sharp transition occurring at 65°C. The temperature (T), dependence of conductivity σ, in solid polymer electrolytes is related by Vogel-Tamman-Fulcher (VTF) and Williams-Landel-Ferry (WLF) relationships in the form [24],

$$\sigma(T) = AT^{-1/2} \exp [-E_a / R (T - T_o)] \qquad \text{Eq. 3.8}$$

This means that ideally amorphous materials display gently curved temperature dependence in a log σ vs 1/T plot. It is known that PEO based polymer electrolytes contain a mixed morphology; the crystalline spherulitic regions of the polymer melt at 65°C [25]. Consequently, the mobility of the charge carriers increases contributing to the ionic conductivity that is responsible for the presence of the 'knee' leading to an increase in conductivity at that temperature. Apart from this, a small and broad peak is observed at low

temperature that may be attributed to the release of charge carriers from the traps as the temperature rises.

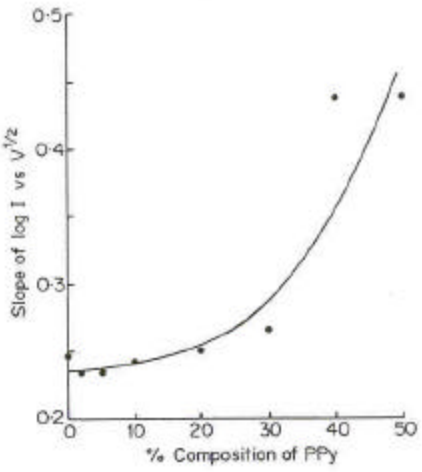

Fig. 3.11 Slopes of log I vs $V^{1/2}$ with respect to the composition of PPy for PPy/PEO-$CuCl_2$ ex-situ blends

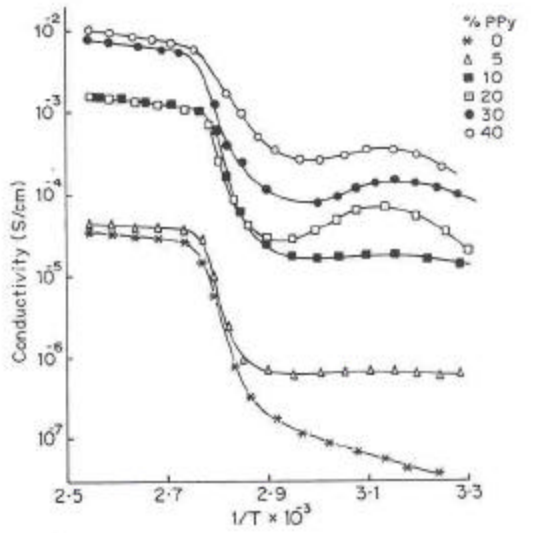

Fig. 3.12 Temperature dependence of conductivity in the PPy/PEO-$CuCl_2$ ex-situ blend

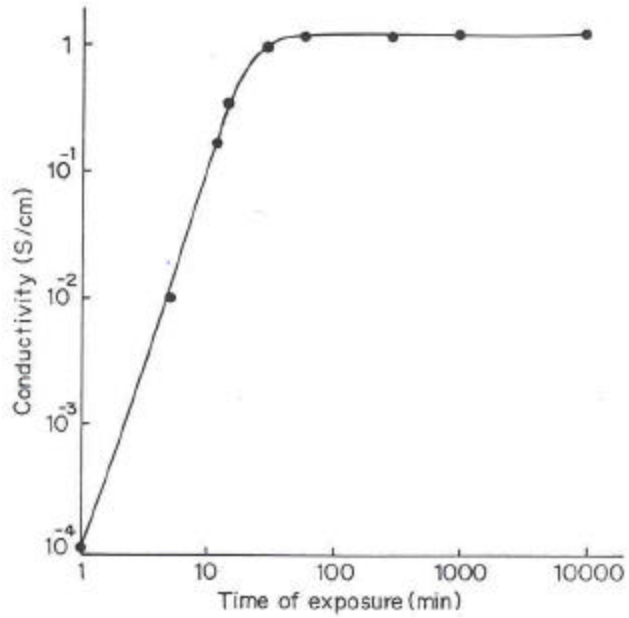

Fig. 3.13 Variation of conductivity with time of exposure to pyrrole vapours for 8:1 monomer/mole PEO-$CuCl_2$

3.3.3 Charge transport in PPy/PEO-$CuCl_2$ in–situ blend:

The studies were carried out in two configurations viz. the surface mode (interdigited cells) and the sandwich mode (multilayered cells).

(a) Time dependence of conductivity:

The time dependence of conductivity was carried out to know the extent of rise in conductivity with the duration of exposure to pyrrole vapours. A typical plot for 8:1 PEO-$CuCl_2$ composition is exhibited in the **Fig.3.13.** The initial portion of the plot indicates a rise in conductivity by almost four orders in magnitude for an exposure duration of 30 minutes. This is followed by saturation in conductivity inspite of further exposure to pyrrole. Thus a conductivity increase to 1 S/cm is observed due to the formation of PPy in the PEO-$CuCl_2$. The formation of PPy occurs at the cost of $CuCl_2$ [26]. The initiation of the polymerization takes place along in the crystalline boundaries in the PEO-$CuCl_2$ complex. As time proceeds, more growth of PPy occurs that leads to the formation of network-like structure. The increase of PPy content enhances the conductivity of the blend. At higher exposure duration, the vapour phase polymerisation reaction goes to completion due to complete conversion of $CuCl_2$ to CuCl and no more PPy is formed. Consequently, the conductivity of the blend reaches a steady value of 1 S/cm. Similar findings were recorded for the blends containing varying amounts of $CuCl_2$. The rise in conductivity is higher in the case of blends containing more $CuCl_2$.

(b) Compositional dependence of conductivity:

Conductivity of the blends was plotted against the $CuCl_2$ concentration in the blend as illustrated by the **Fig.3.14.** Curve (A) represents the conductivity variation for the PEO-$CuCl_2$ alone (without PPy), curve (B) represents the conductivity for the blends exposed to PPy for 2 minutes duration while curve (C) indicates the conductivity of the blends when exposed to pyrrole for 24 hours till saturation. The curve (A) indicates a conductivity rise from 10^{-9} S/cm for PEO to 10^{-6} S/cm with 0.25 M addition of $CuCl_2$ (4:1 monomer/mole $CuCl_2$) and then shows a small decrease with further increase in $CuCl_2$. As discussed in Chapter I, for PEO-salt complexes the charge transport is governed by ionic conduction. When a dopant salt is introduced into the polymer matrix, conductivity increases rapidly due to an increased number of charge carriers. However, at higher salt concentrations, the salt

also crystallizes out of the PEO systems. Maximum concentration of the salt retained in a complex form exhibits higher conductivity. This optimum is observed to be achieved at 4:1 PEO:$CuCl_2$ monomer /mole concentration in the present case as evidenced by the conductivity plot. Vapour phase deposition of PPy in the PEO-$CuCl_2$ matrix for two minutes duration increases the conductivity of the system by almost four orders of magnitude as indicated by the curve (B). The conductivity increases quite sharply with respect to the molar concentration to a value of 10^{-1} S/cm at 0.25M $CuCl_2$ content, whereafter it is observed to be steady irrespective of the $CuCl_2$ change. Actually, it is expected that the conductivity should rise with the increase in dopant ion continuously. But Cheung et. al.[27] have found out that the larger amount of dopant in the film may result in high degree of conjugation but not higher conductivity. This has been explained on the basis of the factors limiting the conductivity i.e. the carrier mobility and the carrier concentration. Carrier mobility depends on the intramolecular and intermolecular transport, which is concerned with hopping from one backbone to other and interparticle transport. Thus the densely packed films would have higher conductivities. The conductivity of the blends after exposure to pyrrole till saturation are indicated by the curve(c) wherein a saturation value of 1 S/cm is obtained for the blends with $CuCl_2$ content beyond 0.25 M.

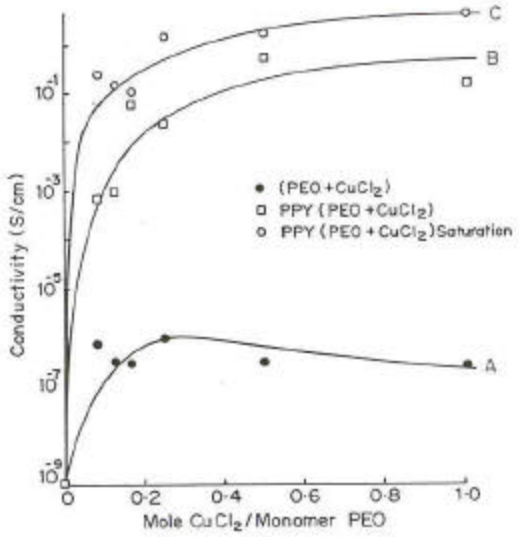

Fig. 3.14 Dependence of conductivity on the $CuCl_2$ content in PEO for PPy/PEO-$CuCl_2$ insitu blend. Curves correspond to (a) PEO-$CuCl_2$ alone (b) PEO-$CuCl_2$ with exposure to pyrrole for 2 min (c) PEO-$CuCl_2$ exposed to pyrrole till saturation

The compositional dependence is similar to that observed for the ex-situ blend as observed

in the **Fig 3.6**. This occurs due to the two-phase morphology of the ex-situ as well as the in-situ type of blend. The PEO-$CuCl_2$ film shows a polycrystalline nature with many amorphous regions. During the in-situ deposition, the preferential growth of PPy in the inter spherulitic-crystalline regions creates conducting regions (domains) separated by non-conducting regions [28]. The mean free path of an electron will thus remain confined to the conducting domain. The microstructure is similar to the M-I-M structure as described in the ex-situ blend system but the dimensions are drastically reduced to sub-micron scales in the in-situ blend. Hence a composite-like behaviour as observed in the case of the ex-situ blends is expected. At low time exposure, low concentrations of PPy are formed. Hence these blends can be said to be below the percolation threshold as represented by the curve (B). However, at higher exposure times, continuous PPy network is formed and the blends are said to be above the percolation threshold as indicated by the curve (C).

(c) I-V characteristics of PPy/PEO-$CuCl_2$ in-situ blends:

The I-V characteristics of the PPy/PEO-$CuCl_2$ blend system with partial deposition of PPy with varying $CuCl_2$ contents are shown by the **Fig 3.15.** It is observed that the I-V curves are non-linear and the degree of non-linearity increases as the $CuCl_2$ concentration increases. These were then analyzed for the exact conduction mechanism. The SCLC mechanism was ruled out as the value of n in $I \alpha V^n$ is less than 2. Plots of $\log I / V^{1/2}$ were made as depicted in the inset of **Fig.3.15** yielding a linear dependence implying a Poole-Frenkel or Schottky type of conduction mechanism; the slopes of which are also indicated (see **Fig.3.16**). It is observed that the slopes rise with the increase in $CuCl_2$ till 0.25 M concentration and then remains constant. This can be again explained on the basis of the factors governing the variations of the slope. In case of the blends with low dopant (initiator) concentration i.e. 0.08, 0.125, and 0.167 the PPy content is also low, the interparticular distance ($d^{1/2}$) is high giving rise to barriers at the PPy / PEO-$CuCl_2$ interface. The addition of $CuCl_2$ to the matrix, decreases the interdomain distance, d, reducing the barrier width at the interface consequently increasing the slope of the $\log I / V^{1/2}$ plot.

The I-V characteristics for the PPy/PEO-$CuCl_2$ blends that are saturated with PPy and hence above the percolation threshold are depicted in the **Fig.3.17**. Curves (A) and (B) represent I-V characteristics for 12:1 and 8:1 PEO-$CuCl_2$ monomer/mole concentration. It is clear that the I-V characteristics are all linear irrespective of the $CuCl_2$

CO

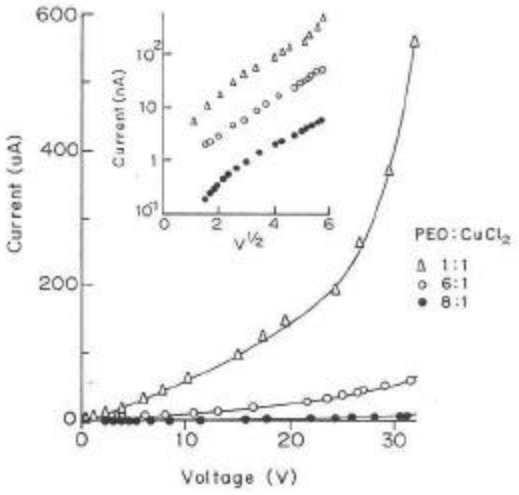

Fig. 3.15 I-V characteristics for the PPy/PEO-$CuCl_2$ in-situ blend with partial exposure to pyrrole for the compositions 8:1, 6:1 and 1:1 monomer/mole PEO-$CuCl_2$. Inset shows the linear dependence of conductivity on square root voltage

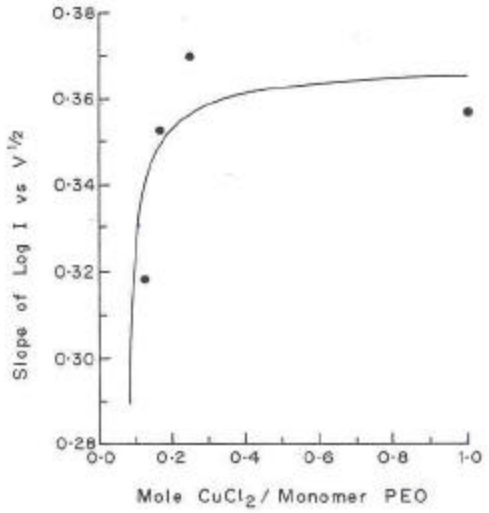

Fig. 3.16 Variation of slopes of log I vs $V^{1/2}$ with $CuCl_2$ concentration for the PPy/PEO -$CuCl_2$ in-situ blend

ncentration. The ohmic nature of the I-V curves clearly brings out that no barriers are present between the PPy domains and network is formed throughout the matrix in the saturated blend.

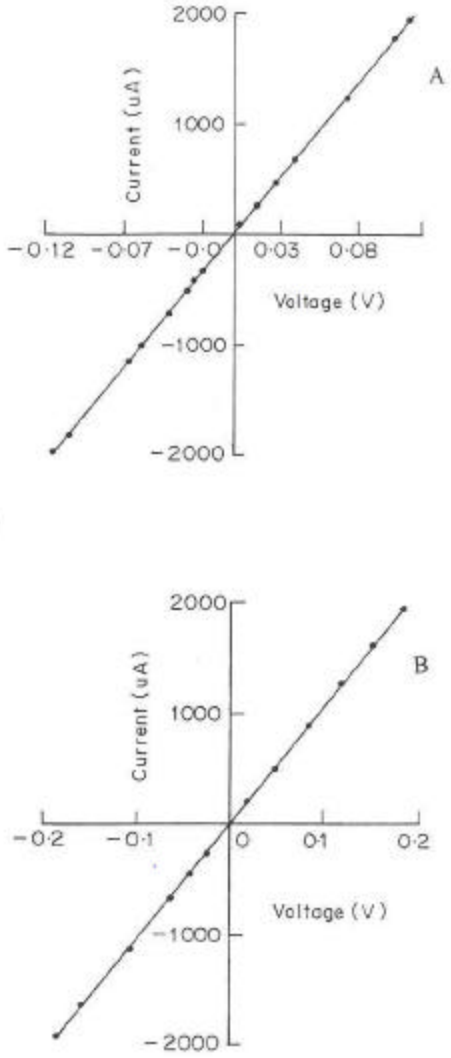

Fig. 3.17 I-V characteristics for the PPy/PEO-$CuCl_2$ in-situ blends saturated with pyrrole. Curves (A) and (B) correspond to 8:1 and 12:1 monomer/mole PEO-$CuCl_2$ concentration

(d) Temperature dependence of conductivity:

The temperature dependence of conductivity for the PPy/PEO-$CuCl_2$ in-situ blend with different $CuCl_2$ was carried out as is represented by the **Fig 3.18.** It can be noticed that the log σ vs. 1/T plots having low concentrations of $CuCl_2$ show the presence of a transition near the T_m of PEO. The blend containing 8:1 PEO-$CuCl_2$ exhibits a rise in the conductivity till 89^oC and shows a small decrease at higher temperatures. A similar behaviour is observed for the blend containing 6:1 PEO-$CuCl_2$ with the peak in conductivity shifting to a higher temperature of 103^oC. The increase in the conductivity at the transition is by magnitude of more than 1 order in the blends with 8:1 and 6:1 PEO-$CuCl_2$. As discussed in section 1.3.2 (C), the transition at the T_m of PEO is influenced by the viscosity of the blend, which changes by the addition of PPy. Formation of PPy by in-situ method is more at a higher dopant (initiator) concentration of the matrix. Hence the viscosity of the blend increases as the $CuCl_2$ increases. At lower concentrations of $CuCl_2$, the ionic mobility increases as well as some deformation in the conducting domains occurs at the T_m that reduces the intergranular distance. Practically this phenomenon is observed as a transition in the case of 8:1 and 6:1 in-situ blends. However as the viscosity of the blends increases, the ionic mobility successively decreases, lowering the sharpness and magnitude of the transition at the T_m.

The temperature variation of conductivity for the in-situ blends saturated with PPy i.e. above the percolation threshold are markedly different than observed for the partially deposited blends. No transition is observed in the conductivity-temperature plots. It is thus evident that more the amount of PPy available for blend formation with PEO-$CuCl_2$ more is the thermal stability of the material. Formation of PPy network eliminates the barriers at the interface, hence conduction occurs via interchain and intrachain hopping. As discussed in the Chapter I, Mott's variable range hopping model [29] has a relationship as,

$$\sigma = \sigma_o \exp (-T/T)^{1/4} \qquad \text{Eq. 3.9}$$

The significant feature of σ is its dependence on exp $(-T_o/T)^{1/4}$. Hence plots of σ-T were represented as log σ against $T^{-1/4}$ as shown in the **Fig 3.19**. It is observed that the plots follow a linear dependence hence obeying the equation 1.1. It can be said that the conduction occurs by variable range hopping model in the case of blends saturated with PPy. Lefrant et al [30] have observed that above the percolation threshold, a temperature dependence of the conductivity characteristic of VRH model is obeyed in the case of PPy/PVA-$FeCl_3$

composites. This holds good in the present case also where continuous PPy domains are formed in case of higher PPy blends.

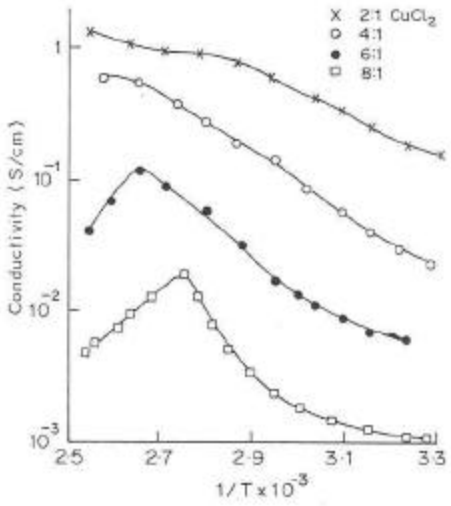

Fig. 3.18 Temperature dependence of conductivity for the PPy/PEO-$CuCl_2$ in-situ blends

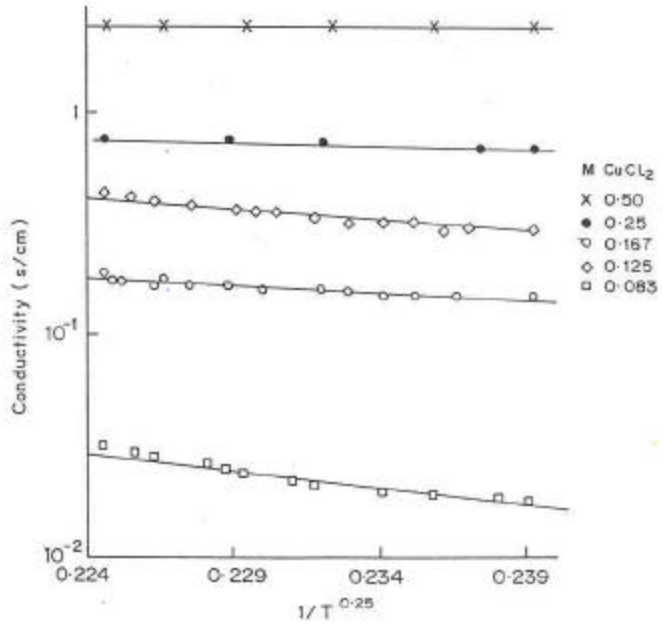

Fig. 3.19 Temperature dependence of conductivity for the PPy/PEO-$CuCl_2$ in-situ blends saturated with PPy

3.3.4 Charge transport at PPy/PEO-$CuCl_2$ and other solid polymer electrolytes :

Typical I-V characteristics were obtained for the in-situ blends containing 2:1 and 4:1 PEO-$CuCl_2$ for the ITO/PPy(PEO-$CuCl_2$)/Au cell and are shown in **Fig.3.20**. Sharp steps in current at a certain applied potential are observed in both increasing and decreasing cycles which are similar to switching type of characteristics [31]. In order to investigate this further, single junction studies were carried out at the PPy/PEO-$CuCl_2$ interface by making a sandwich cell of electrochemically deposited PPy and the PEO-$CuCl_2$ (4:1) across ITO and Au electrodes. The I-V characteristics of the device are depicted in the **Fig.3.21**, which exhibit a similar switching type of behaviour. To understand this fully, charge transport was studied across single junctions of PPy in contact with solid polymer electrolyte consisting of PEO complexed with KCl. The I-V characteristics for the cell exhibited a large anodic current superimposed on a small cyclic wave noted in the cathodic region (see **Fig.3.22**). These were similar to rectifying type of characteristics. Single junction studies were also carried out in contact with liquid electrolyte as a comparative study between the solid and the liquid electrolytes. The cyclic voltammogram of PPy cycled in $CuCl_2$ and and KCl are given in the **Fig3.23 (a)** and **(b).** Distinct changes are observed in the charge transport processes at the PPy/SPE and the PPy/liquid electrolyte interface. Similar studies were carried out in contact of SPE and the liquid electrolytes with different salts like $LiClO_4$, $NaCl_4$, and Na_2SO_4; the I-V characteristics of which are depicted in the **Fig. 3.24, 3.25** and **3.26**. The I-V curves are found to be of rectifying nature in all the cases using SPEs. It may be mentioned herein that the PEO-based SPE has comparatively high resistivity; thus, much lower current values are expected in these type of cells than those with the liquid electrolytes. Furthermore, it may be noted that the potentials in the case of SPE are with reference to gold, whereas those in liquids are with respect to SCE. The former are hence much higher (~0.8 V) than the latter.

The cyclic voltammetry of PPy films in the liquid electrolytes has been studied by several authors, and is well documented in the literature [32-35]. Although there are some changes in the actual potential values from report to another, the overall features in the I-V characteristics are the same. Two peaks are observed in the I-V characteristics that correspond to the reduction and the oxidation of the PPy films; for example the cyclic

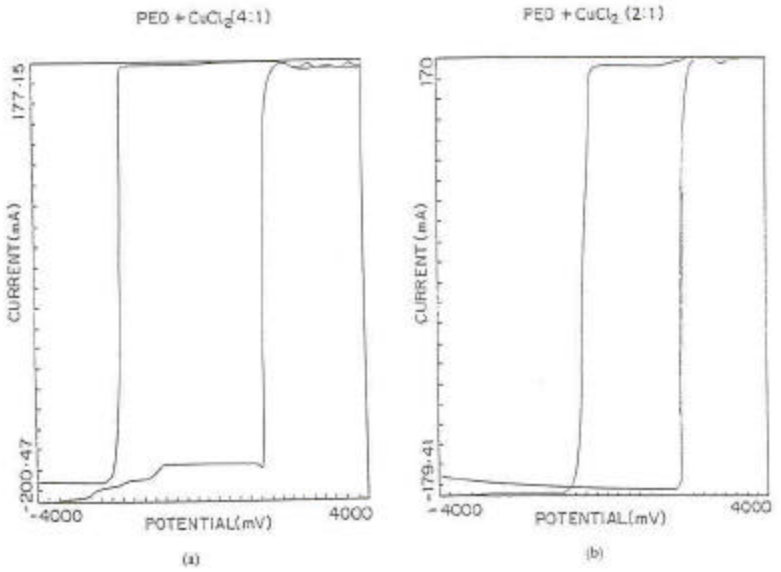

Fig. 3.20 Current-voltage characteristics for the solid-state cell containing the composite of PPy/PEO-$CuCl_2$ with PPy deposited in-situ (a) 4:1 complex and (b) 2:1 complex

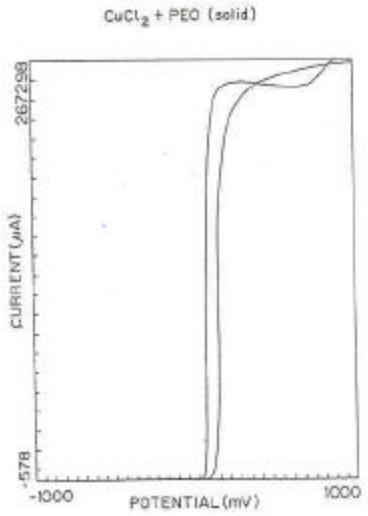

Fig. 3.21 Cyclic voltammogram of PPy film in $CuCl_2$ electrolyte, as PEO complex solid electrolyte concentration of 4:1 monomer/mole. Scan rate 30mV/s with gold as reference electrode

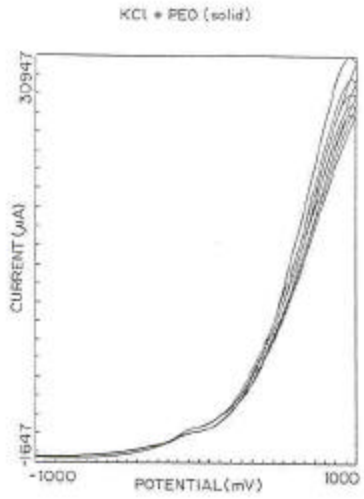

Fig. 3.22 Cyclic voltammogram of PPy film in KCl electrolyte as solid electrolyte with an electrolyte concentration of 4:1 monomer/mole

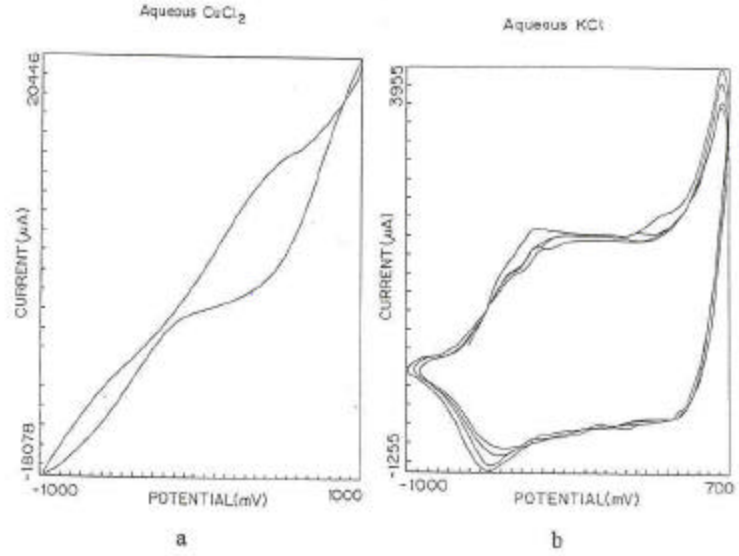

Fig. 3.23 Cyclic voltammograms of PPy film in aqueous electrolytes containing 0.1 M $CuCl_2$ and 0.1 M KCl in curves (a) and (b) respectively. Scan rate 30mV/s, SCE as reference electrode

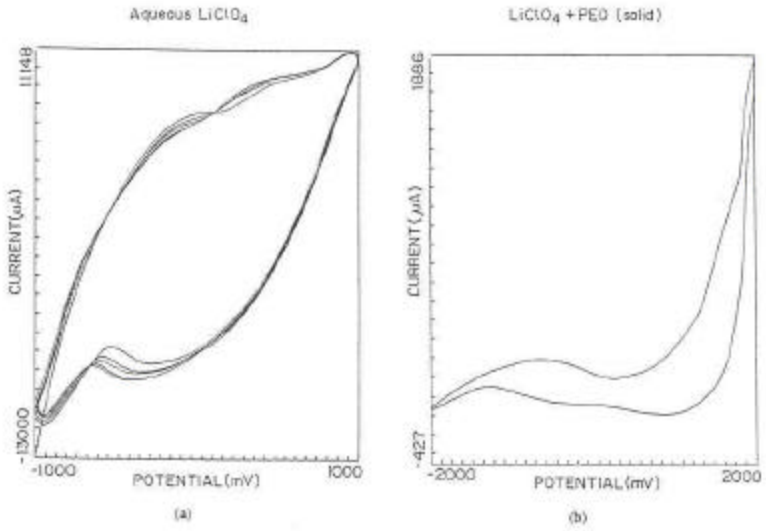

Fig. 3.24 Cyclic voltammogram of PPy film in $LiClO_4$ electrolyte (a) aqueous and (b) as PEO complex solid electrolyte

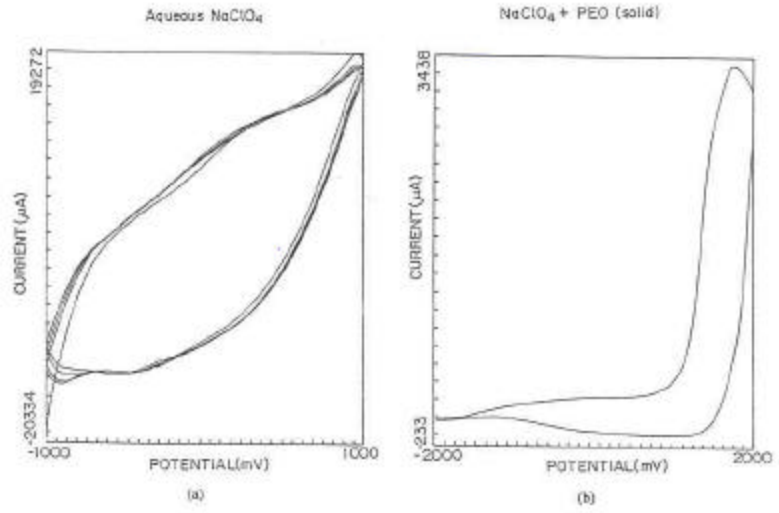

Fig. 3.25 Cyclic voltammogram of PPy film in $NaClO_4$ (a) aqueous and (b) as PEO complex solid electrolyte

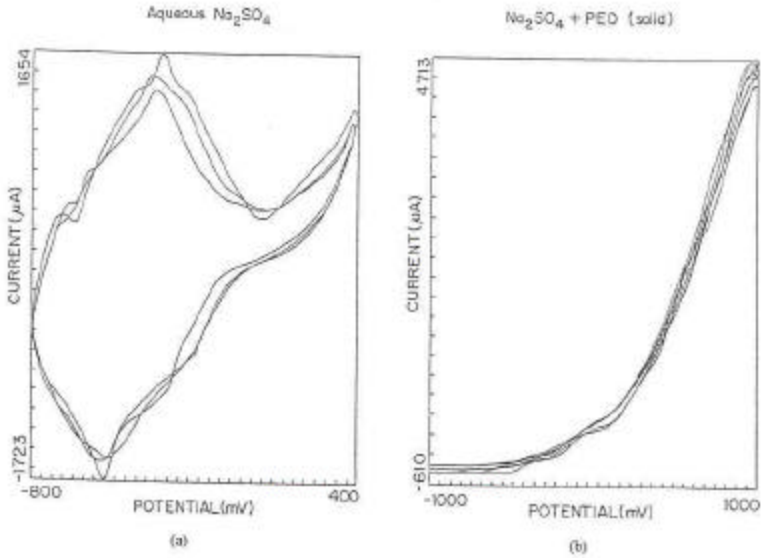

Fig. 3.26 Cyclic voltammogram of PPy film in Na_2SO_4 (a) aqueous and (b) as PEO complex solid electrolyte

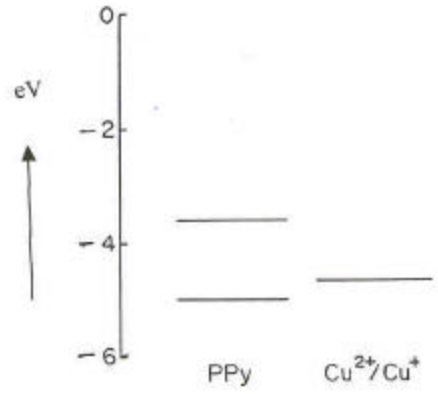

Fig. 3.27 Band diagram of PPy/PEO-$CuCl_2$

voltammogram for PPy in aqueous KCl (**Fig.** 3.**22 b**) shows the presence of two distinct peaks in the I-V at –0.4V and –0.15V corresponding to reduction and oxidation of the PPy.

This process of reduction and oxidation of the PPy is understood in terms of the transport of ions/charge carriers in and out of the polymer. The peak position and its sharpness depend on the nature of the dopant ion present in the electrolyte. The present observations for the PPy in liquid electrolytes are essentially in agreement with these reports. It is thus clear that freely mobile ions should be available for the doping/undoping process to take place, and these are present in the case of liquid electrolytes, whereas in the SPE, there will be less mobility of ions and a different type of behaviour would be expected. A few authors have mentioned the use of SPE, together with conducting polymers and note similar I-V curves as in liquid electrolytes. Because the ionic transport in SPE is governed by the type/size of the ions, temperature, crystallinity, etc. [36-38], the similarity of the I-V curves would be observed only in certain cases where the ion transport is not hindered through the SPE (probably in $LiClO_4$ and $NaClO_4$), as well as the interface of the SPE and the conducting polymer. Large differences in the diffusion constants for the ions in the SPE (of the order of $5x10^{-7}$), compared with liquid electrolytes ($>3x10^{-5}$), have been reported by Geng and colleagues [39]. Thus, one may expect the I-V characteristics to change at least in the value of currents and peak position when the SPE is used in place of liquid electrolyte.

In the present case, significant differences were noted in the I-V characteristics when the SPE was replaced by a liquid electrolyte, with the former exhibiting high anodic currents, compared with cathodic ones. There can be mainly two reasons for this type of behaviour:

(1) the charge transport across the PPy/SPE interface is easier in one direction than the other, and /or

(2) the SPE allows transport of only one type of ion.

In the SPEs, PEO is known to form complexes with alkali metal salts by binding the metallic ions within the helical matrix by coordination with oxygen atoms[40,41]. Thus it appears that one of the charge species would be more mobile than the other in such electrolytes, compared with the liquid electrolytes, wherein both the species are mobile. This may lead to the unusually non-symmetric I-V characteristics observed in the case of the SPEs. Furthermore, PPy has a work function of 5.0 eV, whereas the PEO has a workfunction of 3.95 eV [42] as represented in the band diagram, **Fig 3.27**. This can give rise to a potential barrier for the charge transport at the interface, because of the mismatch in the energy levels of the two polymers. Thus, the charge transport across the interface of PPy and SPE is also

quite different from that at PPy and liquid electrolyte. These various effects can give rise to the type of I-V characteristics described herein.

Now, considering the case of $CuCl_2$ complexed with PEO as the electrolyte, it may be noted that the rapid switching type characteristics were observed especially for those samples that were made by in-situ polymerization technique. In this process, the PPy formation takes place according to ref [43]:

$$N\,\mathrm{Py} + m\,\mathrm{CuCl_2} \longrightarrow [(\mathrm{Py})_x\,\mathrm{Cl}^-_{x-1}]_n + m\,\mathrm{CuCl} \qquad \text{Eq. 3.10}$$

where N(= nx) and m(= nx-n) are molar concentrations of monomer and dopant, respectively; and x is some fraction indicating dopant concentration in the polymer. The above equation is a generalized form of that reported for x = 2. This clearly suggests the formation of CuCl during the polymerization step. This component remains in the SPE during subsequent experiments and changes the nature of the I-V characteristics. It may be of interest to note herein that the PPy has a work function of 5.0 eV which implies that its valence band is 5.0 eV below vacuum level (0.0 eV), and the Fermi level that exists between the bipolaronic states have been reported to be 1.7 eV apart above the valence band (i.e., at 2.2 eV below the vacuum level). Furthermore, the Cu^{++}/Cu^{+} redox is expected at 4.653 eV below the vacuum [44]. Thus, the transfer of electrons from the bipolaronic state to the redox state in such a case is very much facilitated, whereas the reverse process is blocked. To confirm the role of CuCl, separate set of experiments were conducted by deliberately incorporating CuCl into the liquid electrolytes containing $CuCl_2$. **Fig. 3.28 (a), (b)** and **(c)** shows the cyclic voltammograms for PPy in liquid electrolyte containing 10, 20 and 30% CuCl (of the total salt concentration). It is clearly revealed from these that I-V characteristics exhibit additional waves that correspond to the oxidation and reduction of Cu^{+} species. This wave becomes more pronounced and sharp with the increase of CuCl [compare **Fig 3.27(a,c)**]. At a high concentration of CuCl, the overall shape of the I-V resembles a sharp step-like characteristic similar to those in the **Fig.3.20**. With a difference that, in the latter case, the step is much steeper and the currents are much higher in the case of PPy in liquid electrolyte. These differences in the I-V characteristics of **Fig 3.20** and **Fig. 3.21** can be understood as follows. In the case of PPy film immersed in liquid electrolyte containing $CuCl_2$/CuCl [**Fig 3.21 (b)**], there is a single junction formed at the interface of the polymer and the electrolyte, whereas in the case of PPy deposited in the SPE containing $CuCl_2$ (and in situ formed CuCl), there are a large number of such junctions formed at the PPy domains

that are connected in series and parallel. Thus, the effect observed at each PPy-electrolyte junction gets amplified in the case of PPy deposited in the SPE, and one observes much higher current values, as well as a sharp step in their I-V curves. It may be also mentioned that the charge transfer to the redox sites within the SPEs is much more efficient when the electroactive component is dispersed in it [45]. Hence, one would also expect a higher rate of charge transfer in the PPy/SPE composite than for discrete two layer structures. It may be of interest to mention herein that the differences in the I-V curves have been observed when the rate of analyte transport near the electrode (e.g., in the case of microelectrode systems, compared with macroelectrode-based cells) [46]. In the former, the I-V is sigmoidal, whereas in the latter it exhibits typical I-V peaks. The present results on the PPy/SPE composite cells seem to suggest that these behave more like microsystems in which each domain of PPy acts as a microelectrode on which the electrochemical reaction takes place.

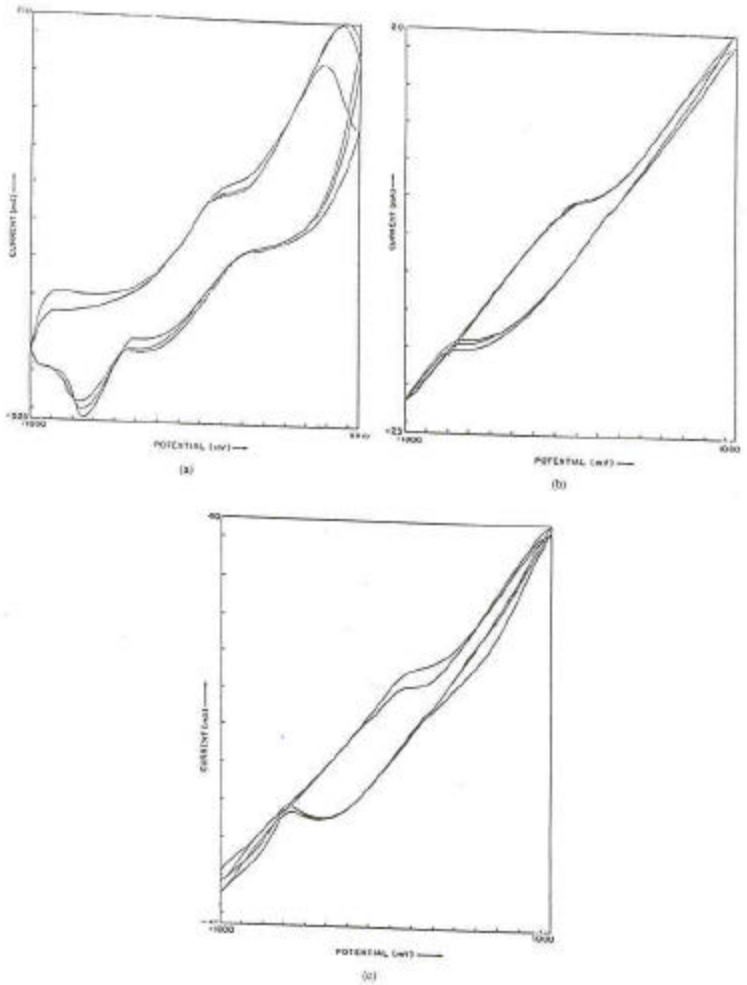

Fig. 3.28 Cyclic voltammograms of conducting PPy films in aqueous 0.1M $CuCl_2$ containing additional CuCl (a) 10% (b) 20% and (c) 30% CuCl

3.3.5 PPy/CuPc in composite:

These composites were made by vapour phase deposition of PPy on PEO-$CuCl_2$ films containing CuPc in the range of 2% to 45% by weight.

(a) Time dependent kinetic studies:

The variation of composition in the CuPc composite system urged the need to investigate the kinetics of vapour phase polymerization of PPy. The variation of conductivity of the composites with exposure time is depicted in the **Fig. 3.29**. It is observed that the conductivity rises very rapidly in case of the compositions containing CuPc represented by curves (b), (c), (d), (e), (f) and g containing CuPc of 16.7, 23.1, 28.6, 33.3, 37.5 and 44.4 % composites as compared to the 0% CuPc (i.e. PEO-$CuCl_2$) indicated by the curve (g) (PEO-$CuCl_2$ is same in all cases, 4:1). The rapid rise in the conductivity of the composites for a shorter exposure time to pyrrole suggests that CuPc influences the vapour phase polymerization process of pyrrole. It may be of interest to note that the conductivity values at zero exposure i.e. without PPy are also found to vary with the CuPc composition. The exposure to pyrrole causes the conductivity of the composites containing 2% and 5% CuPc to rise by almost 4 orders of magnitude in the initial 100 seconds. It is observed to saturate beyond an exposure time of 500 seconds. On the contrary, the 0% CuPc shows a slow rise in conductivity till around 900 seconds and then reaches the saturation limit. At higher concentrations of CuPc, the conductivity saturates at relatively higher time of exposure. The composite containing 25% CuPc is observed to saturate around 200 seconds while that containing 38% and 45% CuPc takes 300-400 seconds to saturate.

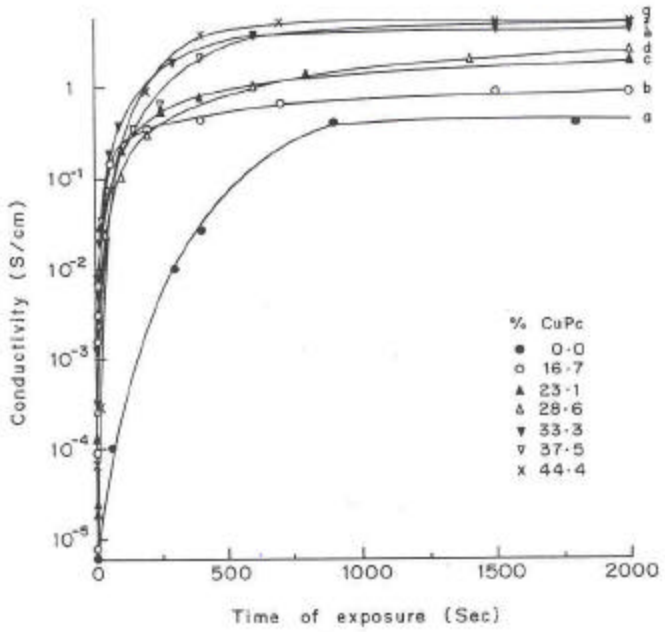

Fig. 3.29 Variation of conductivity with the exposure to pyrrole for the PPy/CuPc in-situ composites with PEO-$CuCl_2$ (4:1 monomer/mole). Curves (a) to (g) correspond to a CuPc concentration of 0, 16.7, 23.1, 28.6, 33.3, 37.5 and 44.4 by weight

In order to understand the variations in the rate of deposition of PPy, morphological studies of the composites were carried out using an optical polarizing microscope. **Fig 3.30 (a), (b)** and **(c)** depicts the optical micrographs of the composite containing dispersion of 0.5, 1 and 5% CuPc in PEO-$CuCl_2$.

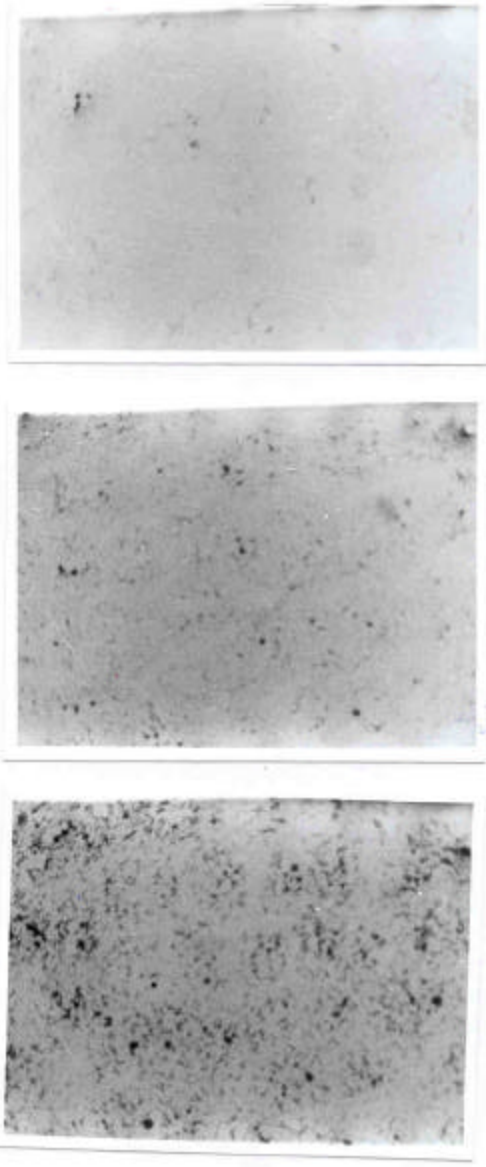

Figure 3.30 Optical polarising micrographs of CuPc dispersion in PEO-$CuCl_2$ (4:1 monomer/mole) containing 0.5, 1 and 2% CuPc

It can be easily observed that the CuPc particles are associated with the domains in the matrix. There can be a possibility of some kind of chemical interaction between CuPc and

$CuCl_2$ due to which these are found in close vicinity in the matrix. Another interesting fact noticed, is the greater association of CuPc with the domains as more CuPc is dispersed in the matrix. A comparison of the particle size of CuPc dispersed in the matrix suggests that the particle size of CuPc increases at higher (e.g. 28%) CuPc. Dyes such as phthalocyanines are reported to form agglomerates at a higher compositions [47-49]. Similar phenomenon of agglomeration can be observed to occur in the present composites as evidenced by the increasing particle size of CuPc. Exposure of these composites to pyrrole show the presence of black deposits of PPy as indicated by the **Fig. 3.31(a) and (b).** An interesting fact observed in these micrographs is the exclusive deposition of PPy on the CuPc particles. These micrographs also show a networking of the PPy deposits all throughout the matrix whereas no networking is observed in the case of PEO-$CuCl_2$ exposed to pyrrole for the same time interval. It is thus clear that the CuPc-$CuCl_2$ association provides sites for initiating the vapour phase polymerization process for PPy, which then proceeds in the bulk forming a network.

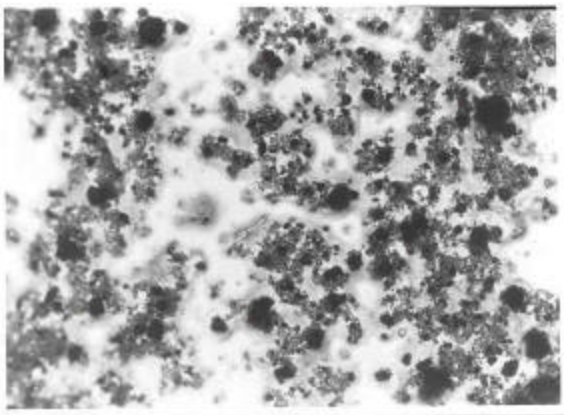

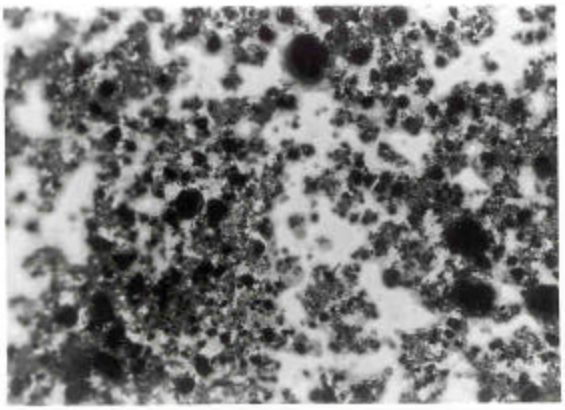

Fig. 3.31 Optical micrographs of PPy/CuPc in-situ composite with CuPc containing (a) 5 and (b) 23% CuPc respectively. Exposure to pyrrole 30 sec

The above findings suggest that CuPc associated with $CuCl_2$ acts as an initiator and hence a

catalyst in the polymerization process of PPy which results in a fast deposition of PPy and hence a rapid rise in the conductivity. The time dependence of the reaction was further investigated by applying the conventional equation for kinetics [50].

$$\ln t = a \ln x + bx^c + d \qquad \text{Eq. 3.11}$$

where a = (1-n),

d = - ln (1-n) k

$x = [\sigma_{(t)} - \sigma_{(0)}] / [\sigma_{(\alpha)} - \sigma_{(0)}]$

t is the time, n the reaction order, k the rate parameters;

a,b,c are the constants, x the fractional change in conductivity,

$\sigma_{(0)}$, $\sigma_{(t)}$ and $\sigma_{(\infty)}$ the electrical conductivities at time 0, t and ∞ respectively.

Plots of x or ΔR {as $[\sigma_{(t)} - \sigma_{(0)}] / [\sigma_{(\infty)} - \sigma_{(0)}]$} against the time on a log-log scale was made for the initial rise in conductivity as depicted by the **Fig.3.32**, where the $\sigma_{(0)}$ as taken as the conductivity value at zero time exposure, while $\sigma_{(\alpha)}$ was taken as the conductivity at the saturation limit. The plots are observed to be straight lines with varying slopes that are plotted with respect to the CuPc composition as in the **Fig.3.33**. It is observed that 2% CuPc composition exhibits a maximum denoting a faster rise in the conductivity. It may be expected that at higher concentrations of CuPc, the more number of nucleating sites present would give rise to a much-enhanced deposition of PPy yielding a high rate of reaction. But exactly the opposite phenomenon is observed, wherein the rate is seen to decrease at higher concentrations of CuPc. This can be understood as follows. Referring to the **Fig 3.31** again, one can notice that there is agglomeration of the CuPc particles resulting in the formation of large particles. Thus, the surface to volume ratio is found to be lower in the case of agglomerates than for the individual particle. , the initiation of polymerization reaction occurring mainly on the active surface of CuPc. Due to the agglomeration of CuPc, the net active area available for the polymerization reaction reduces leading to lower rate than that at lower CuPc content. (It is still higher than the case of 0% CuPc. Hence an optimum surface of 2% CuPc content is observed which gives the most rapid deposition of PPy.

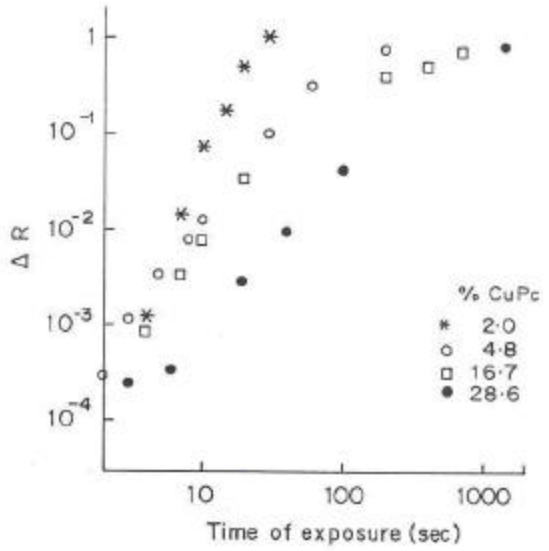

Fig. 3.32 Variation of the ΔR with the time of exposure on a log-log scale

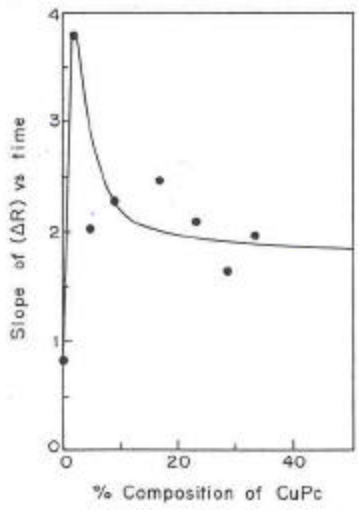

Fig. 3.33 Dependence of slope of ΔR vs time on the composition of CuPc for the in-situ PPy/CuPc composite

(b) Compositional dependence of conductivity:

Investigations were made for the dependence of conductivity on CuPc concentration as well as $CuCl_2$ doping level. **Fig 3.34** shows the variation of conductivity with CuPc concentration varying from 2% to 45% by weight with $CuCl_2$ concentration being held constant at 4:1 m/M in the PEO matrix. Curve (A) corresponds to the original PEO-$CuCl_2$ matrix with no PPy while curves B and C correspond to the partially exposed and fully exposed samples respectively. It is evident from the above figure that incorporation of small amount of CuPc (even <10%) leads to a large increase of conductivity after PPy deposition. There is some increase of conductivity by incorporation of large quantity of CuPc (> 20%) even in PEO-$CuCl_2$ by itself but the change in conductivity after PPy formation is almost 6 orders of magnitude. If the dopant ($CuCl_2$) content was varied keeping CuPc concentration the same, (40%), the conductivity was again seen to increase with the increase of $CuCl_2$ concentration as shown in the **Fig. 3.35**. In this case it is also seen that the exposure to pyrrole (short or long time) leads to a tremendous increase of conductivity at all concentrations.

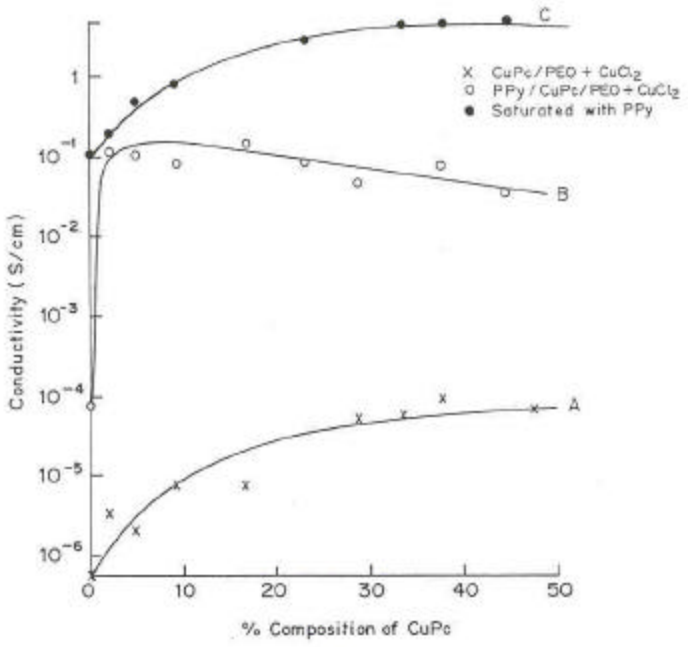

Fig. 3.34 Compositional dependence of conductivity with respect to the CuPc concentration for the PPy/CuPc in-situ composite. Curves represent (A) CuPc in PEO-$CuCl_2$ (B) CuPc/PEO-$CuCl_2$ exposed to pyrrole for 1 minute and (C) exposed to pyrrole till saturation

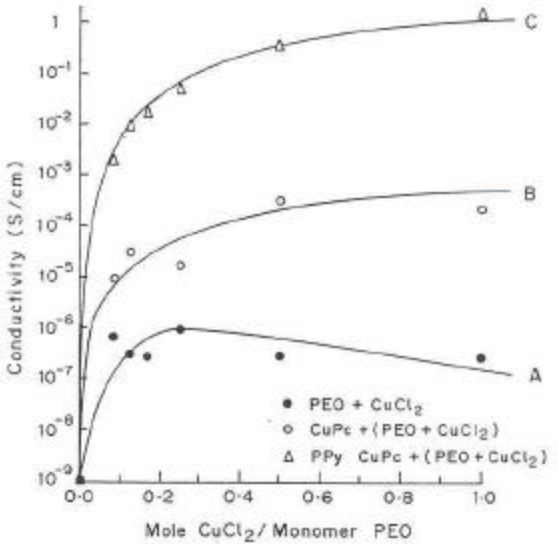

Fig. 3.35 Dependence of conductivity on the $CuCl_2$ content in PEO for the PPy/CuPc in-situ composite containing 40% CuPc. Curves (A) to (C) correspond to PEO-$CuCl_2$, CuPc/PEO-$CuCl_2$ and PPy/CuPc/PEO-$CuCl_2$ (partially exposed to PPy)

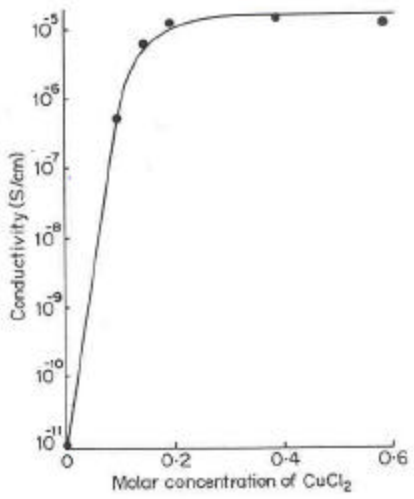

Fig. 3.36 Variation of conductivity of CuPc with $CuCl_2$ doping

These various findings can be explained as follows. The incorporation of CuPc in PEO-$CuCl_2$ leads to slight increase in conductivity, which is possibly due to doping of CuPc by

electron acceptors such as $CuCl_2$ or even chlorine ions. On the other hand, exposure of these composite films to pyrrole, causes PPy deposition on these various semiconducting domains making them more conducting and finally highly conducting due to the formation of continuous network of conducting PPy. As mentioned in the earlier section 1.3.5 (a), CuPc may be acting as a catalyst/initiator for the PPy formation. In order to confirm these hypothesis, further investigations were carried out to study the interaction between CuPc particles and $CuCl_2$ as well as the formation of PPy in these composite films.

The **Fig 3.36** illustrates changes occurring in the conductivity of CuPc powder by using different concentrations of $CuCl_2$. 0.5 gm of CuPc powder was dropped in methanolic solution of $CuCl_2$ in the concentration range of 0.05 to 0.6 M. The powder obtained was filtered and dried. An increase in the conductivity of CuPc from 10^{-8} S/cm to 10^{-5} S/cm is observed till 0.2 M addition of $CuCl_2$ where after it saturates. The increase in the conductivity of CuPc by doping with iodine is well reported by several authors [51-53]. The rise in conductivity by 8 to 15 orders of magnitude has been obtained for $MpcI_x$ where the x varies from 0.2 to 1.7. Similar possibility of 'doping' of CuPc by $CuCl_2$ can be envisaged in the present case. It is clear from the plot that highest conductivity corresponding to the maximum doping occurs at 0.2M $CuCl_2$. Micro-analytical studies were carried out for the CuPc-$CuCl_2$ complex possessing the saturated conductivity. The analysis showed the presence of 1.22% chlorine content. In recent years, an intensively growing number of partially oxidized metal phthalocyanine derivatives have been reported [54,55]. Among these systems particularly interesting are the I_2 doped, co-facially assembled, salt-like aggregates obtained from simple metal phthalocyanine units or polymeric metalloxanes of formula $[M(Pc)O]_n$, (M=Si,Ge) and simplified as $PcNi(I_3)_{0.33}$ and $\{M(Pc)O]I_{1.1}\}_n$. Common features of these doped materials are:

(a) ligand-centered interaction, with the central metal ion experiencing in all cases a stable oxidation state,

(b) attainment by each Pc unit in the stacked polymer, of a non-integral oxidation state, i.e. +0.33, or close to it,

(c) associated presence of parrallel chains of I_3^- ions,

(d) electrical conductivity measured on polycrystalline samples in the range 0.1 to 1 S/cm.

Thus similarities can be drawn in the present context, with the iodine doping occurring in phthalocyanines. The doping process may occur via bridging of the CuPc molecules. The chlorine in $CuCl_2$ forms a coordinate bond with the central metal ion-Cu in the phthalocyanine ring that is originally connected by two covalent and two dative with the nitrogen atoms of the ring. $CuCl_2$ thus acts as a source of Cl ions, which create bridges between the CuPc linking them together forming a network of CuPc. In these compounds, the phthalocyaninato ligand (dianionicligand) forces the central metal atom in a square planar configuration. The highly conductive material is built up of stacks of metallophthalocyanine units and chains of polyhalide anions [56-57]. Structurally, the $CuCl_2$ can be imagined to be present in the interstitial spaces between the CuPc lattice stackings. The bridging of CuPc thus leads to a conjugation in the system resulting in an electrically conducting CuPc. It may be interesting to note that the doping of CuPc by $CuCl_2$ through bridging of the central Cu atoms of phthalocyanine would render a partial charge on the nitrogen atoms of the porphyrin ring structure inducing more polarity in the Cu-N bonding. The distribution of charges was further investigated by XPS analysis of the CuPc with different levels of $CuCl_2$. The C_{1s}, and N_{1s} core level spectra for 0.1, 0.15 and 0.2 M $CuCl_2$ content are indicated by the **Fig. 3.37**. The various species obtained after deconvolution and the areas under the respective peaks are presented as **Table 3.5**. It is observed the C_{1s} does not show a reasonable change in the peak area. On the other hand, the N(I) species exhibits a considerable decrease in the relative contribution from 65.6% to 37.4% as the doping level of CuPc increases whereas the N(II) and N(III) species indicate an increase in their respective contributions. N(II) shows an increase from 21.5% to 47.1% in case of 0.2M $CuCl_2$ while N(III) rises from 13% to 15.5%.

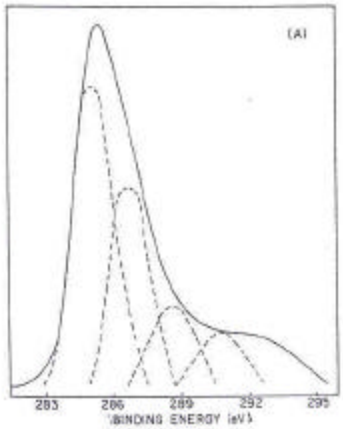
(A)
283
286
289
292
295
BINDING ENERGY (eV)

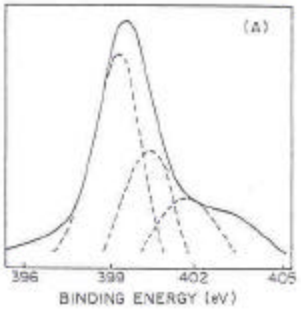
(A)
396
399
402
405
BINDING ENERGY (eV)

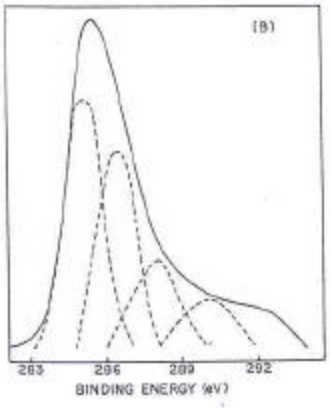
(B)
283
286
289
292
BINDING ENERGY (eV)

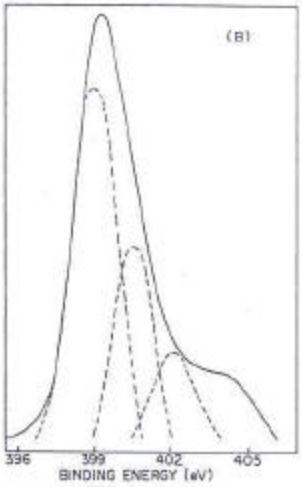
(B)
396
399
402
405
BINDING ENERGY (eV)

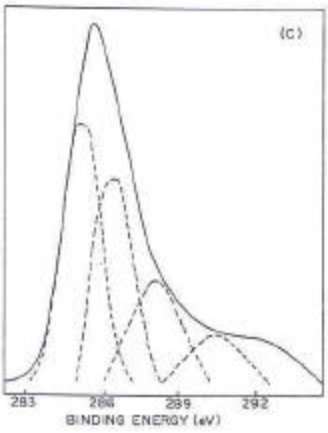
(C)
283
286
289
292
BINDING ENERGY (eV)

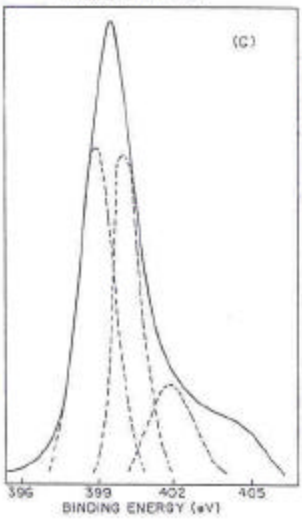
(C)
396
399
402
405
BINDING ENERGY (eV)

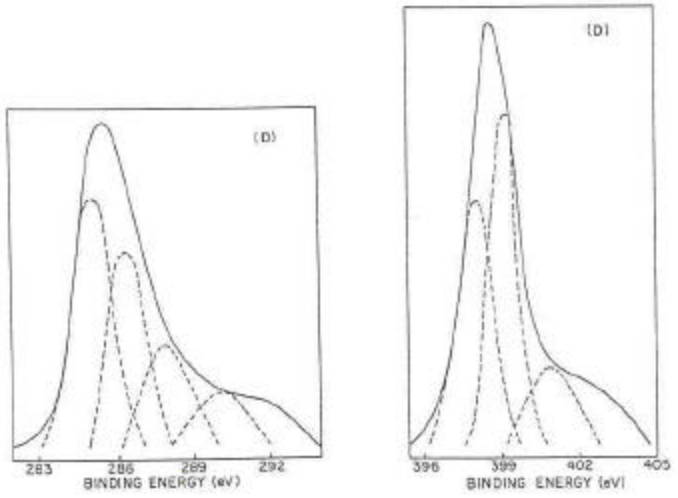

Fig. 3.37 C_{1S} and N_{1S} XPS core level spectra for CuPc doped with $CuCl_2$. $CuCl_2$ concentrations are (A) 0.0 M, (B) 0.5 M, (C) 0.75 M, (D) 0.1 M

Table 3.5 XPS results for CuPc powder doped with different $CuCl_2$ concentrations

Chemical species		CuPc powder doped with $CuCl_2$			
		Relative percentage contribution			
		0.0 M $CuCl_2$	0.5 M $CuCl_2$	0.75M $CuCl_2$	0.1M $CuCl_2$
C_{1s}	C(I)	51.0	44.82	38.78	40.62
	C(II)	29.0	29.27	31.84	30.40
	C(III)	11.4	16.52	20.21	8.53
	C(IV)	7.8	9.38	9.18	10.44
N_{1s}	N(I)	55.0	65.58	48.11	37.34
	N(II)	31.0	21.51	36.98	47.13
	N(III)	13.9	12.90	14.90	15.52

Thus it is clear that CuPc gets doped by $CuCl_2$ resulting in highly charged N_{1s} species. This

implies that CuPc conductivity increases in the presence of $CuCl_2$ leading to higher conductivity in PEO-$CuCl_2$ containing CuPc.

Morphological studies indicate the presence of domain structures as observed in the optical micrograph represented by **Fig. 3.30 (a), (b)** and **(c**). It is also noticed that the individual CuPc particles get closer as the CuPc concentration increases. Comparison of the micrographs indicates that the domain size as well as the distribution changes with CuPc addition. The domains are seen increasing in size along with a decrease in the interdomain distance. An important fact to be noted is that the CuPc is confined to the domains and is not randomly distributed in the matrix. PPy deposition also results in an increase in the conductivity of the system that is indicated by the **Figs.3.33** and **3.34.** The optical micrographs for the composites show a network formation on exposure to PPy (see **Fig 3.38** (a) and (b) for the composite containing 5% CuPc, exposed to pyrrole for 20 and 45 sec respectively), which implies that PPy connects the domains together by establishing conducting channels yielding a higher conductivity. In the case of composites partially exposed to pyrrole the CuPc content plays an important role in deciding the ultimate conductivity. In this case the CuPc particles get coated with PPy, which leads to a decrease in the interparticulate distance and higher conductivity. This would continue till a stage is reached when a network of conducting particles is formed; either due to high CuPc content or high PPy content. For example, in the composite films exposed to pyrrole till saturation is reached, the conductivity exhibits a rise in the conductivity till 16% CuPc addition and then saturates to a value of 4 S/cm. The high conductivity of these composites can be attributed to the PPy network formation.

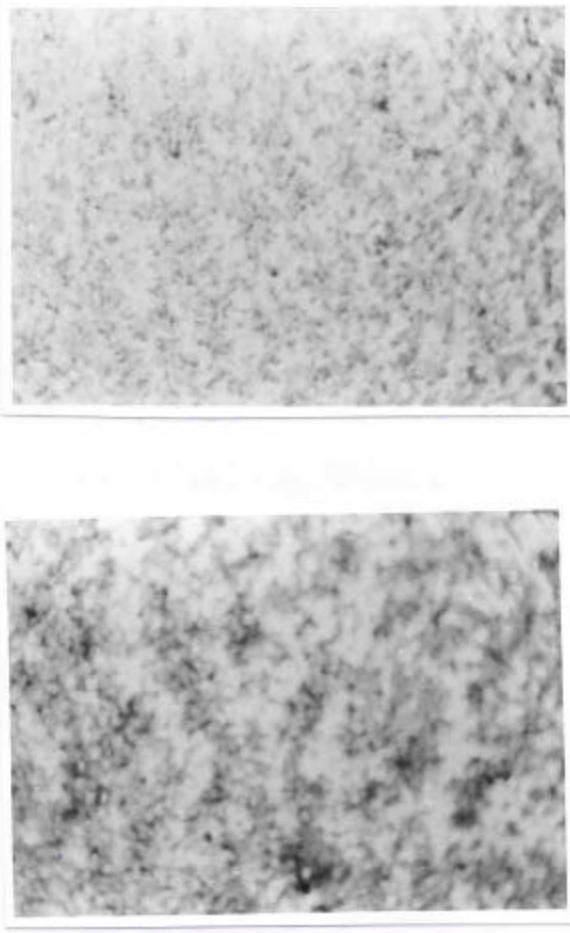

Figure 3.38 Optical micrographs of PPy/CuPc in-situ composite containing 5 % CuPc exposed to pyrrole for (a) 20 sec and (b) 45 sec respectively

The thermal stability of PPy composites with CuPc was studied using TGA. **Fig. 3.39 (A),**

(B), (C) and **(D)** denote the TGA curves in an inert atmosphere at a heating rate of 10°/min, for PEO-$CuCl_2$ (4:1 monomer/mole) and the composites containing 0, 5, 40 % CuPc exposed to pyrrole till saturation respectively. TGA analysis of PEO-$CuCl_2$ (see curve A) depicts two steps in the temperature region of room temperature to 300° C. The first peak occurring at 145°C may be attributed to the entrapped solvent: methanol/water while the second peak around 284.6°C may be due to the decomposition of $CuCl_2$ due to the loss in the chlorine content resulting in the formation of CuCl. The degradation of pure PPy is gradual over the entire temperature range with a total weight loss of 79.5%. The PPy formed in the composite can be estimated using the relation,

The observed weight loss	=	The calculated weight loss of PEO	+	PPy degradation	Eq 3.12

The weight percent of PEO was calculated from the composition used. Content of PPy calculated along with the actual percentage weight loss observed are tabulated as **Table**. **3.6.**

It is clearly observed from the results that the PPy content increases as the CuPc increases. The composite with 28% CuPc contains around 19.6% of PPy that remains more or less constant even as the CuPc increases and is supported by the conductivity against composition studies.

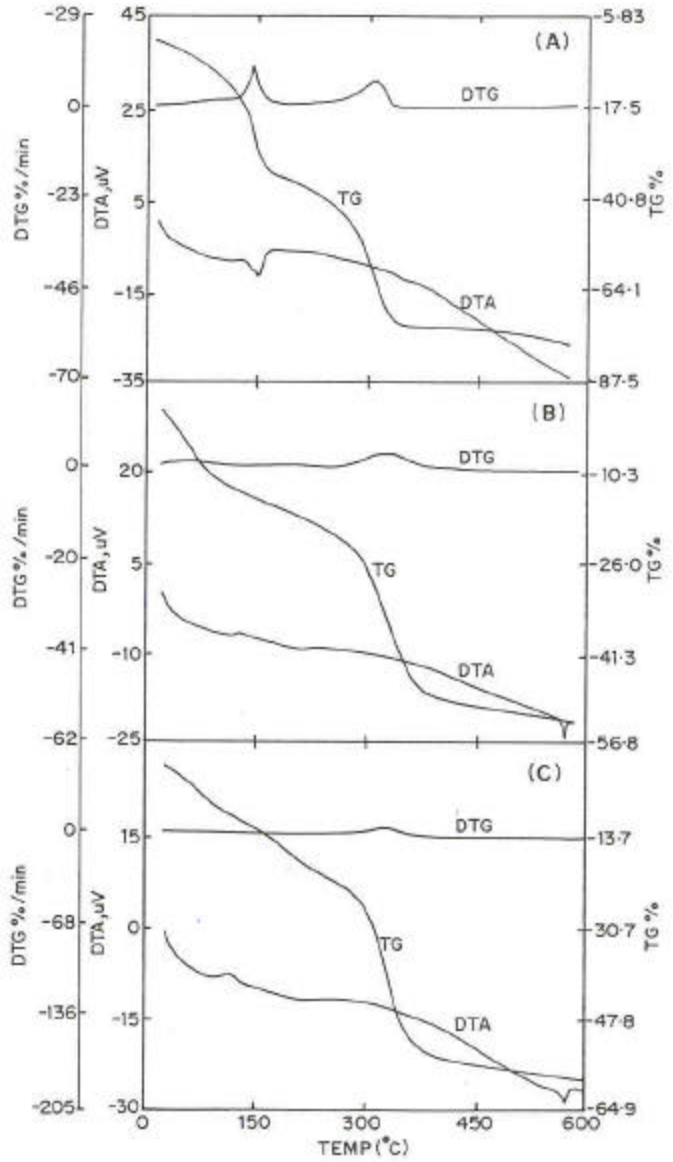
(A)
(B)
(C)
DTG
TG
DTA
DTG %/min
DTA, μV
TG %
TEMP (°C)
0
150
300
450
600

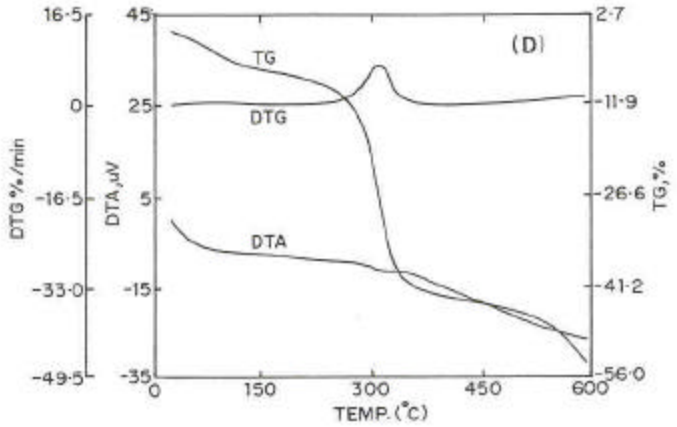

Fig. 3.39 TGA analysis of the PPy/CuPc in-situ composites. Curves correspond to (A)PEO-$CuCl_2$ (4:1 monomer/mole), (B) PPy/PEO-$CuCl_2$, (C) PPy/ CuPc/PEO-$CuCl_2$ containing 5% CuPc, (D)containing 23% CuPc. (B), (C) and (D) are exposed to pyrrole till saturation

Table 3.6 Amount of PPy determined from TGA analysis

% Composition of CuPc in PEO-$CuCl_2$	% PPy content as determined from TGA analysis
0	10.91
5	16.51
9	16.57
28	19.62

(c) I-V characteristics of the PPy/CuPc in-situ composite:

The charge transport processes in the in-situ composite without PPy and with exposure to pyrrole were carried out by recording the I-V characteristics. The influence of parameters such as the dopant ion concentration and the CuPc composition was also investigated.

(1) Variation of $CuCl_2$:

The I-V characteristics of the CuPc/PEO-$CuCl_2$ composites were investigated as a function of the $CuCl_2$ concentration with a constant CuPc content of 28% and are indicated in the **Fig. 3.40**. It is observed that the I-V curves are non-linear; the degree of non-linearity is found decreasing with increasing $CuCl_2$. These were then analyzed for the Poole-Frenkel type of conduction mechanism by making plots of log I Vs $V^{1/2}$ that are found to be straight lines as illustrated in the **Fig. 3.41(inset)**. The slopes of the log I Vs $V^{1/2}$ plots exhibit a decrease with respect to an increase in the $CuCl_2$ concentration (see **Fig 3.41**). These findings suggest of a barrier formation at the CuPc/PEO-$CuCl_2$ interface. Considering the energy band diagram as given in the **Fig. 3.42**, it can be noticed that a barrier of 0.3 eV exists at the interface of the materials causing non-linearity in the I-V characteristics. The decrease in the non-linearity of the I-V curves and hence the decrease in the slope with the rise in $CuCl_2$ from 8:1 to 1:1 monomer/mole, can be understood in terms of doping of CuPc. Higher doping results at increased $CuCl_2$ contents in PEO-$CuCl_2$. This introduces trapping centers in CuPc resulting in lowering the barrier at the CuPc/PEO-$CuCl_2$ interface at higher $CuCl_2$ contents causing lower slopes.

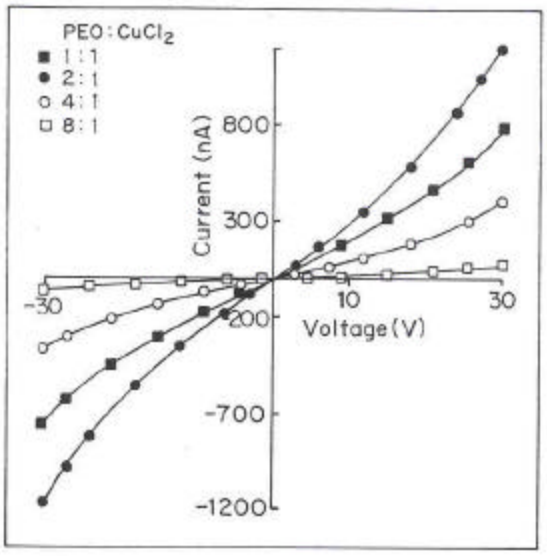

Fig. 3.40 Current-voltage characteristics for 23% CuPc dispersed in PEO-$CuCl_2$ containing varying $CuCl_2$ content

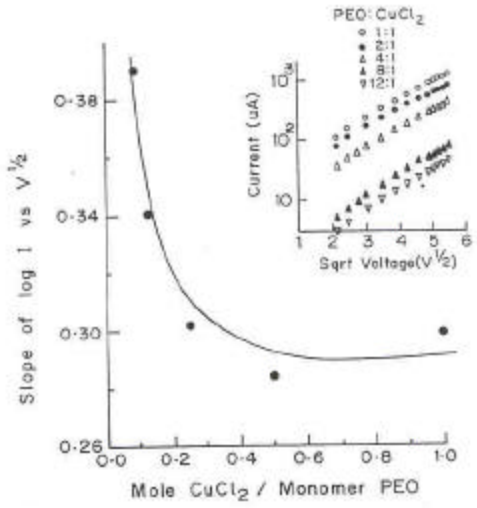

Fig. 3.41 [Inset showing the linear dependence of log I on $V^{1/2}$]
Variation of slope of log I vs $V^{1/2}$ with respect to the $CuCl_2$ concentration

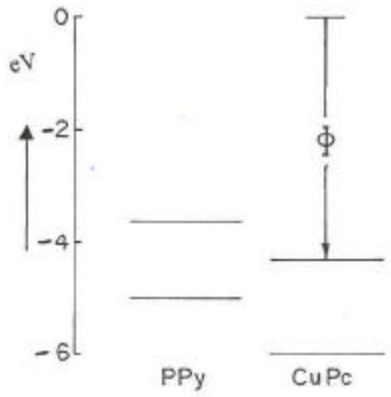

Fig. 3.42 Band diagram showing the energy levels for PPy, CuPc

Exposure of the above composites to pyrrole, yields I-V curves that tend to be less non-linear in nature in comparison to that without PPy deposition (see **Fig 3.43**). The I-V curves

were plotted as log I vs $V^{1/2}$. The plots followed a linear dependence; the slopes of which are presented as a function of the $CuCl_2$ concentration in the **Fig.3.44.** An increase in the slopes is observed as the $CuCl_2$ increases causing a decrease in the interdomain distance hence reducing the interparticulate distance between the PPy deposits leading to an increase in the slope of the logI / $V^{1/2}$ plot. PPy deposition takes place along the CuPc particles that form a charge transfer complex with $CuCl_2$. Increased deposition of PPy takes place at high $CuCl_2$ contents as discussed in section 1.3.5 (b). The deposition of PPy on CuPc increases the size of the particles decreasing the interparticle distance hence the slope of log I / $V^{1/2}$ is observed to be affected more at higher $CuCl_2$ contents. Taking into account the energy levels of PPy and CuPc, it can be noted that a barrier of 0.7 eV is present at the PPy/CuPc interface.

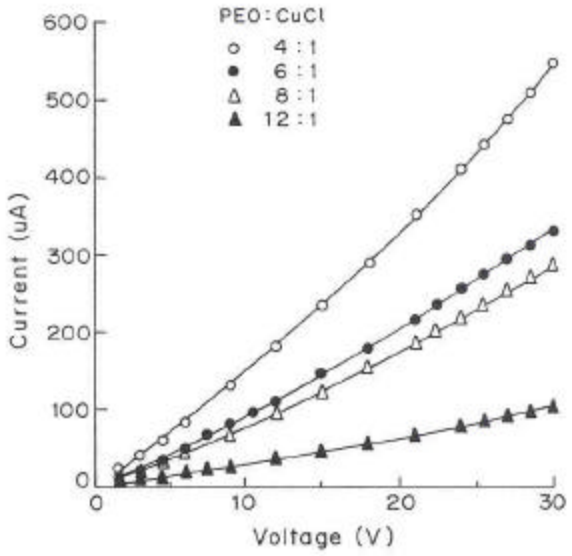

Fig. 3.43 I-V characteristics for the PPy/CuPc/PEO-$CuCl_2$ composite with varying $CuCl_2$ (CuPc 23%, exposure to pyrrole 1 min)

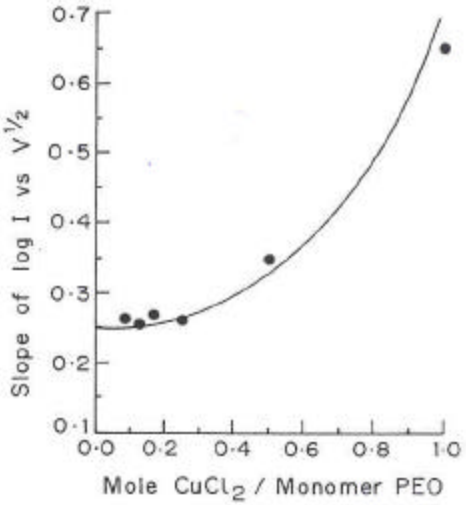

Fig. 3.44 Variation of slope of log $I/V^{1/2}$ with the $CuCl_2$ content for the PPy/CuPc in-situ composite

In order to investigate the junction at the PPy/CuPc, single junction studies were carried out

[58]. A multilayered cell was constructed using electrochemically deposited PPy and vacuum deposited CuPc. The I-V characteristics exhibited strong non-linearity and sometimes-peculiar features such as a peak in the current and negative resistance characteristics above certain applied voltage which depended on the thickness of the CuPc film (see **Fig.3.45**). These characteristics are reminiscent of tunneling type of behaviour observed in thin film semiconductor/insulator structures [59-61]. In the case of Fowler-Nordhiem tunneling, the I-V characteristics are governed by the equation, [62]

$$J = (3.38 \times 10^{10} F^2 / \Phi)\exp(-0.69\phi^{3/2} / F) \qquad \text{Eq. 3.13}$$

With

$$F = V/d$$

Where J is the current density (in A/cm^2), F is the electric field, V the voltage, d the thickness and Φ the barrier height in eV. **Fig 3.46** shows the Fowler-Nordhiem plot, log (I/V^2) against (1/V), for the initial rising portion of the I-V characteristics for the samples having different thicknesses of CuPc. The linearity in all the cases is evident but with a slight change in the slope especially for thicker CuPc films. In the latter cases, there will be some potential drop across the CuPc prior to the active region and hence the applied voltage will not appear wholly across the interface, giving rise to a change of slope in the above graph. A barrier of 0.9 eV can be calculated from the energy band diagram.

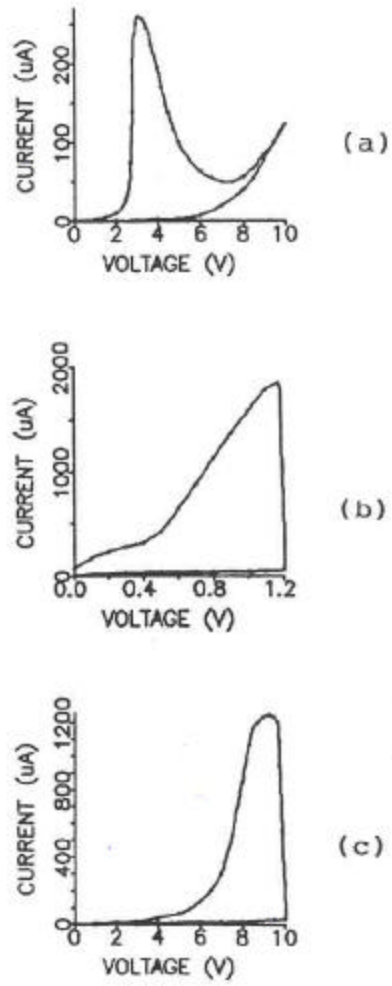

Fig. 3.45 I-V characteristics of Au/PPy/CuPc/Al junctions showing tunneling type behaviour. The CuPc thickness is (a) 35 nm (b) 58 nm (c) 140 nm respectively. Device area is 0.25 cm^2.

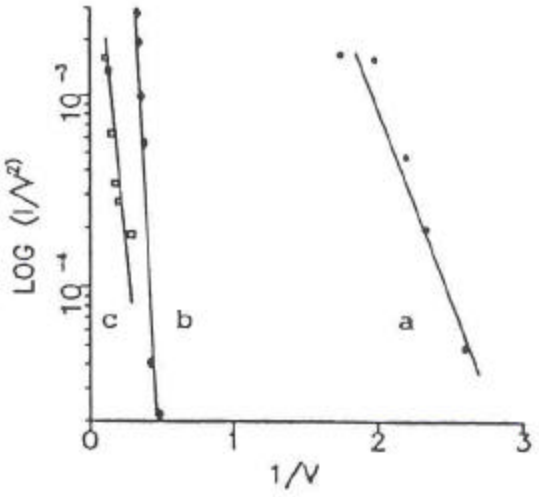

Fig. 3.46 Fowler-Nordhiem plot for the initial part of the I-V characteristics depicted in the Fig. 3.45

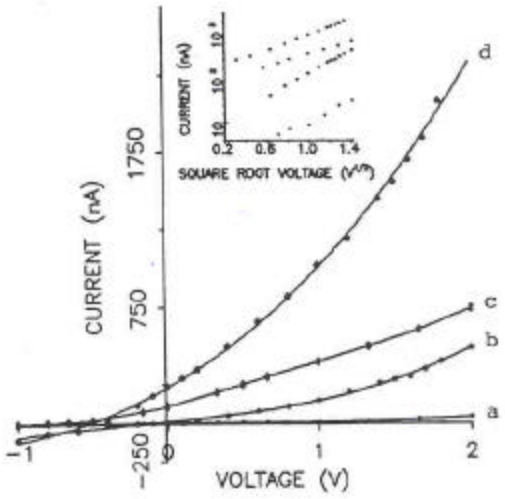

Fig. 3.47 I-V characteristics of Au/PPy/CuPc/Al junctions deposited on substrates with polyvinyl butyral backing layer. The curves (a) and (c) are for dark and illumination (2 mW/cm^2) with CuPc thickness of 28 nm while (b) and (d) are similar curves for CuPc thickness of 43 nm respectively. The inset shows the linearity of log I- $V^{1/2}$ plot as per the Schottky equation. Device area 0.25 cm^2.

Interestingly, the samples having polyvinyl butyral (PVB) backing layer not only showed different behaviour than above but also exhibited high photosensitivity. **Fig. 3.47** depicts the

typical I-V characteristics in these cases. Although the I-V characteristics are strongly non-linear, there was no tunneling type characteristic observed for the whole range of thickness for CuPc used. On the other hand, these follow Richardson-Schottky equation (see the inset of the **Fig.3.47**):

$$J = AT^2 \exp(-\phi/kT) \exp(\beta V^{1/2}/d^{1/2}kT) \qquad \text{Eq. 3.14}$$

where A is constant, T the temperature, k the Boltzmann constant and β the Schottky parameter dependent on the dielectric constant. It may be of interest to mention here that such type of characteristics have been reported for conducting polymer-Rhodamine B junctions [63]. These differences in the nature of the I-V characteristics could be associated with the crystalline nature and morphology of the CuPc films obtained in the two cases of substrates with backing PVB film and those without the backing layer. It may be noted that PVB does not come in contact with the top junction layer. Hence, detailed studies were carried out on the nature of the CuPc films deposited on the bare substrates and those precoated with PVB prior to deposition. These films were observed under the optical polarizing microscope and it was noted that the CuPc films without backing layer appeared amorphous, uniform without any grains while those deposited on the substrates with backing layer were granular (see **Fig. 3.48**).

a

b

Fig. 3.48 Morphology of vacuum deposited CuPc films on (a) bare glass substrate and (b) substrate precoated with polyvinyl butyral.

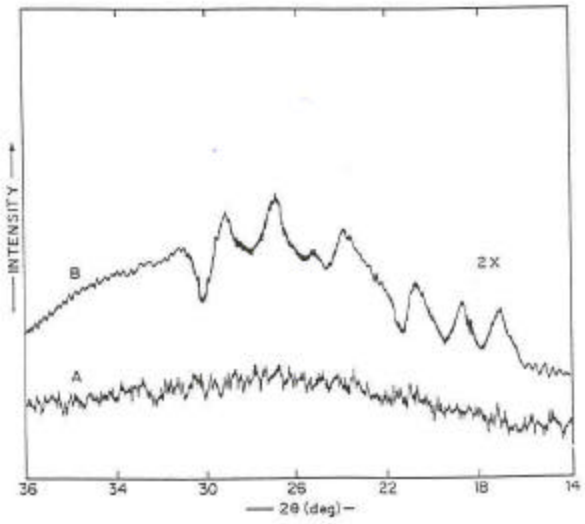

Fig. 3.49 X-ray diffraction scans of CuPc films on glass substrates without preconditioning (curve A) and with precoating of PVB (curve B). For the latter case the sensitivity was increased to two times

These CuPc films were further characterized by X-ray diffraction (XRD). **Fig.3.49** shows the

XRD scans for the CuPc films deposited on glass substrate (curve A) and those deposited on treated substrates (curve B). The latter was taken at higher sensitivity scale in order to bring out the small peaks superimposed on the broad amorphous background. It is clearly seen that whereas the CuPc films on bare glass substrates are wholly amorphous, those deposited on pretreated substrates exhibit some crystallinity. The detailed analysis of these XRD peaks revealed that the films contain a mixture of α and β phases of CuPc. Strong influence of the substrate on the crystalline nature and morphology of CuPc has been reported earlier [64-66]. The nature of the CuPc films can change from amorphous to crystalline and even epitaxial by change of the substrate temperature and/or its crystalline state. In the present case the substrate temperature was low (25°C) and hence only amorphous CuPc was obtained on plain glass substrates (as mentioned in the references) but these films become granular and slightly crystalline on the PVB coated substrates.

From the above discussion it is observed that a Schottky barrier exists at the PPy/CuPc interface. These are present as discrete junctions in case of the composites. This leads to the formation of multiple junctions yielding properties that is a collective effect of the discrete junctions.

The composite system as described above, when saturated with PPy exhibits linear I-V characteristics. The network formation destroys the barriers leading to ohmic I-V characteristics. A comparison of the I-V characteristics of the unexposed, partly exposed and fully exposed composites containing 4:1 PEO-$CuCl_2$ is presented in the **Fig.3.50**. A gradual change in the nature of I-V characteristics from non-linear to linear is clearly brought out. Gradual exposure of the composites to pyrrole gives rise to the formation of a continuous network of PPy in the matrix. Thus the barrier at the PPy/CuPc interface is present at lower PPy contents while higher exposure leads to short-circuiting of the barriers and hence linear I-V characteristics as is clearly noticed.

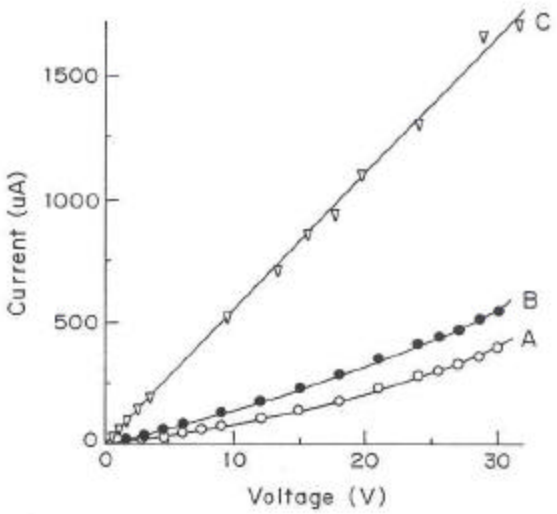

Fig. 3.50 I-V characteristics of PPy/CuPc in-situ composite containing 23% CuPc. Curves (A) to (C) represent CuPc/PEO-$CuCl_2$ unexposed, partly exposed and fully exposed to pyrrole. [Voltage in mV for data plotted in (c)]

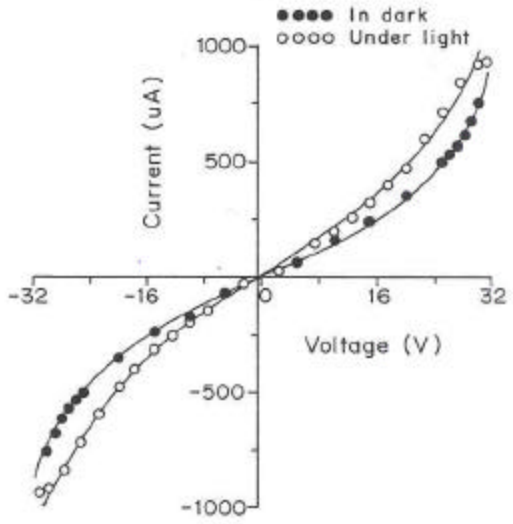

Fig. 3.51 I-V characteristics of PPy/CuPc in-situ composite containing 2% CuPc with PEO -$CuCl_2$ (4:1 monomer/mole concentration)

(2) Variation of CuPc:

The I-V characteristics obtained for the composite system with partial deposition of PPy are found to be non-linear in nature for the compositions ranging from 2 to 40% CuPc by weight (see **Fig 3.51** for the composite containing 2% CuPc). The I-V characteristics were then plotted as log I vs. $V^{1/2}$; the slopes of which are depicted in the **Fig. 3.52**. The variation of the slope showing a decrease from 0.7 to around 0.35 at 28% and then rises further almost to 0.65 at 40% CuPc composition. This decrease in the slope of log I / $V^{1/2}$ can be understood by considering the dependence of the slope on the interparticle distance, 'd'. Dispersion of CuPc in the PEO-$CuCl_2$ matrix results in the formation of aggregates as evidenced by the micrographs. Thus the particle size increases reducing the surface to volume ratio and hence the area of contact. As the CuPc dispersion increases, the extent of agglomeration is also raised yielding bigger particles of CuPc. Consequently, the interparticle distance ($d^{1/2}$) increases resulting in a higher slope. On the other hand, at higher compositions, the concentration of the aggregates in the matrix increases hence decreasing the particle to particle distance that brings about an increase in the slope of the log I / $V^{1/2}$.

In case of the composites saturated with PPy, the I-V characteristics are linear in all the cases exhibiting an ohmic type of conduction. This implies that no barriers exist at the PPy/CuPc interface due to extensive network formation of PPy throughout the matrix.

(d) Temperature dependence of conductivity:

Fig 3.53 illustrates the variation of conductivity against temperature for the PPy/CuPc composites with partial deposition of PPy.

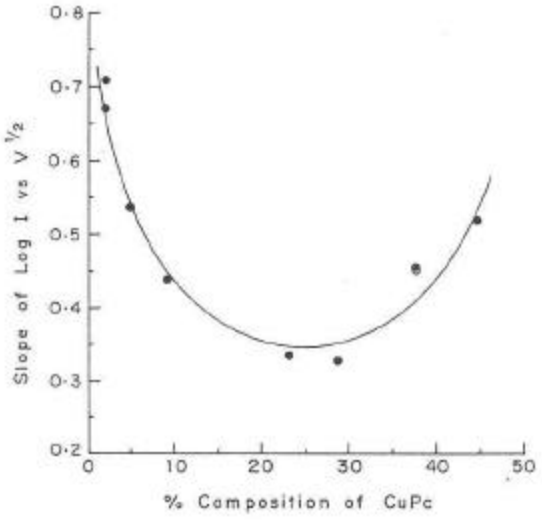

Fig. 3.52 Variation of slope of log I/ $V^{1/2}$ with respect to the composition of CuPc in the PPy/CuPc composite

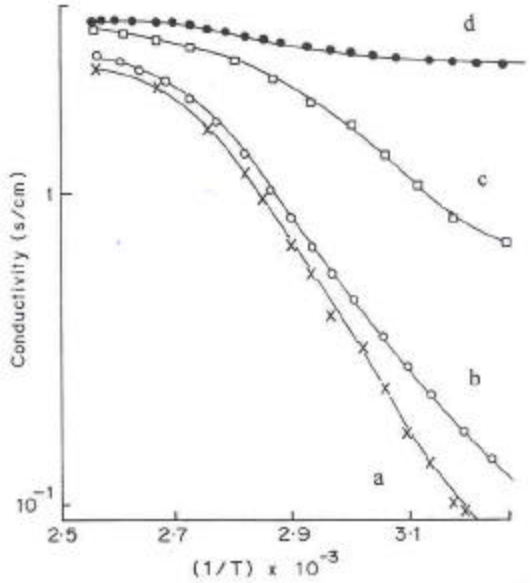

Fig. 3.53 Temperature dependence of conductivity for PPy/CuPc in-situ composite with partial deposition of PPy. Curves (a), (b), (c) and (d) correspond to 0.5, 16.7, 28.6 and 44.4 % CuPc composition

It is observed that the σ-T plots follow a 1/T dependence of temperature. The slopes are

found to decrease with the CuPc composition and then remain almost constant. The activation energies are calculated using the Arrhenius equation as,

$$\nabla E = 1.98 \times 10^{-4} \left\{ \frac{\log_{10} I_2 / I_1}{1/T_2 - 1/T_1} \right\} \qquad \text{Eq. 3.15}$$

and are presented in the **Fig 3.54**. These are observed to decrease till 25% CuPc composition and then almost remain constant. This can be co-related with the lowering of the barrier width at the PPy/CuPc interface due to the increased deposition of PPy till 25% CuPc content beyond which the agglomeration reduces the deposition of PPy content and the barrier width is restored slightly exhibiting an increase in the activation energy.

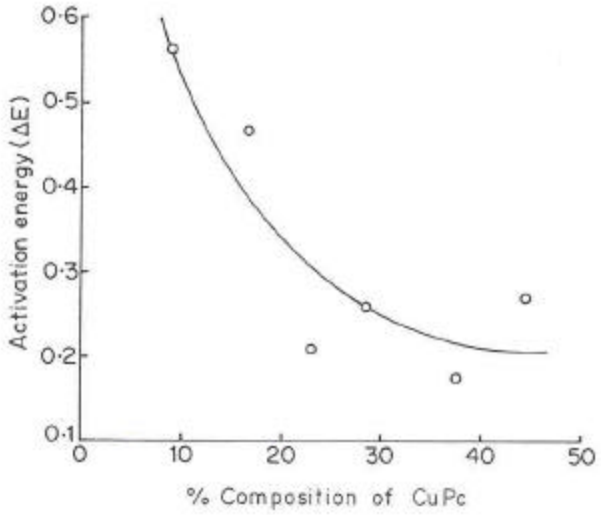

Fig. 3.54 Decrease of activation energy with varying CuPc content for the PPy/CuPc in-situ composite

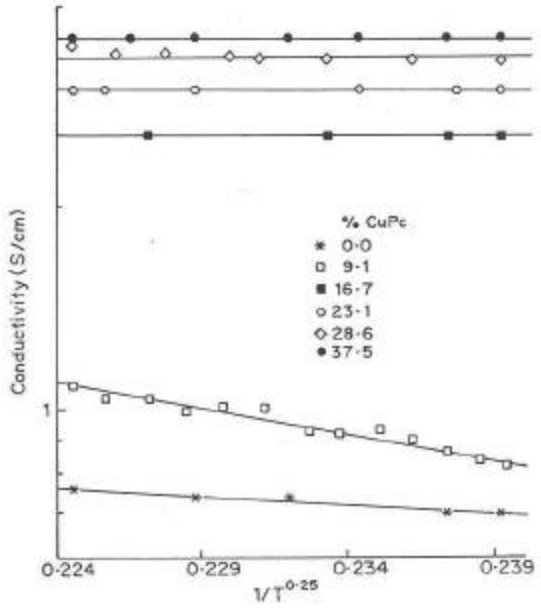

Fig. 3.55 Temperature dependence of conductivity for the PPy/CuPc in-situ composites saturated with pyrrole

Composites saturated with PPy exhibit σ-T plots as presented in the **Fig. 3.55**. The electrons hence experience no barriers for conduction due to the conducting network formation.

(e) Photosensitivity:

The light sensitivity factor (S) was calculated as I_l / I_d. A maximum sensitivity of 1.6 is observed for the composite containing 10% CuPc in PEO- $CuCl_2$. Higher photosensitivity was expected due to the barrier formation at the PPy/CuPc interface. Charge carriers would be generated due to illumination. These would then undergo separation at the under the influence of the surrounding field and get transferred to PPy resulting in a large photocurrent. A large photocurrent is thereby expected due to the formation of multiple junctions. On the contrary, a very low photocurrent is observed for the system. This can be understood on the basis of doping effect CuPc. The formation of a charge transfer complex with $CuCl_2$, gives rise to trapping centers in the energy band gap. Thus, the formation of charge transfer complex with $CuCl_2$ gives rise to trapping centers in the energy band gap. During the process of excitation, most of the excited electrons are trapped by the impurity centers that further undergo recombination. The excitation process is thus dominated by trapping and recombination phenomena. Consequently, very less electrons are available for conduction resulting in a low photoconductivity.

3.4 Conclusions:

PPy/PEO blends exhibit a variation in the charge transport behaviour due to a difference in the method of synthesis. The conductivity of the ex-situ blend follows the percolation model and shows a percolation threshold at 2.5% PPy content. The presence of a barrier at the PPy/PEO-$CuCl_2$ is well reflected in the I-V characteristics and the blend obeys a Poole–Frenkel type of conduction mechanism. In case of the in-situ blend, the dispersion of PPy/PEO-$CuCl_2$ is achieved at a microscopic level exhibiting a much higher conductivity (1 S/cm) and a quite lower percolation threshold. An easy switching of PPy between the conducting and the non-conducting states was achieved across the PEO-$CuCl_2$ solid polymer electrolyte, indicated the presence of Cu^{+}/Cu^{++} couple that facilitated the transfer of electrons between the bipolaronic states of PPy and the redox couple. This was also evidenced by the single junction studies at the PPy and the SPE but with a difference that only Cu^{++} takes part

in the reaction as against the redox in the in-situ case. Hence the role of PEO-$CuCl_2$ as an efficient solid polymer electrolyte is clarified.

The PPy/CuPc in-situ composite depicted the formation of a dispersion of CuPc in the SPE on a nanoscale. A charge-transfer complex was found to form between CuPc and $CuCl_2$, imparting CuPc conductivity well in the semiconducting range. Due to the doping phenomena, CuPc exhibited a role of a catalyst and an initiator in the vapour phase polymerization process of PPy. This resulted in a rapid deposition of PPy as well as improvement in the conductivity of the composites. The presence of barriers was observed at low PPy contents that showed some photoconducting property. The charge transfer was found to follow the Poole-Frenkel model of conduction. The junctions disappeared on saturation implying a network formation of PPy in the matrix. In case of the PPy/CuPc single junction, the charge transport across the barrier occurs by tunneling mechanism in cases of low film thicknesses and is found to be sensitive to the morphology of the backing layer whereby it changes to Schottky mechanism. Similar type of behaviour is not observed in the case of composites because the doping of CuPc by $CuCl_2$, which introduces impurity centers in the CuPc and consequently decreases the barriers at the PPy/CuPc interface.

3.5 References:

1. Naarman H and Strohriegel P, "Handbook of Polymer Synthesis", Ed.Kricheldorf H.R, Marcel Dekker, New York,1992, p.1374
2. Yosomiya R, Hirato M, Haga Y, An H and Seki M, Makmol Chem, Rapid Comm 7 (1986) 697
3. Chao T.H, March J, J Polym Sci, Polym Chem A26 (1988) 743
4. Machida S, Miyata S, A Techagumpuch, Synth Met 31 (1989) 311
5. Rapi S, Bocchi B, Gardini G P Synth Metals, 24 (1988) 217
6. Sak-Bosnar M, Budimir M V, Kovac S, Kukulj D and Diuc L, J Poly Sci Part A, Poly.Chem., 30 (1992) 1609
7. Zhang J, She Y, Lu B, Zhou Y, Fu K, Chin J Polym Sci 11(4) (1993) 337
8. Radhakrishnan S and Saini D R, Synth.Met. 58 (1993) 243
9. Park Y W, Heeger A J, Drug M A and MacDiarmid A G, J.Chem.Phys. 73 946
10. Sessler G M, in "Electronic Properties of Polymers", Ed.O.Mort and

O.Fister, John Wiley, New York p.59 (1982)

11. Seanor D A, "Electrical Properties of Polymers", Academic Press, New York (1982)

12. Braunlich P, "Thermally Stimulated Relaxation in Solids", Springer Verlag Berlin (1979)

13. (a)Chen S A, Tsai Y C and Chem J H, Synth. Met. 28 (1989) C151
(b)Rehwald W and Kiess H G in "Conjugated Conducting Polymers", Ed.H.G.Kiess, Sringer Verlag, Berlin Chapt.3 (1992)

14. Alexander L E, "X-ray Diffraction Methods in Polymer Science",John Wiley, New York, p.379 (1969)

15. Radhakrishnan S, Mandale A B ,Synth Met 62 (1994) 217

16. Kaelbe E, "Handbook of X-rays", McGraw Hill, New York (1961)

17. Dilks A, in "Development in Polymer Characterization", Vol.2 Ed.J.V.Dawkinws, Applied Science, London, p.145 (1980)

18. Sherman R D, Middleman L M and Jacobs S M, Polymer Engineering and Science, vol23, No 1, Jan 1983

19. Sichel E K, Carbon Black Polymer Composites, Marcel Dekker, New York, 1982 p.110

20. Radhakrishnan,Polymer Commun 26 (1985) 153

21. Yin X H, Kobayashi K, Yoshino K, Yamamoto H, Watanuki T, Isa I, Synth Met 69 (1995) 367

22. Ezquerra T A, Mohammadi M, Kremer F, Vilgis T and Wegner G, J Phys C: Solid State Phys. (1988) 927

23. Miyauchi S, Hattori Y, Takamatsu T and Sorimachi Y, J Appl Poly Sci, 44 (1992) 377

24. Scrosati B, Science and Applications of Conducting Polymers, Chapman and Hall, London (1993)

25. Sircar A P, Weissman P T, Kumar B, Marsh R A, Thermochim Acta, 226 (1993) 281

26. Radhakrishnan S, Saini D R, Synth Met 58 (1993) 243

27. Cheung K M, et al , J Mater Sci, 25 (1990) 3834

28. (a)Kiess H, Conjugated Conducting Polymers, Sringer-Verlag, Berlin 1993
(b)Khedkar S P, Radhakrishnan S, Thin Solid Films 303 (1997) 67

29. Mott N F and Davis E A, Electronic Processes in Non-Crystalline Materials, Clarendon Press, Oxford, 1979.

30. Makhlouki M, .Morsli M, Bonnet A, Conan A, Pron A and Lefrant S, J Appl Poly Sci 44(1992) 443

31. Radhakrishnan S, Unde S, J Appl Poly Sci 71 (1999) 2059

32. (a) Garnier F.,Tourillon G, J Electroanal Chem 148 (1983) 299
(b) Marque P, Roncali J, Garnier F, J Electroanal Chem 218 (1987) 107

33. Huq R, Yang L L, Farrington G C, Conducting Polymers: Special Applications; Alcacer,L, Ed. Reidel Publishers; Dordrecht, 1989; p.89

34. Owen J, Comprehensive Polymer Science, Allen G, Bevington J C, Eds.Pergamon: Oxford, 1989, p.669

35. MaCallum J R, Vincent C A, Polymer Electrolyte Reviews, Vol 1, Elsevier: London,1987,p.1

36. Skothiem T,Appl Phys Lett 38 (1981) 712

37. Pantaloni S, Passerini S, Scrosati B, j Electrochem Soc 134 (1987) 753

38. (a)Doeff M A, Lampert C M, Viso S J, Ma Y P, Proc SPIE 1992, p.1727
(b)TadaH, BitoY, Fugino K, Kawahara H, Solar Energy Mater, 16(1981) 509

39. (a)Geng L, Reed R A, Longmire M, Murray R W, J Phys Chem 91(1987) 2908
(b)Murray R W, Reed R A, Lanmire M J, Murray R W, J Electroanal Chem 208 (1986) 185

40. (a) Cowie J M G, Cree J H, Ann Rev Phys Chem 40 (1989) 8
(b) Armand M B, Solid State Ionics9/10 (1983) 1101

41. Ratner M A, Shriver D E, Chem Rev 88 (1988) 109

42. (a)Jenkins A D, Polymer Science, Vol II, North Holland: Amsterdam, (1972) Ch. 17
(b)Topart P, Josowicz M J, J Phys Chem 96 (1992) 7824

43. (a)Khedkar S P, Radhakrishnan S, Polym Degrad Stab 57 (1997) 51

(b)Rapi S, Bocchi V, Gardini G P, Synth Metals 24 (1988) 217
(c)Chao T H, March J, J Polym Sci, Polym Chem 26 (1988) 743

44. Weast R C,Astle A J, Eds.Boca Raton CRC Handbook of Chemistry and Physics, CRC Press: Florida 1980, p.d-157

45. Penner R M, Lewis N, Chem Ind 4 (1991) 788

46. Martin C R, Renner R M, van Dlyke L S, Functional Polymers, Bergbreiter D E, Martin C R,Eds, Plenum Press: New York, 1989, p.119

47. Nevin W A, Lin W, Greenberg S, Hempstead M R, Marcuccio S M, Melnik M, Leznoff CC, Lever ABP, Inorg Chem 24 (1985) 1765

48. Yang Y C, Ward J R, Seiders R P, Inorg Chem 24 (1985) 1765

49. Abkowitz M, Monahan A R, J Chem Phys 58 (1973) 2281

50. Radhakrishnan S, J.Mat.Sci.Lett.6 (1987) 145

51. Shramm C J, Scaringe R P, Stojovic D R, Hoffman B M, Ibers J A, Marks T J, J Amerchem Soc 102, (1980) 1902

52. Hoffman B M, Ibers J A, Accounts Chem. Res 16 (1983) 15

53. Grigoryan L S, Simonyan M V, Sharoyan E G, Phys Stat Solidi A 84 (1984) 597

54. Paoletti A M, Pennesi G, Rossi G and Ercolani C, Inorg Chem 34 (1995) 4780

55. Shultz H, Lehmann H, Rein M, Hanack M, Struct Bonding 74 (1991) 41

56. Peterson J L, Schram C S, Stojakovic D R, Hoffman B M and T J Marks, J Am Chem Soc, 99 (1977) 286

57. Marks T J and Kalina D W in Extended linear chain compounds, Ed. J Miller(Plenum New York) Vol 1, 1982,197

58. Radhakrishnan S, Unde S, Thin Solid Films 347 (1999) 229

59. Simmons G J, in : L I Maissel , Glang R, (Eds.) Handbook of Thin Film Technology, McGraw Hill, New York, 1970 pp.14

60. Simmons J G, J Appl Phys 34 (1963) 1793

61. Chopra K L, Thin Film Phenomena, McGraw Hill, New York, 1969

62. Seanor D A, Electrical Properties of Polymers, New York, 1982

63. Uhera K, Takanishi K, Yamano S, Tanaka M, J Polym Sci Polym Lett26 (1988) 95

64. Ashida M, Bull Chem Soc,Jpn 2625 (1966) 2632

65. Goswami A, Radhakrishnan S, Ind J Pure Appl Phys 13 (1975) 332

66. Saji T, in: Leznoff C C, A.B.P.Lever (Eds.) ; Phthalocyanine Properties and Applications,2, VCH New York 1993, p.163

Chapter 4 - PPy/PVC-$CuCl_2$ based blends and composites

4.1 Introduction:

Polyvinyl chloride is one of the few commodity thermoplastics, which can be processed by both, solution as well as melt techniques. Its application in coatings and films is well known. In order to provide electrostatic dissipation one can incorporate conducting polymers in the same[1]. The processability of PVC can be effectively put to use in the synthesis of blends and composites of PPy. In the present studies chemically synthesized PPy was blended with PVC containing $CuCl_2$. In another case, the blends were prepared by vapour phase polymerization technique. The properties of the blends were modified later by adding CuPc to make a molecular composite.

4.2 Experimental:

(a) Synthesis of PPy/PVC-$CuCl_2$ ex-situ blend:

PVC was dissolved in tetrahydrofuran (THF) and 10% $CuCl_2$ was added with continuous stirring so as to obtain a clear green solution. PPy synthesized by the chemical route using $CuCl_2$ as an oxidizing agent was added to PVC-$CuCl_2$ in various compositions such as 2,5,10 to 50% w/w. The solution was stirred continuously so as to obtain thick slurry, which was then applied on interdigited electrodes and the solvent evaporated at room temperature. Samples were dried for 24 hrs and placed in desiccator under dry conditions.

(b) Synthesis of PPy/PVC-$CuCl_2$ in-situ blend:

PVC-$CuCl_2$ solution containing varying amounts of $CuCl_2$ was prepared in THF. The interdigited electrodes were coated with the solutions containing 1:1, 2:1, 4:1, 6:1, 8:1 and 12:1 monomer/mole of PVC and $CuCl_2$. The films thus obtained were dried thoroughly and then exposed in a dessicator presaturated with pyrrole vapours. The exposure time was varied from 1 minute to 20 hours yielding two sets of blends (1) partially exposed as well as (2) fully saturated samples.

(c) Synthesis of PPy/PVC-$CuCl_2$ in-situ composite with CuPc:

The composite was synthesized with respect to the concentration of CuPc as well as $CuCl_2$. In one case, the PVC-$CuCl_2$ (monomer/mole) ratio was kept constant to 4:1 while the CuPc content was varied from 2,5,10 to 50% w/w. The solution was stirred continuously and then applied on interdigited electrodes. The cells were then exposed to

pyrrole vapours in a dessicator for duration of 1 minute to 20 hours. In the other case, composites were prepared by varying the $CuCl_2$ amount in PVC from 1:1 to 12:1 monomer to mole ratios while keeping the CuPc amount constant at 28.5%. This paste was then applied on the interdigited electrodes, dried and exposed to pyrrole so as to form PPy in-situ.

(d) Fabrication of PPy/PVC-$CuCl_2$ single junctions:

Single junctions were fabricated across PPy and PVC-$CuCl_2$ interface in a multilayered form by using electrochemically deposited PPy on gold electrodes (see Chapt.2). Semitransparent Au as counter electrode was dip-coated with PVC-$CuCl_2$ solution in THF of the ratio 4:1m/M, and dried thoroughly. This counter electrode was then placed over PPy forming a sandwiched cell configuration. Similar single junction was fabricated using CuPc. The electrochemically deposited PPy was dip-coated with PVC-$CuCl_2$ and then dried. CuPc was vacuum deposited on counter electrode Au and then combined with the PPy/PVC-$CuCl_2$ to form a multilayered cell of the type Au/PPy/PVC-$CuCl_2$ /CuPc/Au. In another set of experiments, the CuPc was deposited over a transparent conducting ITO to form a sandwich cell by coupling with PPy/PVC-$CuCl_2$.

4.3 Results and discussion:

4.3.1 Charge transport in PPy/PVC-$CuCl_2$ ex-situ blends:

(a) Compositional variation of conductivity:

The variation of conductivity was studied as a function of the PPy, which was added externally to form the PPy/PVC-$CuCl_2$ blend is presented in the **Fig.4.1**. The magnitude of conductivity increases from 10^{-9} S/cm to 10^{-4} S/cm till 50% addition of PPy and then saturates to 10^{-3} S/cm approaching the conductivity of pure PPy at high concentration. The plot resembles percolation behaviour as discussed earlier in the Chapter 3. A plot of conductivity, σ against the weight fraction of PPy added, (φ), was made on a log-log scale as illustrated in the **Fig.4.2**. The plot is observed to be a straight line. The slope of the plot, yielding the value of 'f' in the eq 3.1, is found to be 4. A clear percolation threshold is observed at 2.5 weight % of PPy in PVC-$CuCl_2$, which implies that formation of a network of PPy starts at 2.5% that results in an increase in conductivity, by almost 5 orders of magnitude till 40-50% addition. Studies on similar

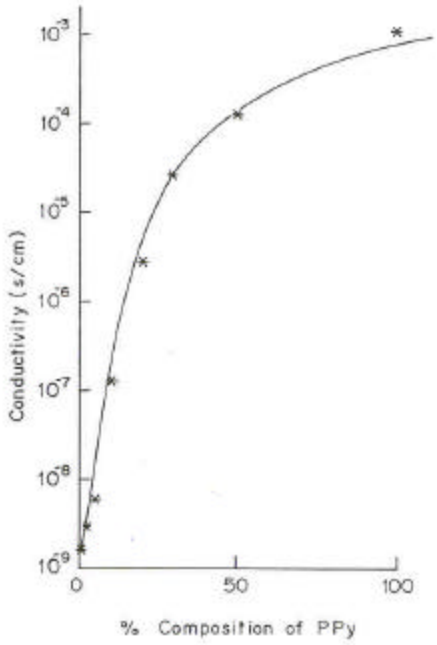

Fig. 4.1 Variation of conductivity with PPy composition for PPy/PVC-$CuCl_2$ ex-situ blends

systems report a percolation threshold at a high PPy loading of 20% [2]. However, lower percolation thresholds have been reported by Mandal[3]. A continuous rise in the conductivity is observed at 3.4 weight % of PPy loading in PPy/PVC blend in THF wherein the PPy particles are isolated by using a stabilizer.

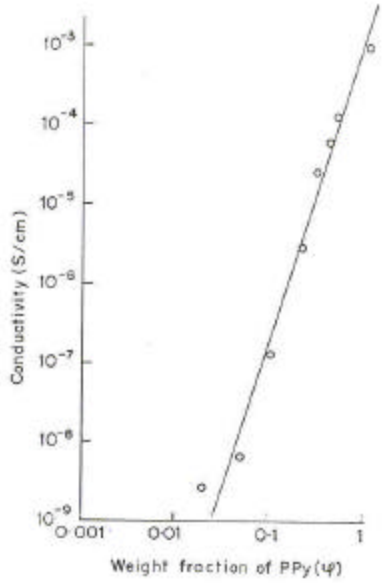

Fig. 4.2 A log-log plot of conductivity against the weight fraction of PPy for the PPy/PVC -$CuCl_2$ ex-situ blends

(b) I-V characteristics of PPy/PVC-$CuCl_2$ ex-situ blends:

The I-V characteristics for the ex-situ blend system were observed to be non-linear in nature as shown in the **Fig.4.3**. The degree of non-linearity is seen to decrease with the increase of PPy. In order to investigate the charge transport mechanism, the I-V curves were plotted on a log-log scale, the slopes of which were found to be between 1 and 2. Hence, the SCLC mechanism was ruled out. Log I vs. $V^{1/2}$ plots were made and are

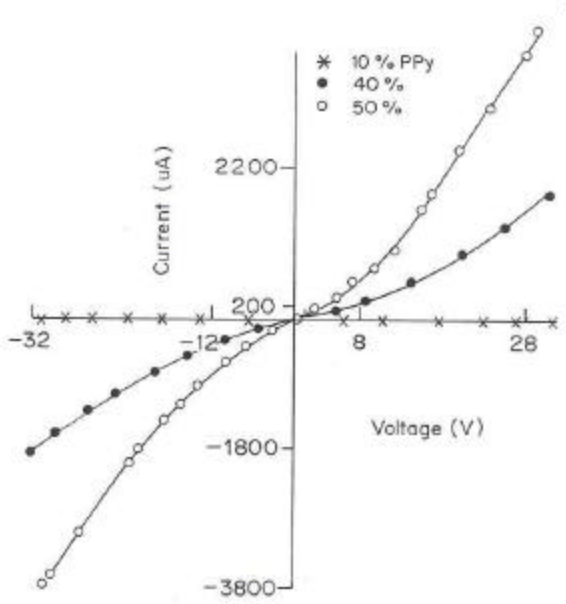

Fig. 4.3 I-V characteristics for the PPy/PVC-$CuCl_2$ ex-situ blends containing 10, 40 and 50 % PPy

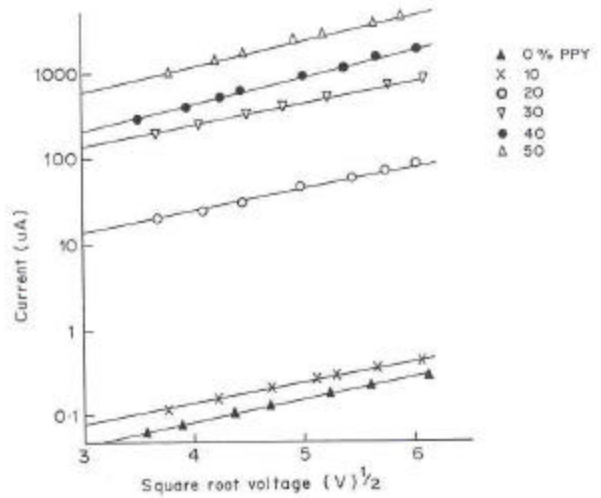

Fig. 4.4 Linear dependence of log I/ $V^{1/2}$ for the PPy/PVC-$CuCl_2$ ex-situ blends containing 10, 20, 30, 40 and 50 % PPy

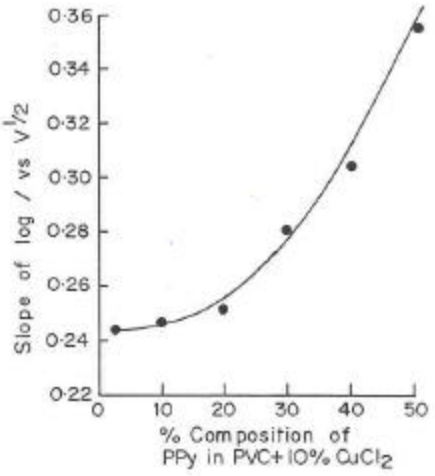

Fig. 4.5 Variation of the slopes of log $I/V^{1/2}$ with respect to the composition of PPy for the PPy/PVC-$CuCl_2$ ex-situ blends

indicated in the **Fig.4.4**. It is observed that the plots are straight lines implying a linear dependence. Hence, the equation (section 3.4.2) governing the Schottky/Poole-Frenkel effect holds good in the present case. The slopes of the plots were determined and are represented graphically in the **Fig.4.5**. It can be clearly noticed from the plot, that the slope of log I / $V^{1/2}$ increases with the increase of PPy in the PVC-$CuCl_2$. This can be associated with the parameters influencing the slope, which can be given as,

$$\text{Log } I / V^{1/2} \alpha \beta / kT\, d^{1/2} \qquad \text{---------- (Eq.4.1)}$$

In the present system, the increase of PPy content in the PVC-$CuCl_2$ matrix decreases the interparticular distance '$d^{1/2}$' between the PPy particles. This reduces the barrier width at the PPy/PVC-$CuCl_2$ interface and hence an easy lowering of the barrier by the application of voltage under Poole-Frenkel effect. The overall effect is the lowering of the interfacial barrier width and hence a better conduction. The charge transport can be well understood by considering the energy band diagram for PPy and PVC as illustrated by the **Fig.4.6**. It can be noticed that the valence band of PPy lies at 5.0 eV which presents a mismatch with the work function, Φ, of PVC i.e. 5.13 eV [4]. This presents a barrier of a very low magnitude of 0.13eV at the PPy/PVC-$CuCl_2$ interface as is brought out by the I-V characteristics.

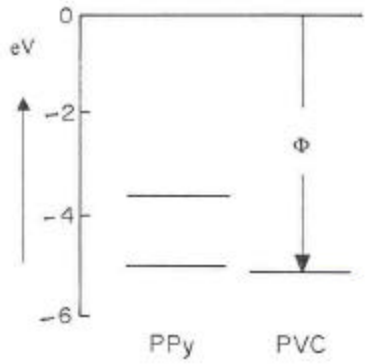

Fig. 4.6 Energy band levels of PPy and PVC

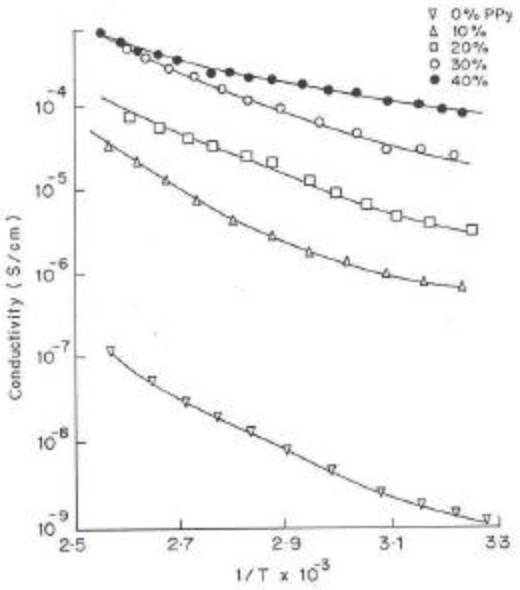

Fig. 4.7 Temperature dependence of conductivity for the PPy/PVC-$CuCl_2$ ex-situ blends containing 0, 10, 20, 30 and 40 % PPy

(c) Temperature dependence of conductivity:

The temperature dependence of conductivity is presented as log σ vs. 1/T plots, which are indicated in the **Fig.4.7**. It may be observed that the plots are linear and that the Arrhenius relation is followed. The slope of the graph, which represents the variation of the activation energy, was determined and its variation with the composition is shown in

Fig.4.8. It is observed that the activation energy decreases with the increase of PPy concentration. Thus, there is easy conduction path with lower activation energy in the blend containing high PPy content.

4.3.2 Charge transport in PPy/PVC-$CuCl_2$ in-situ blends:

(a) Time dependence of conductivity:

The variation of conductivity of the blends with time of exposure to pyrrole was studied. A typical composition of 4:1 (monomer/mole) PVC-$CuCl_2$ is represented in the **Fig.4.9**. The initial rising portion of the plot shows a rise in conductivity from $6x10^{-8}$ S/cm to $3x10^{-6}$ S/cm during a period of 60 seconds of exposure to pyrrole vapours, while the subsequent region exhibits a saturation of conductivity to 5×10^{-5} S/cm after 1500 seconds. Similar rise in conductivity is found in the blends containing different amount of $CuCl_2$. As discussed in Chapter 3, $CuCl_2$ acts as an initiator and a dopant and hence the conductivity rise is more in the blends containing more $CuCl_2$ due to more amount of PPy formation.

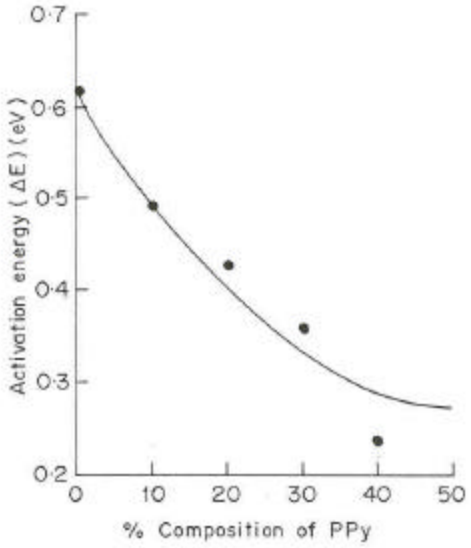

Fig. 4.8 Decrease in the activation energy with higher PPy for the PPy/PVC-$CuCl_2$ ex -situ blends

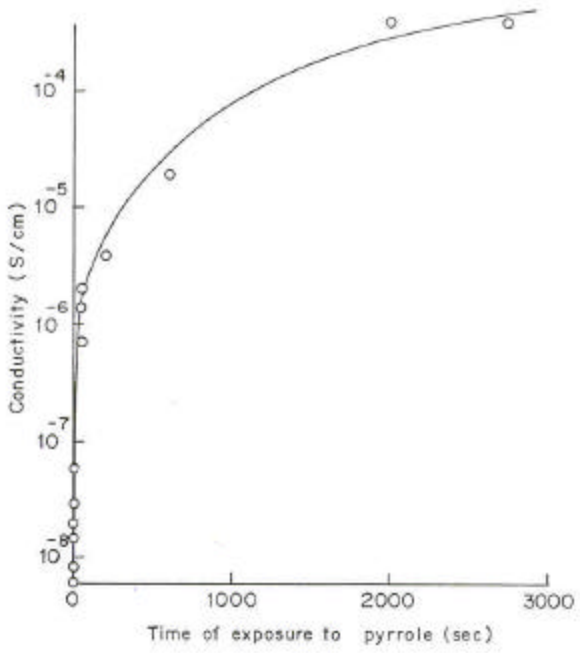

Fig. 4.9 Variation of conductivity with the exposure to pyrrole for 4:1 monomer/mole PVC-$CuCl_2$

(b)Compositional variation of conductivity:

The variation of conductivity with respect to $CuCl_2$ concentration is presented in the **Fig.4.10**. Curves **(a), (b)** and **(c)** indicate the conductivity variations for the PVC-$CuCl_2$ alone, PPy/PVC-$CuCl_2$ partially deposited and PPy/PVC-$CuCl_2$ having maximum PPy in the blends respectively. The conductivity is observed to rise with the increasing amounts of $CuCl_2$ in all the three cases. The rise in the conductivity of PVC with the

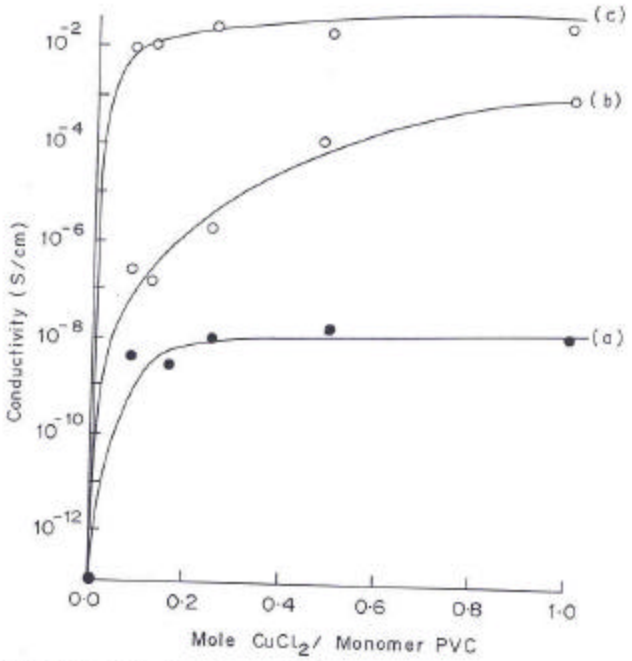

Fig. 4.10 Dependence of conductivity on the $CuCl_2$ mole/monomer concentration in PVC. Curves (a), (b) and (c) represent PVC-$CuCl_2$ alone, partial exposure (1 min) to pyrrole and exposure to pyrrole till saturation (maximum PPy) respectively

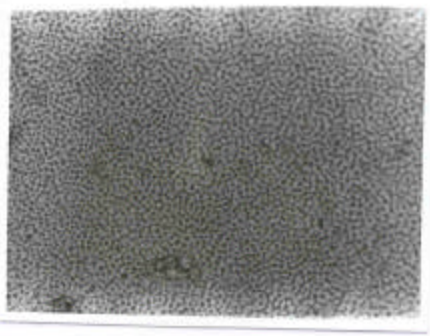

Fig. 4.11 Optical micrograph of PVC-$CuCl_2$ showing a phase-segregated morphology

addition of 0.08 mole/monomer of PVC is almost five orders of magnitude as shown by the curve (a), which saturates to a value of 1.5 x 10^{-8} S/cm beyond 0.25 mole /monomer concentration of $CuCl_2$. When exposed to PPy for 1 min duration, the conductivity is seen to increase further by two orders of magnitude for 0.08 moles of $CuCl_2$. At high concentrations of $CuCl_2$, the conductivity of the blend increases to 8 x 10^{-4} S/cm. For PPy/PVC-$CuCl_2$ having high PPy content (curve c), the magnitude of conductivity rises

from 9 x 10^{-3} S/cm to 3 x 10^{-2} S/cm with the increase in the amount of $CuCl_2$ from 0.08 to 1.0 mole/monomer $CuCl_2$.

These various results can be explained by taking into account the role of $CuCl_2$ as a dopant as well as an initiator for the polymerization of pyrrole. Optical microscopic studies carried out for PVC-$CuCl_2$ (4:1 monomer/mole) reveal a phase-segregated morphology as illustrated by the **Fig 4.11**, which imply no complex formation between PVC and $CuCl_2$ but the $CuCl_2$ is observed to be uniformly distributed in the matrix. On exposure to pyrrole, the $CuCl_2$ acting as an initiator for the polymerization reaction, results in the formation of a blend of PPy in the PVC-$CuCl_2$ matrix. It is reported that a uniform distribution of PPy domains is formed due to a good penetration of the oxidant $FeCl_3$ in PVC rather than in the case of PVAc during oxidative polymerization [5,6]. The morphology of PPy has been found sensitive to the substrate material. Earlier reports [7] reveal that no ordering or crystalline growth in the case of PPy vapour phase deposited on amorphous substrates such as polystyrene, polyvinyl acetate, polyvinyl alcohol, etc. Hence deposition of PPy in a crystalline ordered structure as observed in the case of PEO-$CuCl_2$ [8] does not take place in the PVC-$CuCl_2$ matrix. As the $CuCl_2$ concentration increases, more of PPy is formed in the matrix, which imparts more conductivity to the blend as evidenced by the **Fig.4.10**. Similar kind of work has been reported by Ueno et. al. [9] wherein vapour phase polymerization of pyrrole was carried out in PVC-$FeCl_3$ matrix. However, blends containing a high $FeCl_3$ to PVC (g/g) ratio of 7/4 exhibit a conductivity value less by an order of magnitude as compared to the present case.

(c) I-V characteristics of PPy/PVC-$CuCl_2$ in-situ blends:

The I-V characteristics of the PPy/PVC-$CuCl_2$ in-situ blends are non-linear in nature. Those containing lower $CuCl_2$ amounts i.e. 8:1 and 12:1 monomer/mole exhibit more non-linear character as indicated by the **Fig.4.12**. A plot of log I vs. log V was made to verify the SCLC mechanism. However, the magnitude of the slope is found to be $1<n<2$ suggesting that the SCLC mechanism is not obeyed. Hence, a plot of log I versus $v^{1/2}$ was made. All the compositions represent straight-line graphs, which suggests that the probable mechanism may be Poole Frenkel or Schottky type. The slopes of the log I-$\sqrt{v}$ were determined which are represented in a graphical form in the **Fig.4.13**. It is observed that the value of slope increases initially from 0.22 to 0.35 as the $CuCl_2$ concentration increases to 0.5 M. This variation in the slopes can be correlated with the change in the interdomain distance 'd', with the composition. Since $CuCl_2$ only gets

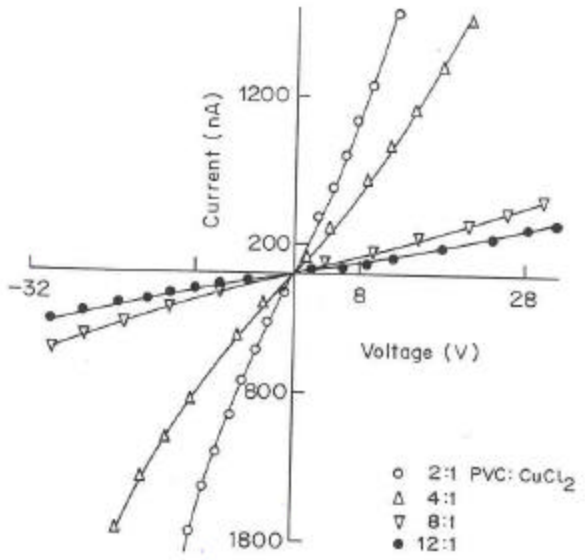

Fig. 4.12 I-V characteristics of PPy/PVC-$CuCl_2$ in-situ blends with partial exposure to pyrrole. Concentration of PVC-$CuCl_2$ is 2:1, 4:1, 8:1 and 12:1 monomer/mole ratio

deposited in the PVC matrix, the PPy formed will be at these sites and hence number of PPy domains will depend on the $CuCl_2$ concentration. These results predict a barrier at the PPy/PVC-$CuCl_2$ as represented by the energy band diagram discussed in the **Fig.4.6**.

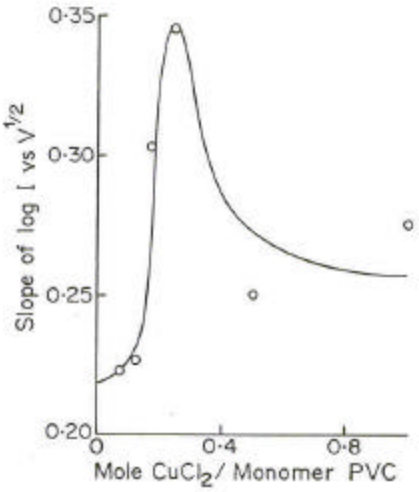

Fig. 4.13 Variation of slope of log I/ $V^{1/2}$ with the $CuCl_2$ concentration for PPy/PVC-$CuCl_2$ in-situ blends

Exposure of these blends to pyrrole for a longer duration induces high conductivity. The I-V curves are as illustrated in the **Fig.4.14**. These are all linear in nature. This suggests that there are practically no barriers present for the charge transport in the system, which is consistent with the band diagram studies.

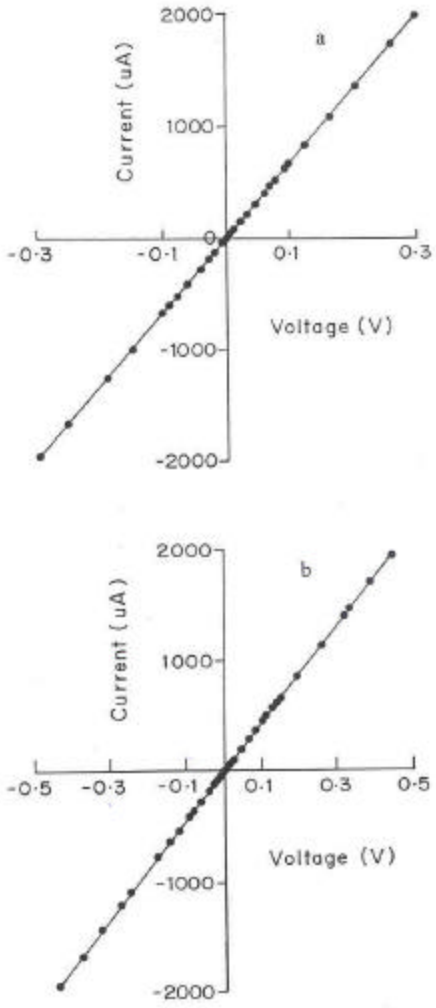

Fig. 4.14 I-V characteristics for PPy/PVC-$CuCl_2$ in-situ blends containing 4:1 and 12:1 monomer/mole PVC-$CuCl_2$ exposed to pyrrole till saturation

In order to check the charge transport mechanism and the type of junction formed at the interface of PPy/PVC-$CuCl_2$, I-V characteristics were recorded for the multilayered cells as described below.

(i) I-V characteristics for Au/PPy/PVC-$CuCl_2$/Au sandwich cell:

The IV characteristics obtained for these cells are illustrated in the **Fig.4.15**. It is observed that the plot is linear. Considering the energy band diagram given in **Fig.4.6**, it can be noticed that there is very little barrier present at the PPy/PVC-$CuCl_2$ interface for the hole transport while there is a barrier for the electron transport. Hence a decrease in overall current is observed in the reverse bias while the I-V curves are slightly non-linear. The effect of illumination was also studied by exposing the cell to light through the PVC-$CuCl_2$ face. Curve (L) in the figure indicates the I-V characteristics under illumination wherein a small photocurrent is observed. Possibly very few of the charge carriers generated in PPy may have undergone a separation at the interface, which are transferred to the trapping sites in PVC. This capture of the photo excited electrons by the trapping sites created by $CuCl_2$ results in a small photocurrent.

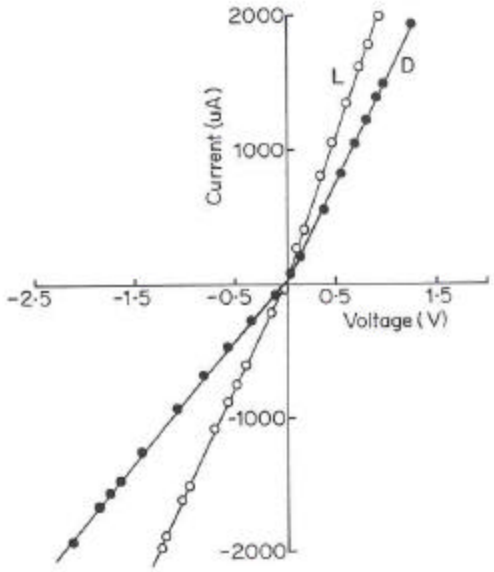

Fig. 4.15 I-V characteristics for Au/PPy/PVC-$CuCl_2$/Au cell using PVC-$CuCl_2$ 4:1 monomer/mole concentration. Curves (D) and (L) indicate the I-V characteristics in dark and light

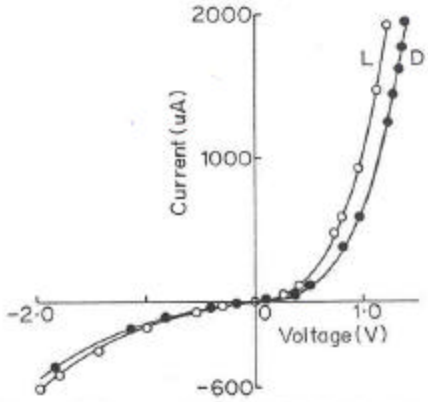

Fig. 4.16 I-V characteristics for Au/PPy/PVC-$CuCl_2$/ITO cell Curves (D) and (L) indicate the I-V characteristics in dark and light

(ii) I-V characteristics for Au/PPy/PVC-$CuCl_2$/ITO sandwich cell:

The change of the counter electrode from Au to ITO, changes the nature of the I-V curves considerably from linear to non-linear and rectifying as shown in the **Fig.4.16**. The work function of ITO is 4.3eV while that of Au is 4.8 eV and hence it acts as a blocking contact to PPy. A depletion region is created at the PPy/ITO interface under

reverse bias conditions that gives rise to rectifying characteristics. Negligible photocurrents are seen under illumination. The I-V curves were further analyzed by making a plot of log I-$V^{1/2}$ as shown in the **Fig.4.17**. It is observed that the plot is a straight line obeying the $V^{1/2}$ dependence.

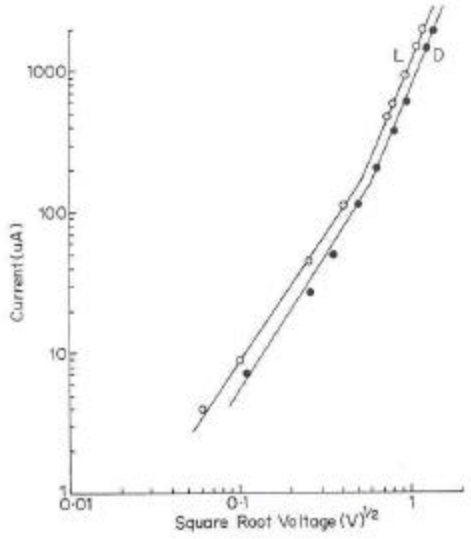

Fig. 4.17 Log I/ $V^{1/2}$ plot for Au/PPy/PVC-$CuCl_2$/ ITO that shows a linear dependence

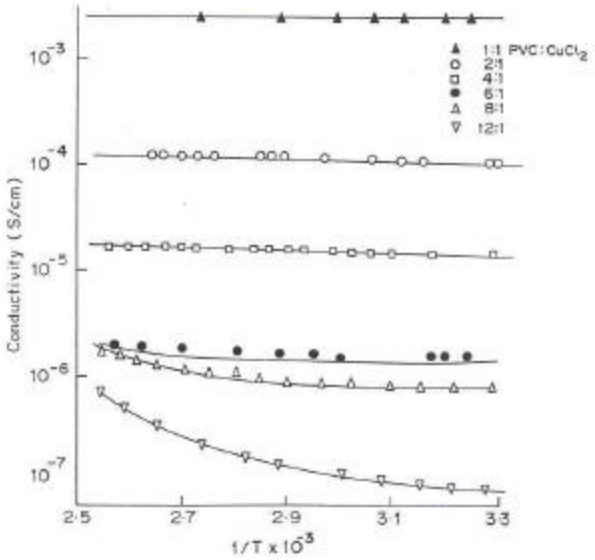

Fig. 4.18 Temperature variation of conductivity for the PPy/CuPc in-situ blends with PVC -$CuCl_2$ concentration of 1:1, 4:1, 6:1, 8:1 and 12:1 monomer/mole

Hence it is observed that the charge transport at the PPy/PVC-$CuCl_2$ interface is of Schottky type. Similar type of discrete junctions are formed in the blend that gives a collective effect on a macroscopic level.

(d) Temperature dependence of conductivity:

The conductivity against temperature plots for the partially exposed blends are shown in the **Fig.4.18**. It is observed that the plots are straight lines thus obeying the Arrhenius law. Activation energy was determined from these plots and is presented in the **Fig.4.19**. It is observed that the blend system possesses low activation energies. An activation of 0.175 eV is observed for the 12:1 composition that decreases rapidly to 0.015 eV in the case of 4:1 m/M PVC-$CuCl_2$. Thus as PPy concentration is increased (due to increase of $CuCl_2$) the interdomain distance decreases and the activation energy for the charge transport (hopping from one domain to the other) decreases.

The conductivity shows practically no change against temperature in the case of blends fully saturated with PPy. In the samples containing high concentration of PPy (saturated) there is an extensive contact/network formation between the conducting domains. Hence, the linear I-V characteristics are observed for these samples. A plot of log I against $1/T^{-4}$ was made and observed to be a straight line. Thus the temperature dependence of conductivity for the same is according to the VRH model [10].

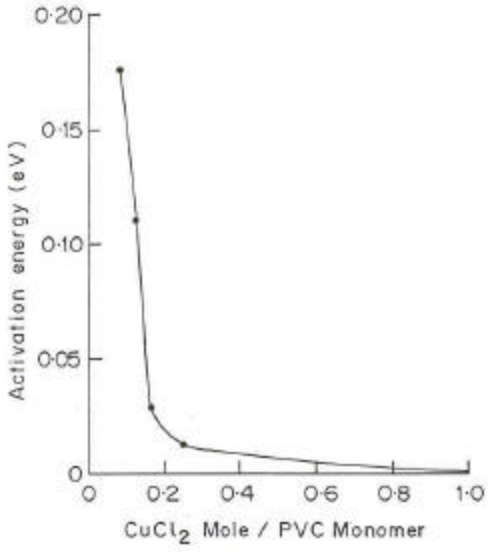

Fig. 4.19 Variation of activation energies for PPy/PVC-$CuCl_2$ in-situ blends with respect to the $CuCl_2$ mole/monomer concentration

4.3.3 Charge transport in PPy/CuPc in-situ composite with PVC-$CuCl_2$:

(a) Time dependent kinetics studies:

The conductivity versus time of exposure of the PVC-$CuCl_2$ matrix (in the ratio 4:1 monomer/mole concentration) containing various amounts of CuPc to pyrrole is shown in the **Fig.4.20**. It is clearly observed that the overall process of deposition is fast in the

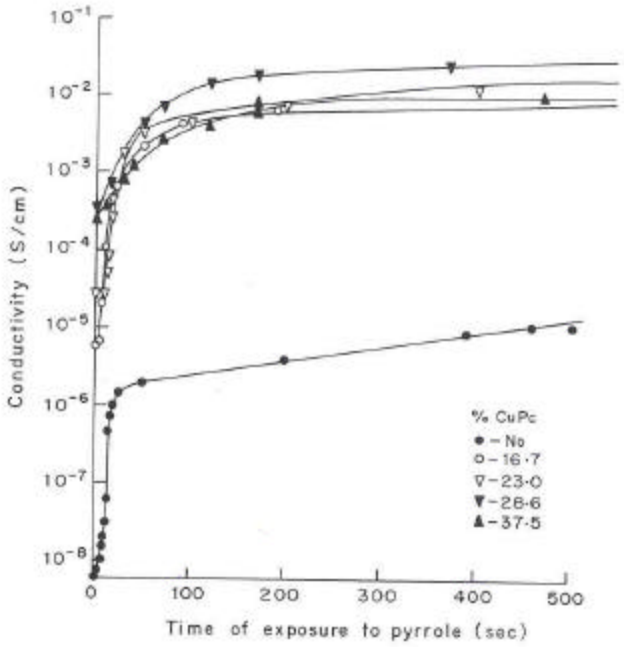

Fig. 4.20 Time dependent conductivity variation for CuPc/PVC-$CuCl_2$ on exposure to pyrrole containing 0, 16.7, 23, 28.6 and 37.5 % CuPc. Concentration of PVC -$CuCl_2$ is 4:1 monomer/mole

CuPc containing samples and the conductivity saturates within 100 seconds of exposure time (curves **b, c, d,** and **e**). The conductivity in the composite formed without CuPc attains an upper value at a much higher time of around 2000 seconds (curve **a**). This suggests that CuPc plays an important role in the formation of PPy in these composites. In order to check the exact nature of role played by CuPc, these curves were analyzed

further to determine the kinetics of polymerization as discussed in Chapter 3 [Section:3.3.5 (a)].

In order to analyse the present system, a plot of log ΔR vs. log t was made as illustrated by the **Fig.4.21** for the rising portion of the conductivity–time curves. The plots represent straight lines with varying slopes. Slopes of these plots were determined and are plotted against the CuPc composition as shown in the **Fig.4.22**. It is observed that the slope in case for PPy/CuPc composite containing 2% CuPc, exhibits a maximum. This implies that the rate of reaction is highest for 2% composite than rest of the cases.

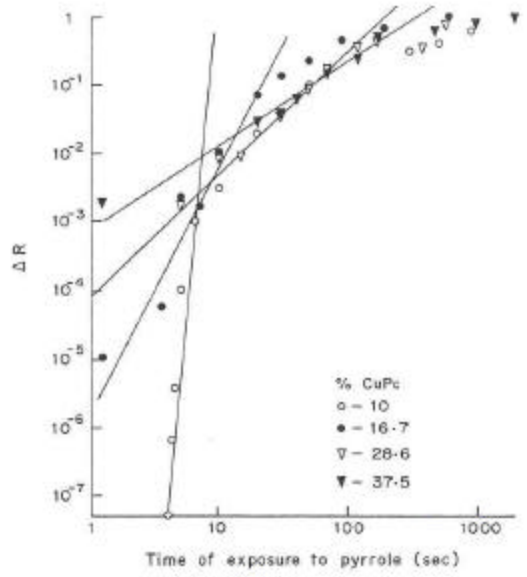

Fig. 4.21 Log ΔR against log t for the rising portion of the plots presented in Fig 4.20

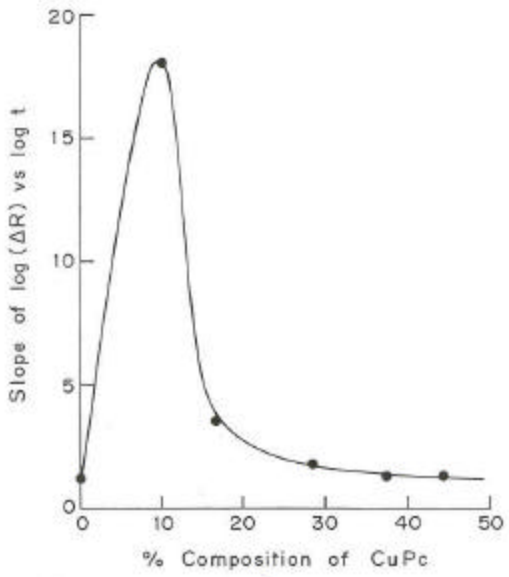

Fig. 4.22 Variation of the slopes of the log Δ R/ log t plots with the CuPc concentration

In order to understand the variation in the rate of polymerisation, morphological studies were carried out by optical microscopy technique for unexposed and the samples exposed to pyrrole. The films were very uniform with the colour changing from green to blue with the addition of CuPc. **Figs.23, 24** and **25** show the optical micrographs for composites containing 0.5, 1, and 2% CuPc dispersed in the PVC-$CuCl_2$ respectively. It is clear from

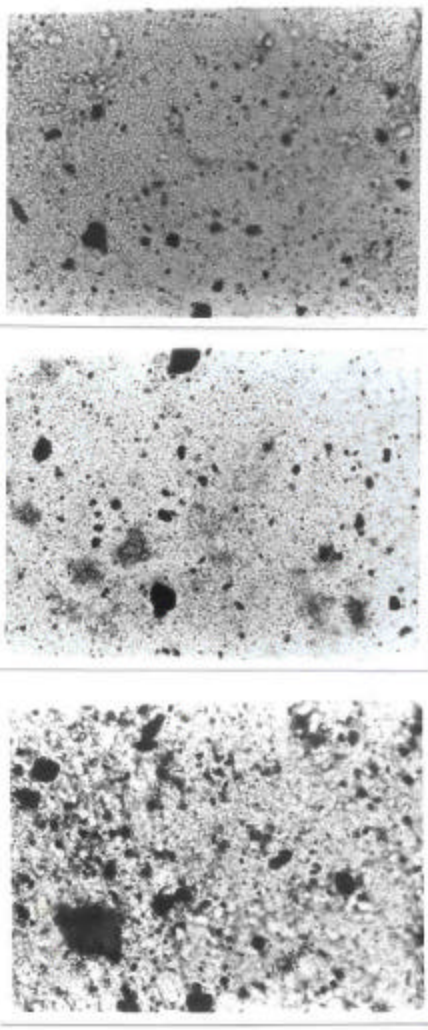

Fig.4.23, 4.24 and **4.25** Optical micrographs for PVC-$CuCl_2$ containing 0.5, 1 and 2% CuPc represented by (a),(b) and (c) respectively

these optical micrographs that the distribution of CuPc becomes increasingly non-uniform with the increase of concentration. The comparison of **Figs. 4.26, 4.27,** & **4.28** (at lower magnification) clearly bring out the fact that as the CuPc concentration increases, the intergranular distance decreases and that agglomeration of CuPc particles also takes place at higher CuPc concentration. Moreover, the distribution of CuPc is random and uneven in nature. Vapour phase deposition of PPy in these matrices

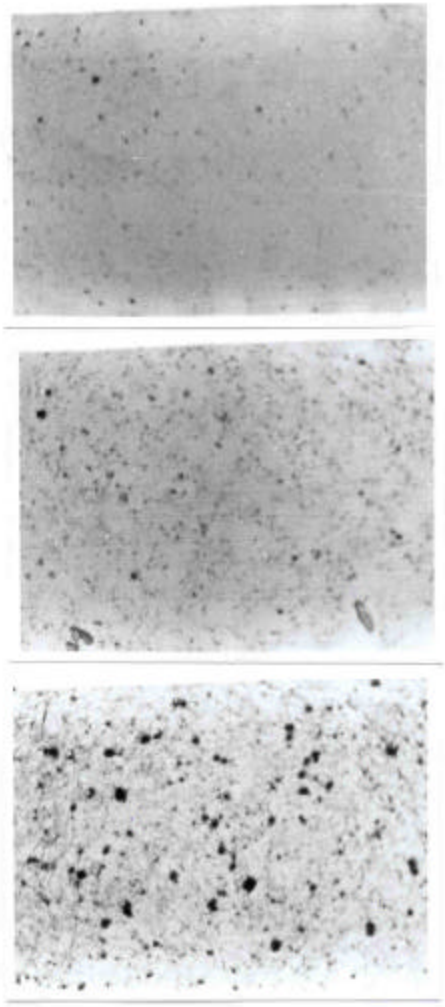

Fig. 4.26, 4.27 and **4.28** Same as Fig. 4.23, 4.24 and 4.25 but with lower magnification

containing 1 and 2% CuPc is indicated by the **Figs. 4.29 & 4.30** respectively which show the morphology of the composites after exposure to pyrrole vapours for 30 seconds. It is observed that PPy is formed preferentially on the CuPc particles even in this case as observed for PEO-$CuCl_2$/PPy composites. The formation of PPy on CuPc increases the size of CuPc, which can lead to contact formation at a particular concentration of CuPc and exposure time to pyrrole vapours. For such composites continuous network of PPy

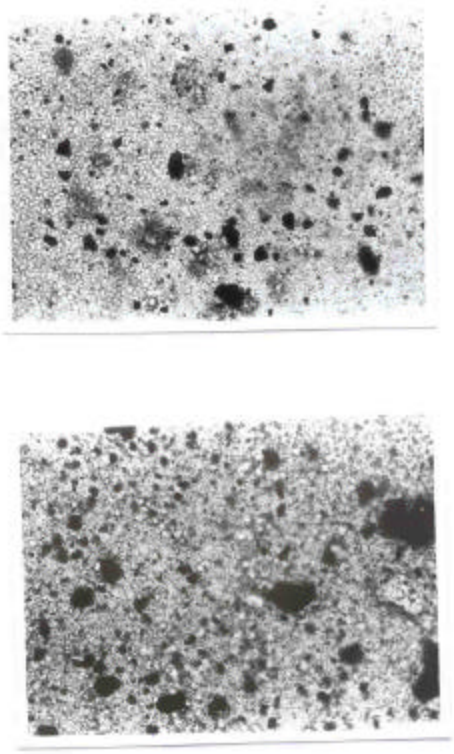

Fig. 4.29 and 4.30 Vapour phase deposition of PPy in the PPy/CuPc in-situ composites with PVC-$CuCl_2$ containing 1 and 2% CuPc. Exposure to pyrrole :30 sec

may take place. This can be clearly observed in **Fig.4.30** which depicts the morphology of PVC-$CuCl_2$ with 2% CuPc after PPy formation.

The kinetic study of vapor phase deposition of PPy in the PVC matrix, containing $FeCl_3$ has been studied by Ueno et al as mentioned earlier. The dependence of conductivity on reaction time was studied by taking different ratios of $FeCl_3.6H_2O$: PVC. It was observed that the matrix containing highest $FeCl_3$: PVC ratio is 7:4 g/g showed a

rapid increase in conductivity than those containing 5:4 and 4:4 g/g and the time taken for saturation was almost 2-3 minutes exhibiting a conductivity of 8 x 10^{-4} S/cm while in the present case. In the present case, an optimum surface to volume ratio is achieved at 2% CuPc due to a good dispersion that yields a higher deposition of PPy. This gives rise to a rapid rise in conductivity at this composition as is evidenced by the rise in slope of ΔR against time.

(b) Compositional variation of conductivity:

The effect of addition of CuPc on conductivity of the composite formed by in-situ method is presented in **Fig.4.31**. Curves **(a), (b)** and **(c)** represent the conductivity variation for PVC-$CuCl_2$ containing CuPc alone, with partially deposited PPy and with maximum PPy respectively. The $CuCl_2$ concentration was held constant in all the cases i.e. 0.25 mole/monomer PVC. It is observed that the overall conductivity increases with the addition of CuPc. In curve (a), the increase in the conductivity is very sharp beyond 5% addition of CuPc, and is almost 4 orders of magnitude saturating at 20% CuPc to a value of 3 x 10^{-5} S/cm. The curve represents a classical percolation behaviour governed by the equation 3.2 (chapter 3). Conductivity, σ, against the weight fraction of CuPc added in PVC was plotted on a log-log scale as shown in the **Fig.4.32**. The plot is a straight line with slope, f = 5.225. The system thus represents conducting particles dispersed in an insulating matrix of PVC similar to carbon black filled polymers [11]. This behaviour can be understood by considering the charge-transfer complex formation between CuPc and $CuCl_2$ giving electrically conducting CuPc that is dispersed in the insulating PVC matrix. The interparticulate distance decreases at higher CuPc concentrations, which effectively leads to contact formation at a critical concentration denoted by the percolation threshold. The percolation threshold is at 4.8% as inferred from the plot.

The conductivity variation of the system (CuPc/PVC-$CuCl_2$) after exposure to pyrrole for 1 minute is represented by a sharp rise of conductivity in the initial region of the plot and reaches saturation at a lower concentration of CuPc i.e. 10% as compared to the CuPc in PVC-$CuCl_2$ alone [see curve (a)]. The increase of conductivity occurs by three orders of magnitude to a value of 8x10^{-3} S/cm. This occurs due to the formation of conducting paths of PPy, interconnecting the CuPc particles. Moreover, the deposition of PPy on the surface of CuPc causes an increase in the size of the CuPc particle facilitating an interparticulate contact formation at a much lower composition of CuPc. Addition of

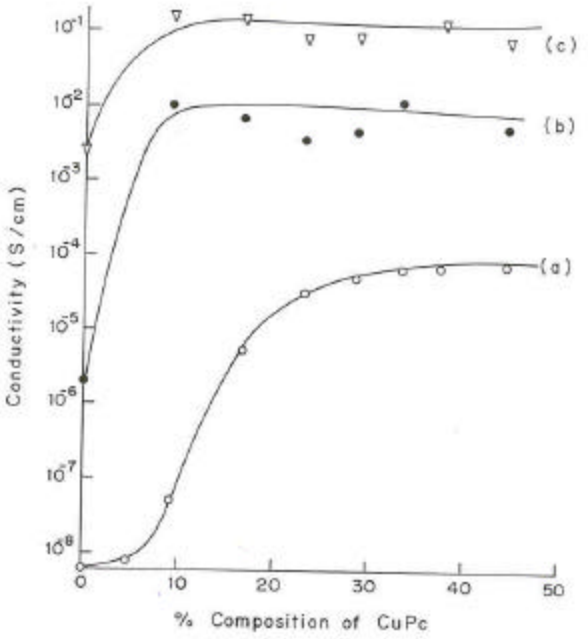

Fig. 4.31 Effect of CuPc addition on the conductivity of the PPy/CuPc in-situ composites with PVC-$CuCl_2$. Curves (a), (b) and (c) represent the conductivity variation for PVC-$CuCl_2$ alone, with partially deposited PPy and with maximum PPy respectively. Concentration of PVC-$CuCl_2$ is 4:1 monomer/mole

CuPc reduces the interparticutae distance effectively touching each other at the 10% composition forming a network.

Curve (c) represents the conductivity of the composite system after deposition of maximum PPy. The variation of conductivity follows the same trend as in curve (a) and (b) with a difference that the increase of conductivity is around two orders of magnitude

which saturates to almost 1 x 10^{-1} S/cm. The formation of extensive PPy network imparts a higher conductivity to the composite.

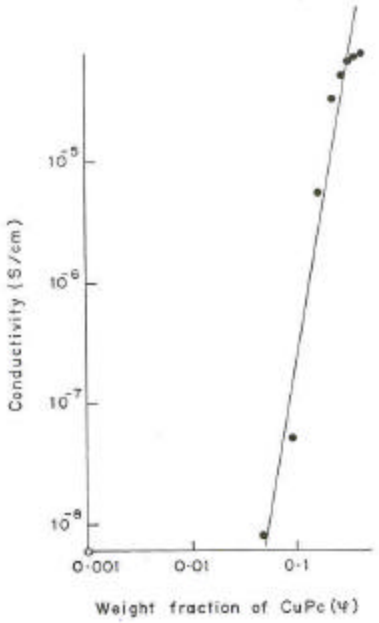

Fig. 4.32 Conductivity against the weight fraction of CuPc [data from Fig. 4.31(c)] on a log -log scale

The variation of conductivity was also studied with respect to the amount of $CuCl_2$ in the PVC matrix and is presented in the **Fig.4.33**. The curves **(a), (b)** and **(c)** indicate the variations for the PVC-$CuCl_2$, containing 28.6% CuPc and with partial exposure to Py

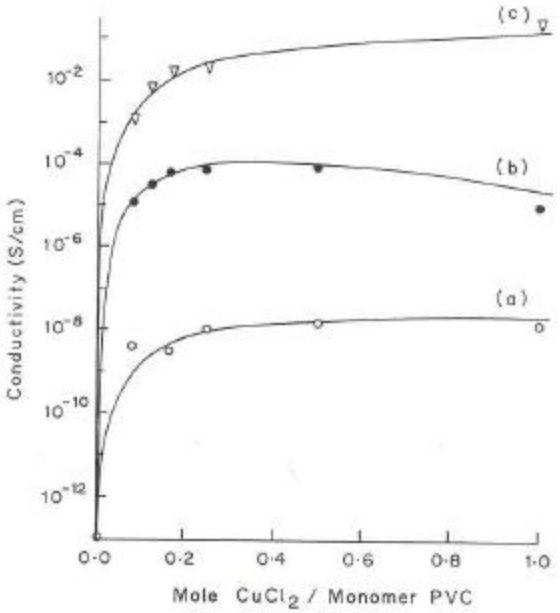

Fig. 4.33 Dependence of conductivity on the $CuCl_2$ amount in PVC. Curves (a), (b) and (c) indicate the conductivity variation for PVC-$CuCl_2$, PVC-$CuCl_2$ containing 28.6% CuPc and with partial exposure to pyrrole respectively

respectively. It can be observed that the conductivity increases with higher $CuCl_2$ in all the cases. The variation of conductivity in the case of PVC-$CuCl_2$ illustrated by the curve (a) is well discussed in the earlier section. Addition of CuPc to this matrix increases the conductivity by almost 3 orders of magnitude from 10^{-8}S/cm to 10^{-5}S/cm, which is brought out by the curve (b). Continuous rise in conductivity is seen till 0.25 M addition of $CuCl_2$ that further saturates at $9x10^{-5}$S/cm. The formation of charge-transfer complex

of CuPc-$CuCl_2$ induces a higher conductivity to the system. A similar trend is observed in the case of the system partially exposed to PPy. The conductivity exhibits a limiting value at 0.25M $CuCl_2$ concentration whereby a value of $2.7x10^{-1}$ S/cm is attained.

The thermal stability of the PPy/CuPc composites with PVC-$CuCl_2$ was investigated using TGA analysis similar to that of PPy/CuPc composites with PEO-$CuCl_2$ (Chapter 3). The TGA/DTG curves are indicated in the **Fig. 4.34**. Curves **(a), (b)** and **(c)** represent the % weight loss with respect to temperature for PVC-$CuCl_2$ alone, saturated with PPy and PVC-$CuCl_2$ with 5% CuPc saturated with PPy. It is observed that the weight loss of PVC-$CuCl_2$ is a very rapid process. The initial portion of the TGA curve can be attributed to the evaporation of THF. This proceeds to complete the degradation process at 300^0C giving a weight loss of 67%. PVC is reported to degrade very rapidly at 300^0C giving a 60% weight loss. The onset temperature of degradation is around 240^0C and degrades 75% at 500^0C.

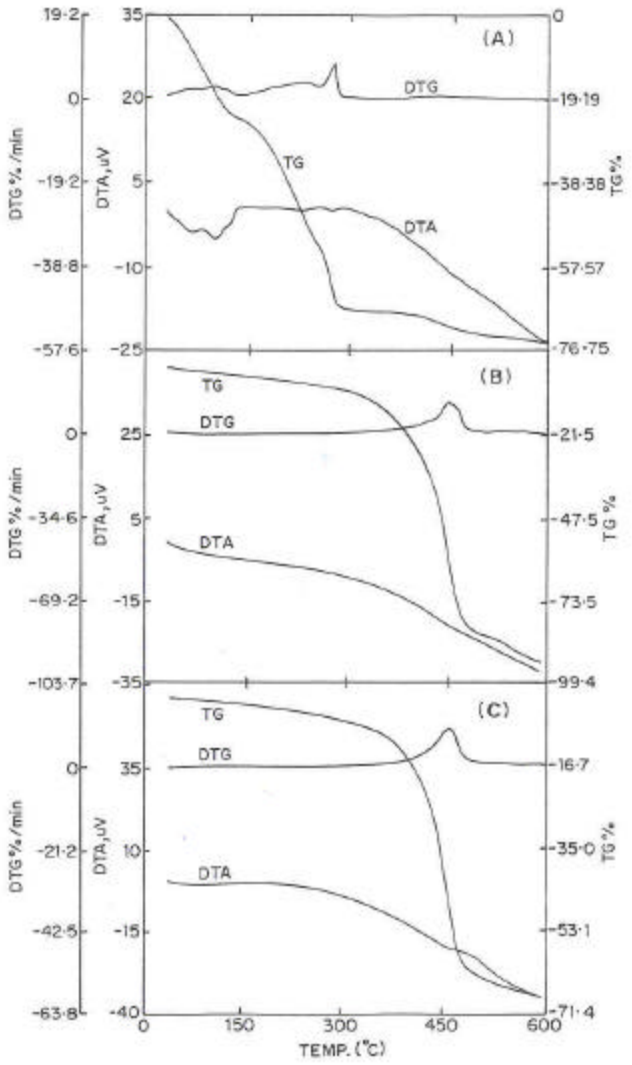

Fig. 4.34 TGA/DTG curves for the PPy/CuPc in-situ composites with PVC-$CuCl_2$ (4:1 monomer/mole). Curves (a), (b) and (c) represent the % weight loss with respect to temperature for PVC-$CuCl_2$ alone, saturated with PPy and PVC-$CuCl_2$ with 5% CuPc saturated with PPy

The TGA curve for the blend saturated with PPy [curve (b)] PPy (PVC-$CuCl_2$) indicates that the blend is stable over a long range of temperature. A rapid weight loss of the blend starts around 370°C and the degradation completes by 500°C. The TGA for the composite with 5% CuPc is shown in the curve (c). The composite is observed to be stable till 360-370°C. Similar TGA plots are obtained for the composites containing 10 &

28.5 % of CuPc, which show a small rise in thermal stability as the CuPc increases. No step-wise degradation of the components was observed. Hence, it was not possible to deduce the weight loss of PPy and hence the composition.

Similar kind of thermal studies have been carried out by De Paoli et al [12] for PPy/PVC blends which are electro-polymerized onto Pt coated PVC films from a solution of acetonitrile containing tetra ethyl ammonium fluoroborate (0.119M) and monomer pyrrole (0.00619M). The TGA curves show that the films are stable to heating till 280°C beyond which they lose weight rapidly in comparison with the decomposition temperature of PVC/PPy films. The thermal stability achieved in the present blends and composites is higher than in the reported case. This may be related to the method of synthesis of the blend and composite. Electro-polymerization process allows the polymerization of pyrrole to take place in the pores and voids of PVC matrix. Thus conducting channels of micrometer range are formed throughout the matrix [13]. In the present case, vapour phase polymerization technique gives an insitu deposition of PPy forming a semi-interpenetrating network. An intimate mixing of the components is ensured during this process.

The problem of thermal stability in PVC has been tackled by adding various heat or UV stabilizers ranging from purely organic chemicals to metallic soaps to complex organometallic compounds[14]. Dehydrochlorination is the main cause of degradation of PVC, which involves three steps: initiation of HCI loss, rapid zip-elimination of HCI and simultaneous formation of polymers in the PVC chain, termination of the zipping process.

PVC degradation occurs by both free radical and ionic reactions where the latter is a more important route. Lewis acid catalysts such as zinc chloride or hydrogen chloride can accelerate the dehydrochlorination of the polymer, which can occur in the case of $CuCl_2$ added to PVC.

Heat stabilizers serve different functions such as: absorption of hydrogen chloride, replacement of labile chlorines, prevention of autoxidation, etc. In the present case, the PVC dispersion with $CuCl_2$ is observed to become thermally stable only after the vapour phase deposition of PPy. This suggests that either PPy itself or the by-products formed during the course of the reaction act as heat stabilizers for PVC. There is a possibility of absorption of HCl by PPy which effectively gets doped forming a charge transfer complex. Thus the HCl formation is arrested. Another factor would be the breaking of labile of C-C1 bonds and doping of PPy with the Cl radical. This would in principle

arrest the indication of HCl formation. On the basis of the by-product CuCl formed during the vapour phase polymerisation of pyrrole it can also be proposed that the loss of Cl is replaced by CuCl. This would also arrest the HCl formation and increase the thermal stability of the composite. More investigations need to be carried out to find the exact mechanism that makes the composite to degrade as a whole than as single components.

(c) I-V characterization for PPy/PVC-$CuCl_2$ in-situ composites:

(1) Variation of $CuCl_2$:

The IV characteristics of the system CuPc (PVC-$CuCl_2$) containing various amounts of $CuCl_2$ are represented in the **Fig.4.35** and can be easily differentiated due to varying non-linear nature for each composition. The degree of non-linearity is seen to decrease with increasing $CuCl_2$ content. Analysis of the IV curves was done in order to find the exact conduction mechanism. The log-log plot of the I-V curves for the composites 12:1, 8:1, 6:1, 4:1, 2:1 and 1:1m/M represent a straight line but the slope is $1<n<2$. This implies that the mechanism is not SCLC but Poole-Frenkel or Schottky type. This was verified by plotting the log $I/\sqrt{v}$ for all the composition that are found to be linear in nature implying that the $\sqrt{v}$ dependence is followed, the slopes for which are represented in the **Fig.4.36**. It is observed that the slope is less at lower concentration of $CuCl_2$ denoting a higher non-linearity, which increases beyond 0.25 M of PVC:$CuCl_2$ from 0.24 to almost 0.305. The optical microscopy reveals a phase-segregated morphology for PVC-$CuCl_2$ while CuPc is found in close association with $CuCl_2$. This effectively results in a conducting CuPc phase dispersed in the PVC matrix. This not only increases the overall conductivity but also affects the barrier at the CuPc/PVC-$CuCl_2$ interface. The energy band diagram (**Fig.4.37**) depicts a barrier of the 0.87eV at the interface of the materials. Collins et al [15] have studied the IR response of PbPc exposed to Cl and I. Generation of acceptor levels within the band gap due to doping led to the splitting of the valence band. The position of the Fermi level shifts towards the valence band edge [16-18], on increased doping. This effectively increases the p-type conductivity of

the material. Similar trapping centres can be introduced in CuPc causing a lowering of the barrier in the present case. Hence, the I-V curves tend to be linear with higher $CuCl_2$.

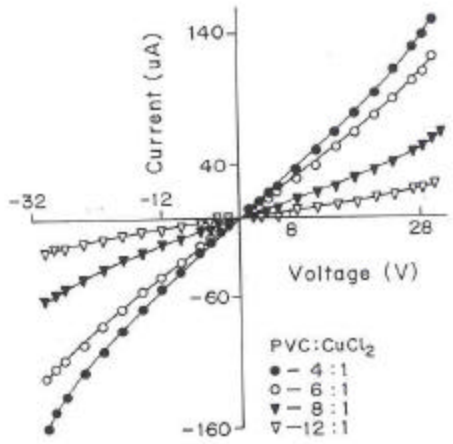

Fig. 4.35 I-V characteristics of the CuPc/PVC-$CuCl_2$ containing 28.6% CuPc and varying amount of $CuCl_2$ in PVC viz. 4:1, 6:1, 8:1 and 12:1 monomer/mole

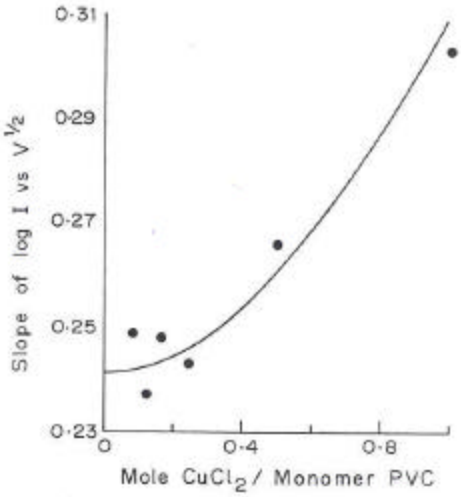

Fig. 4.36 Variation of the slope of log $I/V^{1/2}$ against the $CuCl_2$ concentration for the PPy/CuPc in-situ composites

A partial exposure of CuPc/PVC-$CuCl_2$ containing varying amounts of $CuCl_2$ to pyrrole yields I-V characteristics, which were found to be non-linear in nature as shown in the

Fig.4.38. The initiation of polymerisation at the CuPc generates CuPc particles covered with PPy that are embedded in the PVC-$CuCl_2$ matrix. This results in the increase of particle/domain size of the conductivity component and at high concentration of CuPc and/or high PPy deposition (saturation) these touch each other giving rise to continuous path.

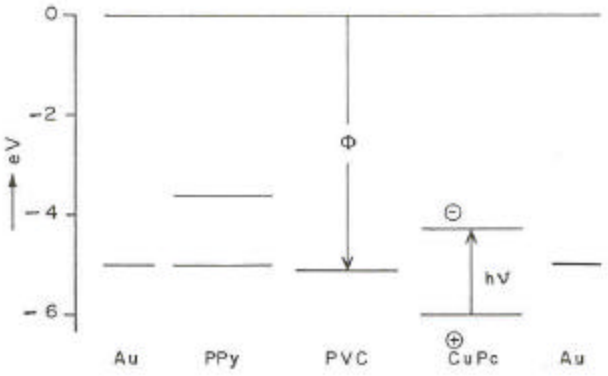

Fig. 4.37 Band diagram depicting the energy levels for PVC and CuPc

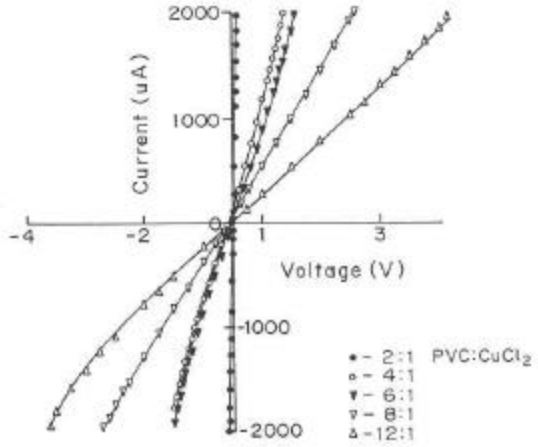

Fig. 4.38 I-V characteristics for PPy/CuPc in-situ composites with PVC-$CuCl_2$ containing 28.6% CuPc with a partial exposure to pyrrole

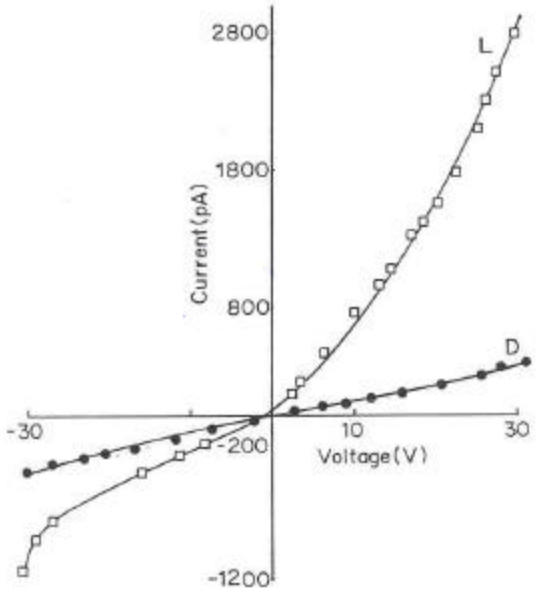

Fig. 4.39 I-V characteristics for Au/PVC-$CuCl_2$/CuPc/Au cell, concentration of PVC-$CuCl_2$ is 4:1 monomer/mole. Curves (D) and (L) indicate the I-V characteristics in dark and light

Hence the charge transport in the PPy/CuPc in-situ composites with PVC-$CuCl_2$ was found to be of Poole-Frenkel type. I-V characteristics of multilayered cells were carried out in order to check the charge transport at the PVC-$CuCl_2$ / CuPc interface. These are presented as follows.

(i) I-V characteristics for Au/PVC-$CuCl_2$/CuPc/Au sandwich cell:

The I-V characteristics obtained for this cell are found to be non-linear in nature (see **Fig. 4.39**) and the conductivity of the cell is observed to be quite low (the current is in pA). These were then plotted as log I vs. $V^{1/2}$ as illustrated in the **Fig.4.40**. It is clear from the plot that the $V^{1/2}$ dependence is absolutely followed. Au forms an ohmic contact to CuPc [19-20]. Referring to the energy band diagram (Fig 4.37), it can be noticed that a barrier of 0.87eV exists at the interface of the materials that gives rise to non-linear I-V characteristics. High photocurrents are noticed as given by the curve L. The hole-electron pair created in CuPc gets separated at the CuPc/PVC-$CuCl_2$ interface. A photosensitivity factor of 7 was determined.

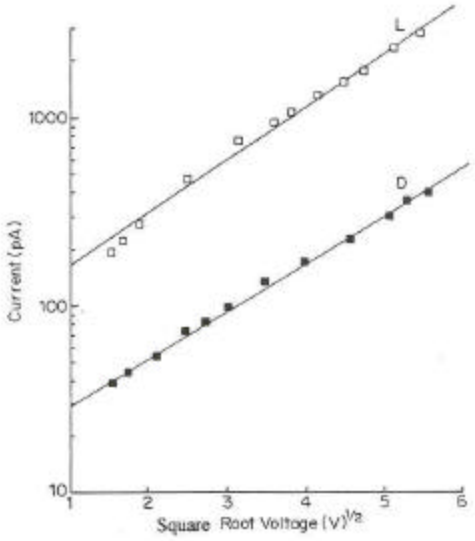

Fig. 4.40 Log I/ $V^{1/2}$ plot for Au/PVC-$CuCl_2$/CuPc/Au cell exhibiting a linear graph

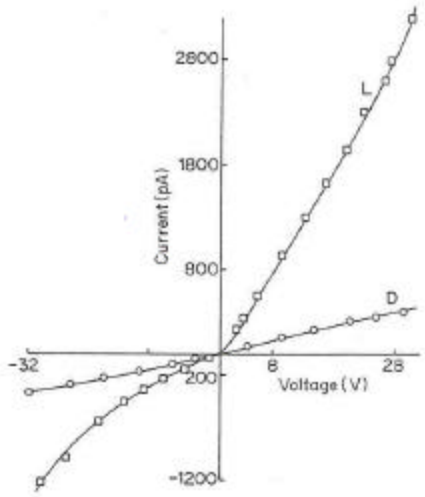

Fig. 4.41 I-V characteristics for the Au/PVC-$CuCl_2$/CuPc/ITO cell. Curves (D) and (L) indicate the I-V characteristics in dark and light

(ii) I-V characteristics for Au/PVC-$CuCl_2$/CuPc/ITO sandwich cells:

I-V characteristics similar to those obtained for the cell with Au are observed in the present case (see **Fig.4.41**). However, larger photocurrents are observed in the forward bias i.e. $ITO^{\oplus}$, than with $Au^{\oplus}$ as CuPc is a hole-transporting layer while ITO acts as an effective hole collector, moreover ITO also ohmic to CuPc [21]. A plot of log I against $V^{1/2}$

was made as shown in the **Fig.4.42**. It can be noticed that the plot is a straight line implying the presence of Schottky barrier at the PVC-$CuCl_2$/CuPc interface. A light sensitivity factor of 8 could be determined.

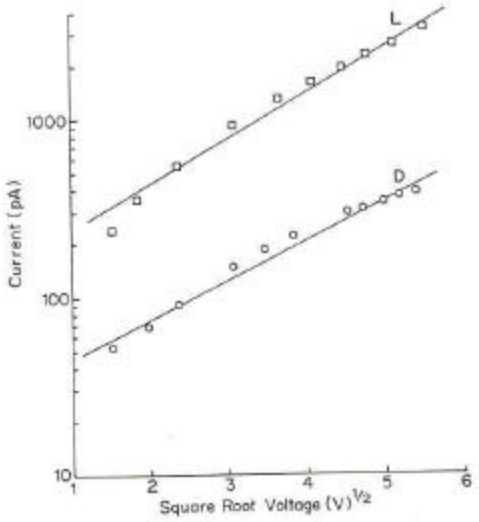

Fig. 4.42 Log $I/V^{1/2}$ for the Au/PVC-$CuCl_2$/CuPc/ITO cell

(iii)I-V characteristics for Au/PPy/PVC-$CuCl_2$/CuPc/Au multilayered cell:

Rectifying I-V characteristics similar to those obtained for cell (i) and (ii) are observed and presented in the **Fig.4.43**. The charge transport mechanism was found to be of Schottky type. Photocurrents were also observed indicated by the curve (L). It is interesting to note that the currents are higher in 10^{-6} A as compared to 10^{-9} A obtained for cells (c) and (d). This is due to the presence of PPy that acts as an efficient hole-transporting layer.

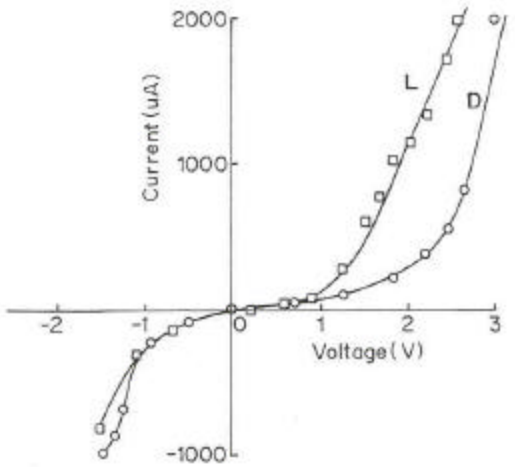

Fig. 4.43 I-V characteristics for the Au/PPy/PVC-$CuCl_2$/CuPc/Au multilayered cell exhibiting rectifying characteristics

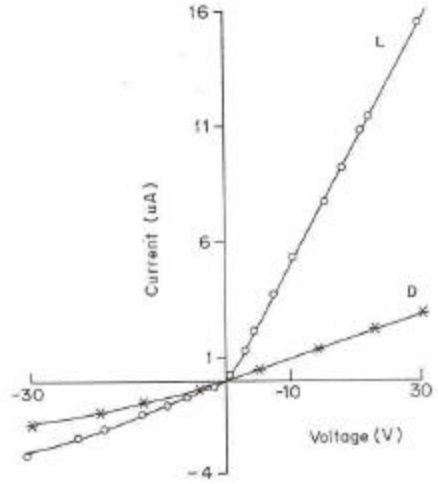

Fig. 4.44 I-V characteristics for Au/PPy/PVC-$CuCl_2$/CuPc/ITO multilayered cell

---

(iv) I-V characteristics for Au/PPy/PVC-$CuCl_2$/CuPc/ITO multilayered cell:

Similar rectifying I-V characteristics are obtained when ITO is used as a counter electrode (see **Fig.4.44**). High currents as well as photosensitivity of a factor of 5.9 are observed.

These various results suggest that Schottky barrier exists at the CuPc/PVC-$CuCl_2$ interface that also exhibits photosensitivity.

(2) Variation of CuPc:

The I-V characteristics for the samples with varying CuPc exposed to pyrrole for 15 seconds are shown in the **Fig.4.45**. It is observed that the I-V curves are mostly linear in nature with some non-linearity in the case of the composites containing higher CuPc. The non-linearity in the I-V characteristics usually occurs at higher electric fields. Since the intergranular gap decreases with the increase of CuPc, there will be high electric strength (V/d) for such composites. Hence, any barrier or space charge effect present will get reflected in the I-V curves for such composites. The log $I/\sqrt{v}$ curves were plotted to find out the influence of CuPc concentration on the charge transport process. The log I vs. $V^{½}$, gave a linear dependence, the slopes of which are represented graphically with respect to the CuPc composition. It is obvious from the **Fig. 4.46** that the slope increases from 0.35 to 0.41 as the CuPc composition increases from 0 to 20% w/w. Slope then reach a steady value as the CuPc is further increased. The decreasing trend of the slope which increasing CuPc decreases the interparticular distance $d^{1/2}$ parameters leading to an increase in the slope till 20 to 30%.

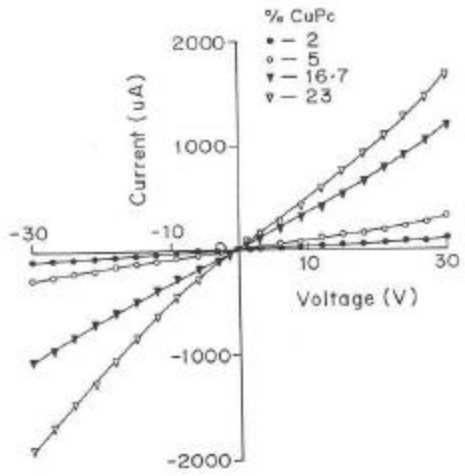

Fig. 4.45 I-V characteristics for PPy/CuPc in-situ composites with PVC-$CuCl_2$ containing 2, 5, 16.7, and 23 % CuPc exposed to pyrrole for 15 sec

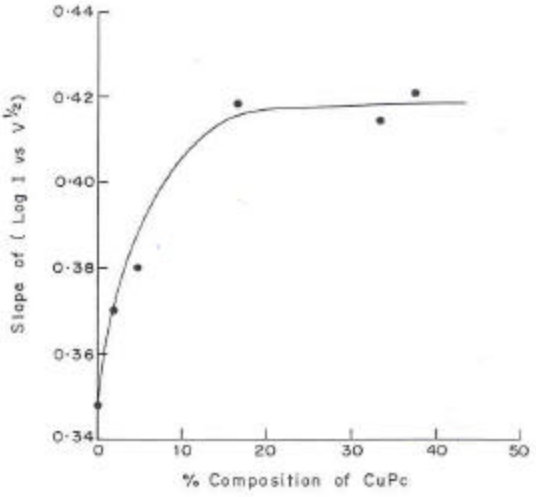

Fig. 4.46 Variation of slopes of log I/ $V^{1/2}$ with respect to the CuPc composition

I-V characterization was also carried out for the above system exposed to pyrrole till saturation. It is observed from the **Fig.4.47** that the curves are exclusively linear irrespective of the composition of CuPc showing that there is continuous conduction path for the charge carriers. The formation of conducting paths of PPy, leads to shorting of CuPc/PVC-$CuCl_2$ junctions and ohmic type of I-V characteristics are obtained.

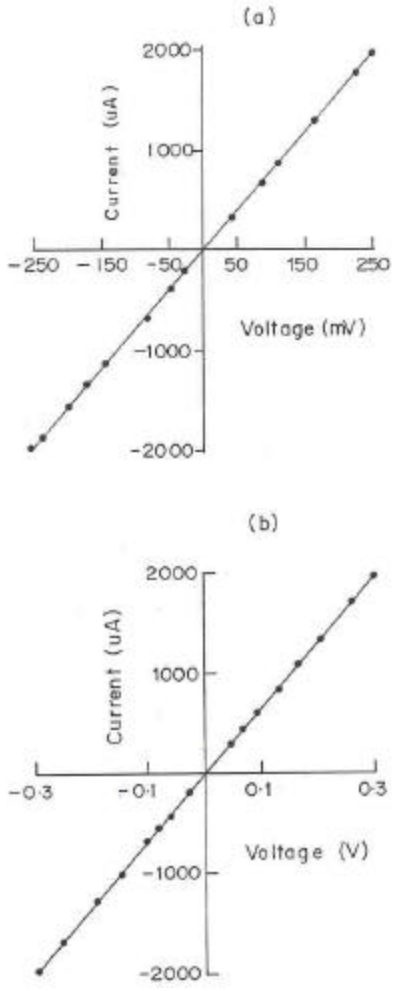

Fig. 4.47 I-V characteristics of the PPy/CuPc in-situ composites with PVC-$CuCl_2$ exposed to pyrrole till saturation

(d)Temperature dependence of conductivity:

The variation of conductivity with temperature was studied in the range of 30^0C to 120^0C for CuPc alone in PVC-$CuCl_2$ (without PPy). It was found that the conductivity rises with rising temperature and the plots of log I vs. 1/T was obtained as shown in the

Fig.4.48. The plots are more or less linear with 0, 9, 16, and 23% showing two distinct slopes for the high temperature and low temperature region. The activation energies were calculated from these and **Fig.4.49** shows the change in ΔE with respect to the CuPc concentration. A sharp change in ΔE from 0.17eV to 0.065eV was observed till 16% of CuPc whereafter it remains almost constant with respect to the CuPc content.

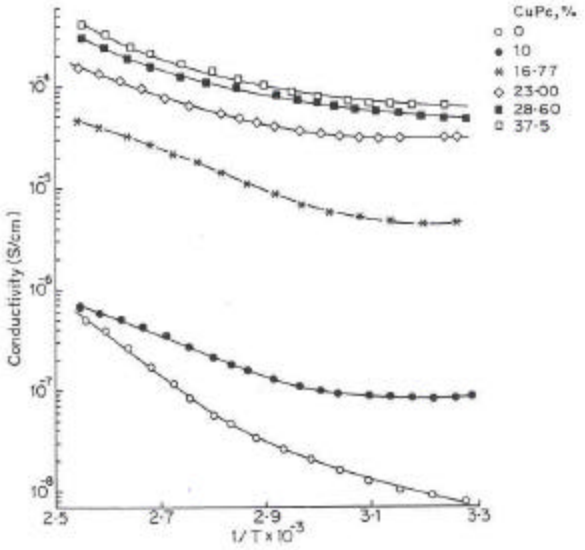

Fig. 4.48 Temperature dependence of conductivity for CuPc/PVC-$CuCl_2$ containing 0, 10, 16.7, 23, 28.6 and 37.5% CuPc

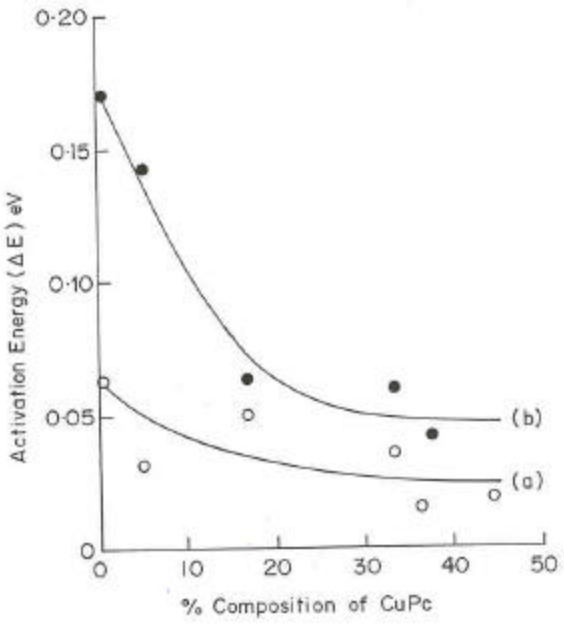

Fig. 4.49 Decrease in activation energy with respect to the CuPc concentration. Curve (a) represents the E_A for low temperature region and curve (b) the E_A for high temperature region

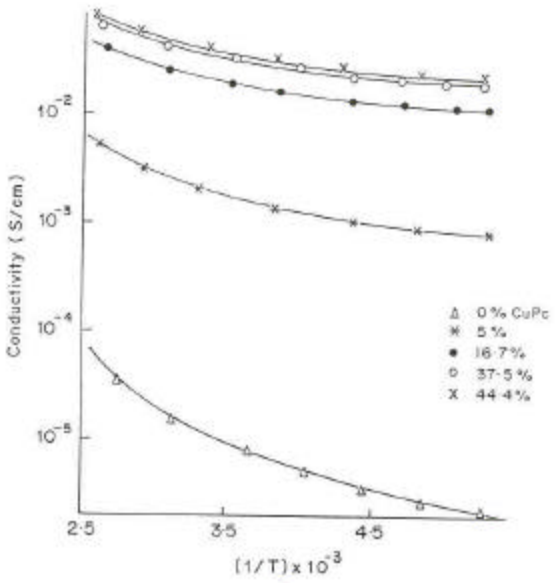

Fig. 4.50 Variation of conductivity with temperature for the PPy/CuPc in-situ composites with PVC-$CuCl_2$ with a less exposure to pyrrole

The dependence of conductivity on the temperature for CuPc/PVC-$CuCl_2$ composites after little exposure to pyrrole, is illustrated in the **Fig.4.50** with temperatures ranging from -100 to 110^0C. It is observed that the plot is a straight line in the low temperature region. Activation energy was determined from these plots and is presented graphically as **Fig.4.51** with respect to CuPc concentration. It can be seen that by comparison with

Fig.4.49, the ΔE is very low for all the compositions due to the formation of PPy providing conducting channels in the composite.

In the case of composites containing high PPy content (exposure to saturation), the temperature dependence of conductivity follows essentially $T^{-1/4}$ law as depicted in the **Fig.4.52**, which is as per the Mott's VRH model.

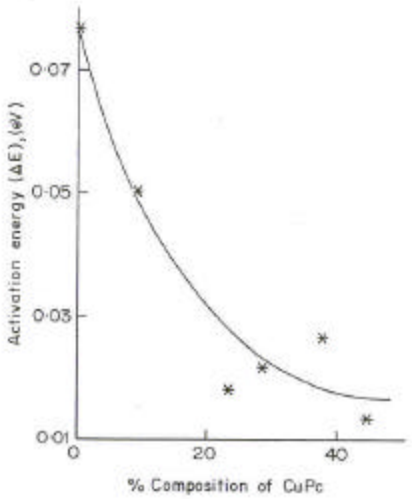

Fig. 4.51 Activation energies for the PPy/CuPc in-situ composites with PVC-$CuCl_2$ determined using the Arrhenius equation

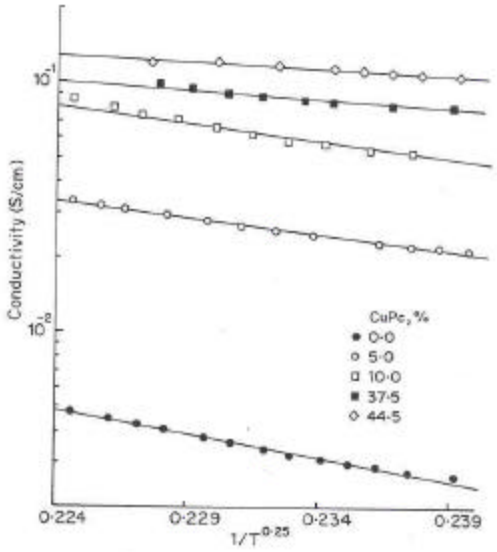

Fig.4.52 Variation of conductivity with respect to $1/T^{0.25}$ according to the VRH model for PPy/CuPc composites with PVC-$CuCl_2$ exposed to pyrrole till saturation

(e) Photosensitivity:

The photosensitization effect of CuPc was carried out for the present composite system. The IV characteristics in dark and under illumination were observed to more or less overlap in case of all the compositions. Hardly any photosensitivity was observed in

the present system. This is because there is no barrier at the interface of the materials. A barrier is one of the prerequisites for the presence of photoconductivity. The inert matrix PVC does not provide a polar environment in the vicinity of the dispersed CuPc particles [22]. This leads to a low rate of separation of the hole-electron pair created due to excitation by the interaction with visible light. Moreover the fraction of charges which get separated under the action of applied electric field get trapped at the impurity centres and thus are not available for giving a photocurrent.

4.4 Conclusions:

The charge transport processes in the PPy/PVC-$CuCl_2$ blends and composites can be explained on the basis of the various results discussed above. In case of the ex-situ blend, charge transport occurs by percolation method. The single junction studies depict a small barrier at the PPy/PVC-$CuCl_2$ interface. The in-situ blends exhibit a higher conductivity than the ex-situ blends. This occurs due to the formation of interpenetrating network of PPy yielding a high conductivity. Moreover, PVC-$CuCl_2$ has a phase-segregated morphology hence PPy deposition take place uniformly in the matrix. Hence a more uniform blending is achieved in the in-situ case.

The in-situ composite of PPy/CuPc with PVC-$CuCl_2$, exhibits conductivity as high as $1x10^{-1}$S/cm. Actually, a barrier is seen to exist at the interface of CuPc/PVC-$CuCl_2$ in the single junction studies that also exhibits considerable photosensitivity. However, in case of the composites, the CuPc gets doped by $CuCl_2$ that consequently introduces impurity states and hence reduces the barrier at the CuPc/PVC-$CuCl_2$ interface and hence a loss in the photosensitivity. The charge transport in the blends and the composite follow a Poole-Frenkel type of conduction mechanism while the studies carried out at the interface of the materials exhibit contact-limited Schottky emission. Network formation at higher PPy contents causes short-circuiting of the CuPc/PVC-$CuCl_2$ barriers and conduction by VRH model.

4.5 References:

1. Chilton J A, Goosey M T, Special Polymers for Electronics and Optoelectronics, Chapman and Hall, London 1995

2. Cooper E C, Vincent B, J Phys D: Appl Phys **22** (1989) 1580

3. Mandal T K, Mandal B M, Makromolecules : New Frontiers, Proc IUPAC, Int. Symp. Adv. Poly. Sci.Technol. **Vol.1**, 296, Edt. Srinivasan K S V, Allied Publ. Ltd. New Delhi 1998

4. Seanor D A, Electrical Properties of Polymers, Eds. Frisch K C and Patsis A, Ch.3, Technomic Publ. Co, Wesport, Conn 1972 p.37-51

5. Kang T J, Miyaki Y, Han J H, Motobe T, Whang Y E, Miyata S, Prog Pac Polym Sci 3, Proc Pac Polym Conf 3rd 307, Edt. Chiggino K P, Springer: Berlin Germany

6. Kang T J, Miyata S, Miyaki Y, Polm Bull 31(5) (1993) 593

7. Radhakrishnan S, Mandale A B, Synth Met 62 (1994) 217

8. Unsworth J, Jin Z, Lunn B A, Innis P C, Polym Int 26(4) (1991) 245

9. Ueno T, Arntz Hans-Detlef, Flesch S and Bargon J, J Makromol Sci-Chem, A 25(12) (1988) 1557

10. Mott N F and Davis E A, Electronic Processes in Non-Crystalline Materials,

Clarendon Press, Oxford, 1979.

11. Sichel E K, Carbon Black Polymer Composites, Marcel Dekker, New York, (1982) 110

12. De Paoli M A, Waltman R J, Diaz A F, and Bargon J, J Poly Sci : Polym Chem Ed vol23, (1985) 1687

13. Niwa O, Hikita M, Tamamura T, Appl Phys Lett, 46 (1985) 444

14. Polymer Durability, Edt. Clough R L, Billingham N C, Gillan K T, Adv Chem Series 249, ACS, Washington DC, 1996

15. Collins R A, Abass A K, Krier A, Thin Solid Films 239(2) (1994) 268

16. Sharma G D, Sangodkar S G, Roy M S, Mater Sci Eng B, B41(2) 1996) 222

17. Xavier F P, Goldsmith G J, Bull Mater Sci 18(3) (1995) 269

18. Pfeiffer M Beyer A, Fritz T Leo K, Appl Phys Lett 73(22) (1998) 3202

19. Takeuchi M, Ohtsu S, Takeoka H, Naganuma S, Nagasaka H, Tech. Dig.-Int Photovoltaic Sci and Eng Conf, Ist 263-6, Tokyo, Japan 1984

20. Remaki B, Guillaud G, Mayes D, Opt Mater 9(1-4) (1998) 240

21. Yamamoto N, Tonomura H , J Appl Phys, 52(9) (1981) 5705

22. Minami N, Sasaki K, Tsuda K, J Appl Phys 54(11) (1983) 6764

Chapter 5 - PPy/$CuCl_2$ based CdS composites

5.1 Introduction:

The use of $(CH)_x$ as a photosensitive material was reported by Heeger's group by a demonstration of p-$(CH)_x$/n-ZnS heterojunction that gave an open circuit potential of 0.8 V [1]. PPy has been used in combination with CdS mainly to prevent photo anodic decomposition of semiconductors [2]. The semiconducting photoanode materials are all susceptible to oxidative decomposition when photogenerated holes (h^+) rise to the top of the valence band. All n- type non-oxide photo-anodes suffer irreversible decomposition when exposed to light in aqueous electrolyte solutions. In order to stabilize n- type semiconductors against photo-anodic decomposition, a PPy film is usually electropolymerized on the semiconductor electrode. Visible light water cleavage has been reported by PPy-coated n-CdS photonode on which RuO_2 was attached [3]. However, little work describing the semiconductor contacts and photovoltaic applications has been reported in the literature. The present chapter deals with the electrical and photoconductive properties displayed by a PPy/CdS heterojunction. The influence of the type of the materials used and the method of fabrication was on the charge transport process across the junction was investigated.

PPy/CdS heterojunctions have been fabricated in the present case, in the form of a composite by vapour phase deposition technique. The virtue of achieving interpenetrating network of PPy by the vapour phase deposition method in the solid polymer electrolyte – (PEO-$CuCl_2$) was put to use in the case of in-situ composites. Multiple junctions were also prepared by making a composite of PPy with CdS by ex-situ method. The charge transport at each of the micro-junctions was carried out by constructing PPy/CdS single junctions. The charge transport and photosensitivity has been investigated with respect to the composition of PPy and CdS. The CdS used in all dispersions was encapsulated with PEO. It is well known that the polymer composites consisting of photoconducting powder dispersed in a polymer matrix exhibit high photosensitivity especially at high fields, high intensities [4]. Such photoconducting composites have found wide application especially as photo resistors and electrophotographic layers [5]. CdS encapsulated in various polymers like PMMA, PS, etc. was reported to have light sensitive effect. These results have been compared with those obtained using commercially available grade, which definitely shows a lower photosensitivity.

5.2 Experimental:

(a) Synthesis of in-situ CdS:

Nanoparticulate CdS was prepared by in-situ technique. A reaction of $CdCl_2$ with Na_2S was carried out in methanol containing PEO. A 2:1 ratio of PEO:$CdCl_2$ was used. $CdCl_2.2½ H_2O$ (6 gms) and PEO (2gms) were dissolved in 250ml methanol containing 50 ml water. To this was added a 50 ml methanol solution containing 2.4gms Na_2S without stirring. The solution was then digested overnight and then stirred to obtain fine colloidal precipitate. The precipitate was filtered and dried in air for 24 hrs.

(b) Synthesis of the PPy/CdS in-situ composite:

The PPy/CdS in-situ composite was synthesized by using vapour phase polymerized PPy. The composite was prepared by two methods wherein in one case the PPy was generated by the VPP technique first and then CdS was added to it, whereas in the other case, CdS was dispersed in PEO-$CuCl_2$ and then the CdS/PEO-$CuCl_2$ dispersion was exposed to pyrrole so as to obtain in-situ PPy in the matrix containing CdS.

(1) PPy/CdS in-situ composite (I):

A solution of PEO-$CuCl_2$ was prepared in methanol with a PEO-$CuCl_2$ ratio of 4:1 monomer/mole. The solution was then poured in a large petridish and then exposed in a desiccator previously saturated by pyrrole vapours. The duration of exposure was 24 hours. The PPy/PEO-$CuCl_2$ thus obtained was the dried thoroughly in a dessicator and used for preparation of the composites.

The composites were prepared by dispersing CdS-IS in a constant quantity of PPy in various amounts ranging from 20, 30, 40, 50, 60 and 80 % by weight. The two were thoroughly mixed making a thick paste in methanol. The solvent then evaporated and the residue was dried in air. The resulting powder was scraped off the petridish and pelletized under a pressure of 3 tons. Air-drying silver paste was applied on one face of the pellet while the counter electrode used was transparent conducting ITO coated glass so as to form a sandwich cell configuration.

(2) PPy/CdS in-situ composite (II):

The composites were prepared by adding different quantities of the in-situ grade CdS (CdS-IS) to a 5 ml methanol solution of PEO-$CuCl_2$ (4:1). The amount of CdS was varied from 20, 30, 40, to 50% by weight keeping the quantity of PEO-$CuCl_2$ constant. The slurry was prepared by continuously stirring for thirty minutes and then applied uniformly over interdigited gold-coated glass substrate. The films were dried in a desiccator and then exposed to pyrrole vapours in a closed chamber. The exposure time was one minute so that limited PPy was formed. Excess PPy gives high conductivity but no photosensitivity. The various parameters like stirring time and time of exposure to pyrrole were strictly controlled. I-V characteristics of these films were studied by using IT0 as the top electrode. Commercial grade CdS was also used instead of the in-situ prepared CdS. In another set of experiments the $CuCl_2$ content was varied by changing the PEO-$CuCl_2$ ratio from 4:1 to 8:1, 16:1 and 32:1 monomer/mole. The composites were prepared in the same manner as in the above case. The effect of variation of $CuCl_2$ concentration on the I-V characteristics was noted.

(c) Synthesis of PPy/CdS ex-situ composite:

An ex-situ composite was prepared by using PPy-synthesized by chemical polymerization technique.

The chemically synthesized PPy using $CuCl_2$ as the oxidant was used in making a dispersion of PPy and encapsulated CdS. 10% PEO by weight was used as a binder for preparing the composite. PPy was added in various compositions of 10, 20, 30, 40 and 50% by weight to CdS containing 10% PEO. The slurry was prepared in methanol and applied on interdigited gold electrodes resulting in the formation of surface cells.

(d) Synthesis of PPy/CdS single junctions:

Single junctions were created in a sandwich cell mode having a multilayered structure of the type Au/PPy/CdS/Au. Firstly, electrochemical deposition of PPy on gold coated substrates was carried out. Commercially available CdS was vacuum evaporated on the PPy films for various durations to vary the thickness of the CdS film. A thin layer of gold as a counter electrode was the vacuum deposited on top of the multilayered structure using a mask. Electrical connections were made by air-drying silver paste.

5.3 Results and discussion:

5.3.1 Charge transport in PPy/CdS ex-situ composite with PEO-$CuCl_2$:

A composite was prepared by an ex-situ method wherein PPy was externally added to the encapsulated CdS. This was done by dispersion of PPy powder in encapsulated CdS using 10% PEO as a binder.

(a)Compositional variation of conductivity:

The conductivity of the system increases with the increase in the PPy composition as exhibited by the **Fig.5.1.** It is observed that the conductivity increases from $4.5x10^{-10}$S/cm, (which is the conductivity of encapsulated CdS) to $1x10^{-6}$S/cm with PPy addition till 20% whereafter it attains limiting value. As discussed in Chapter 3, percolation threshold denotes the critical concentration at which the conduction occurs by percolation method. It may be estimated from the log-log plot as indicated by (see **Fig 5.2**). It was found to be almost 1wt.% PPy, which is similar to that obtained for the blends discussed so far. The increase in amount of PPy yields a network formation of PPy around CdS particles, leading to a high conductivity.

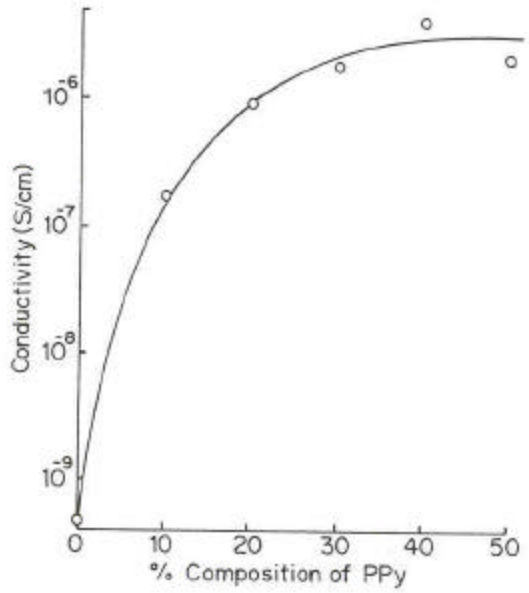

Fig. 5.1 Conductivity variation with respect to PPy composition in the PPy/CdS ex-situ composites with PEO-$CuCl_2$

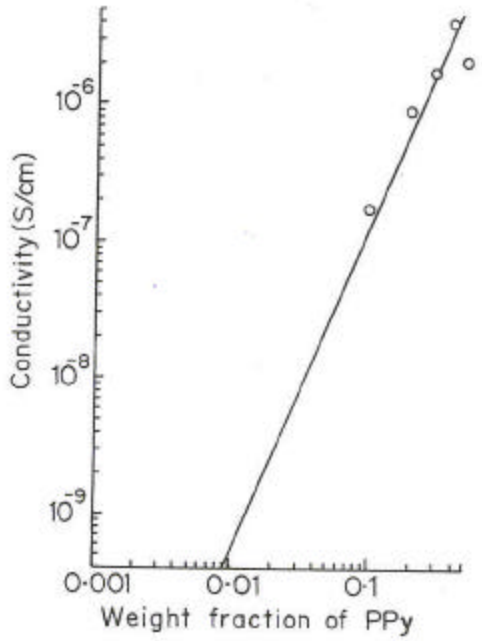

Fig. 5.2 Log-log plot of conductivity against the weight fraction of PPy in the PPy/CdS ex-situ composites with PEO-$CuCl_2$

(b)I-V characteristics of the PPy/CdS ex-situ composites:

The I-V curves for the PPy/CdS dispersed system are found to be non-linear in nature with the degree of non-linearity decreasing with the higher composition of PPy **Fig.5.3**. The I-V curves were then analyzed by making a plot of log I against $V^{½}$. It was found that the plots exhibit a linear dependence as illustrated by the **Fig. 5.4**, implying the presence of a barrier at the interface of these materials. The slopes of the plots show an increase with higher PPy content as indicated by the **Fig.5.5**. This behaviour can be explained on the basis of the variation involved in the distance between the PPy particles as the composition changes. The increase in the PPy content in the PEO-CdS, brings about a decrease in the interparticular distance (d), between the PPy particles. This results in a higher slope with a higher PPy composition.

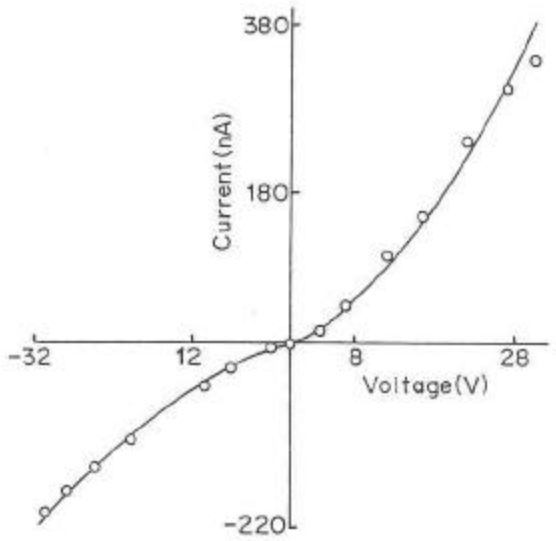

Fig. 5.3 I-V characteristics of the PPy/CdS ex-situ composites with PEO-$CuCl_2$ containing 10% PPy

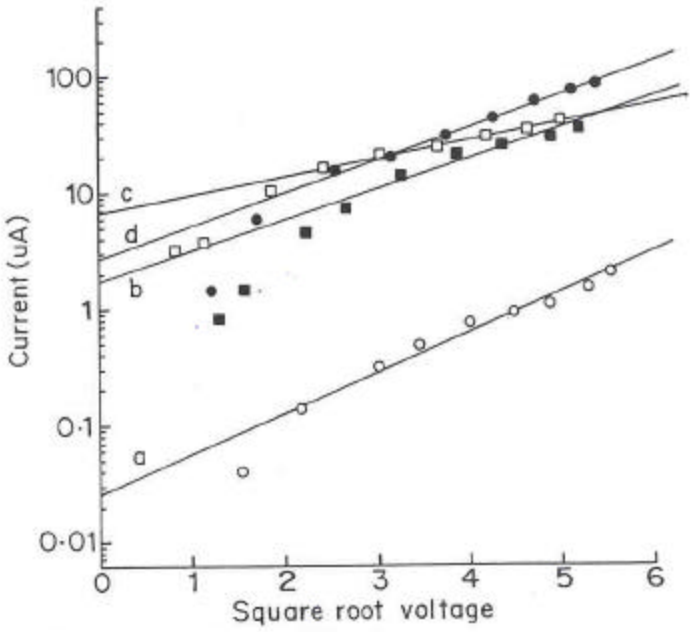

Fig. 5.4 Log I against $V^{1/2}$ dependence for the PPy/CdS ex-situ composites with PEO -$CuCl_2$ containing 20, 30, 40 and 50% PPy indicated by curves (a) to (d)

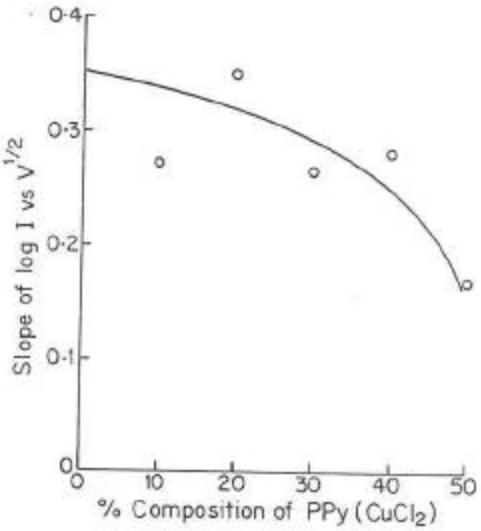

Fig. 5.5 Variation of slopes of log I/ $V^{1/2}$ with the PPy composition for PPy/CdS ex-situ composites with PEO-$CuCl_2$

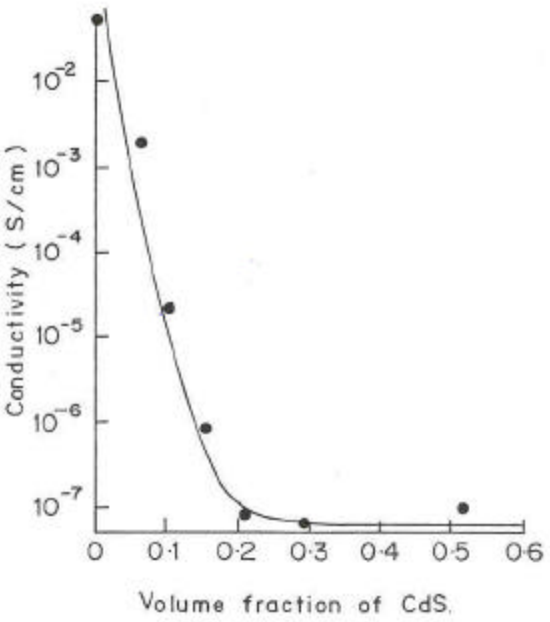

Fig. 5.6 Dependence of conductivity on the volume fraction of CdS for the PPy/CdS in -situ composite (I) with PEO-$CuCl_2$

Hence a barrier exists at the PPy/CdS interface and the charge transport takes place by Poole-

Frenkel mechanism.

5.3.2 Charge transport in PPy/CdS in-situ composites with PEO-$CuCl_2$:

The charge transport studies were carried out by using vapour phase polymerized PPy. A compositional variation was done in order to investigate the influence of CdS content on the photoconductive properties of the system. All the studies were carried out in a sandwich cell configuration.

(A) PPy/CdS in-situ composite (I):

As discussed in the section 5.2, the present composite was obtained by dispersion of CdS in the VPP PPy.

(a) Compositional dependence of conductivity:

The dependence of conductivity for the PPy/CdS composite system on the composition of CdS is exhibited in the **Fig.5.6** as log σ against the volume fraction of CdS. It is observed that the conductivity decreases as the volume fraction of CdS increases. It decreases abruptly from $9x10^{-1}$ S/cm to $5x10^{-7}$S/cm as the volume fraction of CdS increases to 0.17 after which the conductivity remains almost constant. This composition of CdS where the conductivity of the system saturates corresponds to the critical composition of the filler in a composite at which the particles of CdS form a contact with each other resulting in a continuous phase. Thus the percolation threshold is achieved at 40% CdS composition in the present case. This behaviour can be understood as follows. Discontinuities are created in the conducting PPy network due to the incorporation of CdS. Increase of CdS leads to a successive replacement of the existing PPy network by CdS. The conductivity at the critical composition corresponds to that of pure CdS, which remains constant in spite of the change in the composition on account of the continuous network formed.

(b) I-V Characteristics for PPy/CdS in-situ composite (I):

The I-V characteristics are found to be non-linear in nature. Furthermore, the degree of non-linearity is seen increasing with increasing CdS content as observed in the **Fig. 5.7 (a), (b), (c), (d), (e)** and **(f)** corresponding to 20, 30, 40, 50, 60 and 80% CdS. The system thus consists of the n-type CdS phase dispersed in the interpenetrating, p-type PPy phase. However

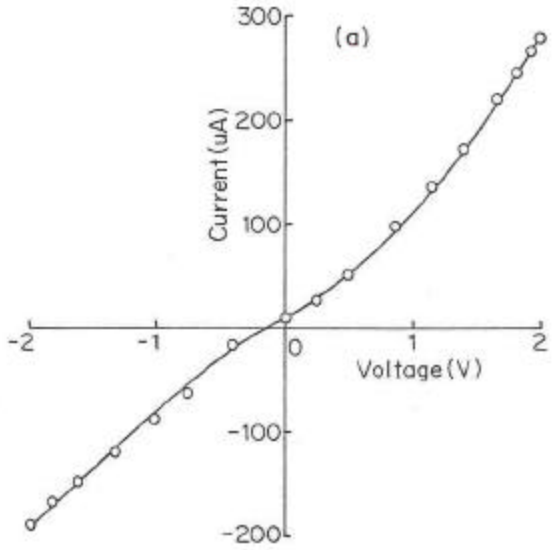
(a)
300
200
100
-100
-200
Current (uA)
-2
-1
0
1
2
Voltage (V)

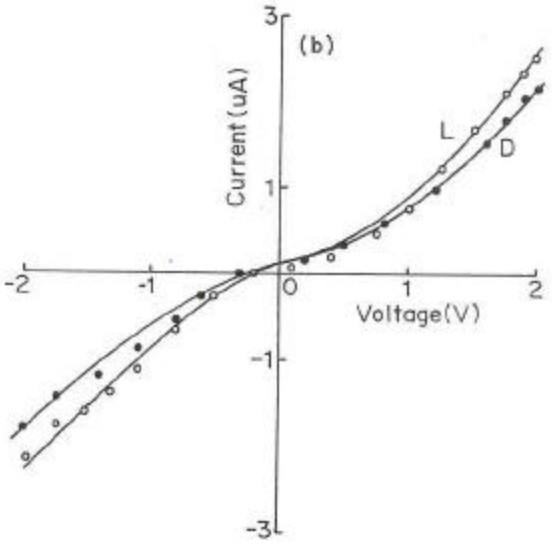
(b)
3
1
-1
-3
Current (uA)
L
D
-2
-1
0
1
2
Voltage (V)

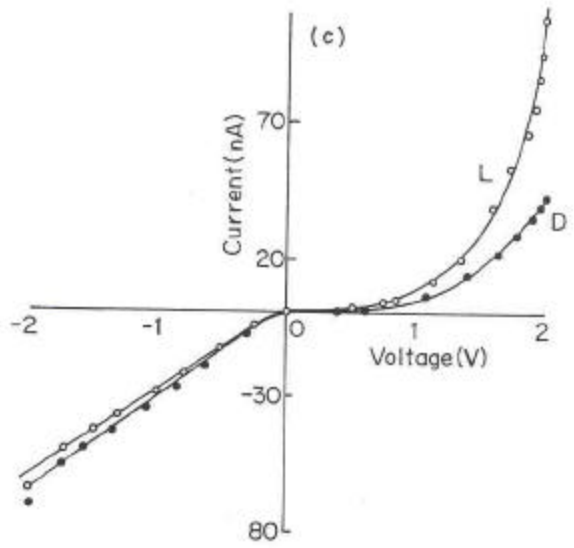
(c)
Current (nA)
70
20
-30
80
-2
-1
0
1
2
Voltage (V)
L
D

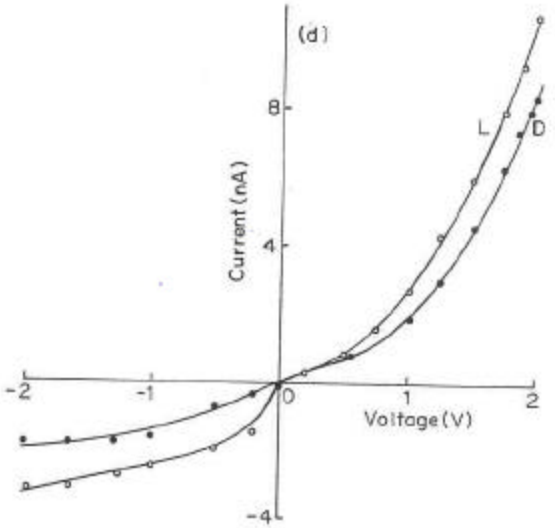
(d)
Current (nA)
8
4
-4
-2
-1
0
1
2
Voltage (V)
L
D

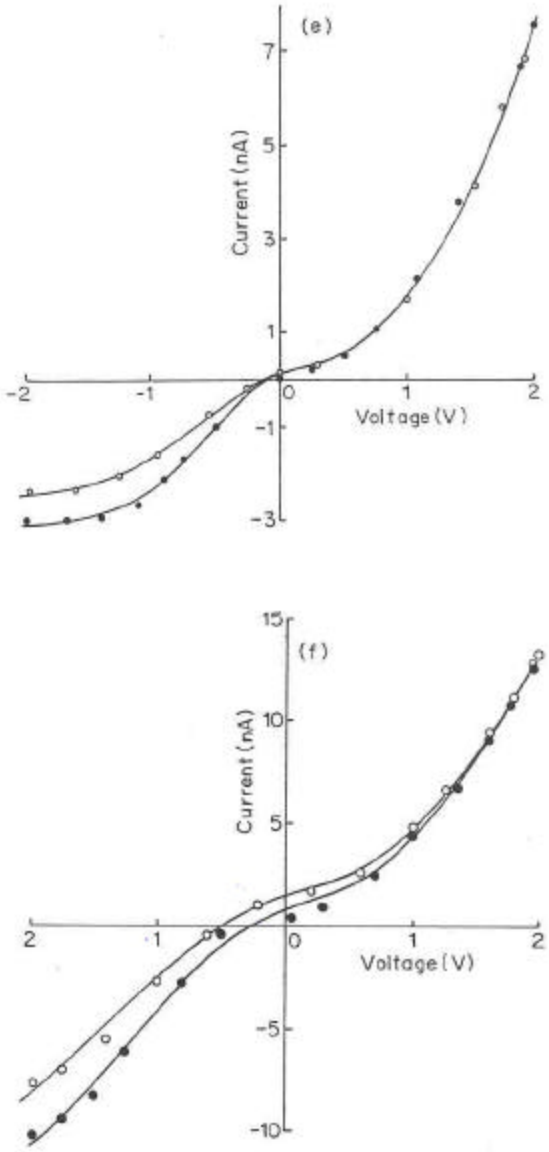

Fig. 5.7 I-V characteristics for the PPy/CdS in-situ composite (I) with PEO-$CuCl_2$ containing (a) 20, (b) 30, (c) 40, (d) 50 (e) 60 and (f) 80 % CdS

a considerable change in the I-V characteristics was observed with the increase in CdS. The

curves (a) and (b) appear non-linear in nature which increasingly become rectifying at higher concentrations as indicated by curves (c), (d) and (e). Variation of CdS content was expected to effectively control the thickness of PPy between the CdS particles. No chemical reaction of the vapour phase polymerized PPy with CdS was envisaged. The CuCl that is obtained as a by-product of the VPP process reacts with CdS only at high temperatures above 90^oC [6]. An experiment to verify this was done by pouring a 20% aqueous solution of CuCl over 80% CdS composite. This was then filtered and palletized. The resistance was found to be 14MΩ and is comparable to the pure CdS ensuring no reaction between the two.

Further, the I-V curves for the composites containing 20 and 30% CdS were analyzed by plotting on a log-log scale. However, the slopes of the plots were less than two, hence the SCLC mechanism was ruled out. A plot of log I against $V^{½}$ was made as exhibited by the **Fig.5.8 (a)** and **(b)**. The plots are linear showing a dependence on Richardson-Schottky equation. This behaviour can be understood as follows. The 20 and 30% CdS composites are well below the percolation threshold wherein PPy is present as a continuous network. This results in short-circuiting of the PPy/CdS barriers. The conduction hence takes place via interchain and intrachain hopping process along the PPy chains. All these composites are tested in a sandwich cell configuration using Ag and ITO as the electrodes as mentioned in the experimental. Ag is ohmic to PPy while ITO acts as a blocking contact [7]. Hence non-linear characteristics obtained for 20 and 30% CdS compositions are due to the space charge created at the PPy/ITO interface, caused by the blocking nature of ITO (ITO acting as a low work-function metal, $\Phi \gg 4.7$ eV).

The microstructure of the composite becomes exactly reverse when a higher concentration of 40% CdS is dispersed in the vapour phase deposited PPy. Formation of CdS network, gives rise to barriers at the PPy/CdS interfaces. Considering the energy band diagram of the materials (**Fig.5.9**), an energy barrier of 1.5 eV can be determined due to the mismatch of the energy levels causing a the barrier at the interface of PPy and CdS. A barrier of 0.8 eV is reported by Skothiem [8]. The I-V curves for 40, 50, 60 and 80% CdS tend to be more rectifying and are similar to those obtained for p-n junctions [Fig 5.7 (c), (d), and (e)]. The curves were then analyzed for the SCLC conduction mechanism by plotting on a log-log scale as shown in the **Fig.5.10 (a), (b)** and **(c)** for the composites containing 40, 50 and 60% CdS. It can be

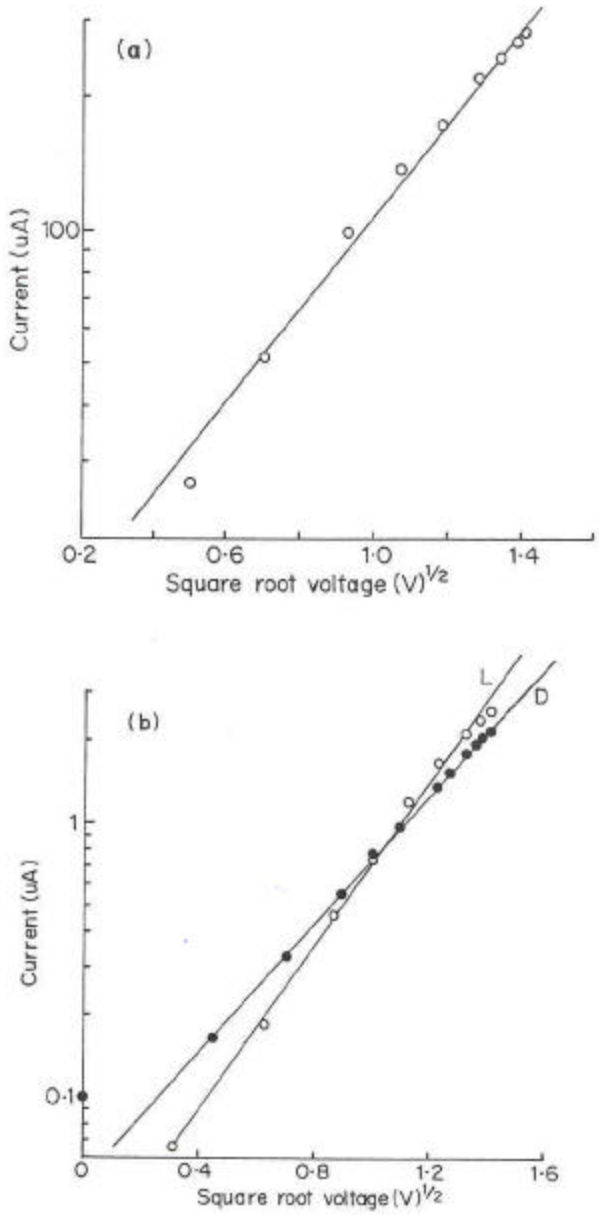

Fig. 5.8 Log I/ $V^{1/2}$ dependence for (a) 20% and (b) 30% CdS in PPy/CdS in-situ composites (I) with PEO-$CuCl_2$

observed that the magnitude of the slopes of these plots turned 2 at higher voltages. The

current in SCLC is given by,

$$I = \frac{8}{9} m q \left[V^{n+1} / d^{(2n+1)} \right] \qquad \text{Eq.5.1}$$

where μ is the mobility, d the film thickness, θ is a parameter which takes into account the trapping center (impurity centers) concentration and their distribution and n is an integer having values 0, 1, 2 etc.

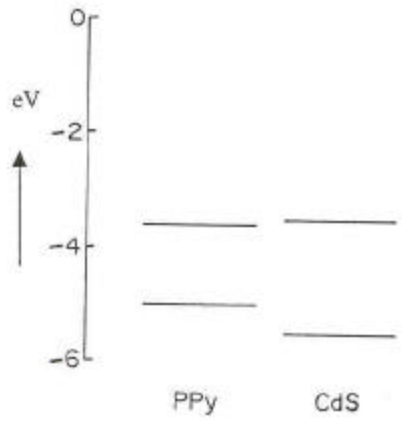

Fig. 5.9 Energy band diagram for PPy and CdS

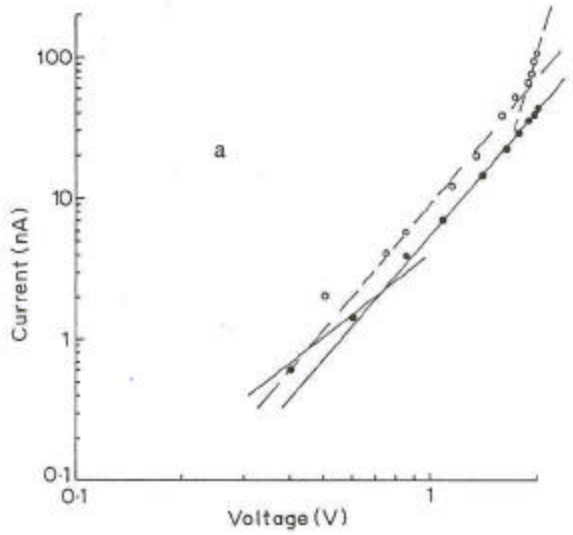

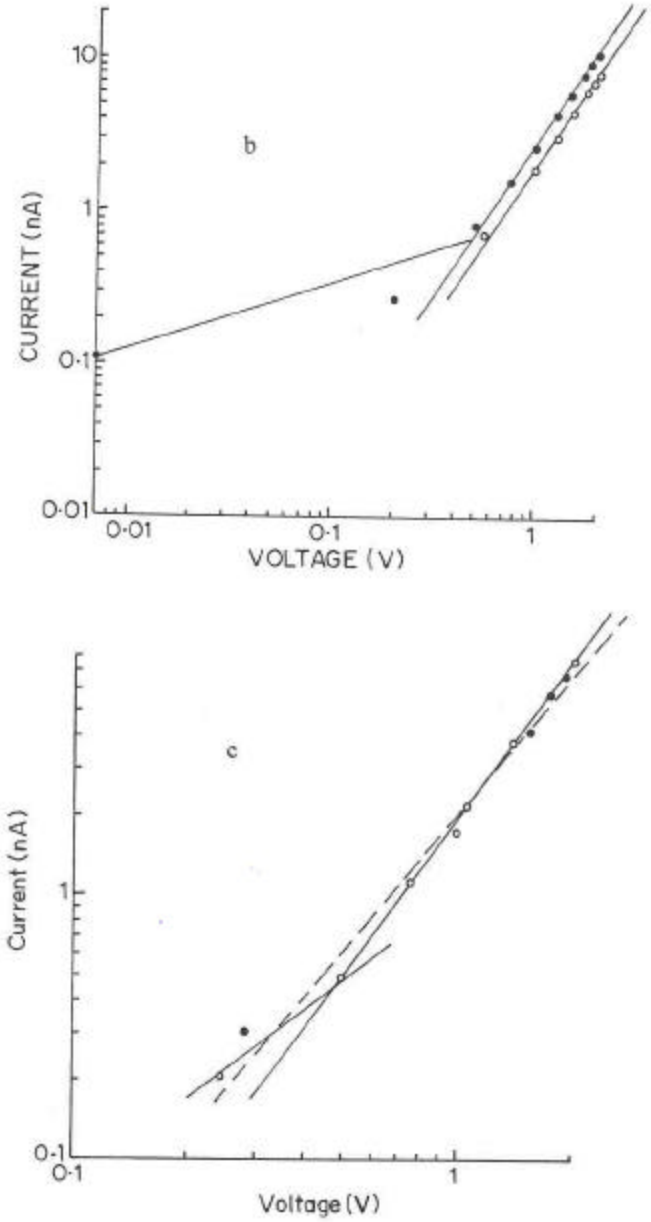

Fig. 5.10 Log-log plot of the I-V characteristics for the PPy/CdS in-situ composite (I) with PEO-$CuCl_2$ containing (a) 40 (b) 50 and (c) 60% CdS

This clearly denotes that the power law with exponent 2 is obeyed for the composites

containing CdS beyond the percolation threshold. The changeover of the junctions from PPy/ITO to PPy/CdS is clearly brought out by the varying nature of the I-V characteristics. The conduction takes place according to the SCLC mechanism as the composition of CdS increases. Similar type of diode characteristics have been obtained by Skotheim and Inganas [8]. The results have been explained on the basis of a Schottky barrier formation at the PPy/CdS interface. Studies on poly(methyl thiophene) /CdS in solid state also show a rectifying heterojunction formation as reported by Frank and Glenis [9].

The above studies were carried out for PPy/CdS barriers in a composite form. In order to investigate the charge transport at the interface of PPy/CdS alone, single junctions were constructed across the interface of electrochemically deposited PPy and vacuum deposited CdS.

The I-V characteristics of the device Au/PPy/CdS/Au in a sandwich mode were strongly rectifying in nature as indicated by the **Fig 5.11 (a).** These curves were then analyzed for the conduction behavior. SCLC seemed to be the most appropriate one amongst all the various mechanism available for conduction. A plot of I-V was made on a log-log scale as shown in the **Fig 5.12**. It is evident from the log-log curves that the relation, $I \propto V^n$ is indeed followed. The value of n equals unity depicting an Ohmic behavior at lower voltage while at higher voltages $n \geq 3$, indicating a space charge limited current. Zuleeg [10] has reported SCLC in In/CdS/Au sandwiches in which indium made the ohmic contact. The plot obeyed $I \propto V^3$ law with $I \propto V^2$ in the intermediate region suggesting an SCLC behaviour. These changes in the value of n can be interpreted as filling of impurity centers giving rise to linear, square and superlinear type of I-V characteristics. The V_{TFL}, the voltage at which majority of the traps get filled, was determined from the plot and was found to be 2.065 V. V_{TFL} was also determined in a similar manner under reverse bias conditions and was found to be 2.0 V.

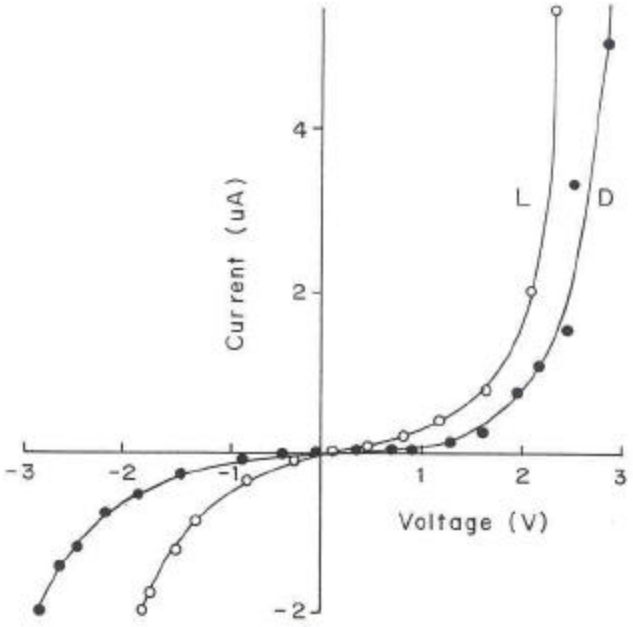

Fig. 5.11 I-V characteristics for the Au/PPy/CdS/Au multilayered cell

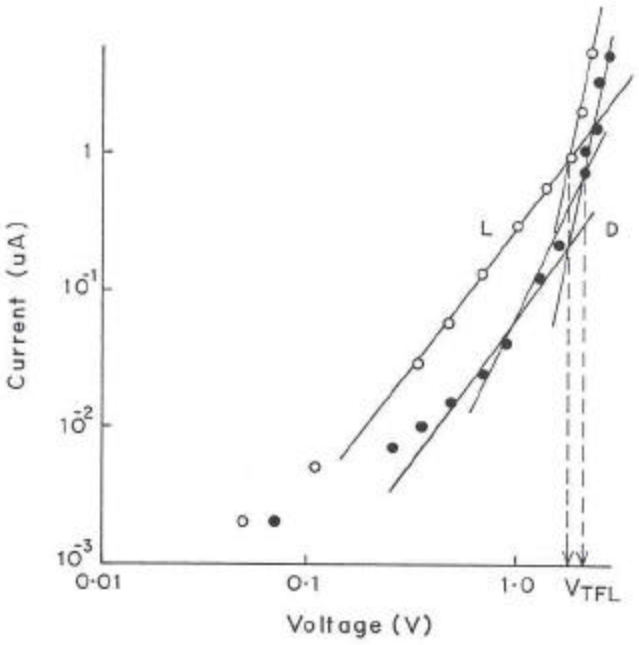

Fig. 5.12 I-V characteristics for PPy/CdS single junction on a log-log scale

PPy being synthesized by electrochemical route is highly doped ($\sigma \geq 1$S/cm) and has a p-type

character. Gold makes an ohmic contact with PPy as discussed in Chapter 3. Metal /CdS contacts have been well studied in the past and Au is reported to form a blocking contact to CdS [11]. But it is known that with a modest voltage across the thin barrier, a tunneling of electrons takes place from the Au electrode. Hence a Schottky barrier is observed at low voltage while the contact becomes injecting as the tunneling of electrons takes place. The device as a whole then becomes forward bias with respect to CdS. The p-nature of PPy in the present multilayered structure increases the possibility of a p-n junction formation as reflected by the rectifying I-V characteristics.

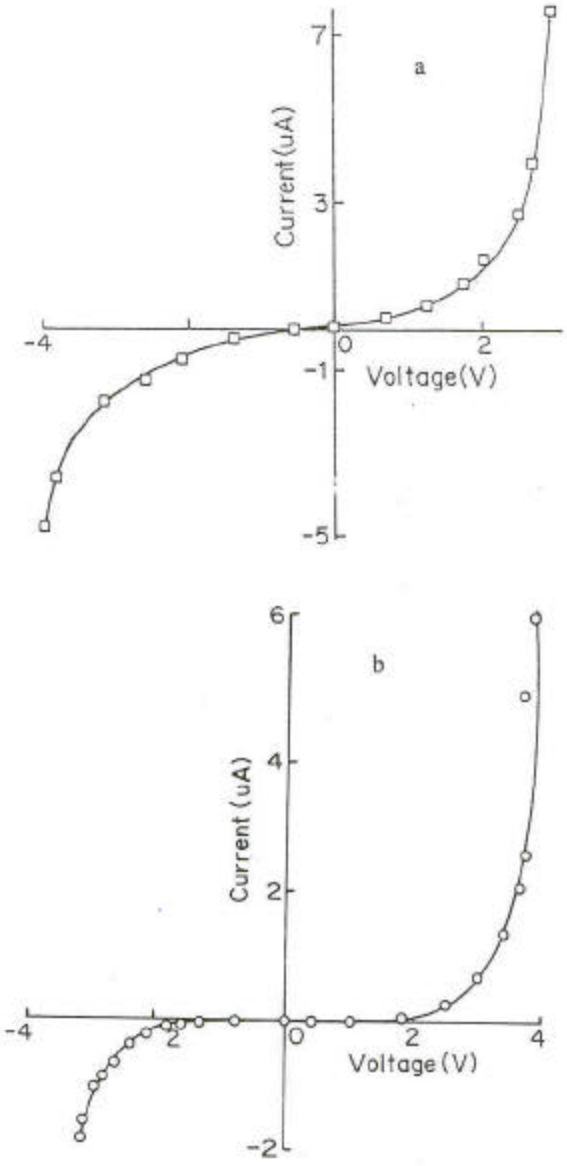

Fig. 5.13 I-V characteristics of PPy/CdS single junctions with increasing thickness of the CdS vacuum deposited layer represented by curves (a) and (b)

The junction characteristics were also studied by varying the thickness of CdS layer. **Figs.5.13 (b)** and **(c)** denote the I-V characteristics for the sandwich cells with increasing CdS thickness. An SCLC mechanism is observed in all the cases. A remarkable variation can be observed in the V_{TFL} values, which are seen to be increasing with the increasing thickness of the CdS layer. The results are presented in the **Table 5.1**

Table 5.1

Sample-No.	V_{TFL}	
	Forward bias	Reverse bias
a	2.06	2.45
b	2.40	2.85
c	2.62	3.00

When a thicker layer of CdS is added, the barrier width of the Au/CdS Schottky junction increases thus increasing the voltage required for the electrons to overcome the barrier. Also, the number of trapping centers rise, as CdS layer grows thicker. The voltage required to achieve the trap filled limit increases. Under reverse bias conditions a rectification is observed since electrons are minority carriers and a depletion region is created at the PPy/CdS interface.

Photosensitivity at the PPy/CdS heterojunctions was also studied. The I-V characteristics under illumination are presented along with the I-V curves in dark (see Fig 5.11(a). CdS has a relatively wide energy band gap and acts as a window material in most of the solar devices [12,13]. Comparatively, PPy is a less photoactive material. The recombination probabilities are high in PPy due to the presence of midgap states. Hence the photoresponse observed is due to the excitations occurring in CdS. The sample was illuminated through the CdS face rather than through PPy to avoid light absorption by the polymer layer causing less PPy/CdS interface. The mechanism of photoexcitation and conduction is similar to conventional p-n junctions. Absorption of energy during illumination generates excited electron-hole pairs in CdS. These get separated under the action of field in the space charge region at the PPy/CdS interface since most of the depletion layer is concentrated in CdS. CdS transfers the excited electrons to PPy resulting in a photocurrent. The I-V curves under illumination were analyzed for the SCLC mechanism. It was found that the V_{TFL} under illumination was reached at a lower voltage than under dark as observed in the Fig. 5.13 (b) and (c). The V_{TFL} was seen shifting from 2.06V in dark to 1.77V under

illumination in the case of curve (a) while it shifts from 2.4V to 1.88V in the case of curve (c). The reason may be that the photoexcited electrons are trapped by the impurity centers in addition to the injection of charge from the cathode. This brings out the filling of traps at a lower voltage under illumination as is evident by the shift of V_{TFL} to a lower value.

Hence it is clear that the charge transport in PPy/CdS in-situ composites (I) below the percolation threshold, i.e. for 40,50, 60 and 80% occurs by SCLC type of conduction mechanism due to the creation of PPy/CdS barriers. Photoconductivity of the present composite was also studied. I-V characteristics under illumination were recorded and are represented in the respective figures along with the I-V curves recorded in dark. The photosensitivity exhibited by the composites containing 20, and 30% CdS is due to metal-semiconductor Schottky barrier formation. The illumination of these junctions creates some photocarriers, which undergo separation in the space charge region created at the IT0/PPy interface-giving rise to a small photocurrent. The photosensitivity was determined by taking the I_L/I_D and was found to increase with decreasing PPy concentration as indicated by the **Fig.5.14**. The I-V curve under illumination for 40, 50,60 and 80% CdS depicts an SCLC behaviour similar to that observed in dark. However, in the case of 40% PPy/CdS composite, the V_{TFL} is seen shifting to a lower value of 0.92 V from 1.8V (see Fig.5.10). This is an example of filling of the traps by the photoexcited carries at a low voltage. The photocurrent exhibited in the reverse direction increases with increasing CdS content while the photocurrent in the forward direction decreases as the p-n junction character increases with the increase in CdS. The overall sensitivity is low.

However, the charge transport for the PPy/CdS ex-situ composites is of Schottky type while the in-situ composites exhibit SCLC type of conduction behaviour. It is known that PPy behaves as a p-type material depending on its degree of oxidation, which is also reflected in the conductivity. The formation of a p-n junction between PPy and CdS is expected in the present case. The conductivity of chemically synthesized PPy in the formation of the ex-situ composites is of the order of 10^{-3} S/cm, which is quite low as compared to the vapour phase polymerized PPy in the in-situ case. PPy/CdS junctions were investigated with respect to the degree of oxidation by Hagemeister and White [14]. The authors have observed that the electrical properties of solid-state photovoltaic devices with redox conductive or electronically conductive polymer film depend strongly on the extent of polymer oxidation. It was found that

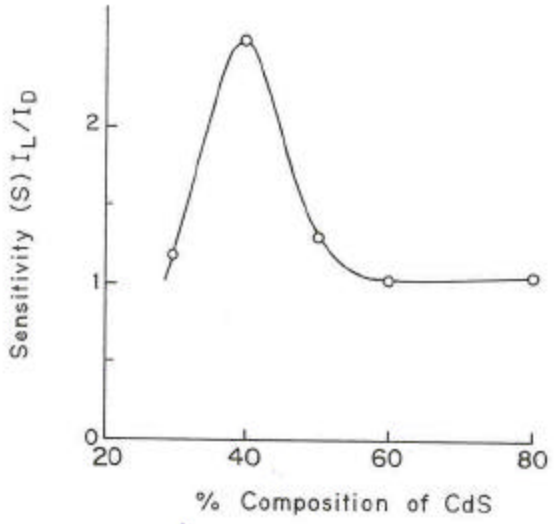

Fig. 5.14 Variation of the light sensitivity against the CdS composition for the PPy/CdS in-situ composites (I) with PEO-$CuCl_2$

PPy in the partially oxidized and charged state, $PPy^{0/+}$, yielded normal rectifying behaviour,

while in the fully reduced and neutral state it behaves as a thick insulating layer. From the conductivity data it can be inferred that the chemically synthesized PPy is in a partially doped form having a less 'p'-character in comparison to the latter. Probability of formation of p-n junction is thus reduced in the former case

(B) PPy/CdS insitu composite (II):

These composites were prepared by the partial vapour phase deposition of PPy in the PEO-$CuCl_2$ matrix containing CdS. The composition of $CuCl_2$ in PEO was increased from 32:1, 16:1, 8:1 to 4:1 monomer/mole ratio.

(a) Compositional variation of conductivity:

The conductivity exhibited a decrease in the conductivity with respect to the CdS composition in case of the 32:1 PEO-$CuCl_2$ composition. It is observed that the conductivity decreases in the case of composites containing higher amounts of CdS. This is understood as the filler-CdS is a semiconducting material. The system can be schematically described as CdS particles being dispersed in the PEO-$CuCl_2$ matrix. Beyond a critical concentration the CdS, the particles contact each other disturbing the connectivity of the PPy chains that decreases the conductivity. Similar results are observed for the composites containing increased $CuCl_2$. The **Fig.5.15** illustrates a consolidated plot of the conductivity of PPy/CdS composites containing varying amounts of $CuCl_2$. A decrease in the conductivity with higher CdS is observed in all the cases. An interesting feature to be noticed is that the change in conductivity is higher for the composites containing higher $CuCl_2$. For instance, the curve (d) indicates a rise in the conductivity by three orders of magnitude i.e. from 10^{-7}S/cm to 10^{-4}S/cm, which is somewhat similar as observed in curve (c), whereas curve (b) and (a) exhibit an increase by 4 and 6.5 orders respectively. An abrupt change in the conductivity at almost 50% CdS composition is observed for the composite containing 32:1 and 16:1 PEO-$CuCl_2$ while in the composite containing 4:1, the percolation threshold is seen to have reached at 35% CdS content. This behaviour may be due to the varying $CuCl_2$ content affecting the PPy formation in the composite. Accordingly, more PPy is formed in the composite containing more $CuCl_2$ (initiator /dopant). This in turn influences the ultimate conductivity of the composite.

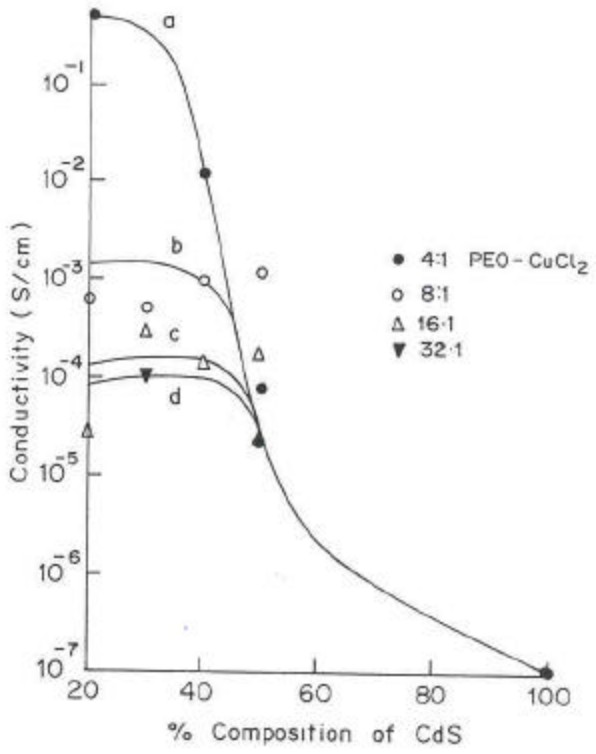

Fig.5.15 Consolidated plot of conductivity of PPy/CdS in-situ composites with PEO -$CuCl_2$ for varying $CuCl_2$. Curves (a), (b), (c) and (d) correspond to the PEO -$CuCl_2$ concentration of 4:1, 8:1, 16:1 and 32:1 monomer/mole

(b) I-V characteristics for PPy/CdS in-situ composites with PEO-$CuCl_2$:

In the case of the PPy/CdS in-situ composite containing 32:1 monomer/mole PEO-$CuCl_2$, the I-V characteristics are non-linear and tend to be rectifying in nature as the CdS content increases as indicated by the **Fig 5.16**. Curves **(a) (b) (c)** and **(d)** correspond to 20, 30, 40 and 50%. These were then analyzed for the SCLC mechanism by plotting on a log-log scale, however the slope of the plots is found to be between $1<n<2$. The I-V curves were then analyzed for Schottky or Poole-Frenkel behaviour by making a plot of log I against $\sqrt{v}$ which is presented in the **Fig. 5.17 (a), (b)** and **(c).** The slopes of the log I-$\sqrt{v}$ plots are plotted against the CdS composition as depicted in the **Fig.5.18**.

Similar non-linear I-V characteristics are observed in the case of the composites with 16:1 PEO-$CuCl_2$, containing 20, 30, 40 and 50% CdS content as depicted in the **Fig 5.19.** It is clearly observed that the degree of non-linearity decreases with the composition of CdS. The plots were then analyzed for log I-$\sqrt{v}$ analysis, that could be delineated into two straight lines in the case of 20 and 30% CdS composites while a single slope could be determined for 40 and 50% CdS addition [**Fig.5.20 (a), (b)** and **(c)**]. The variations in the slope of the plots are presented graphically as **Fig 5.21**.

The I-V characteristics of the composite system containing 8:1 PEO-$CuCl_2$ are highly non-linear exhibiting rectifying characteristics. **Fig.5.22 (a), (b), (c)** and **(d)** depict the IV curves for 20, 30, 40 and 50% CdS content. These were plotted on a log-log curve as shown in the **Fig.5.23 (a)** and **(b)** for the composites containing 20 and 50% CdS, yielding straight lines with slopes varying as the I-V characteristics are hence seen to follow an SCLC mechanism. Similar non-linear/asymmetric I-V characteristics that also show some extent of rectification are observed for the composites containing 4:1 monomer/mole PEO-$CuCl_2$. **Fig 5.24 (a)** to **(c)** represents the I-V curves for PPy/PEO-$CuCl_2$ with 20, 40 and 50% CdS content respectively. These I-V characteristics, similar exhibit strong rectification, accompanied by a marked difference in the magnitude of current and the degree of rectification. The plots were then analyzed to find out the exact conduction mechanism. **Fig. 5.25** indicates the I-V curve in dark and under illumination for 20% CdS content plotted on a log-log scale. The curves were found to be linear with the slope $n >> 3$. Since the slope shows a variation from linear to superlinear nature, SCLC mechanism of conduction was found to be most appropriate in the present case.

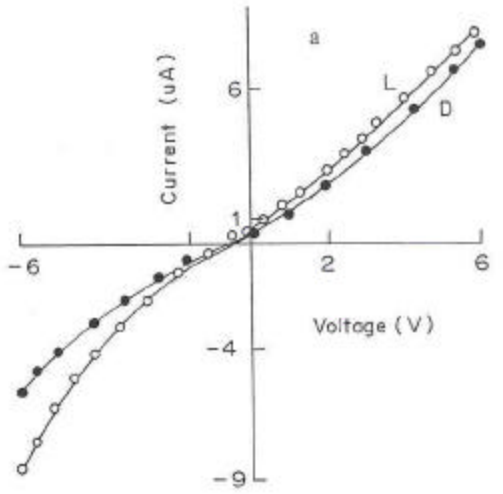
a
Current (uA)
6
1
-4
-9
-6
2
6
Voltage (V)
L
D

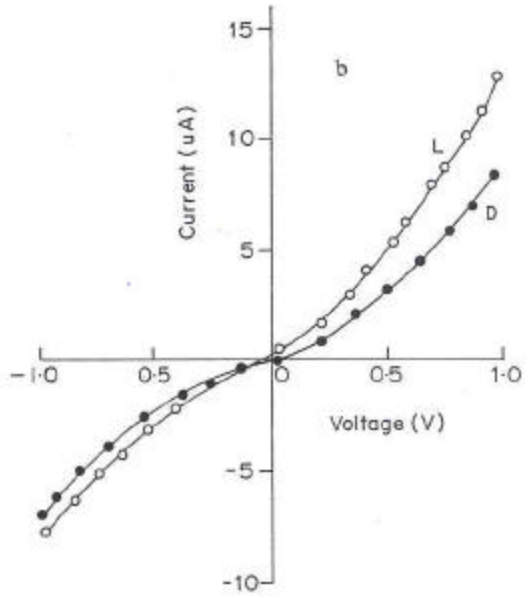
b
Current (uA)
15
10
5
-5
-10
-1·0
0·5
0
0·5
1·0
Voltage (V)
L
D

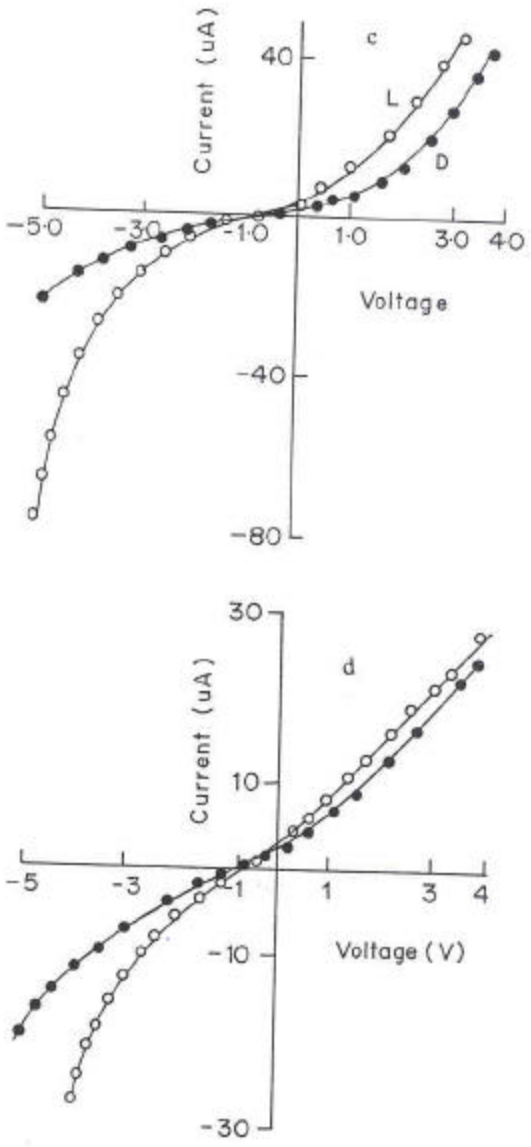

Fig. 5.16 I-V characteristics for the PPy/CdS in-situ composites (II) containing 32:1 M/m PEO-$CuCl_2$. Curves (a), (b), (c) and (d) represent 20, 30, 40 and 50% CdS concentration

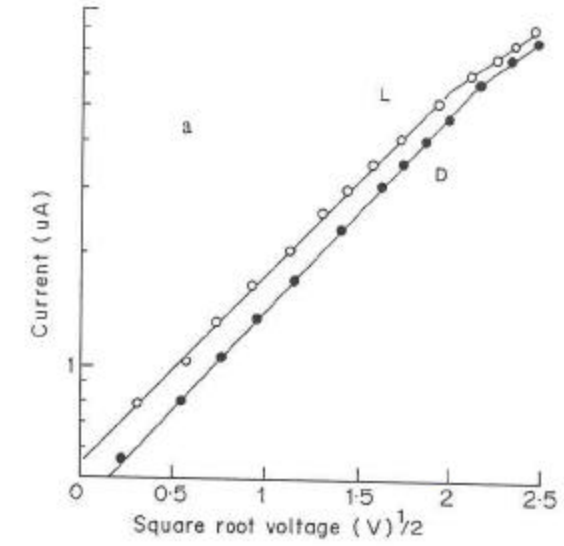
a
L
D
Current (uA)
1
0
0·5
1
1·5
2
2·5
Square root voltage (V)1/2

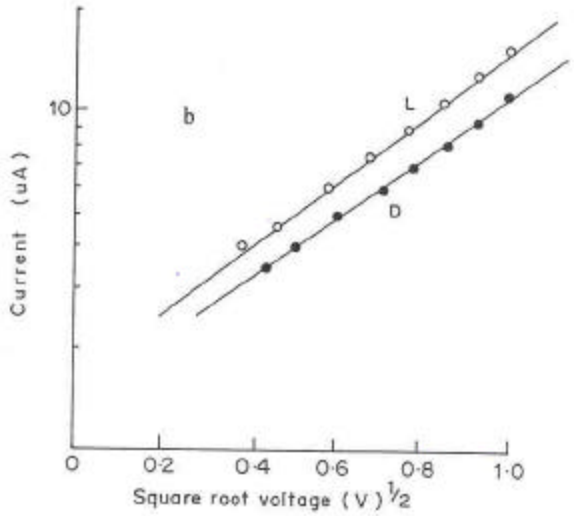
b
L
D
Current (uA)
10
0
0·2
0·4
0·6
0·8
1·0
Square root voltage (V)1/2

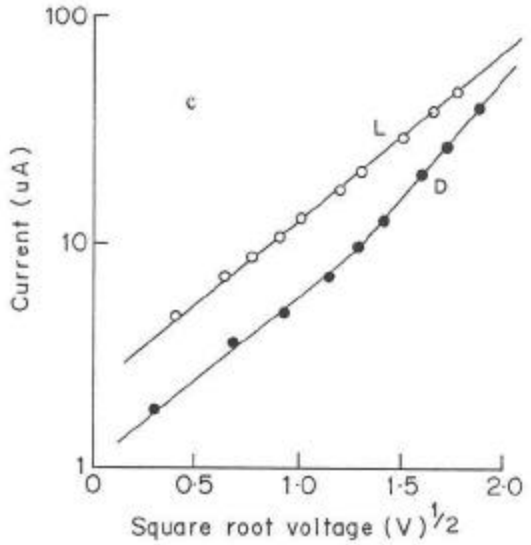

Fig. 5.17 Log I / $V^{1/2}$ plot of the I-V characteristics of PPy/CdS in-situ composites (II) with 32:1 M/m PEO-$CuCl_2$ containing (a) 20, (b) 30, and (c) 40% CdS respectively

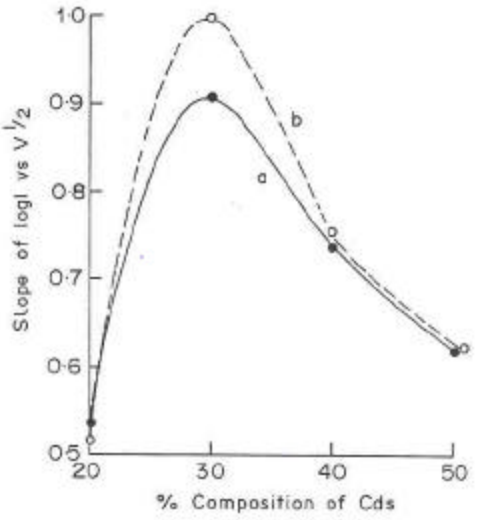

Fig. 5.18 Dependence of slopes of log I/ $V^{1/2}$ on the CdS in-situ composites (II) with 32:1 M/m PEO-CdS

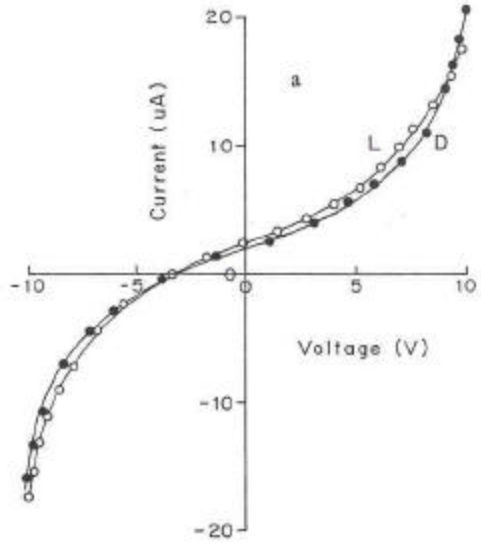
a
Current (uA)
Voltage (V)
L
D
20
10
-10
-20
-10
-5
0
5
10

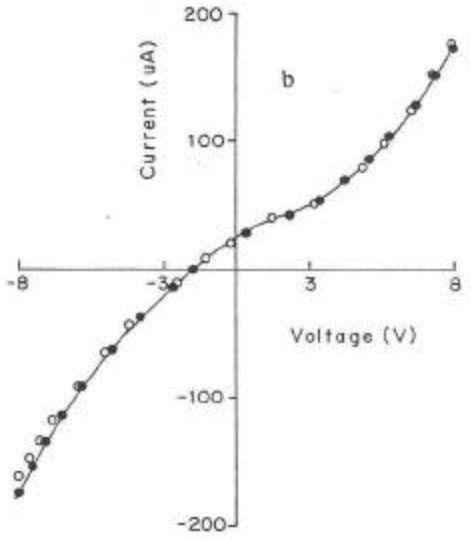
b
Current (uA)
Voltage (V)
200
100
-100
-200
-8
-3
3
8

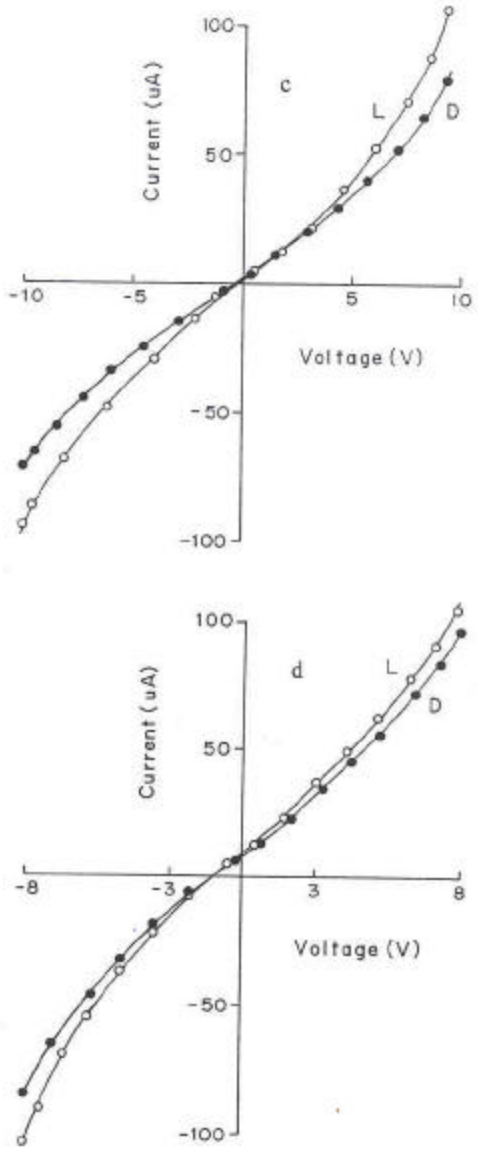

Fig. 5.19 I-V characteristics for the PPy/CdS in-situ composites (II) with 16:1 PEO -$CuCl_2$ containing 20, 30, 40 and 50% CdS as indicated by curves (a), (b), (c) and (d) respectively

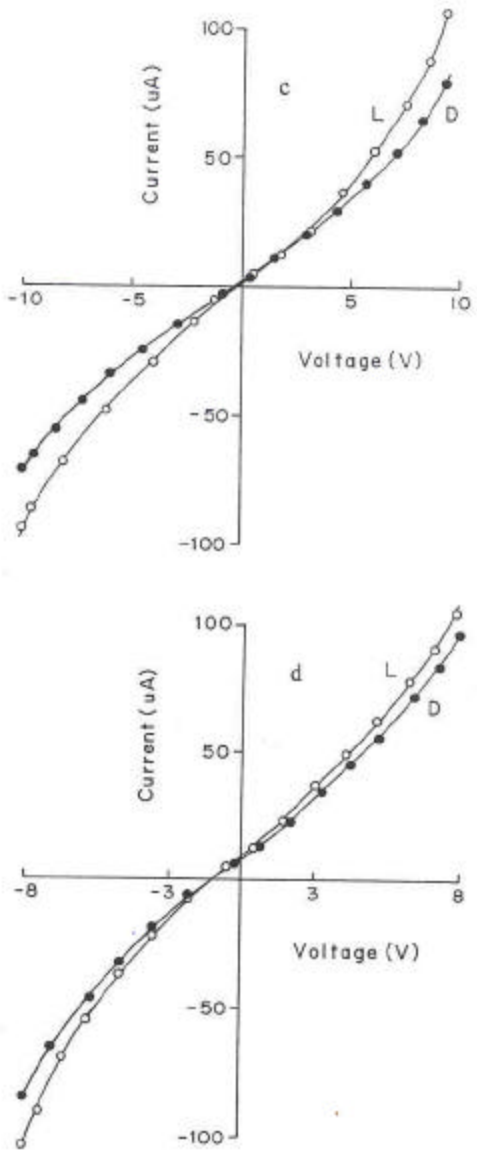

Fig. 5.19 I-V characteristics for the PPy/CdS in-situ composites (II) with 16:1 PEO -$CuCl_2$ containing 20, 30, 40 and 50% CdS as indicated by curves (a), (b), (c) and (d) respectively

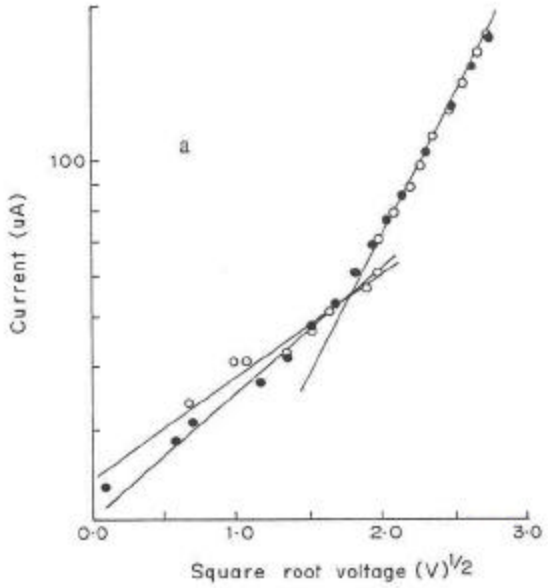
a
100
Current (uA)
0·0
1·0
2·0
3·0
Square root voltage (V)1/2

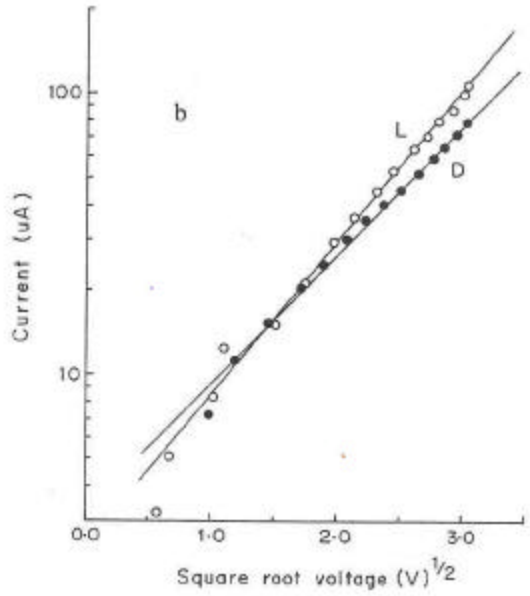
b
100
10
L
D
Current (uA)
0·0
1·0
2·0
3·0
Square root voltage (V)1/2

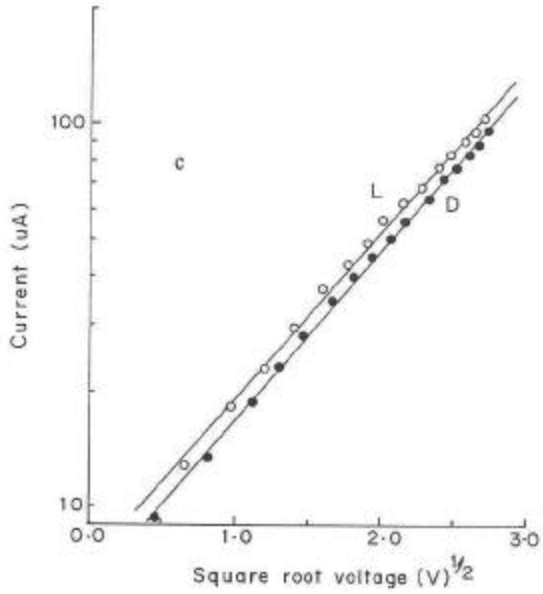

Fig. 5.20 Linear dependence of Log I on $V^{1/2}$ for PPy/CdS in-situ composite (II) with 16:1 M/m PEO-$CuCl_2$ containing 30, 40 and 50% CdS as indicated by curves (a), (b), and (c) respectively

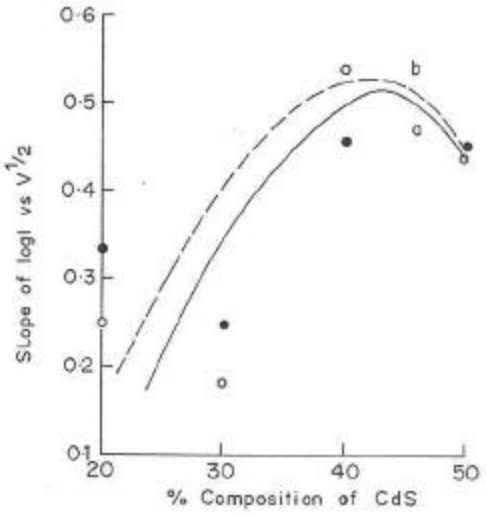

Fig. 5.21 Variations in the slope of log $I/V^{1/2}$ with respect to the CdS composition for the PPy/CdS in-situ composite (II) with 16:1 M/m PEO-$CuCl_2$

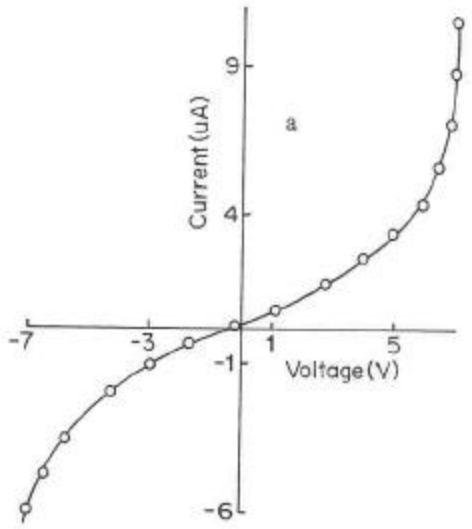
a
Current (uA)
9
4
-6
-7
-3
-1
1
5
Voltage (V)

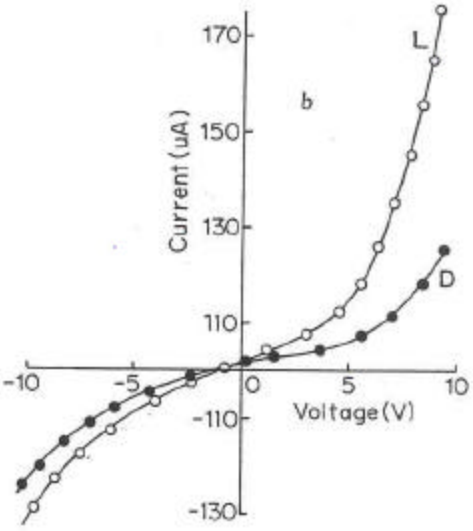
b
L
D
Current (uA)
170
150
130
110
-110
-130
-10
-5
0
5
10
Voltage (V)

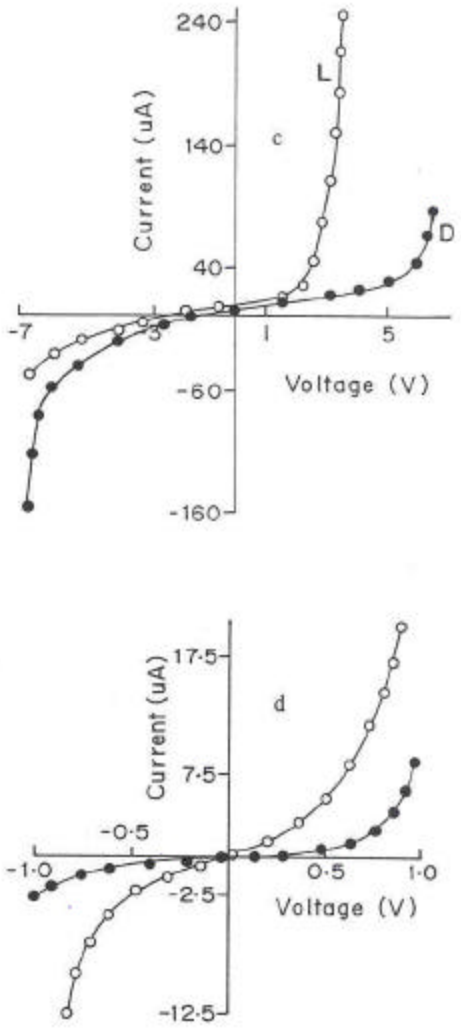

Fig. 5.22 I-V characteristics for PPy/CdS in-situ composite (II) with 8:1 M/m PEO-$CuCl_2$ containing (a) 20, (b) 30, (c) 40 and (d) 50 % CdS

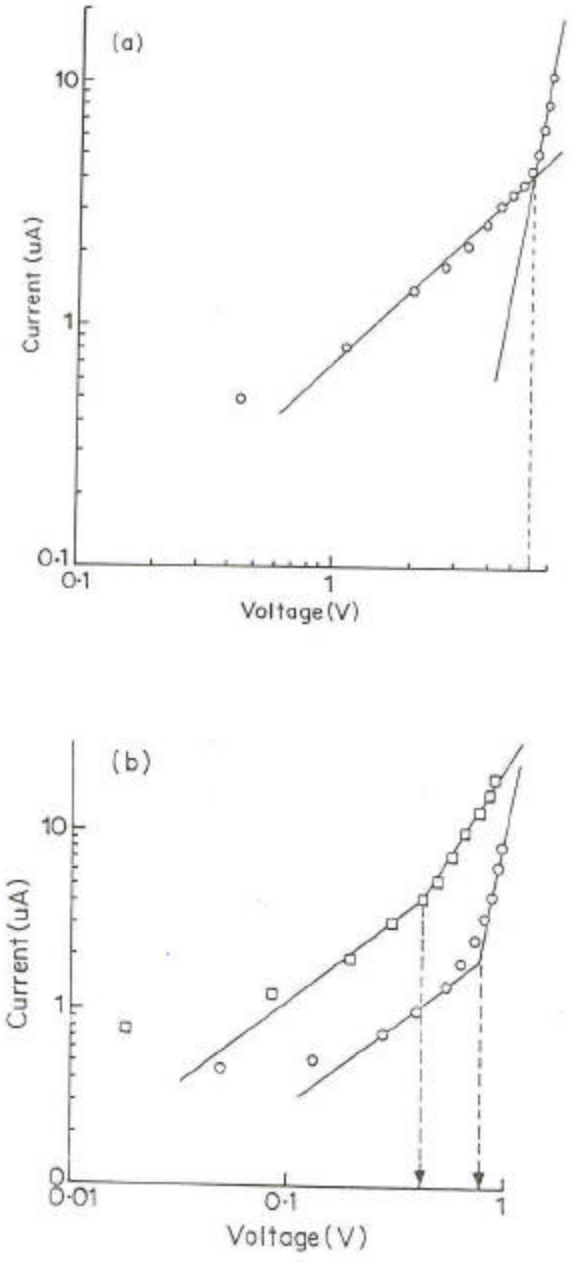

Fig. 5.23 I-V characteristics for PPy/CdS in-situ composite (II) with 8:1 M/m PEO-$CuCl_2$ containing (a) 20 and (b) 40% CdS on log-log scale

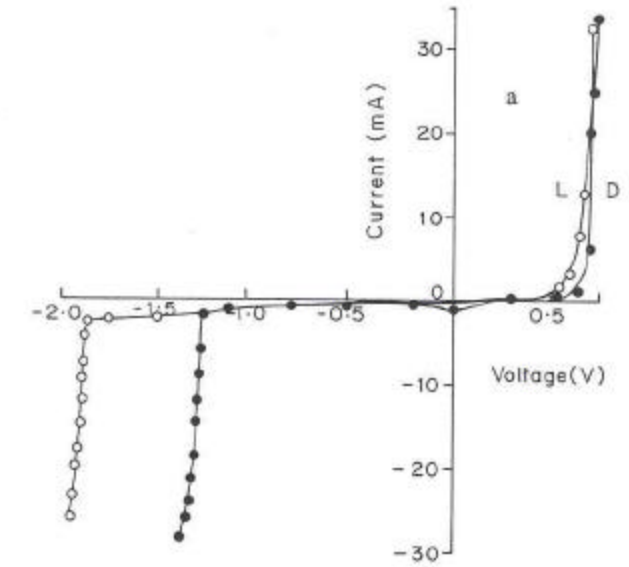
a
Current (mA)
30
20
10
0
-10
-20
-30
L
D
-2·0
-1·5
-1·0
-0·5
0·5
Voltage(V)

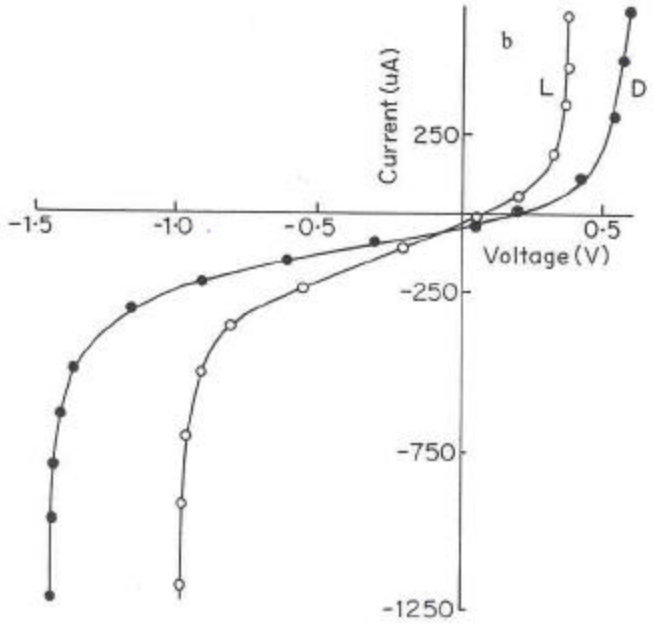
b
Current (uA)
250
-250
-750
-1250
L
D
-1·5
-1·0
-0·5
0·5
Voltage (V)

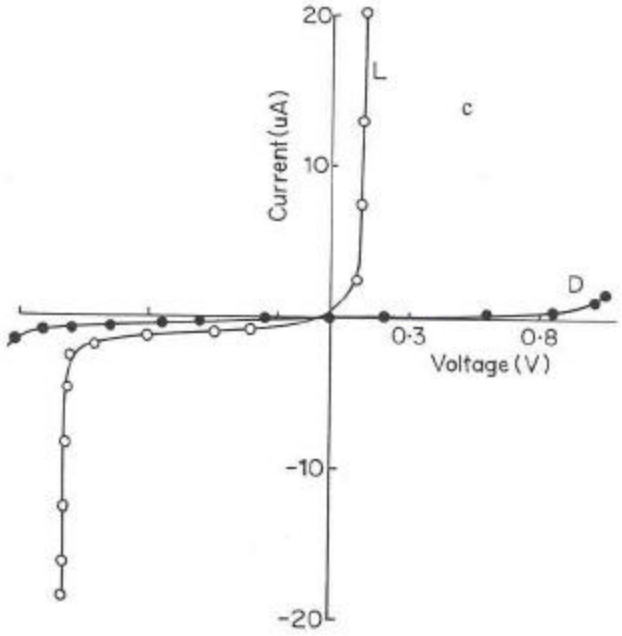

Fig. 5.24 I-V characteristics for PPy/CdS in-situ composite (II) with 4:1 M/m PEO-$CuCl_2$ containing (a) 20, (b) 40 and (c) 50 % CdS respectively

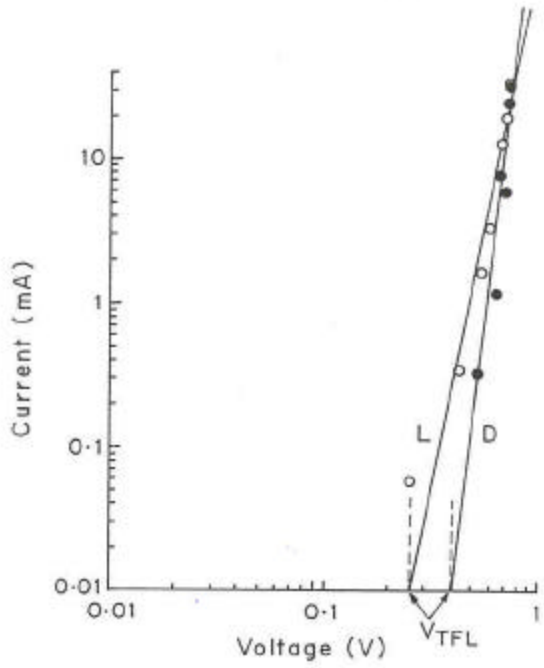

Fig. 5.25 Log-log plot of I-V for PPy/CdS composites (II) with 4:1 PEO-$CuCl_2$ containing 20% CdS

However, the I-V curves also resemble diode characteristics. The forward current

characteristics for a diode can be given as,

$$J=J_O\,(e^{-qV/kT}-1) \qquad \text{Eq.5.2}$$

where J_O is the thermal current, kT/q is the thermal potential and V is the applied field.

Hence, log (I) was plotted with respect to the voltage as represented in the **Fig.5.26**. It is observed that the dependence is followed only at lower voltages whereas at higher voltages the plot deviates. From the above results it can be said that the I-V curves do not follow diode characteristics.

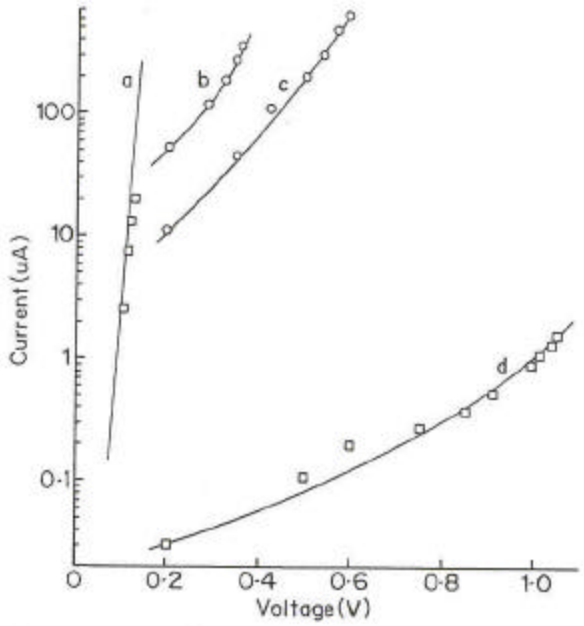

Fig. 5.26 Dependence of log I on the voltage (V) for PPy/CdS with 4:1 M/m PEO-$CuCl_2$ containing 40 and 50% CdS. Curves (a) and (b) represent the I-V characteristics in light for 50 and 40% CdS while (c) and (d) represent the I-V characteristics in dark for 40 and 50% respectively

These various results suggest a Schottky barrier formation in the case of PPy/CdS in-situ composites containing lower $CuCl_2$, i.e. 32:1 and 16:1 whereas the composites containing higher $CuCl_2$ content i.e. 8:1 and 4:1 exhibit SCLC type of conduction mechanism. Thus it is observed that the conduction mechanism of the composite varies with respect to the $CuCl_2$ content. This appears controversial so long as the type of the dopant is same in all the cases that leads to an equal extent of doping of PPy. It is only the amount of the PPy formed that varies with the initiator concentration. Nevertheless, the formation of PPy/CdS junctions is expected to be the same in all the cases under these conditions. Hence it is clear that the nature of conduction for the PPy/CdS in-situ composites depends considerably on the composition especially the concentration of $CuCl_2$. Furthermore, possibility of a reaction between CdS and $CuCl_2$ cannot be ruled out. A change in conduction mechanism may be brought about by a change in the type of junction formation. Moreover, $CuCl_2$ being a strong oxidizing agent operates at room temperature. During the dispersion of CdS, the $CuCl_2$ present may react with CdS according to reaction.

$$xCuCl_2 + CdS \longrightarrow Cu_x S + xCdCl_2 \qquad \text{Eq.5.3}$$

This may result in coating of each particle of CdS with a thin layer of Cu_xS. Moreover, CdS being encapsulated creates a controlled layer of Cu_2S. Swelling of the PEO covering CdS during dispersion facilitates the diffusion of $CuCl_2$ to come in contact with CdS causing a conversion of CdS to Cu_2S. Similar dispersion of CdS/Cu_xS in polymers were carried out by Yamamoto. Higher photoefficiency was found in these composites than CdS/Cu_xS alone [15]. Modification of CdS in dispersed films was carried out by incorporating conductive PPy domains that gave good mechanical strength as well as high photocurrent [16].

The conventional p-type material used with CdS to form a photovoltaic cell is Cu_2S [17]. The CdS/Cu_2S junction is well studied in the past. Cu_2S grown on the surface of CdS acts as a hole injecting contact and is reported to be a p-type material with a resistivity of 2×10^{-2} Ω/cm which is well in the conducting range. It is an indirect gap material with a short diffusion length (~50 nm) that allows an optimum thickness of only about 100nm. The energy band diagram of the CdS/Cu_2S cell can be given as **Fig 5.27** [18]:

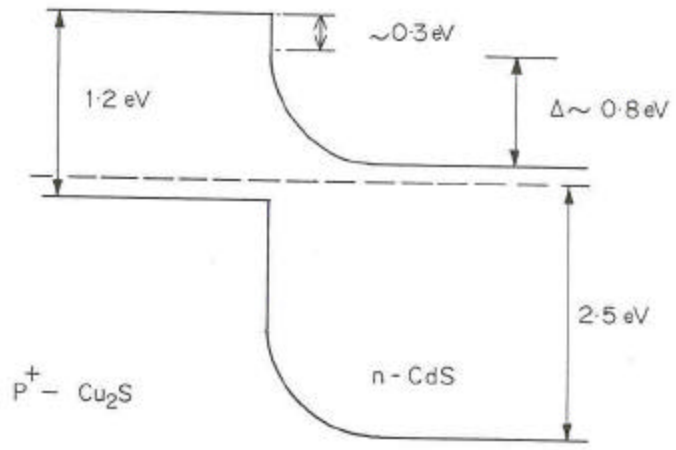

Fig. 5.27 Energy band diagram for CdS/Cu_2S p-n junction

The electron affinity of CdS is 0.30V greater than that of Cu_2S. The Clevite model of

CdS/Cu_2S solar cells, assigns a value of 1.2eV for the band gap of Cu_2S as any direct work function data is absent for Cu_2S [19].

The I-V characteristics in PPy/CdS composite containing PEO-$CuCl_2$ in the ratio 4:1, resemble that obtained for CdS/Cu_xS p-n junctions [20]. Partain et al has reported an SCLC type of conduction mechanism for CdS/Cu_xS. In the present case, Au makes an ohmic contact with Cu_2S while IT0 is ohmic to CdS. The V_{TFL} was determined from the plot and was found to be 0.425 V in dark that changes to 0.261 V under illumination. The I-V curves for 40% and 50% CdS were analyzed in a similar manner and found to follow the SCLC mechanism as depicted in the **Fig.5.28 (a)** and **(b).** V_{TFL} was determined for the composites in forward as well as the reverse bias and are presented in the **Table.5.2.**

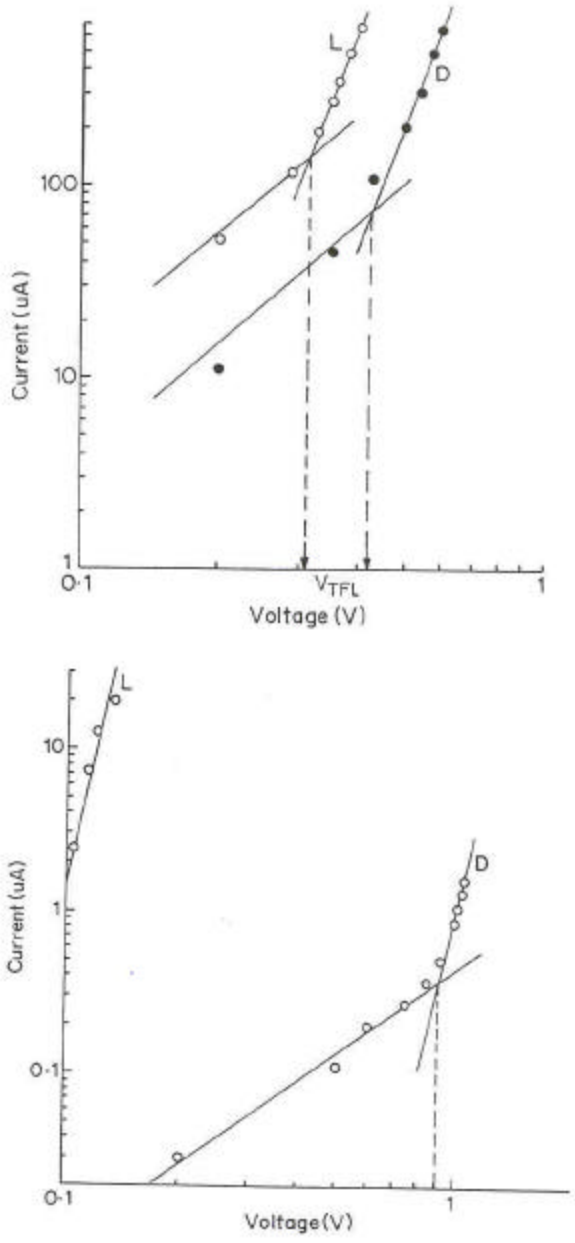

Fig. 5.28 Log-log plot of the I-V characteristics for PPy/CdS in-situ composite (II) with 4:1 M/m PEO-$CuCl_2$ containing 40 and 50 % CdS

Table 5.2

% Composition of CdS	V_{TFL}			
	Forward bias		Reverse bias	
	Dark	Light	Dark	Light
20	0.42	0.26	1.76	1.28
30	0.41	0.30	1.15	0.70
50	0.88	0.10	1.11	0.95

The V_{TFL} was found to vary with the CdS composition. A variation in CdS composition is actually a variation in the interparticulate distance, S. A relation between the two can be given as,

$$V_x = A' S^2/\theta$$

$$S \propto (\phi)^{-1/3}$$

$$\text{Hence } V_x = A' \phi^{-2/3}/\theta \qquad \text{Eq. 5.4}$$

where A' is a constant

θ is the parameter which takes into account the trapping center (impurity centers) concentration and their distribution.

Hence a plot of V_{TFL} against the volume fraction of CdS was made. The variations of $V_{TFL,}$ in the forward and reverse direction in dark are illustrated by the **Fig 5.29 (a)** and **(b).** An increase in the V_{TFL} with the volume fraction of CdS is observed. On the other hand an exactly reverse relation is obeyed as indicated by the Fig 5.29 (b). In fact the SCLC in CdS/Cu_xS originates due to the formation of high-resistance region of Cu compensated CdS at the interface to Cu_xS. The insulating region acts as a gate controlling the carrier flow. Hence a space charge is created at the interface of the Cu compensated region and the Cu_xS. When the CdS content is increased, the ratio of Cu_xS to CdS decreases. Hence under reverse bias conditions, the number of traps reduce due to a reduction in the Cu_xS thickness. It is found that a direct relationship exists between the thickness of the semiconductor layer and the traps or the defects involved. This leads to an early filling of the traps and consequently a lower V_{TFL} than the forward bias. According to this convention, the subsequent decrease in Cu_xS results in

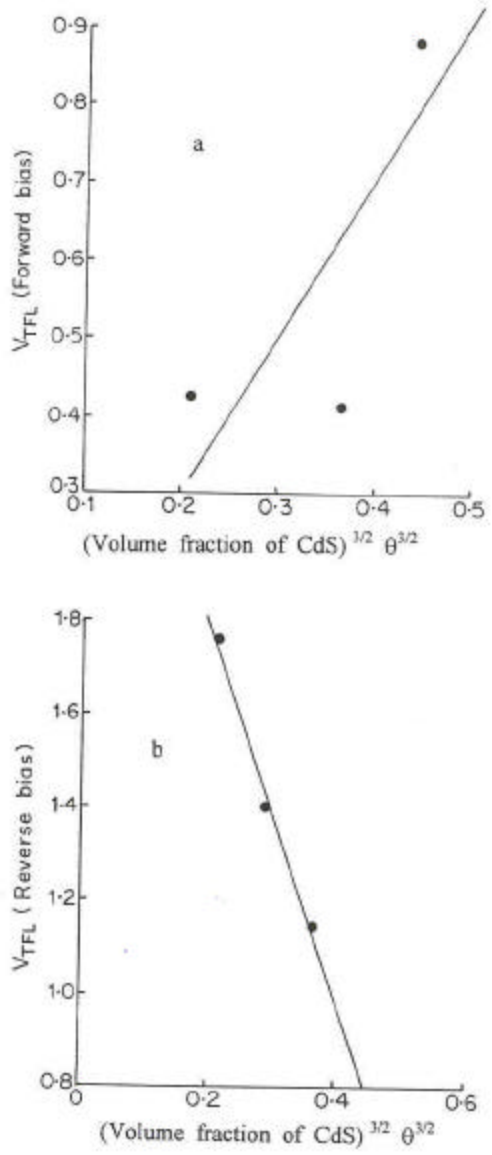

Fig. 5.29 Variations in V_{TFL} in the (a) forward bias and (b) reverse bias in dark with respect to the volume fraction of CdS

a lower V_{TFL} as brought out in the Fig.5.29 (b). A similar decrease in the V_{TFL} is observed in

the case of the PPy/CdS in-situ composite containing 8:1 m/M PEO-$CuCl_2$ (a) in dark and (b) light, is indicated by the **Fig.5.30**. As the $CuCl_2$ content is low, a limited amount of Cu_xS is formed. Hence the relative concentration of Cu_xS to CdS remains almost constant, causing no significant variation in the V_{TFL} under reverse bias conditions.

Considering again the case of the PPy/CdS in-situ composites containing 16:1 and 32:1 PEO-$CuCl_2$, the formation of Cu_xS is hampered on account of low $CuCl_2$ content. Also the formation of PPy would be less than sufficient to yield an interpenetrating network as discussed in the Chapter 3. This reduces the probability of junction formation at the CdS/PPy interface. As a result majority of the junctions are formed at the PPy/PEO-$CuCl_2$ interface that yields Schottky barrier formation.

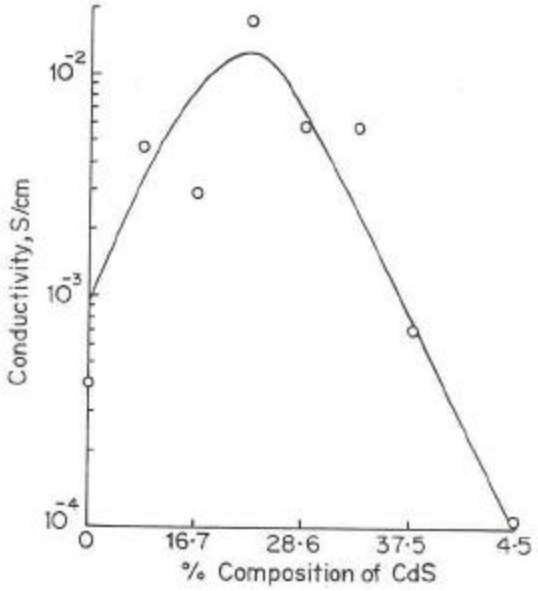

Fig. 5.30 Compositional dependence of conductivity (σ) for the PPy/CdS in-situ composite (III) with 4:1 M/m PEO-$CuCl_2$ using commercial grade CdS

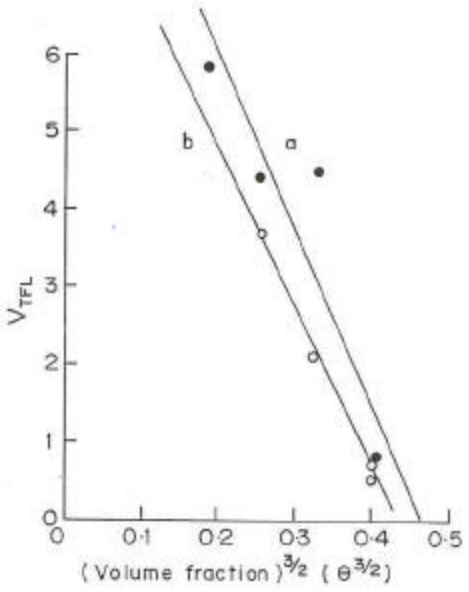

Fig. 5.31 Variations in V_{TFL} in (a) dark and (b) light for the PPy/CdS in-situ composite (II) with 8:1 M/m PEO-$CuCl_2$

As regards photoconductivity, the composites containing lower $CuCl_2$ do not exhibit any notable photocurrent. This is by the virtue of the PPy/PEO-$CuCl_2$ junctions. Conversely, the composites consisting of Cu_xS/CdS junctions i.e 4:1 and 8:1 PEO-$CuCl_2$ with CdS, exhibit considerable photoconductivity that varies with the CdS content. The photosensitivity is seen varying with the CdS. The V_{TFL} in the case of composite containing 4:1 PEO-$CuCl_2$ with 20% CdS was found to be 0.425 V in dark that changes to 0.261 V under illumination. However, a large shift is also observed under reverse bias conditions. The V_{TFL} shifts from 1.8V in dark to 1.3V in light. The mechanism of photoexcitation can be explained by considering that the illumination is from the p-side. Absorption of light in the semiconductor produces hole-electron pairs near the p-insulating region interface. Pairs produced in the depletion region or within a diffusion length of it will eventually be separated by the electric field, leading to current flow in the external circuit as carriers drift across the depletion layer. As the composition of CdS increases, the shift in V_{TFL} also increases as evident by the 50% CdS composition that exhibits a shift from 0.88V to 0.1V under illumination. This is due to the fact that as the CdS content increases, the thickness of the insulating region containing Cu compensated CdS also increases causing a decrease in the dark conductivity. As a result the photocurrent is perceived to rise. Similar variations are observed in the case of the composite containing 8:1 PEO-$CuCl_2$, however, the shift in the V_{TFL} in this case is low as evident from the **Fig.5.30**, where curves (a) and (b) represent the V_{TFL} in dark and under illumination. These findings can be explained on the basis of lower Cu_xS and lesser thickness of the Cu compensated layer. A low thickness of the insulating region results in a less space charge formation causing recombination and trapping as the major phenomenon.

(C) PPy/CdS in-situ composite using commercial grade CdS:

Commercially available CdS was used in order to study the influence of encapsulation on the charge transport behaviour and the photoconductivity. The PEO-$CuCl_2$ content was kept constant at 4:1 monomer/mole while the CdS was varied. PPy was partially deposited.

(a) Compositional variation of conductivity:

It was observed that the conductivity increases from $4x10^{-4}$ S/cm to $4x10^{-3}$S/cm after the addition of 10%CdS. There is not much of change observed in the conductivity till 23% addition of CdS beyond which the conductivity exhibits a sharp decrease to $9.5x10^{-5}$S/cm at 45% composition of CdS (**Fig.5.31**). These results can be explained by considering the direct

reaction of CdS with $CuCl_2$. CdS being not encapsulated does not have any control on the conversion of CdS to Cu_xS. This results in the formation of thicker layer of Cu_xS that increases at higher CdS. The increase in the conducting Cu_2S phase in addition to PPy deposition results in the overall higher conductivity, which reaches saturation around 40% composition of CdS. This behaviour is similar to the above case wherein the insulating filler particles contact each other at critical concentration that corresponds to an abrupt decrease in the conductivity in the present system. Hence the percolation threshold can be said to be reached at 23% CdS composition that contains a network of CdS breaking the PPy continuity and hence a lower

conductivity.

(b) I-V characteristics for the PPy/CdS composites using commercial grade CdS:

I-V characteristics were also recorded for the PPy/CdS composite system using commercial grade CdS as illustrated in the **Fig.5.32** typically for the composite containing 40% CdS. The plots are practically linear irrespective of the CdS composition. Thus a large variation can be observed in the charge transport for these composites depending on the type of CdS used. These variations may be associated with the structural difference between the two. In order to investigate this further, a detailed X-ray diffraction analysis was carried out for the two types of CdS. The **Fig.5.33** depicts the XRD pattern for the commercial grade CdS. CdS is present in two polymorphic forms-α and β. XRD studies have also been reported for the encapsulated CdS [21], the XRD for which is shown in the **Fig.5.34**. The 2θ and 'd' values corresponding to the peaks for both the grades are tabulated as **Table 5.3**. The in-situ formation of CdS using $CdCl_2$ has been reported. A crystal size of about 500 A^o was obtained in that case, showing a mixed α and β phase in the WAXD. An amorphous pattern was obtained for low concentration of $CdCl_2$. On the other hand, the commercial CdS shows the existence of only α phase. Further, width of the peaks in the x-ray diffraction pattern is different suggesting large differences in crystallite size in the two cases.

No photoconductivity is observed. This is because thicker Cu_2S layer causes low illumination of the CdS/Cu_2S junctions and hence a lower photoefficiency. The commercial grade CdS being crystalline in nature, allows the formation of Cu_2S preferentially at the grain boundaries [22]. On the other hand, the composites containing CdS encapsulated with PEO, exhibits a higher photoconductivity as seen earlier. The photoconductive properties vary greatly on the nature and volume of the polymer used as binding material. In conventional dispersion composites binding polymers have been necessary to give mechanical strength required for practical use without reducing the photosensitive properties. The photoconductivity of CdS encapsulated in various polymers like PMMA, polystyrene and polyvinyl carbazole was studied against their dispersions [23]. It was found that the photosensitivity was highest in CdS capsulated with PMMA with a high dispersion rate of 3.04% wt. Compared to the conventional CdS/polymer dispersion composite, the encapsulated CdS composites have improved dispersability and wettability, a more homogeneous sample can be prepared. Kuczkowski has reported a polyester polymer-CdS composite for photoelectronic device applications [24]. Photoelectric properties were investigated for the CdS

composite as a function of component weight ratio, electric field strength and light intensity. It was observed that the composite containing 60-70% by wt. of CdS had the best properties. The ratio of photocurrent to dark current was greater than 10^8 for white illumination of approximately 225 mV/cm^2. CdS in the present case was encapsulated with PEO in view of increasing the compatibility of the composite with the solid polymer electrolytes used in various practical applications of conducting polymers [25].

5.4 Conclusions:

The charge transport in the PPy/CdS composite system is affected largely by the physico-chemical nature of both the constituents. The method of synthesis of PPy greatly influences its p-type character whereas the encapsulation of CdS influences its morphology and structure; consequently the photosensitivity. In case of the in-situ deposited PPy, a reaction of CdS with $CuCl_2$, resulted in the formation of CdS-Cu_xS junctions. The role of PPy was only to act as a transporting layer and an interconnection for all these microjunctions created in the matrix. The Cu_xS/CdS solar cells are usually constructed in thin film form, which face drawbacks in a large-scale production. For the conversion of CdS to Cu_2S in a dipping process, a thicker film of CdS ($\sim$25μm) is required to prevent the diffusion of Cu_2S down the grain boundaries to the base electrode. Relatively, thinner films can be used by spray pyrolysis technique. However, the thin films being poly crystalline in nature, introduce internal surface in the form of grain boundaries which can decrease current generation efficiency, output voltage and the stability of the cells [26]. Another difficulty reported is the necessity for cell series is the interconnection within modules, which should appear to be the most expensive step in CdS/Cu_2S module production. An integrated series connected array can be achieved but losses due to shunting paths and the series resistance could not be avoided [27]. In the present case, each CdS-Cu_xS particle acts as a p-n junction and many more such particles are dispersed in the PEO matrix consisting of the interpenetrating PPy network. This resembles a microsystem, wherein the nano-particulate CdS/Cu_2S junctions are interconnected in series and parallel by PPy in a thin film form. Thus junctions were created in-situ where by they got interconnected as well as encapsulated. The net diode characteristics are hence a

collective effect of all the embedded junctions. This unique method not only imparts processability to the composite but also makes it environmentally stable.

Hence a composite of CdS/Cu_xS photovoltaic junctions was achieved at critical concentration of Cu_xS and CdS. Charge transport was found to occur by SCLC mechanism, which was influenced by the compositional parameters. However, high conversion efficiencies were not achieved as reported for composite systems [28] as against low for the single layered structures due to high recombination and trapping.

The use of commercial grade CdS was found to influence the growth of Cu_xS on the CdS particle. This not only influenced the charge transport properties but also a loss in photoconductivity. An uncontrolled growth of Cu_xS, results in the formation of a shorting of the junctions and a high conductivity. The variations in the encapsulated CdS content caused changes in the PPy interpenetrating network and hence the conductivity. On the other hand, variations in the $CuCl_2$ content caused variations in the Cu_xS layer. This affected the charge transport across the junction as well as the photoconductivity. Hence, the microengineering of these p-n junctions can be brought about by variations in the composition, which makes it possible to create composites with high current and high photoconductivity. Even the ex-situ composite, which have no possibilities of side reactions, showed the existence of heterojunctions between PPy and CdS. A marked difference was observed in the charge transport of the composites containing vapour phase PPy and that synthesized by chemical route. Variation of doping level influences the p-nature of the PPy and hence the junction formed at the PPy/CdS interface. A high doping concentration in the case of vapour phase polymerized PPy, results in the formation of p-n junctions wherein the charge transport occurs by space charge limited conduction mechanism. On the other hand, in the case of chemically prepared PPy, a Schottky barrier is formed at the interface of the materials.

5.5 References:

1. Ozaki M, Peebles, Weinberger B R, Chiang C K, Gau S C, Heeger A J, and MacDiarmid A J Appl Phys lett 35(1) (1979) 83

2. (a)Rabek J F, prog Polym Sci 13(2) 1988 83
   (b)Horowitz G and Garnier F, J Electrochem Soc 132 (1985) 634

3. Frank A J, Honda K, J Phys Chem 86 (1982) 1933

4. Haga Y, Inoue S, Nakajima M, Mater Chem Phys 19(4) (1988) 381

5. (a)Goswami A , Radhakrishnan S, Ind J Pure and Appl Phys 13 (1975) 332
   (b)Zhuravlera T S, Vannikov A V, Mater Sci Forum 21 (1987) 203

6. Goodman A M, J Appl Phy 35 (1964) 573

7. Jayachandran M, and Venkatesan V K, Phys Stat Solidi A(113) (1989) K217

8. Inganas O, Skothiem T Lundstroem I, J Appl Phys 54(6) (1983) 3636

9. Frank A J, Glenis S, and Nelson A J, J Phys Chem 93 (1989) 3818

10. Bube R H, Photoconductivity of Solids, Wiley, 1960

11. (a)Smith R W, Phys Rev 97 (1955) 1525
    (b)Smith M and Behringer J, J Appl Phys 36 (1965) 3475

12. Boakye F and Nusenu D, Solid State Commun 102(4) (1997) 323

13. Neville R C, Solar Energy Conversion : The Solar Cell , Elsevier Sci Publ Co, The Netherlands 1978, 148

14. Hagemeister M, White H S, J Phys Chem 91 (1987) 150

15. Yamamoto T, Taniguchi A, Kubota K, Tominaga Y, Inorg Chim Acta, 104 L1 (1985)

16. IyodaT, Ohtani A, Shimidzu T and Honda K, Polym Prep Jpn 34 (1985) 534

17. Bube R H, J Appl Phys 31 (1960) 2239

18. Johnston W D, Solar Voltaic Cells, Marcel Dekker Inc, New York 1980

19. Shiozawa LR, Augustine F, Sullivan G A, Smith JM, Cook WR, Project Rep. Wright Patterson Air Force Base, Ohio

20. Partain LD, J Appl Phys 63(5) 1988

21. Radhakrishnan S, J. Cryst Growth, 141 (1994) 437

22. (a) Sands T, Washburn J and Gronsky R, Solar energy Mater 10, (1984) 349
(b)Thomas G and Westmacott K H, J Met 37 (1985) 36

23. (a) Yutaka H, Nakajima M, Kyntoku Y, J Angew Makromol Chem 139 (1986) 49
(b) Wu C and Bube R H, J Appl Phys 45 (1973) 648

24. Kuczkowski A, J Phys D, Appl Phys 22 (1989) 1731

25. Lin J, Cates E, Bianconi P A, 116(11) 1994 4739

26. Bube R H, Photoconductivity of solids, New York: Wiley 1960

27. Lampert M A, Mark P, Current Injection in Solids, Academic Press 1980 New York

28. Polycrystalline and Amorphous Thin Films and Devices Edt. Kazmerski LL, Academic Press 1980 New York

Chapter 6 - PANI/PEO-$CuCl_2$ based blends and PANI/PVAc-$CuCl_2$ based blends and composite

6.1 Introduction:

Among the conducting polymers, polyaniline is an extremely interesting material because of its stability in air and its different oxidation states, which are controllable by redox processes [1-4]. Inspite of extensive in polyaniline and its blends/composites with other bulk polymers has attracted much interest because these provide ease of processibility, good mechanical properties and enhanced stability[5]. Composites of polyaniline and polycarbonates composites have been reported by Isa et al [6]. Electrically conductive polymer blends have been prepared in situ by chemical or electrochemical oxidation of aniline in films of thermoplastics PVC, polyolefin's, PMMA, poly (acrylic acid) [7].

Blends were also prepared by the chemical oxidation of aniline monomer sorbed in films of Nylon-6 immersed in an oxidant solution containing a functionalized acid [8]. Using micro porous polycarbonate as the host polymer, Granstorm, Inganas [9] and Martin [10] synthesized a conducting polymer composite with novel structures by chemical or electrochemical oxidation of monomers. In another case, the PANI-PP films synthesized by chemical oxidation polymerization exhibit mechanical properties similar to the micro porous PP [11].

The first major commercial application of polyaniline is used in areas of batteries wherein it was used as an anode in combination with $LiBF_4$ in propylene carbonate [12]. Another interesting application of PANI is evolved in the field of electrochromic devices wherein the displays are fabricated utilizing a solid polymer electrolyte of PEO with $LiClO_4$ [13,14]. All solid state electrochromic devices utilizing alkali metal salts or protonic acids with PEO are reported [15] that have several key advantages such as flexibility, processibility, ease of handling, etc [16]. Hence it is proposed in the present work to synthesize blends of PANI with solid polymer electrolytes such as PEO-$CuCl_2$ and PVAc-$CuCl_2$ by ex-situ method. Further, the charge transport processes in these blends was investigated and the effects of various parameters like the doping level of PANI and the composition of the blend on the conduction behaviour was also studied.

Chemically synthesized polyaniline has been used for preparing blends in the present studies. Two grades of PANI were used: low dopant level PANI-(L) and a highly doped

PANI-(H) for synthesis of blends with PEO-$CuCl_2$. The dispersion by mechanical agitation was found to be quite convenient in making various composition of the blend. PANI blends were also prepared in the same manner using polyvinyl acetate (PVAc)-$CuCl_2$. Further, an organic photoconducting material-CuPc was dispersed in the same to form a composite. The formation of the barriers in the blends and composite was studied mainly by I-V characterization. Barrier modulation by various factors such as change in composition, doping, etc. was carried out and correlated with properties such as chemical sensitivity and light sensitivity.

The charge transport at the interface was studied in a single junction formed using these materials in film form. The various results obtained were then compared with those obtained for the multiple junctions expected to be present in the case of blends and composites.

6.2 Experimental:

(a) Synthesis of PANI:

PANI was first synthesized by chemical polymerization route using ammonium persulphate as the initiator. 5.3gms of ammonium persulphate were dissolved in 100ml distilled water. A solution of 5.5ml conc. HCl was added in 150 ml distilled water to which was added 10ml aniline and stirred. The above solution of ammonium persulphate was added to this by constant stirring. The solution was digested for 24 hours and then filtered. The resulting precipitate was washed with distilled water. The powder after drying appeared brownish green in colour and designated as PANI-(L).

In another case, the HCl quantity was increased to 11ml and the synthesis of PANI was carried out in the same way as before. The PANI powder obtained by using these concentrations was dark green in colour and notified as PANI-(H).

(b) Synthesis of PANI/PEO-$CuCl_2$ blend:

A dry mixture of 3.6 gms of PEO and 0.4 gms (i.e. 10%) $CuCl_2$ was prepared by thoroughly grinding in a pestle-mortar. Polyaniline was synthesized in two forms: PANI-(L) less doped and PANI-(H) highly doped as described above. The powders were crushed and added to 0.25 gms of PEO-$CuCl_2$ was dissolved in 5 ml methanol in a concentration range of 10% to

50% w/w. The solution was continuously stirred to give a thick paste, which was then applied on interdigited electrodes so as to make surface cells.

(c) Synthesis of PANI/PVAc-$CuCl_2$ blend:

PANI-(H) was used for the synthesis of PANI/PVAc-$CuCl_2$ blends. A solution was prepared by dissolving 3.6 gms of PVAc was in methanol to which 10% $CuCl_2$ was added. PANI-(H) was then added in various concentration range 10-50% w/w to the PVAc-$CuCl_2$ and the mixed thoroughly in little methanol to form a thick paste. This was then later applied on interdigited gold electrodes.

(d) Synthesis of PANI/CuPc composite with PVAc and PVAc-$CuCl_2$:

CuPc was dispersed in PVAc and PVAc-$CuCl_2$, in methanol in various compositions ranging from 2,5, 10 to 45% weight by weight. 10% PANI-(H) was then dispersed in PVAc and PVAc-$CuCl_2$. The resulting slurry was then applied on interdigited electrodes.

(e) Fabrication PANI/ PEO-$CuCl_2$ single junction:

PANI was synthesized by electrochemical polymerization technique from an aqueous electrolytic bath containing 0.2M HCl and 0.1M aniline. Gold-coated glass electrodes were used as substrates for the deposition of PANI films. The polymerization was carried out at 0.9V using chronoamperometric technique for 2 minutes.

In order to prepare multilayered structure, an ITO electrode was dip-coated with a methanolic solution of PEO-$CuCl_2$ containing PEO and $CuCl_2$ in the ratio 4:1 monomer/mole. The coating was air dried and then sandwiched over the glass substrate carrying the electrochemically deposited PANI. Electrical connections were made using air-drying silver paste from the edges.

6.3 Results and discussion:

The PANI obtained was characterized by conductivity and IR spectroscopy. The charge transport in the blends and composite was studied with respect to the composition and various properties such as chemical sensitivity, light sensitivity was also studied. The

discussion is divided into two parts dealing with PANI/PEO-$CuCl_2$ and PANI/PVAc-$CuCl_2$ respectively.

6.3.1 Characterization of PANI:

The PANI-(L) and PANI-(H) obtained by chemical polymerization route was characterized with respect to conductivity. The conductivity of PANI-(L) was measured to be 8 x 10^{-6} S/cm, which is in the semi conducting range. On the other hand the PANI-(H) exhibits a higher conductivity of $9x10^{-1}$S/cm. The difference between the two grades arises mainly due to the varying amount of dopant employed during the polymerization process. The various species present were investigated by the IR spectroscopy. **Fig 6.1** represents the IR spectrum for the different grades of PANI [17]. The frequency and the probable assignments of the various peaks are tabulated accordingly. It is observed that the absorption at 1582 cm^{-1} for the quinoidal form is prominent in the case of PANI-(H) whereas PANI-(L) exhibits a weak intensity. Another peak appears at 1506 cm^{-1} in the case of PANI-(H) that corresponds to the benzoid structure. It has been reported that the intensity of the 1570-1590 cm^{-1} band relative to the 1500 cm^{-1} is a measure of the degree of oxidation of the polymer film [18]. In the present case, the PANI-(L) does not show any absorption at 1500 cm^{-1} while the relative ratio for PANI-(H) is 2:1 for the two peaks. This indicates that the PANI-(L) possesses only quinoid structure while both the structures are present in the case of PANI-(H). Hence it appears that it is only partly doped with Cl^- ions [19] while PANI-(H) consists mainly of emeraldine salt i.e. highly doped state which is highly conducting in nature. The peak at 1375 cm^{-1} corresponds to the semiquinoid ring mode [20].

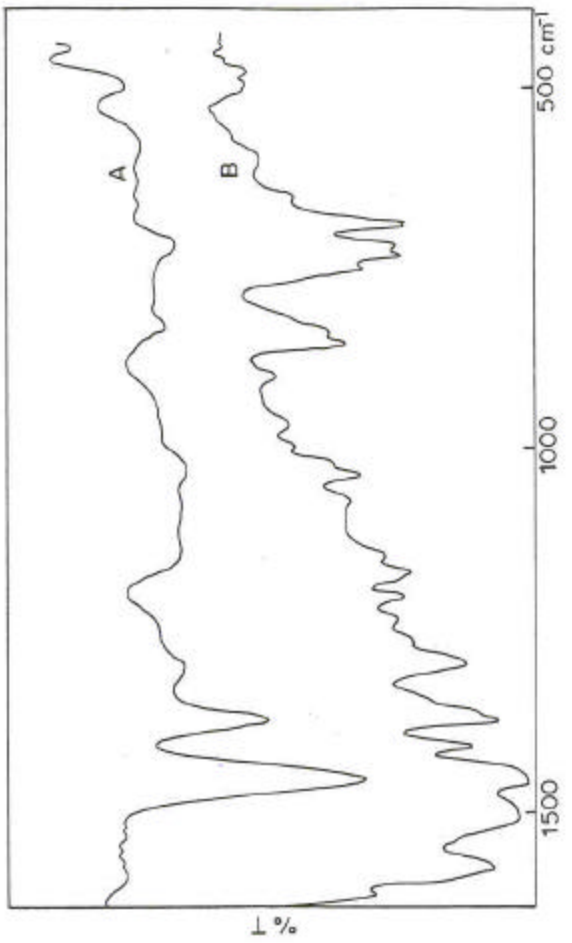

Fig. 6.1 I-R spectra for (a) PANI-(L) and (b) PANI-(H)

6.3.2 PANI/PEO-$CuCl_2$ based blends:

Blends using two different grades of PANI were prepared and investigated for the conduction mechanism as presented below.

(a)Compositional variation of conductivity:

The conductivity variation of the blend containing PANI-(L) against the composition is illustrated by the **Fig.6.2 (a).** It is observed that the plot is of typical percolative nature. The conductivity shows a rise of almost 1.5 orders of magnitude till 20% addition of PANI and is stable thereafter. In order to fit the experimental data in the equation 6.1,

$$\sigma \propto (\phi - \phi_C)^f$$

$$\text{or} \quad \sigma = A(\phi - \phi_C)^f$$

$$\therefore \log \sigma = \log A + f \log(\phi - \phi_C)$$

-----Eq.6.1

A plot of conductivity against the volume fraction of PANI was made on log-log scale. It is observed in the **Fig.6.2 (b)** that the plot is a straight line exhibiting a percolation threshold at 8 % of PANI content with f = 8.01. This type of behaviour is encountered in the case of ex-situ blends wherein a conducting phase is in contact of insulating/semiconducting matrix. The conducting particles make a contact with each other at a critical concentration of PANI. This leads to the formation of PANI network in the blend exhibiting conductivity that is almost equal to that of the pure polymer i.e. 1.5×10^{-6} S/cm.

In the case of blend prepared using PANI-(H), it is observed that the there is a rise in the conductivity with respect to the composition of PANI-(H) added **Fig. 6.3 (a)**. A plot of conductivity against the volume fraction of PANI is depicted in the **Fig. 6.3 (b)** that reveals a percolation threshold at 6 % PANI content. The value of 'f' was noted to be low i.e. 3.6 as compared to that of PANI-(L) blend. A comparison of the percolation thresholds of the two blends suggests a lowering of the percolation threshold as well as the value of 'f' on higher doping of PANI. This behaviour can be understood as follows. Doping introduces impurity centers in the energy band gap of PANI that increase with the magnitude of doping. Consequently, the barrier at the PANI-(H)/PEO-$CuCl_2$ is lowered than in the former case facilitating transport of electrons at a lower PANI-(H) content exhibiting a lower percolation

threshold. The difference between the magnitude of the barrier height of the two blends also influences the value of 'f' since the change in ultimate conductivity depends on the same.

Table 6.1

PANI-(L) Peak (cm^{-1})	PANI-(H) Peak (cm^{-1})	Assignments
1582.9 (w)	1582.3(m)	Quiniod N=Q=N structure
	1506.1(vs)	Benzeniod N-B-N structure
1456.2(vs)	1461.9(vs)	Benzene ring structure
1375.2(s)	1376.7(s)	C-N structure
1302.9(m)	1298.5(s)	C-N structure
	1208.2(ms)	C=N structure
	1173.2(ms)	Vibrational mode of N=Q=N
	1041.3(m)	
1030.4(m)		
	906.6(m)	
	861.1(m)	
834.4(m)		C-H out of the plane
	738.9(ms)	
725.1(m)		
	695.5(s)	
595.8(w)		
508.1(w)		
	486.8(s)	
456.8(w)		

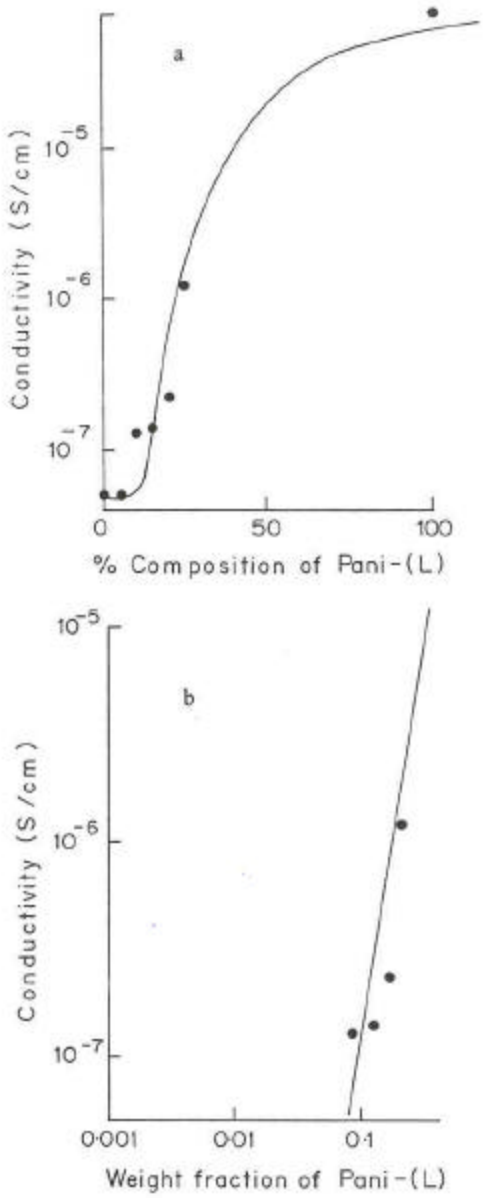

Fig.6.2 (a) Variation of conductivity with respect to the concentration of PANI-(L) for the PANI-(L)/PEO-$CuCl_2$ blends

(b) Dependence of conductivity on the weight fraction of PANI-(L) for PANI -(L)/PEO-$CuCl_2$ blends

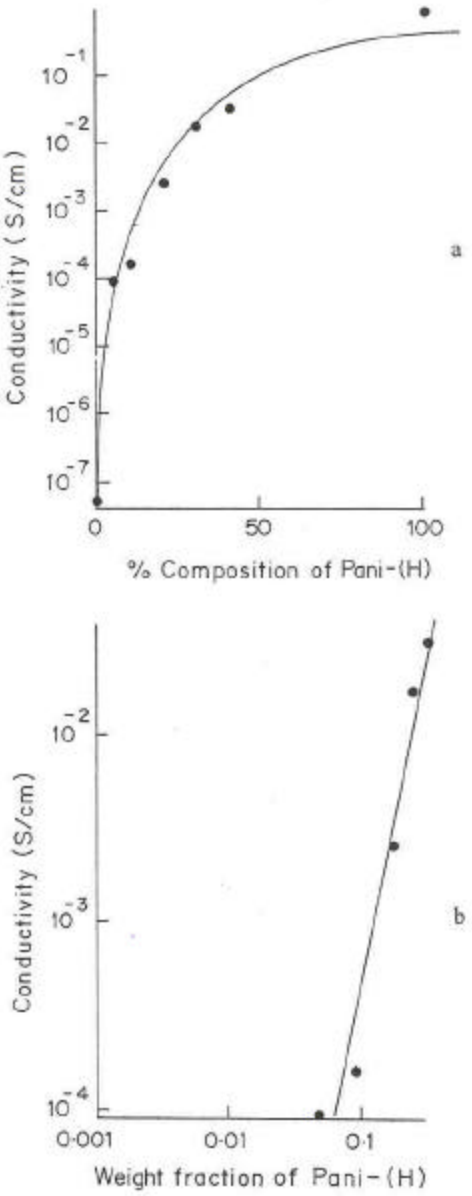

Fig. 6.3 (a) Variation of conductivity with respect to the concentration of PANI-(H) for the PANI-(H)/PEO-$CuCl_2$ blends

(b) Dependence of conductivity on the weight fraction of PANI-(H) for PANI -(H)/PEO-$CuCl_2$ blends

(b)I-V characteristics for the PANI/PEO-$CuCl_2$ blends:

The I-V curves for PANI-(L)/PEO-$CuCl_2$ blend are non linear in nature as observed in the **Fig**. **6.4**. The degree of non-linearity decreases with PANI addition. The I-V curves were then further analyzed for the exact charge transport mechanism by plotting the IV curves on a log-log scale. Slopes of the plots were observed to be between 1 and 2 and thus the system cannot be said to follow the SCLC mechanism. The I-V curves were then analyzed for Schottky or Poole–Frenkel effect. Plot of log I vs $V^{1/2}$ plot made and was noted to follow a linear graph. The slopes of these graphs changed with PANI composition as indicated by the **Fig**.**6.5.** These are observed to rise as the PANI composition increases till 10% and then decrease beyond the percolation threshold. Considering once again the equation 1.7, the factors determining the slope can be given as

$$S \alpha \beta / kT\, d^{1/2} \qquad \text{Eq.6.2}$$

where β is the Poole Frenkel parameter.

Thus as the PANI increases, the intergranular distance 'd' at the conducting PANI sites decreases leading to an increase in the slope of log I vs $V^{1/2}$ curve The dispersion of PANI in the PEO-$CuCl_2$ matrix creates potential barriers at the interface of the materials. The energy band diagram is as shown in the **Fig**.**6.6.** The conducting PANI in the semi-conducting PEO-$CuCl_2$ matrix forms a Schottky barrier at each of the intergranular regions due to dissimilarities in the work function. In order to confirm this single junction of PANI/PEO-$CuCl_2$ was fabricated using electrochemically deposited PANI and dip-coated PEO-$CuCl_2$. The charge transport studies across these were carried out as described in the following.

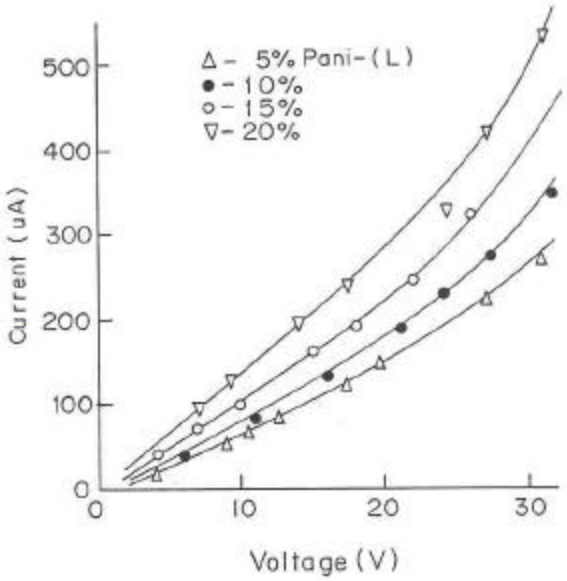

Fig.6.4 I-V characteristics for the PANI-(L)/PEO-$CuCl_2$ blends containing 5,10, 15 and 20% PANI

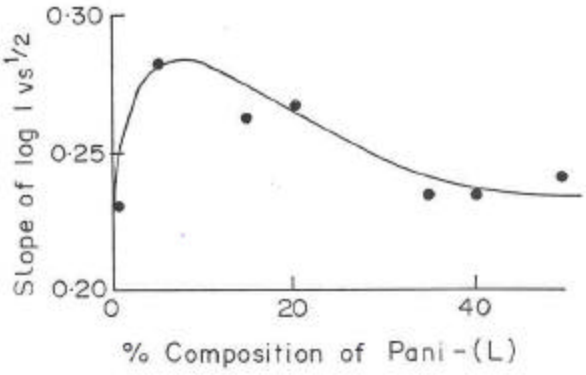

Fig.6.5 Dependence of slopes of log $I/V^{1/2}$ on the PANI-(L) composition

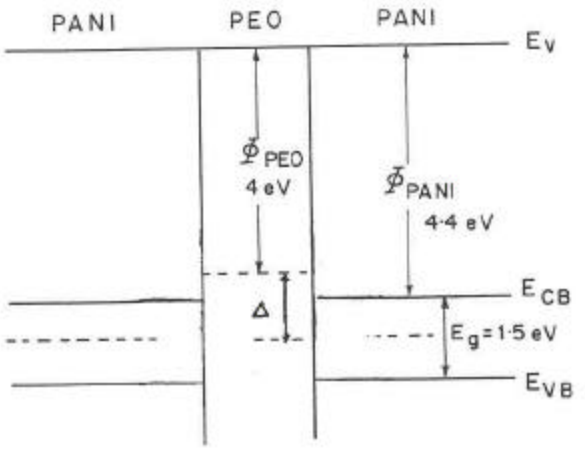

ENERGY BAND DIAGRAM FOR

PEO–PANI

Fig.6.6 Energy band diagram for PANI/PEO

(i)PANI/PEO:

The I-V curves are represented in the **Fig.6.7 (a).** The non-linear nature of the plot clearly suggests a non-ohmic conduction process mostly Schottky type. It was confirmed by making a log I against $V^{1/2}$ plot that followed a linear dependence indicating the presence of a Schottky barrier. Since PANI has a work-function of 4.4 eV [21] and PEO has a work-function of 4.0 eV [22] it can be understood that a barrier of about 0.4 eV exists at their interface as described in the diagram (Fig.6.6).

The I-V characteristics for the cell using ITO are shown in the **Fig.6.7 (b)**. Strong rectification is observed sine ITO acts as a blocking contact for the Au/PANI/PEO/ITO configuration. These were then analyzed by making a log I vs $V^{1/2}$ plot obeying the dependence and giving an evidence of the barrier at the interface. A small photocurrent is observed under illumination, in the reverse bias mode. The electron/hole pairs generated by photon absorption in PANI get separated in the depletion region and overcome the PANI/PEO barrier exhibiting a photocurrent.

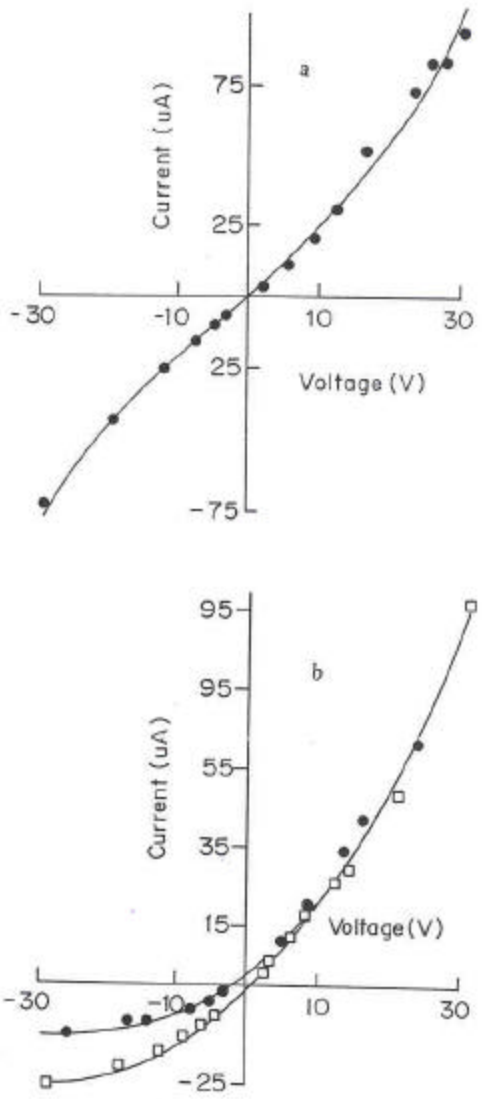

Fig.6.7 I-V characteristics for the PANI/PEO cell using Au/Au and Au/ITO electrodes represented by (a) and (b)

(ii) PANI/PEO–$CuCl_2$:

The I-V characteristics of the PANI/PEO-$CuCl_2$ junction were investigated using Au and ITO as top electrodes. Using Au, a non-linear I-V curve is obtained with a small photocurrent in the forward bias as denoted by the **Fig.6.8 (a).** The plot was analyzed for $\sqrt{V}$ dependence. It was found that the plot was a straight-line graph depicting a Schottky barrier presence at the PANI/PEO-$CuCl_2$ interface. The photoexcited electrons in PANI are trapped by the impurity states in PEO and hence reduce the recombination giving a small photocurrent.

The I-V characteristics are non-linear with ITO top electrode [see **Fig.6.8 (b)**]. However, no rectification in the I-V curves is observed for the PANI/PEO-$CuCl_2$ cell as compared to the PANI/PEO cell using ITO. This may be explained on the basis of the impurity levels created in the PEO energy gap resulting in the lowering of the barrier at the PEO/ITO interface.

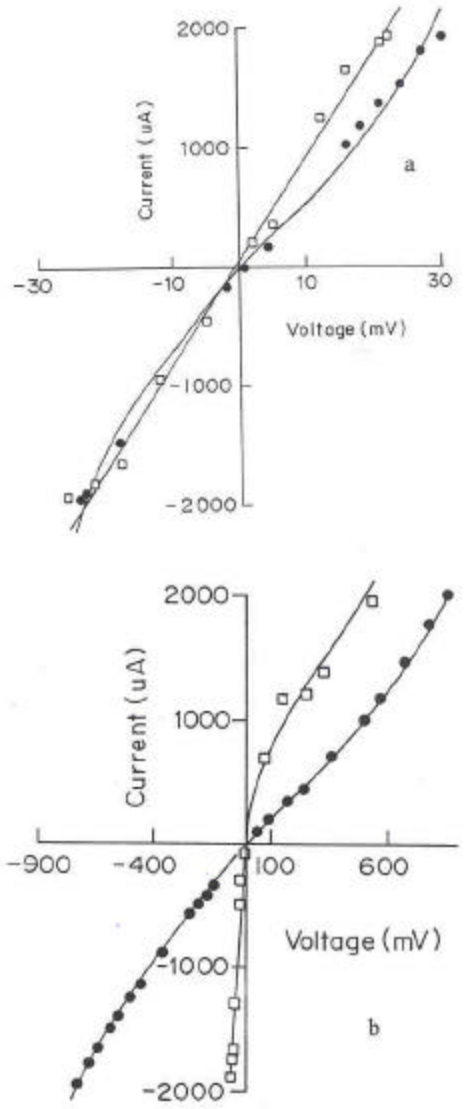

Fig.6.8 I-V characteristics for the PANI/PEO-$CuCl_2$ cell using Au/Au and Au/ITO electrodes represented by (a) and (b)

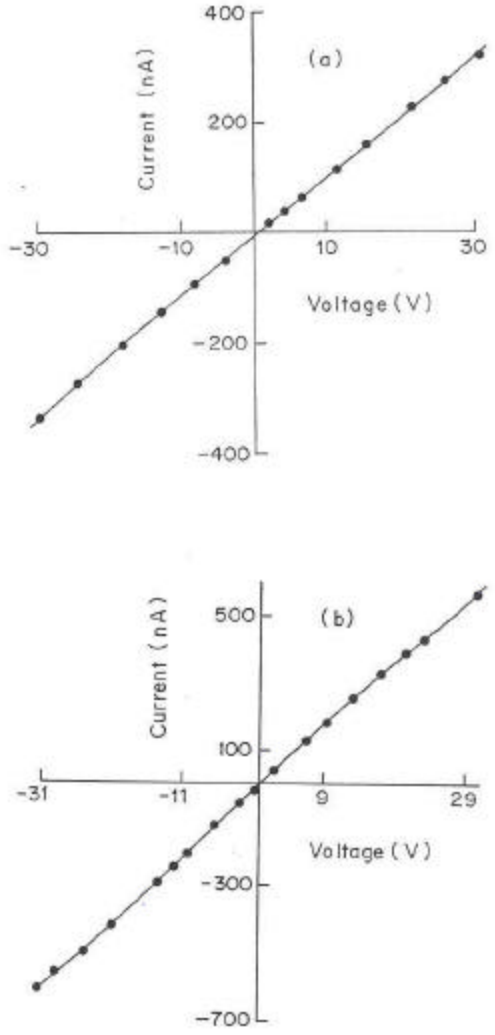

Fig.6.9 I-V characteristics for the PANI-(H)/PEO-$CuCl_2$ blends containing 10 and 20% PANI-(H) indicated by (a) and (b)

The above studies make it clear that a Schottky junction is present at the PANI/PEO-$CuCl_2$

interface. Moreover in a blend system discrete junctions are formed in the solid polymer matrix that gives rise to collective junction effects.

The effect of higher doping on the charge transport was studied using PANI-(H). The I-V curves for PANI-(H)/PEO-$CuCl_2$ blends are non-linear in nature [**Fig.6.9 (a)** and **(b)**]. But the degree of non-linearity is observed to be less than that of PANI-(L)/PEO-$CuCl_2$ blend system. These were analyzed by making a plot of log I against $V^{1/2}$ dependence. The plots were straight lines verifying the Schottky effect. The slopes were determined and plotted against the composition of PANI-(H) in PEO-$CuCl_2$ as seen in the **Fig**.6.10. It is observed from the figure that the slopes exhibit a decrease from 0.24 to almost 0.21 at 10% PANI concentration and remains constant thereafter.

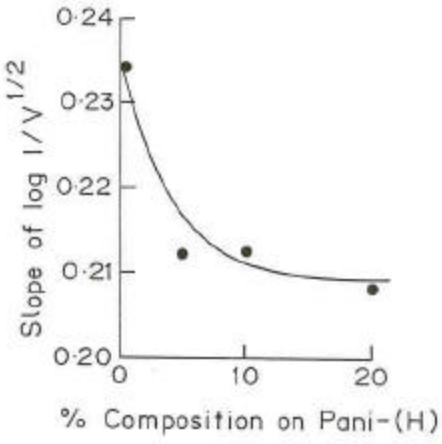

Fig.6.10 Dependence of slopes of log I/ $V^{1/2}$ on the composition of PANI-(H)

A comparison of the I-V characteristics indicate a decrease in the non-linearity with a change in the grade of PANI from PANI-(L) to PANI-(H) and is distinctly reflected in the slopes of the logI vs $V^{1/2}$ plots. This can be understood on the basis of the changes induced in the energy band diagram at the PANI/PEO-$CuCl_2$ interface. Doping introduces trapping levels in the PANI. The concentration of the impurities depends on the degree of doping. Hence more impurities are created in the energy gap of PANI-(H), that reduce the Schottky barrier height at the PANI/PEO-$CuCl_2$ interface [23]. This causes the I-V characteristics to be less non-linear in nature.

Hence the charge transport in the PANI/PEO-$CuCl_2$ blends takes place according to the Schottky type of conduction mechanism. The reduction in the barrier height at the interface of the materials causes linearity in the I-V curves.

(c)Temperature dependence of conductivity PANI/PEO-$CuCl_2$ blends:

The conductivity showed an increase with temperature for the PANI-(L)/PEO-$CuCl_2$ blend. The conductivity was plotted against $1/T^{0.25}$ to verify the VRH model but no linearity was observed which indicated that the Mott's law is not obeyed. Moreover, a sharp transition in conductivity is seen at the T_m of PEO ($\approx 65^0$C) [24]. A plot of log σ vs 1/T was made as shown in the **Fig.6.11 (a).** The plots are dominated entirely by the sharp rise in conductivity within a small range of temperature. The temperature variation of conductivity for the case of PANI-(H), is similar to that obtained for PANI-(L)/PEO-$CuCl_2$. The log σ plotted against reciprocal temperature for PANI-(H) also exhibits a transition around the T_m of PEO as indicated by the **Fig.6.11 (b)**. A close look reveals that the 'knee'-the magnitude of increase in conductivity is not similar for all the PANI compositions in both the blends. Variation of PANI may bring about a change in the viscosity of the system. These differences in the transition can be directly related to the variation in viscosity of the system that arises due to PANI addition.

The conductivity and viscosity are related applying the Stokes law [25]:

$$Z\, q\, E = \sigma\, \pi\, \eta\, r\, \mu\, E$$

The viscous force 'f' acting on the ion is given by $\sigma \pi \eta r \mu E$ where 'r' is the ionic radius, η is the local viscosity and μ the ion mobility. At equilibrium $\vartheta = z q E$ where 'z' is the number of charges on the ion and E is the electric field.

Putting $\mu = \sigma/q n$

$$\sigma = z n q^2/6 \pi \eta r$$

$$\text{or } \sigma = 1/\eta$$

$$\text{or } \sigma \eta = z n q^2/6 \pi r \qquad \text{---------} \qquad \text{Eq 6.4}$$

When n is constant, the above equation is Waldren's rule.

The above equation can also be written as:

$$\sigma (T) \eta (T) = N_0 \exp - (E/kT) q^2/6 \pi r$$

which means that the plots of log [σ (T) η (T)] against the reciprocal of the absolute temperature should yield straight lines.

In short, studies correlate the mobilities of ions and the fludity (which is defined as $1/\eta$) of the medium in which they move and is summarised as Waldren's rule,

$$\Lambda * \eta = \text{constant} \qquad \text{---------} \text{ Eq 6.5}$$

Λ is the equivalent molar conductivity and η is the shear viscosity. This was especially evident in the increase of conductance with temperature in a given solvent which parallels the decrease of its viscosity.

Thus the transition in the present case occurs due to the increased mobility of the ions in melting of the PEO-$CuCl_2$ complex. The viscosity of the blend is no doubt greater than that of the complex on dispersion of PANI, thus reducing the mobility of the ions. As the PANI composition is increased, the viscosity of the blend goes on increasing making the ions tightly bound in the matrix. Consequently, the transition due to ionic mobility is lowered significantly. Moreover, the conductivity changes from ionic to electronic in nature as PANI composition increases. The viscosity at any temperature for a given volume fraction of filler can be summarized in the form of Einstein's equation for dilute solutions,

$$\eta = \eta_o(1+ 2.5 \varphi) \qquad \text{- ----------Eq 6.6}$$

However for a wider range of concentration, the Mooney [26] equation can be given as,

$$\ln \eta_o / \eta = (1-\phi_2/\phi_m) / k_E \phi_2 \text{ ---------- Eq 6.7}$$

Hence $\ln \sigma / \sigma_o = (1- \phi_2/\phi_m) / \phi k_{E\,2}$

where

η = viscosity of the solution

η_o = viscosity of the suspending liquid

k_E = Einstein's constant

ϕ_2 = volume fraction of the filler

ϕ_m = maximum possible filler fraction = 0.9

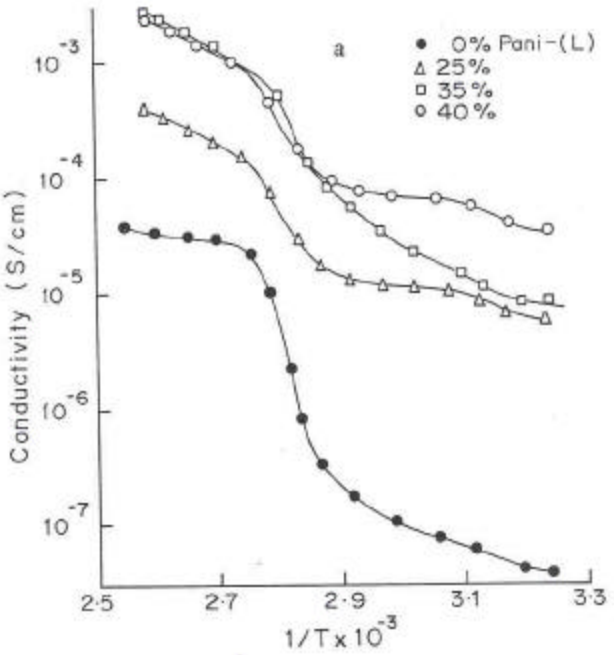

A plot of log σ/σ_o against $(1-\phi_2/\phi_m) / k_E \phi_2$ was made by taking the conductivity values at the beginning and the end of transition occurring in the temperature – conductivity plots. It is

observed from the **Fig.6.12** that the magnitude of transition depends highly on the volume fraction of the filler material – PANI. The plot of Mooney equation is a straight line graph for the PANI-(L) as well as PANI-(H) blends. However the slopes of the plot are different: being higher in the former case (0.656) than the latter (0.273), which is by virtue of the charge transport across the PANI/PEO-$CuCl_2$ barrier. Thus it is clear that the volume fraction of PANI influences the viscosity and hence the conductivity, close to the T_m of PEO. The higher the PANI content more is the viscosity and hence less is the change in conductivity at transition.

Thus the Mooney's equation is obeyed irrespective of the type of PANI used. It is only the fluidity of the matrix and the concentration of the filler that plays an important role in varying the conductivity of the blend.

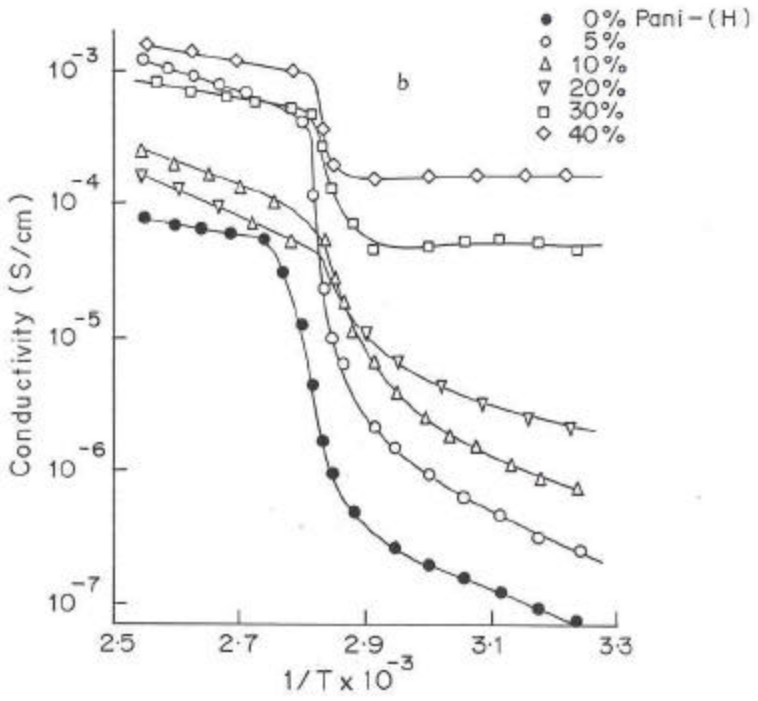

Fig.6.11 Temperature dependence of conductivity for the PANI/PEO-$CuCl_2$ blends. Curve (a) and (b) indicate the log σ Vs 1/T for PANI-(L) and PANI-(H)

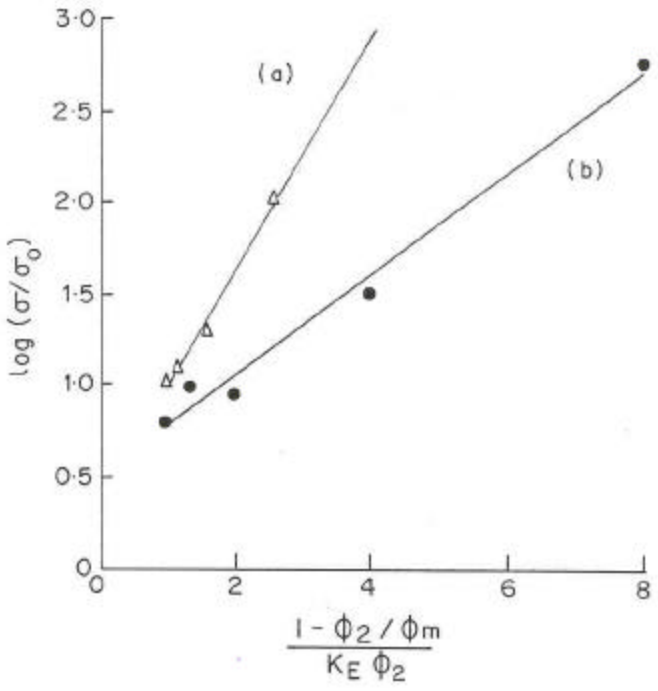

Fig.6.12 Dependence of the change in conductivity on the volume fraction of PANI according to the Mooney's equation

(d) Charge transport in PANI/PEO-$CuCl_2$ blends:

The presence of a barrier at the PANI/PEO-$CuCl_2$ interface due to difference in work function was observed in the case of multiple junctions as well we single junctions. The barrier height at the PANI/PEO-$CuCl_2$ interface was noted to change with the extent of doping of the PANI used as evidenced by the linear nature of the I-V characteristics. Dopants create impurity states in the band gap of PANI leading to more band bending at the PANI/PEO interface and thus a reduction in the Schottky barrier height. This also affects the chemical sensitivity of the blend in turn. The sensitivity is observed to be high in the case of PANI with low dopant concentration than with the higher one. The lowering of the barrier reduces the change induced due to transfer of electrons. Hence there has to be an optimum height of the barrier to achieve higher sensitivity.

(e)Property Measurement - Chemical Sensing:

As mentioned in the Ch 1, this is one of the major application areas of conducting polymers [27,28]. The present system shows the presence of Schottky barriers and is an appropriate material for application in the chemical sensors. The interdigited electrodes were exposed to methanol vapours and are described with varying blend composition.

The response characteristics of the polyaniline-based sensors exposed to methanol are depicted in the **Fig.6.13** and **6.14**. They show a continuous variation in sample resistance after exposed to 330 ppm methanol and recovery after removal of the sensor from the cell. It is clear that there is a sharp decrease in resistance immediately after exposure and minimum value is attained within 1 min while the recovery is quite slow extending over a period of 15 min. It is interesting to note that the decrease in resistance is sharp in all cases, while the recovery depends on the composition of the sensing material (compare curves in **Fig. 6.14**).

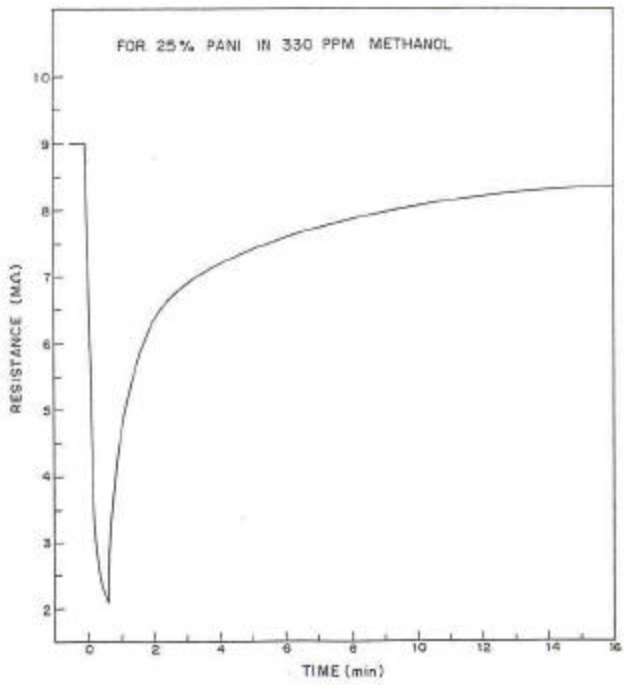

Fig.6.13 Response characteristics of PANI-(L)/PEO-$CuCl_2$ blends containing 40% PANI-(L) exposed to 330 ppm of methanol

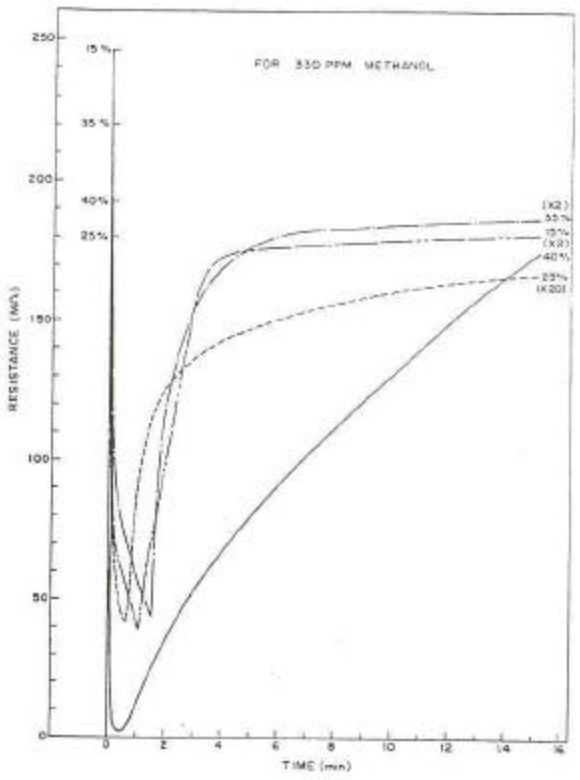

Fig.6.14 A consolidated plot of response characteristics of PANI-(L)/PEO-$CuCl_2$ containing 15, 25, 35 and 40% PANI-(L)

All the sensors with different concentrations of polyaniline were tested in the manner described above and from their response characteristics the various parameters such as

response time (t_t), decay time (t_d) and sensitivity (σ_{max}/σ_0) were evaluated for each dosage level of methanol ranging from 0.02% to 0.06% under ambient conditions. **Figs.6.15 (a)-(d)** show the value of t_t, t_d and S for sensor elements containing 15, 25, 35 and 40% polyaniline respectively. It is seen that these three parameters exhibit maxima or minima with respect to the methanol dosage level and also depend strongly on the composition of the sensor material. Typically S is maximum for methanol dosage of 0.04% (400 ppm) and t_r is minimum for about the same distance while t_d exhibits a maximum or complex behaviour depending on the concentration of the sensor material.

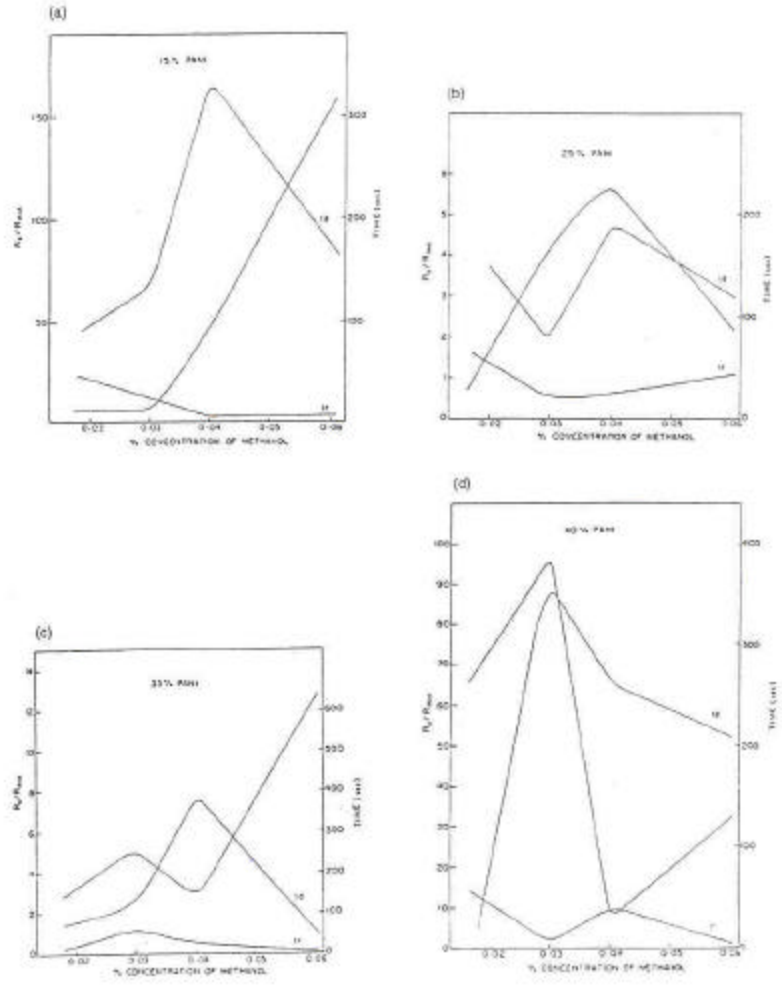

Fig.6.15 Variations of response time, decay time and sensitivity on the dosage level of methanol for the PANI-(L)/PEO-$CuCl_2$ blends containing 15, 25, 35 and 40% PANI-(L)

In order to understand the above results, one has to first look into the interaction between the chemical vapour and the polymeric material as well as the processes involved in the sensing

action [29]. As discussed in the Ch.1, the chemical vapour can react with the adsorbed oxygen on the sensor material and hence cause a change in conductivity or react with the gate material in the case of MIS structures causing a change in the work function or conductivity of the insulating layer [30]. In the present case, the chemisorption effect is important wherein the chemical vapour is absorbed with a transfer of electrons at the substrate.

The conducting polymeric material in the present case can be considered to be a blend of finely dispersed conducting particles (polyaniline) in a semiconducting matrix (polyethylene oxide-$CuCl_2$ complex) as shown schematically in the **Fig.6.16.** In each of the intergranular regions a Schottky barrier is formed owing to dissimilarities in the material and their work function or energy band levels [31]. Additionally, since polymers are of a semicrystalline nature, there are a large number of defects, which give rise to impurity levels in both materials. Polyethylene oxide–$CuCl_2$ complex has a very high resistivity and is a weakly ionic conductor at room temperature. However it has a strong tendency to absorb methanol, moisture, etc. On the other hand, PANI containing dopant molecules (incorporated during synthesis) is mainly an electronic conductor with a low resistivity and hence these domains would not only facilitate the charge transport but would also be expected to respond fast to external changes.

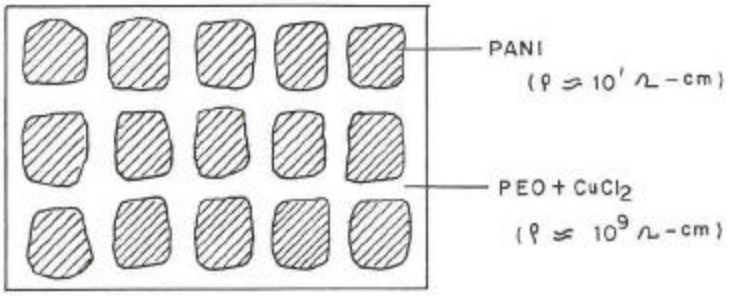

Fig. 6.16 Schematic diagram of dispersion of PANI in the PEO-$CuCl_2$ matrix

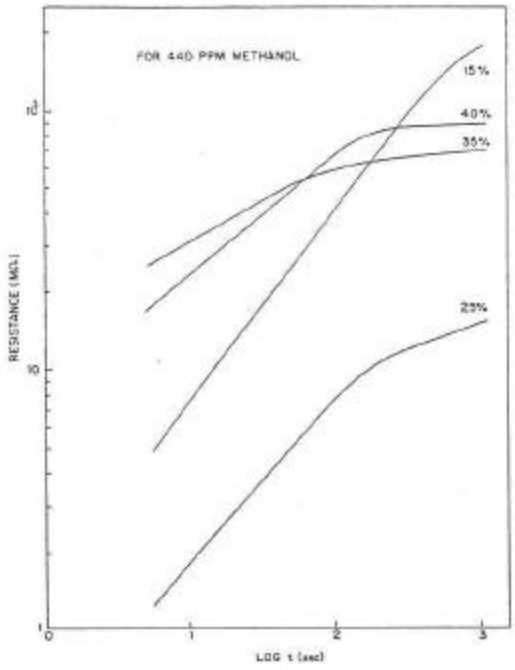

Fig.6.17 Recovery for the PANI-(L)/ PEO-$CuCl_2$ blends plotted on a log-log scale

The action of a chemical vapour, methanol in the present case, on such a blend system would proceed as follows. Firstly, the PEO-$CuCl_2$ matrix, which is the major component, would

absorb the vapour, which then has to diffuse through the interdomain spaces and reach the polyaniline moieties where it would interact with the impurity state and transfer electronic charge. The transfer of electrons leads to a lowering of the potential barrier at the interface, giving rise to an increase in conductivity. From the rapid response of these material to methanol vapour, it may be surmised that the process is of the fast electronic type and that ions are not involved in the charge transport.

The recovery of the sensor after exposure to methanol involves the desorption of vapour molecules and corresponding changes in reverse order as described above. The desorption process is normally expected to follow the diffusion mechanism governed by Fick's second law,[32] i.e.

$$\frac{d_c}{d_t} = -D\frac{d^2c}{dx^2}$$

----------Eq 6.8

where c is the concentration, t is the time, x is the distance along the thickness of the film and D is the diffusion constant. The above equation suggests that the concentration dependence of vapour molecules in the film will follow

$$\frac{d_c}{d_x} = \frac{Co}{(4p\,Dt)^{1/2}} \exp\left(\frac{-x^2}{4Dt}\right)$$

----------Eq 6.9

or to a first approximation at times exceeding 10^{-6} is,

$$\frac{C_t}{C_\infty} \approx \frac{\sigma}{r(Dt/\pi)^{1/2}}$$

----------Eq 6.10

where the molecules are considered to be spherical with radius r and the subscripts t & Co denote the value at time t and after a very long time respectively. Thus one would expect the change in electrical resistance, which is directly related to the methanol concentration in

the polymer during the recovery process to follow a $t^{1/2}$ law. In order to confirm such a time-dependence, the resistance value during recovery was plotted as function of time on log-log scale as shown in the **Fig.6.17**. It is interesting to note that the graphs are linear in all cases only in the initial stage of the recovery process, indicating that resistivity, $\rho \propto t^n$ in this region.

However, the value of n changes from 0.7 to 0.4 with increasing polyaniline concentration in the film. Further there is an increasing tendency for the graphs to become non-linear, suggesting the presence of additional processes other than the diffusion of vapour out of the polymer film. Since these deviations are larger for samples containing higher concentration of polyaniline, the additional process must be associated with the interaction of vapour molecules with polyaniline moities.

The role of the interfacial barrier between polyaniline domains and the PEO matrix in the enhancement of sensitivity is brought out in **Fig.6.18**, which shows the sensitivity factor for these sensor elements as a function of polyaniline contents in the film material. It is interesting to note that the sensitivity increases initially with increasing polyaniline content upto about 40% but then decreases for higher content of polyaniline and is in fact quite low for pure polyaniline. Thus it is seen that there is an optimum concentration (40-50%) of polyaniline at which the sensitivity is maximum. This peculiar behaviour can be explained as follows. At a very low concentration of polyaniline, the barrier width is very large and the charge transport across it is difficult. The barrier width decreases with increasing polyaniline concentration and charge transport is facilitated, giving rise to an increase in sensitivity factor. However, when the polyaniline concentration is increased above 40%, which is near to the percolation threshold for such composite, interparticulate contacts forms and some of the barriers are 'shorted out'. Since pure polyaniline powder by itself does not have much sensitivity, the overall sensitivity decreases for high concentration of polyaniline owing to a decrease in the number of active barriers. This clearly indicates that an optimum height and width of the barrier are necessary for obtaining high sensitivity in such composite films.

The PANI-(H)/PEO-$CuCl_2$ blend was also investigated for chemical sensitivity. Response characteristics of exposure to methanol are similar to for PANI-(L)/PEO-$CuCl_2$ system. The sensitivity factor σ_{max}/σ_0 was calculated and is plotted against the PANI-(H) composition. A maxima of a factor 38 is observed at 10% PANI composition. The decay time (t_d) and the recovery time (t_r) were calculated and are represented by the **Fig.6.19**. The

decay time is similar in all the cases- it is almost two minutes, which the recovery time shows a variation with PANI composition. A lower t_r is seen between 10 - 20% PANI composition where the blend exhibits maximum sensitivity towards methanol. The recovery process was then analyzed by plotting on a log-log scale. Two processes can be clearly delineated from these graphs. These exhibit a maximum slope at 20% PANI composition and then decreases thereafter. The slopes of these plots are lower than that observed for the PANI-(L)/PEO-$CuCl_2$ blend.

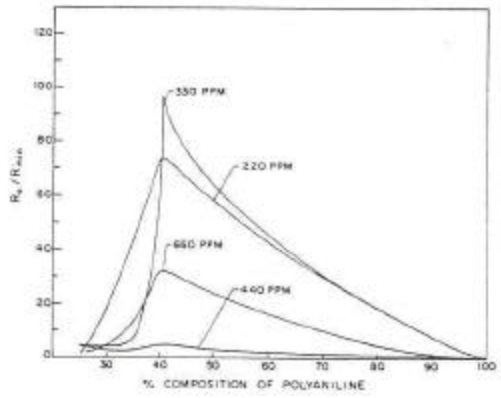

Fig.6.18 Sensitivity for the PANI-(L)/PEO-$CuCl_2$ blends as a function of the composition of PANI-(L) for different dosage levels of methanol

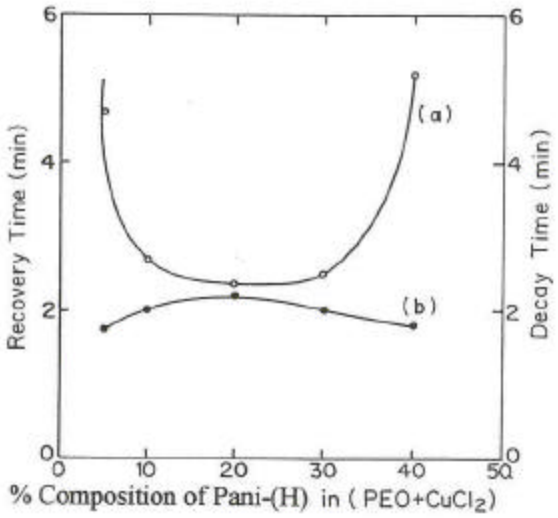

Fig.6.19 Decay time and recovery time as a function of composition of PANI-(H) for the PANI-(H)/PEO-$CuCl_2$ blends

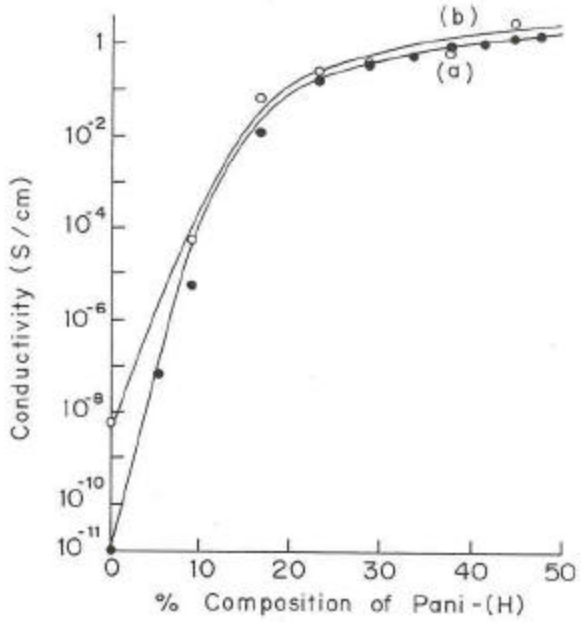

Fig.6.20 Compositional dependence of conductivity for (a) PANI/PVAc blends (b)PANI/PVAc-$CuCl_2$ blends

6.3.3 PANI/PVAc-$CuCl_2$ based blends and composite:

Blends of PANI-(H) were prepared by using PVAc and PVAc-$CuCl_2$. Further, a composite of PANI/CuPc was prepared using PVAc.

(A) PANI/PVAc blends:

(a) Compositional dependence of conductivity:

The conductivity against the concentration of PANI added in the PVAc matrix is as shown in the **Fig.6.20** (curve **a**). The conductivity is seen to increase with the addition PANI composition. A rapid rise in conductivity by almost 10 orders of magnitude is seen at 23% PANI dispersion in PVAc, which saturates to $9x10^{-1}$ S/cm. The curve represents a classical percolation behaviour. Hence a plot of conductivity with respect to the weight fraction of PANI was made on log-log scale as illustrated by the **Fig.6.21**. It is clear that the percolation threshold is achieved at 6 % PANI composition. The matrix PVAc is an insulating material with a conductivity of $2x10^{9}$ S/cm. The addition of conducting particles of PANI to this insulating matrix results in the formation of interparticulate gaps. The junction formation at the interface of the materials is as shown in the **Fig.6.22.** It is clear from the band diagram since the work function of PANI is 4.4 eV and PVAc is 4.38 eV, there is practically no barrier at the interface of the materials. Hence it is only the jump distance that decreases as the PANI content in the blend is increased. Beyond the critical concentration of PANI, the conduction occurs by percolation process.

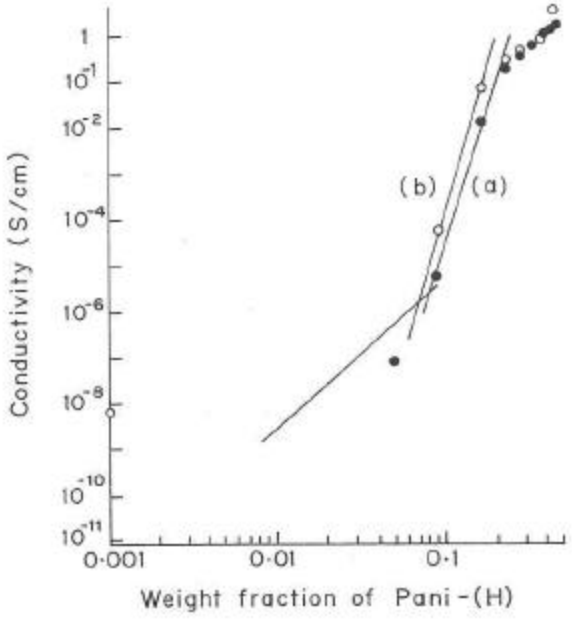

Fig.6.21 Dependence of conductivity on the volume fraction of PANI in PVAc

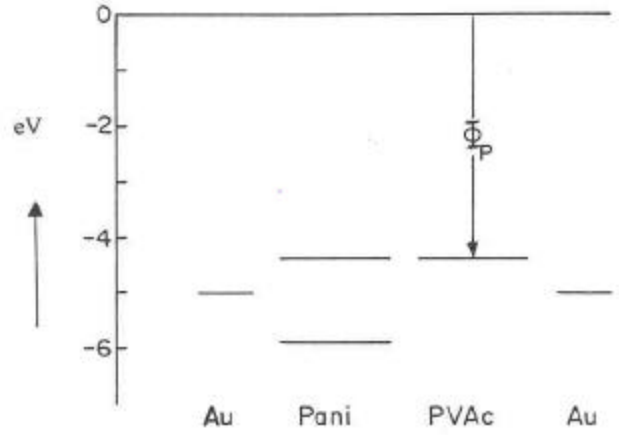

Fig.6.22 Band diagram showing the energy levels of PANI and PVAc

The conductivity versus composition for PANI/PVAc-$CuCl_2$ is as shown in the **Fig.6.20**

(curve **b**). It is observed that the conductivity of PANI/PVAc-$CuCl_2$ increases by almost seven orders on addition of PANI. The conductivity attains a limiting value of 1-2 S/cm at around 20-30% PANI. As compared to the PANI/PVAc blend as represented by (a), the conductivity of the PVAc-$CuCl_2$ matrix itself is observed to rise by 2.5 orders of magnitude. This may occur possibly due to the formation of a complex. It is reported that PVAc contains a small amount of polyvinyl alcohol that may form an ionic complex with $CuCl_2$. The formation of PVA-$CuCl_2$ complex leads to increase in the conductivity of the blend.

(b) I-V characteristics of PANI/PVAc-$CuCl_2$ based blends:

The I-V characteristics for the PANI/PVAc blend for the compositions are found to be non-linear in nature for 10 and 20% PANI content as shown in the **Fig.6.23 (a)** and **(b)** respectively. Rest of the compositions containing higher PANI composition exhibit linear I-V characteristics as in the **Fig.6.23(c)** for 30% PANI composition. The curves were then analyzed by making a plot of log I against log V. The plots were found to delineate in to two straight lines as exhibited by the **Fig.6.24**. The slopes of the plots were found to change from 1 to 2. This type of behaviour is encountered in the case of SCLC type of conduction mechanism as discussed in the chapter 3 (sec 3.3.2). The change of slope can be related to filling of the traps, correlated by the equation. Hence, it can be said that a space charge region is created at the interface of PANI/PVAc that gives rise to the SCLC behaviour. If the contacts to the electrode are ohmic, then the electrodes act as an abundant source of charge carrier which can be injected in to the solid. At sufficiently high fields, the solid is unable to transport all the injected charge and a build-up of charge begins within the solid. Traps are generated in the PANI owing to the dopant ions. The PVAc also contains defect states due to the disordered structure [33]. The conduction proceeds by filling up of these traps depicting an SCLC behaviour. This causes a change in the conduction behaviour from ohmic at lower voltages (n=1) to a square law at higher voltages (n=2). However, at higher compositions such as 30, 40 and 50 %, the conduction mechanism is seen changing to ohmic in nature. This composition range of PANI lies well above the percolation threshold, wherein a continuous phase of PANI is formed as discussed in the earlier section. This leads to a shorting of PANI/PVAc barriers yielding linear I-V characteristics.

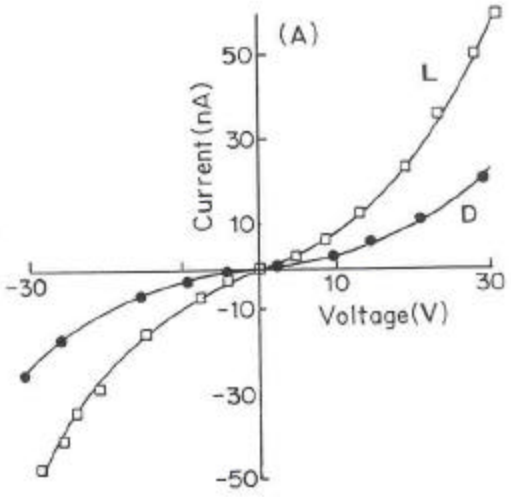
(A)
L
D
Current (nA)
50
30
10
-10
-30
-50
-30
10
30
Voltage(V)

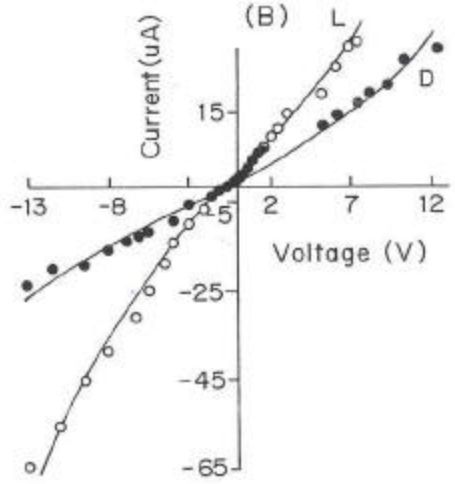
(B)
L
D
Current (uA)
15
-5
-25
-45
-65
-13
-8
2
7
12
Voltage (V)

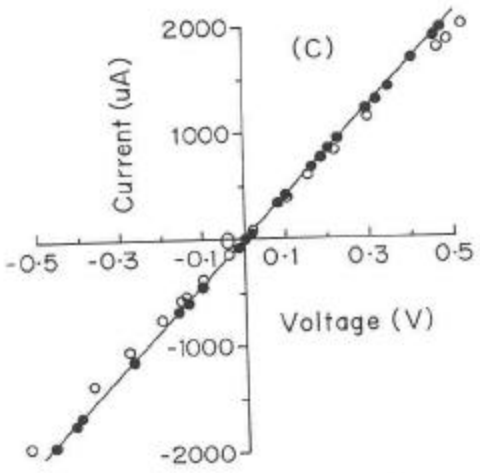

Fig.6.23 I-V characteristics for PANI/PVAc blends containing (a)10 and (b)20 (c)30% PANI respectively

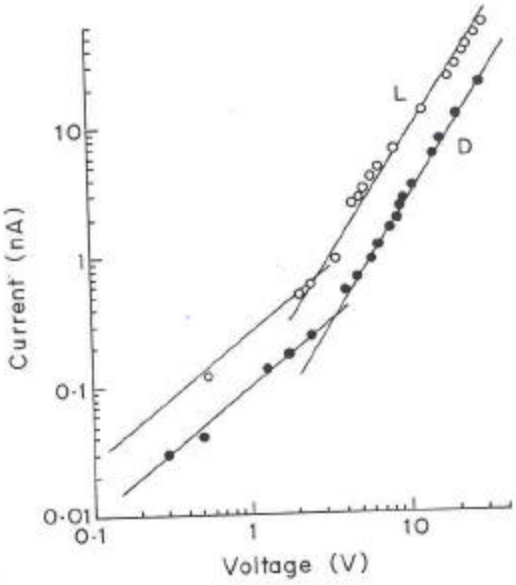

Fig.6.24 A log-log plot of the I-V characteristics for the PANI/PVAc blends containing 10% PANI

In the case of PANI/PVAc-$CuCl_2$ blends, the I-V characteristics were found to be nonlinear in nature, for the lower compositions i.e. 5% and 10% PANI content and linear for the higher compositions i.e. 30% as depicted in the **Fig.6.25 (a), (b) and (c)** respectively. These are similar to that observed for PANI/PVAc blend. These were analyzed by plotting as log I-log V as shown in the **Fig.6.26.** It is observed that the plots can be delineated in to two straight lines, the slopes corresponding to 1 and 2. The change in the slope, 'n' can be associated with the SCLC mechanism as discussed in the case of PANI/PVAc blend. The complex formation of PVAc with $CuCl_2$ results in the introduction of traps in PVAc that get filled at higher voltages. The filling up these of traps yields square law behaviour, as observed in the present case. As observed in the earlier section, the conduction in the blends beyond the percolation threshold takes place by hopping mechanism, as no PANI/PVAc-$CuCl_2$ barriers are present. This explanation holds good in the case of blends wherein each PANI particle is presumed to form a junction at the PVAc interface and these junctions when connected in series and parallel exhibit a net effect as reflected in the I-V characteristics.

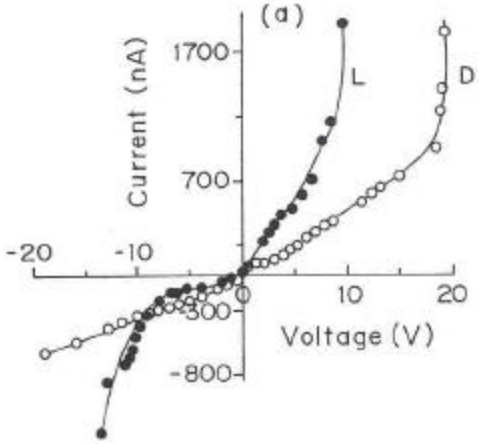
(a)
1700
700
-300
-800
Current (nA)
-20
-10
0
10
20
Voltage (V)
L
D

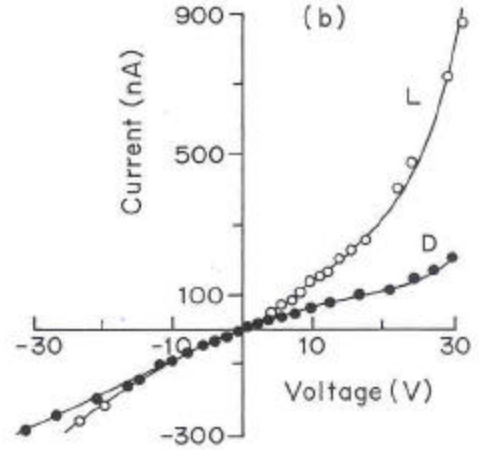
(b)
900
500
100
-300
Current (nA)
-30
-10
10
30
Voltage (V)
L
D

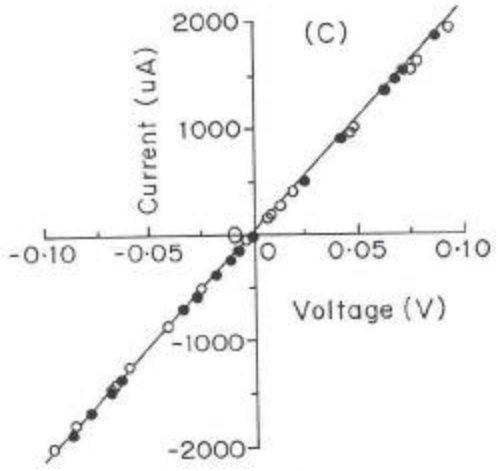

Fig.6.25 I-V characteristics for PANI/PVAc-$CuCl_2$ blends. Curves (a) to (c) correspond to PANI concentration of 5, 10 and 30%

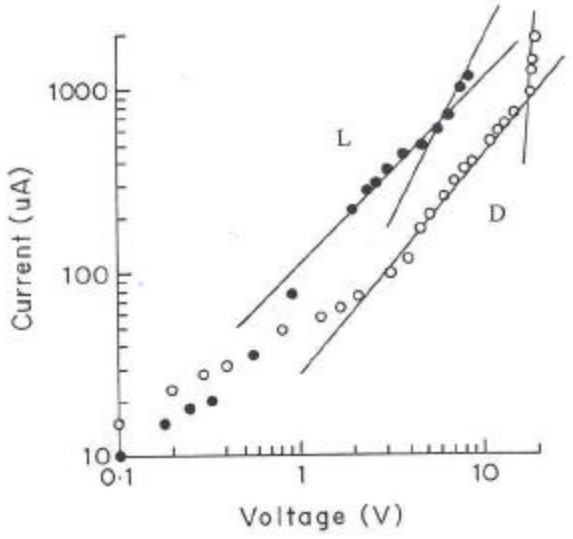

Fig.6.26 Log-log plot of I-V characteristics of PANI/PVAc-$CuCl_2$ blends containing 5% PANI

It can be concluded from the above studies that no barrier exists at the interface of PANI/PVAc and PANI/PVAc-$CuCl_2$ interface. The blend system consists of discrete junctions connected together giving a multiple junction effect. The charge transport takes place by SCLC type of conduction mechanism. These junctions exist only till the percolation threshold whereafter they form short circuit giving rise to a polyaniline network. The conduction occurs by hopping process in the blends containing higher PANI.

(c) Temperature variation for PANI/PVAc-$CuCl_2$ based blends:

The PANI/PVAc blends exhibited a range of conductivity from semiconducting to a conducting state. The effect on the conduction mechanism was clearly observed as a marked differentiation in the I-V characteristics. A similar variation can be noted in the temperature dependence also. **Fig.6.27** denotes the log σ Vs 1/T plots for various compositions from 0 to 40% PANI content. The curves for the low PANI compositions i.e. 5,10 <20% can be delineated into two plots, one representing the high temperature region and the other a low temperature region. A transition is observed at 82-85^oC which is near the T_m of hydrolyzed PVAc (T_m~85^oC) [34]. Hence the blends containing low PANI exhibit a considerable change in the conductivity whereas those containing higher (≥28.7% PANI) exhibit negligible change. This is due to the increase in viscosity of the blends at higher PANI concentrations (as discussed in section 6.3.2.c) that causes the domains to remain intact and hence no effect on the overall conductivity.

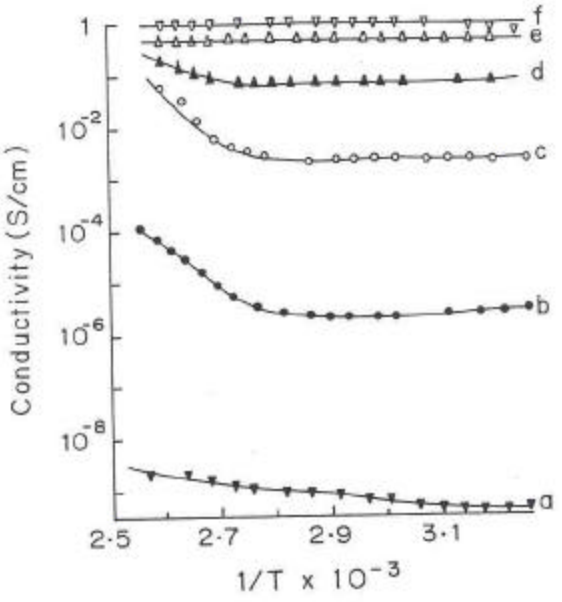

Fig.6.27 Temperature dependence of conductivity for the PANI/PVAc blends containing 0 to 40% PANI

The ΔE was calculated using the Arrhenius equation (eq.3.15). Activation energies calculated are thus tabulated as **Table 6.2.**

Table 6.2:

% Composition of PANI in PVAc	Activation energies (ΔE) in eV	
	At low temp	At high temp
0	0.0847	0.5067
5	0.0388	1.555
20	0.058	1.795

The activation energy is thus seen to decrease with the increase in PANI concentration. This is due to lesser trapping of charge carriers in the PVAc regions between two conducting domains as the PANI content increases.

The temperature variation in the case of PANI /PVAc-$CuCl_2$ blend shows a similar behaviour as in the earlier case. The lower compositions exhibit activation energies that are tabulated as **Table 6.3.**

Table 6.3

% Composition of PANI in PVAc	Activation energies (ΔE) in eV	
	At low temp	At high temp
0	0.08116	0.3887
5	0.0468	1.301
10	0.0463	1.132
20	0.0612	0.199

It is observed that the activation energies are lower than in the earlier case as the conductivity of the matrix increases.

(d) Property measurement:

The properties such as light sensitivity and photosensitivity were investigated for these samples and the results of the same are described in the following sections.

(1) Light Sensitivity:

The I-V characteristics recorded in dark and light for 10% PANI in PVAc are represented in the **Fig. 6.23(a).** The sensitivity factor IL/ID was calculated to be 3 whereas compositions containing higher PANI content exhibit a negligible light sensitivity. Thus it can be observed that the overall sensitivity is low since there are no barriers present at the interface of the materials. The photocarriers generated under illumination in PANI get trapped and a high recombination probability thus exists. A small amount of photoexcited electrons undergo separation due to PVAc polar field, contribute to a small photocurrent as observed.

In the case of PANI/PVAc-$CuCl_2$, the light sensitivity increases to 4.5 (see **Fig.6.28**) as compared to a factor of 3 in PANI/PVAc blend. It may be of interest to note that during the synthesis of PVAc, a small amount of poly(vinyl alcohol) may be produced as a result of hydrolysis [35]. PVA is known to form complexes with nitrate, sulfate, chloride or bromide salt of Cu^{++}[36]. Furthermore, the complex of PVA-$CuCl_2$ is also reported to be photoconductive [37]. Well-dried films of PVA containing Cu^{2+} content as low as 0.015 mole/monomer ratio is sufficient to produce strong photocurrents in PVA-$CuCl_2$ and PVA-$CuBr_2$. When the PVA-$CuCl_2$ film is illuminated at the charge transfer band a reaction is believed to occur [38]. The halogen atom abstracts a hydrogen atom from PVA thereby producing a free radical [39]. When the Cu^{2+} to PVA ratio is high, the halogen atoms interact more with neighbouring halide ions. At this point the reduction reaction involves the production of holes in the network of halide ions. A photocurrent is observed when an electric field is applied to the film. In the present case, the PVA present as impurity yields a similar photoconductive effect. The maximum light sensitivity is shown at 10% PANI composition beyond which it is almost insignificant due to the creation of the network.

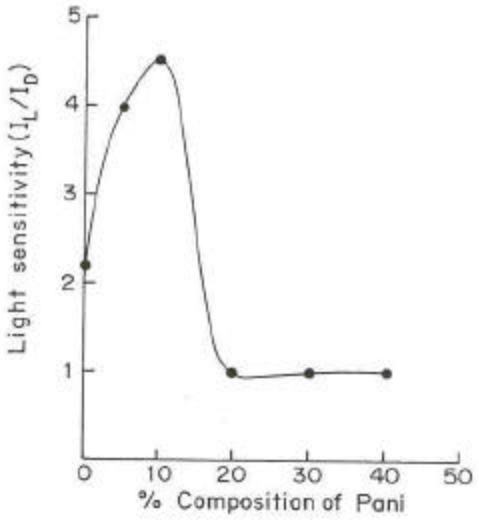

Fig.6.28 Light sensitivity I_L/I_D for PANI/PVAc-$CuCl_2$ blends as a function of the composition of PANI

(2)Chemical Sensing:

The blends have M-I-M structure similar to those studied earlier. The chemical/electronic configuration if altered by the action of an external parameter would cause a change in the conductivity of the materials. The present PANI/PVAc blends were also subjected to the presence of gases like methanol and NO_2. The response characteristics are studied and presented below.

(i)Exposure to Methanol:

The response characteristics of 33 % PANI in PVAc to methanol are illustrated in the **Fig**.**6.29**. It is observed that the conductivity of the blend increases on exposure to methanol. The sensitivity factor $S = \sigma \text{ max} / \sigma \text{ min}$ was determined and is plotted as **Fig**.**6.30**.

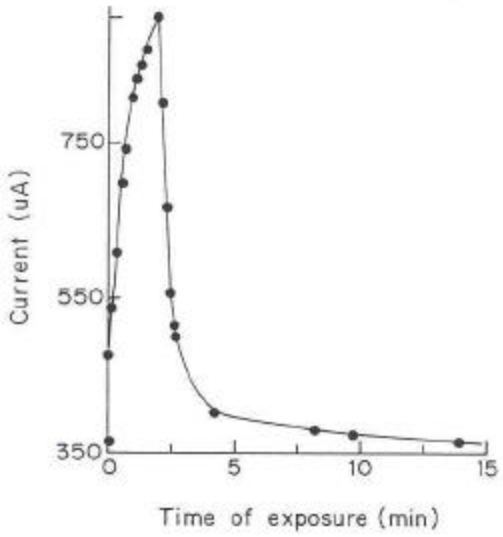

Fig.6.29 Response characteristics of PANI/PVAc containing 33% PANI on exposure to methanol

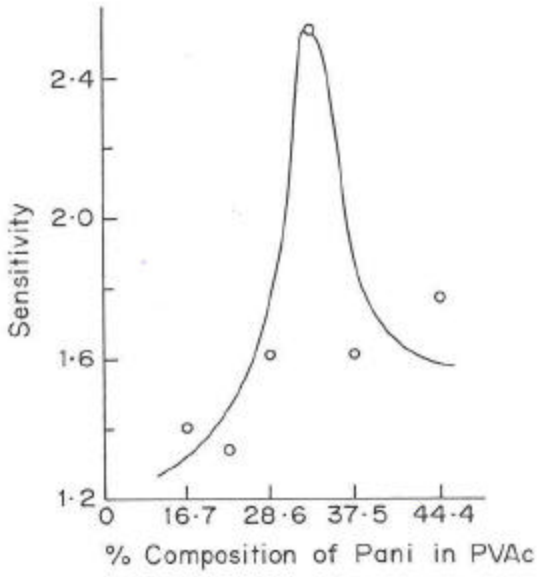

Fig.6.30 Effect of PANI concentration on the sensitivity of PANI/PVAc blends

The overall sensitivity is seen to be quite low. This can be explained taking into consideration the electron transfer occurring in the blend. The action of methanol is similar to that described in the PANI/PEO systems, methanol vapours are absorbed by the PVAc matrix. Methanol contains the donor – OH group which then forms a charge-transfer complex donating the electrons to PVAc. These are then transferred to PANI an electronic conductor. As more electrons are available for conduction the conductivity of PANI increases thus showing a response to the presence of methanol. The magnitude of response depends on the interdomain distance i.e. distance between the two conducting PANI particles. An efficient electron transfer occurs at an optimum interparticulate distance that is seen occurring at 33% PANI composition at which it gives maximum sensitivity. The recovery time and the decay time are also low at this composition as denoted by the **Fig.6.31**. The decay time (td) is around 3 minutes while it recovers in about 6 minutes.

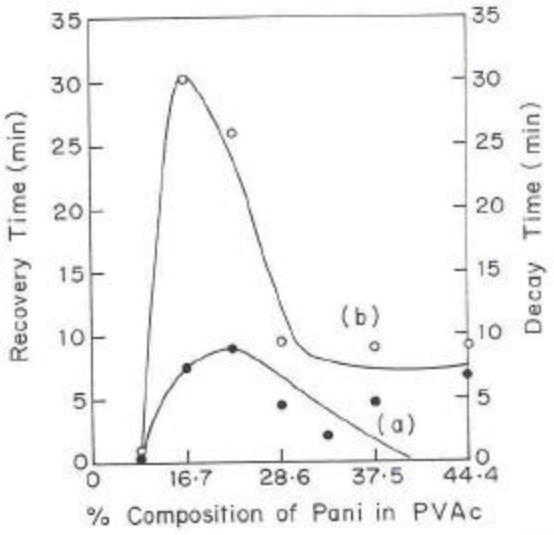

Fig.6.31 Dependence of recovery time and decay time for the PANI/PVAc blends on exposure to methanol

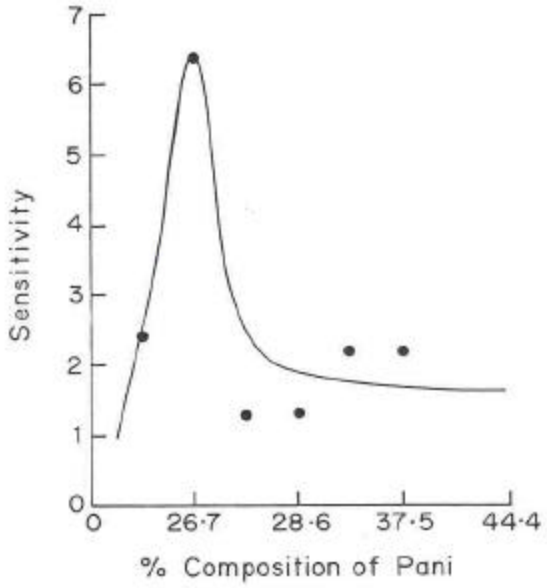

Fig.6.32 Variation of sensitivity with PANI composition for PANI/PVAc-$CuCl_2$ blends on exposure to methanol

In the case of PANI/PVAc-$CuCl_2$, the conduction is of mixed type – ionic as well as of electronic type and hence the response to methanol is expected to be different than that of PANI/PVAc. The response characteristics show an increase in conductivity on exposure to methanol as in the earlier cases. The variation of the sensitivity factor with the PANI composition is depicted by the **Fig.6.32.** It is observed that the sensitivity towards methanol is highest i.e. 6.4 at 20 % PANI composition and decreases to around 2 and remaining constant thereafter. The decay as well as response time show a minimum at optimum concentration of 20 % PANI. The optimum concentration is lower in the present case than in PANI/PVAc blend. This is due to separation of PANI particles by the semiconducting PVAc-$CuCl_2$. The acceptor impurity levels of $CuCl_2$ created in PVAc (PVA-$CuCl_2$) trap the electrons that are donated by methanol consequently increasing the conductivity of the PVAc-$CuCl_2$ and hence of the blend. This results in an enhanced sensitivity towards methanol as compared to the PANI/PVAc blend.

(ii)Exposure to Nitrogen dioxide:

The PANI/PVAc blend was also tested for nitrogen dioxide sensing. Nitrogen dioxide is a strong electron-withdrawing group. Its action is expected to be just opposite of methanol which has a donating group. A decrease in conductivity of the blend on exposure to NO_2 is indeed observed as typically represented by the response characteristics of the blend containing 28% PANI (**Fig.6.33**). The sensitivity factor was determined from the response studied for all the compositions and is plotted as **Fig.6.34**. It is clear that the sensitivity increases with PANI composition and shows a factor of 250 at 37% PANI loading in PVAc. The action of NO_2 would take place by diffusion through the PVAc matrix towards the PANI. The electron withdrawing nature of NO_2 creates deficiency of electrons and hence a transfer of electrons from PANI. This results in a low conductivity, which is reflected as a response to NO_2 detection. But the transfer of electrons back to PANI seems to be quite slow and relatively irreversible.

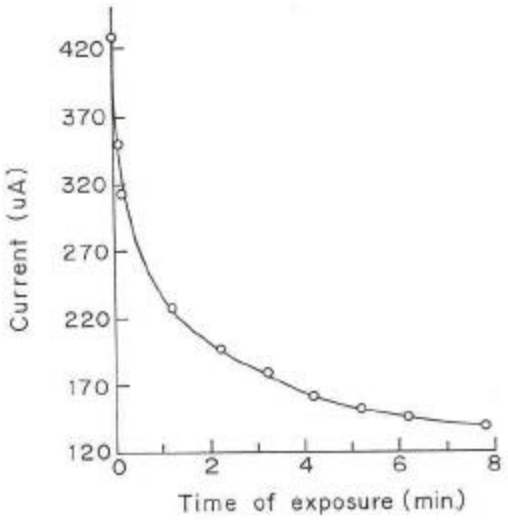

Fig.6.33 Response characteristics of PANI/PVAc blends towards NO_2 containing 28% PANI

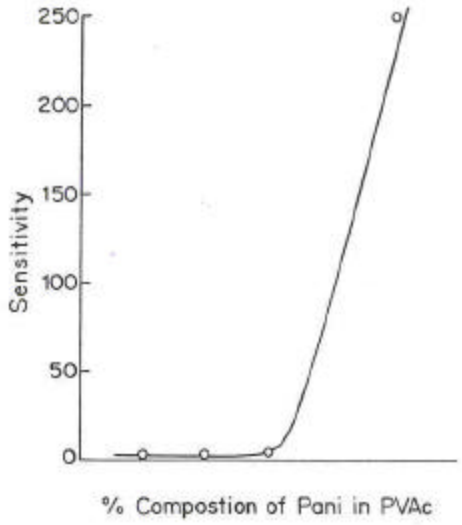

Fig.6.34 Sensitivity towards NO_2 as a function of the composition of PANI in the PANI/PVAc blends

The sensitivity towards NO_2 for PANI/PVAc-$CuCl_2$ is similar to that of the above case. Sensitivity factor shows an increasing trend with the composition of PANI. The

maximum sensitivity is 26, which is an order less than the PANI/PVAc blend. The electronegative Cl ion present in the matrix reduces the affinity of PVAc towards NO_2.

(B) PANI/CuPc composite with PVAc:

PANI/CuPc composite was prepared by dispersion method in PVAc using 10% PANI w/w PVAc. PVAc-$CuCl_2$ was not used for the purpose, as it is known that $CuCl_2$ forms a complex with CuPc consequently increasing the trapping sites in CuPc. The charge transport and properties associated with the materials were investigated and are presented below.

(a) Compositional variation of conductivity:

The variation of conductivity of the PANI/CuPc composite with PVAc depicted in the **Fig.6.35**. It is observed that the conductivity decreases as the CuPc content increases. It drops down from $8x10^{-5}$ S/cm to $2x10^{-9}$ S/cm i.e. by around 4-5 orders of magnitude till 40 % addition of CuPc. Taking into consideration the energy band diagram as shown in the **Fig.6.36**, it can be understood that there exists a very small barrier of 0.1 eV at the PANI/CuPc interface since the work function of CuPc is 4.3eV. The variations in conductivity of the composite can be explained by considering the interparticulate distance between the PANI particles. The jump distance increases as the CuPc content increases and hence results in lowering the conductivity of the composites.

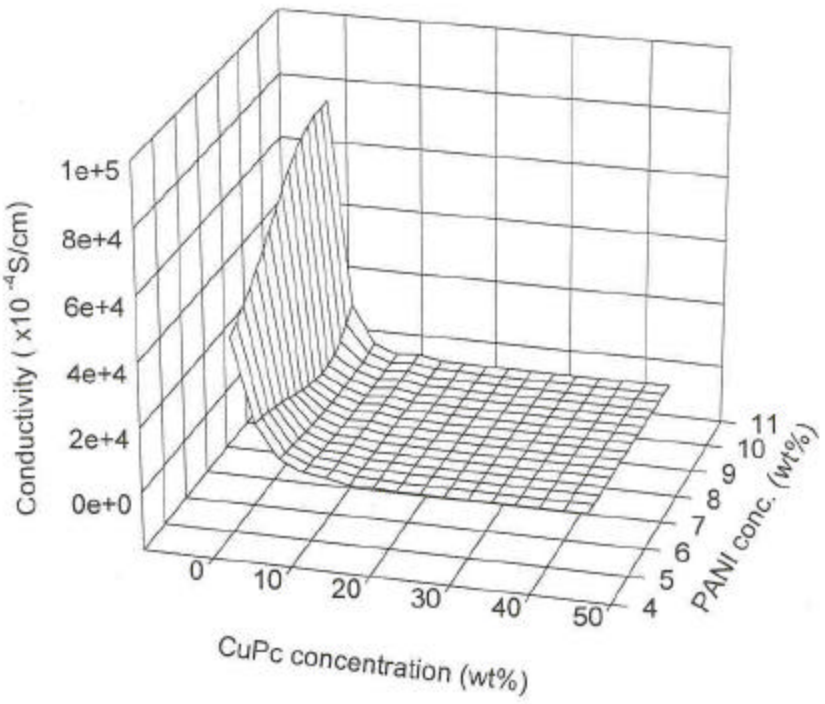

Fig.6.35 Variation of the conductivity of PANI/CuPc composites with PVAc with PANI and CuPc composition

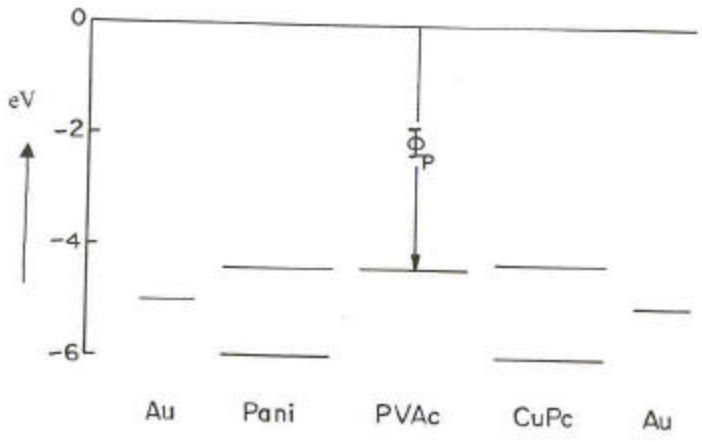

Fig.6.36 Band diagram showing energy levels of PANI and CuPc

(b) I–V characteristics for PANI/PVAc-$CuCl_2$ based composites:

The I-V characteristics were non-linear in nature for the composites containing 5,10 and 20% CuPc while those containing 30 and 40 % CuPc exhibit linear I-V characteristics. The **Fig**.**6.37 (a)** and **(b)** illustrates an IV curve for10 % and 20 % CuPc in PANI/PVAc. The plot was then analyzed by making a plot of log I against log V. The plots could be demarked in to two straight lines with corresponding slopes of 1 and 2 as noticed in the **Figs**.**6.38 (a)** and **(b).** Hence the conduction takes place by SCLC mechanism due to the presence of trapping centers in PVAc as discussed in section 6.3.2. At higher compositions a CuPc network is formed throughout the composite. Au is ohmic to CuPc [40]. Hence the I-V characteristics are linear in nature at higher CuPc contents.

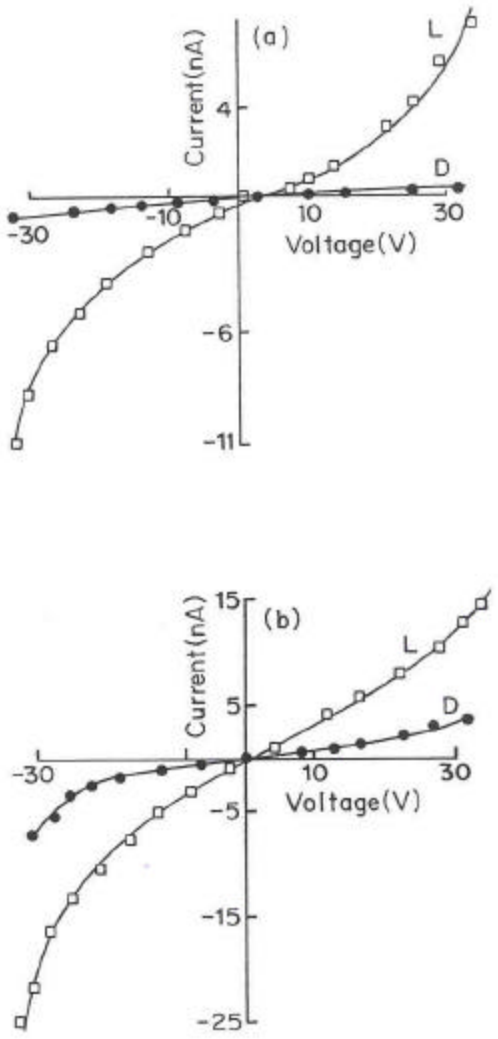

Fig.6.37 I-V characteristics for PANI/CuPc composites with PVAc containing (a) 10 and (b) 20% CuPc

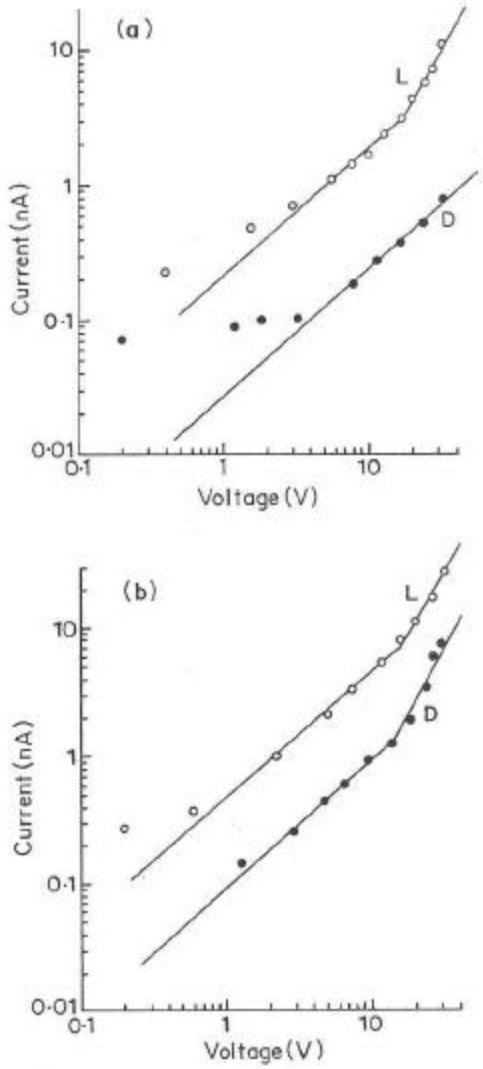

Fig. 6.38 LogI- log V plots for PANI/CuPc composites with PVAc containing (a) 10 and (b)20% CuPc

It is thus observed that no significant barriers are present at PANI/CuPc interface. The charge transport takes place by SCLC type of mechanism in the case of PANI/CuPc

composites with PVAc at lower CuPc contents but it becomes increasingly ohmic at higher concentrations.

(c) Temperature variation for PANI/PVAc-$CuCl_2$ based composites:

The conductivity increases with temperature for all the composition of CuPc. The log σ Vs ^{1}/T plots for the system are illustrated by the **Fig.6.39**, that obey the Arrhenius law as denoted by the straight-line graphs. The log σ Vs 1/T plots for higher compositions of CuPc viz. 28, 37, and 44 % show the presence of two activation energies: one at low temperature and other at higher temperature. It is observed that there is a decrease in the activation energy with increase in CuPc concentration as evidenced by the **Fig.6.40**. This is due to the continuous network formation of CuPc, eliminating the conduction through filling up of trapping centers in PVAc.

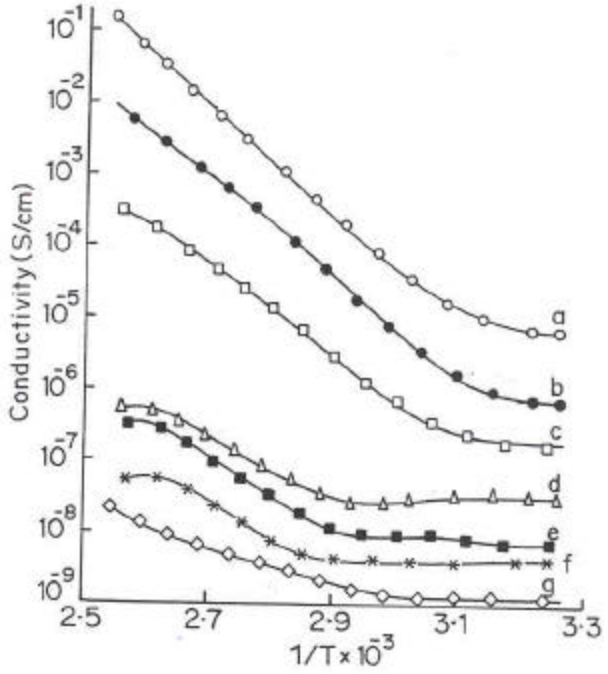

Fig.6.39 Temperature variation of conductivity for the PANI/CuPc composites with PVAc

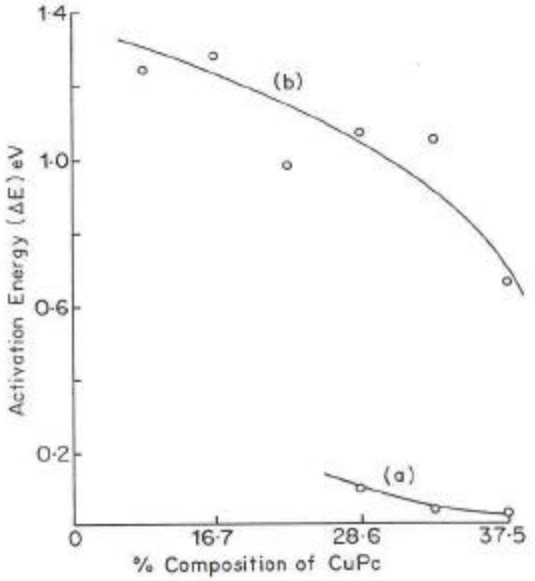

Fig.6.40 Decrease in activation energy with higher CuPc for PANI/CuPc composites with CuPc

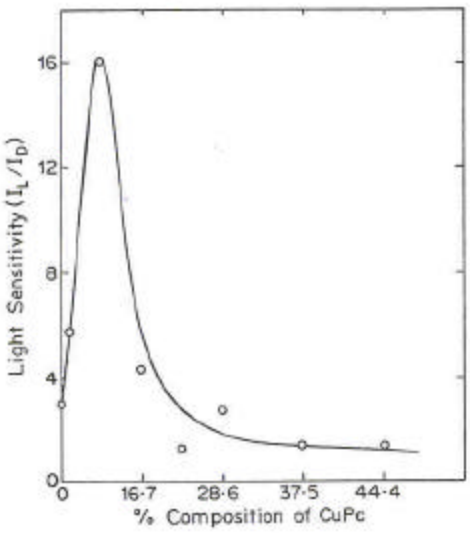

Fig.6.41 Light sensitivity as a function of CuPc concentration in the PANI/CuPc composites with PVAc

(d) Charge transport for PANI/PVAc-$CuCl_2$ based composites:

It is clear from the various results obtained that the charge transport in the PANI/CuPc composites is dominated by the conduction across PANI/CuPc interface, which occurs by SCLC conduction mechanism.

(e) Property Measurement:

1.Light Sensitivity:

The dye sensitized PANI/PVAc/CuPc composite exhibited light sensitivity as evident by the enhanced photocurrent depicted by the I-V characteristics (**Fig 6.37**). The light sensitivity factor IL/ID was determined for all the compositions and is represented by **Fig**.**6.41**. It is observed that 10 % CuPc shows a maximum factor of 16. The phenomenon of sensitization is discussed in Ch. 1. The charge generation in phthalocyanines induced by light is given below [41].

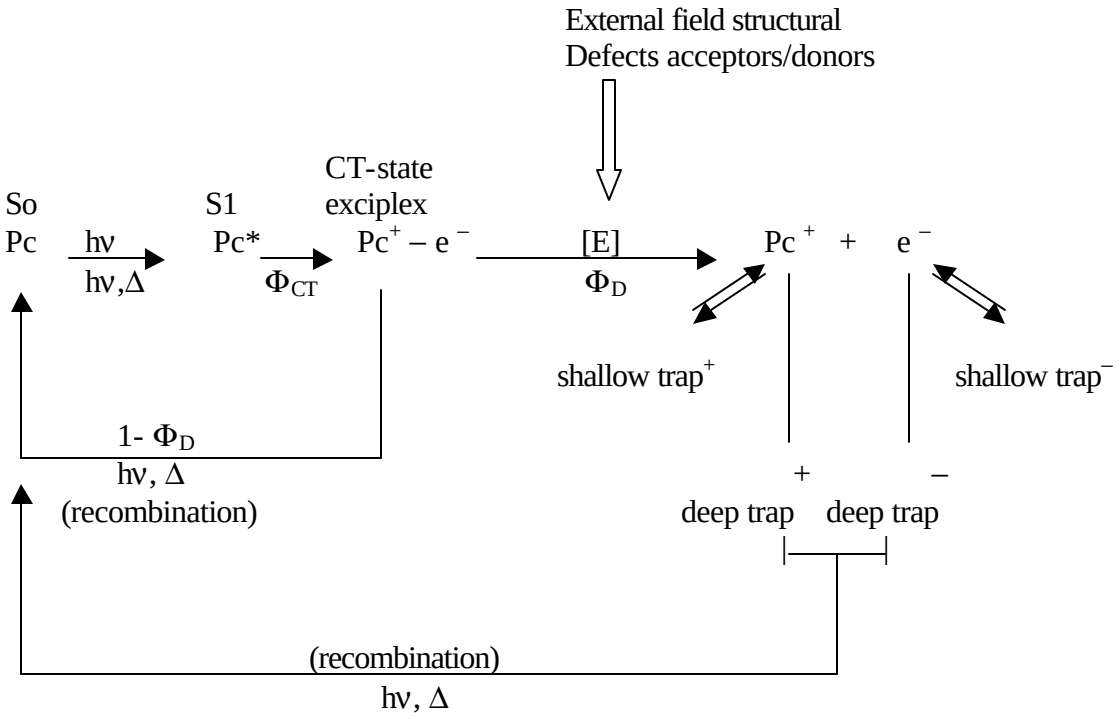

Under illumination, in the absorption region the excited states contribute to the number of charge carriers. In the primary step a localised excited state at one molecule (exciton) is formed. It is known that in organic crystals the exciton can diffuse by energy

transfer and can also recombine (thermally or by emission of photon) or dissociate in an auto-ionizing step into mobile charge carriers. Exciton dissociation in phthalocyanines is believed to occur assisted by electric field. This field can either be established internally by structural defects (intrinsic photoconduction) by charged impurities (extrinsic photoconduction) or externally by applied electric field. The applied field leads to a more efficient dissociation of exictons and collection of charge carriers, which in turn decreases the probability of recombination reactions. The conductivity thus changes as:

$$\sigma_{phot} = e\left(\Delta n\mu_n + \Delta p\mu_p\right)$$

----------Eq 6.11

where Δ_n and Δ_p are changes in electron and hole concentration under illumination

As discussed in Chapter 1, CuPc is used as a photosensitive material in contact with different metals like In, Al. In almost every case, for these photovoltaic cells, a severe loss in power conversion efficiency is noted as the light intensity is increased. This inefficiency is due to the change in chemical and morphological state of the materials during vapour deposition, which critically determine their performance. A new approach to the fabrication of low cost organic cells is the use of particulate semiconductors. The device employs a solvent a solvent-coated dispersion of photoactive particles in a polymer binder on a conductive substrate. Thus the use of a polycrystalline powder than a vapour deposited film preserves the chemical and morphological integrity of the semiconductor. Loutfy et al [42] have reported of metal free phthalocyanine dispersed in a polymer binder like polycarbonate, polyvinyl acetate and polyvinylcarbazole. They have found an improvement in power conversion efficiency at high light intensity and a long-term stability was also observed. The photovoltaic parameters also depend on pigment loading, polymer binder, film thickness, doping, dye sensitization and barrier electrode material. This aspect was further studied in detail by Tsuda [43,44] et al by examining various polymer binders with H_2Pc. The H_2Pc content was maintained at 60% in 40% polymers like PVDF, PVPh, PVK, PVAc, PS, etc. There was a considerable difference on the photovoltaic characteristics of H_2Pc using different binders. The energy conversion efficiency, η, was the highest for PVDF, followed by PAN, PVF, PVAc, etc. This indicates that a polar group- electron attracting or donating is essential indicating their participation in the current production. In organic polymers, the

exciton-excited state created by light absorption should be separated into charge carriers. This is achieved by applying potential and the local field. It has been reported that the site of exciton dissociation is at the H_2Pc particle surface. The binder polymer surrounding the active site (the surface of H_2Pc) may strongly influence the photocarrier generation process. The charge separations occur assisted by local field is PVAc, which has a polar group. Under illumination, absorption of photons by CuPc generates excitons that get separated at the CuPc/PVAc active region. The excited electron further gets transferred to PANI resulting in an enhanced conductivity. A maxima in photoconductivity is observed at a low concentration of 10 % CuPc in the composite. More amount of CuPc reduces the efficiency due to light absorption in the inactive region and the high resistance of the dye layers (recombination process). Hence higher dye concentrations do not contribute to the photo current.

2.Chemical Sensing:

Phthalocyanines have been widely incorporated in chemical sensor as described in Ch.1. When subjected to the presence of a gas, it absorbs or forms a weak bond to undergo a change in conductivity, e.g. it shows an increase in conductivity when stimulated by acceptor gases like oxygen, nitric oxide and nitrogen dioxide while the conductivity decreases with ammonia which is an electron donor [45]. The PANI/PVAc blend is sensitive to the external changes as studied in the earlier section. Incorporation of CuPc was expected to affect the gas sensitivity of the composite as discussed above. Accordingly the composite was tested for sensitivity towards methanol and nitrogen dioxide and the results are presented as follows.

(i) Exposure to Methanol:

As evident from the earlier reports the conductivity of CuPc would be expected to decrease when subjected to methanol vapours. But the recorded response characteristics do not agree with the expectations. On the contrary, an increase in the magnitude of conductivity is observed as illustrated by the response characteristics for 30% CuPc loading shown by the **Fig.6.42**. The sensitivity factor for different CuPc compositions was calculated

as is represented in the **Fig.6.43**. It is observed that a maximum of four occurs at 30% CuPc content.

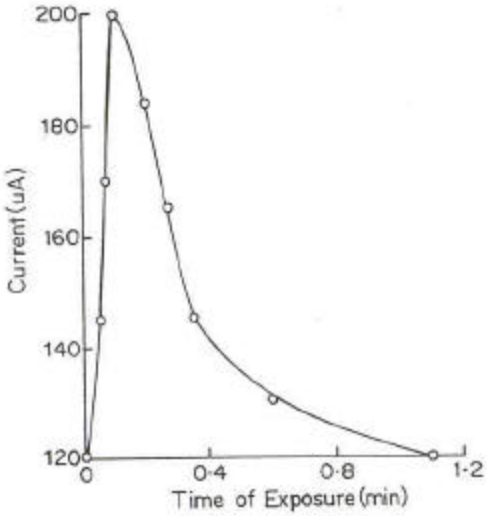

Fig.6.42 Response characteristics of PANI/CuPc composites with PVAc on exposure to methanol containing 30% CuPc

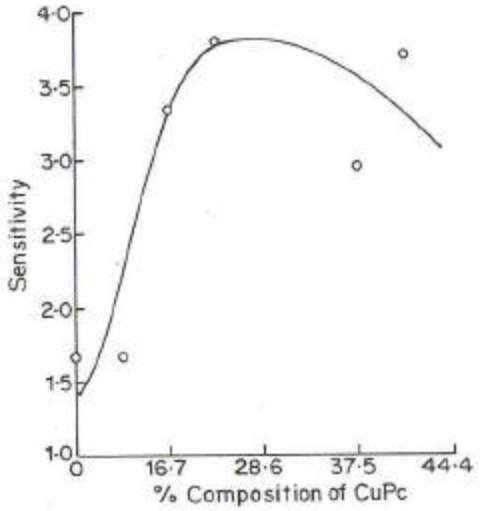

Fig.6.43 Chemical sensitivity towards methanol for PANI/CuPc composites with PVAc

This behaviour of the composite is based on the two components, which can play a role in absorbing or forming a weak bond with methanol. One is the filler CuPc and the other the matrix PVAc that is more sensitive to methanol. Referring to the response shown by PANI/PVAc blend towards methanol, which is quite similar to these in the present case, it can be said that PVAc plays an active role in responding to methanol than CuPc. The latter is known to be less sensitive to electron donors. A typical example would be the response to ammonia by CuPc was a decrease from 8.5 X 10^{-8} to 6.5 X 10^{-8} A [46]. This change can be considered to be small considering the observed one. At lower compositions of CuPc, the action of methanol takes place by transfer of charge from PVAc to PANI. However, increase in CuPc decreases the PVAc relatively, which is the methanol absorbing component. Hence the sensitivity factor remains the same even after addition of CuPc due to the limited charge transfer across PVAc/CuPc barrier.

(ii) Exposure to Nitrogen Dioxide :

Nitrogen dioxide is reported to have large effects (6 to 8 orders of magnitude) on the conductivity of variety of sublimed phthalocyanine films [47]. All the phthalocyanine single crystals also responded initially with a large conductivity increase from 10^{-15} Ω/cm^2 to 10^{-4} to 10^{-8} Ω/cm^2 at saturation. In the present case, a dispersion of CuPc in the PANI/PVAc was expected to cause similar effects. The response characteristics depicted an increase in conductivity on exposure to NO_2 as observed in the **Fig.6.44.** The sensitivity factors for the compositions studied are plotted in the **Fig.6.45**. The plot shows an increasing sensitivity towards NO_2 with the increase in CuPc. Highest sensitivity of 7000 is obtained for 40% CuPc content in the composite. A close look at the response characteristics suggests that the sensor is completely reversible best at 23% and better at 28% composition. Less recovery is observed beyond 28% CuPc content. The decay and recovery times are more or less similar for all the composites. The reports of phthalocyanine single crystals also show partial recovery. On evacuation Ph-, Mn- and Co- phthalocyanine show little changes in the conductivity while other phthalocyanine decreased by a factor of 50 to 1000. Heating under vacuum at 150 ^{0}C returned the metal free Ni, Cu and Zn-phthalocyanine conductivity to within a factor of 5 of the initial level which Ph, Mn and Co phthalocyanines required heating at 250 ^{0}C for 12 hr. to active the effect. In the case of sublimed Pc films different

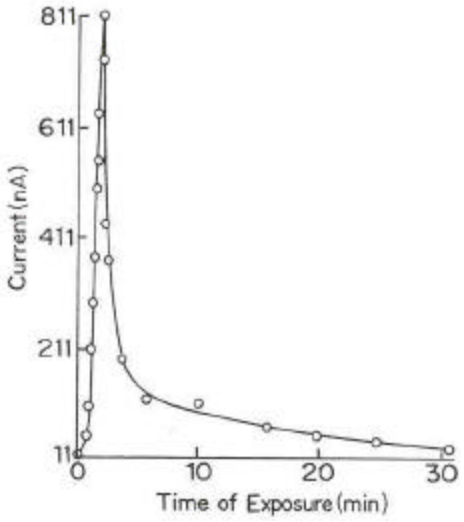

Fig.6.44 Response of the PANI/CuPc composites with PVAc to NO_2 containing 23% CuPc

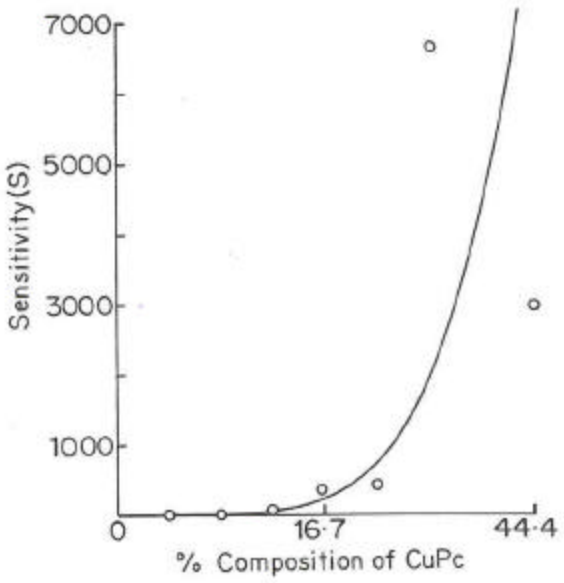

Fig.6.45 Chemical sensitivity of PANI/CuPc composites with PVAc towards NO_2 with respect to the CuPc concentration

conductivity dependence on the concentration of NO_2 were displayed. Evacuation at room

temperature does not completely reverse the NO_2 exposure nor it is completely by exposure to donor gases such as ammonia or hydrogen sulfide [48].

The PANI/CuPc composite also shows a high sensitivity (around 3 orders of magnitude) and comparatively a better reversibility at lower compositions of CuPc. The action of NO_2 would be formation of a charge transfer, complex between CuPc-donor and NO_2 acceptor [49]. As a result holes are produced in the CuPc matrix. NO_2 is a Π electron acceptor and the accepted electron would be delocalized over the planar NO_2 structure. Since the hole is also delocalized over the CuPc structure the coulombic force between the opposite charges is weakened and the charge carrier movement is facilitated. This leads to more conductivity of CuPc. Spectroscopic studies have supported the interaction of CuPc with NO_2. In transmission UV-vis spectrum, exposure to NO_2 causes the strong absorption at 700 and 625 nm to decline in intensity with the appearance of new absorption at 560 nm. These changes were said to be characteristic of formation of phthalocyanine radical cation. The IR transmission spectrum is interpreted to indicate that NO_2 percolates into the phthalocyanine lattice interstitial while the reflective spectrum displays bands corresponding to NO_2^- ion indicating that charge transfer occurs only at the surface.

The response to NO_2 for the lower composition is thus by simple diffusion of the gas in the matrix formation of charge transfer complex and the diffusion of the gas out of the sample when NO_2 is cut off. The process is thus reversible. With higher quantities of CuPc, the charge may get localized on CuPc and form a stronger charge transfer complex with NO_2. The charges are thus retained in the sample and it does not recover. NO_2 may also sit in the lattice structure making the change in conductivity irreversible.

In order to study the influence of introduction of trapping centers in the CuPc towards methanol sensing, the PANI/CuPc composite was prepared using 4:1 PVAc-$CuCl_2$ and tested for the sensitivity measurements.

The response of the PANI/CuPc composite with PVAc-$CuCl_2$, to NO_2 is increase in conductivity, which varies with the composition of CuPc as represented by the **Fig.6.46**. It is observed that the sensitivity exhibits maxima of 145 at 28 % of CuPc composition and thereafter decreases as against the rising plot in case of PANI/PVAc/CuPc. The comparison between the two composites at the same composition that is 44 % CuPc suggests that the response of the composite towards NO_2 decreases by adding $CuCl_2$ to the matrix. This behaviour can be due to the formation of charge transfer complex as described in the earlier

section. CuPc already contains impurity centers generated by $CuCl_2$. As a result, CuPc loses affinity towards NO_2 and hence a reduction in the sensitivity factor.

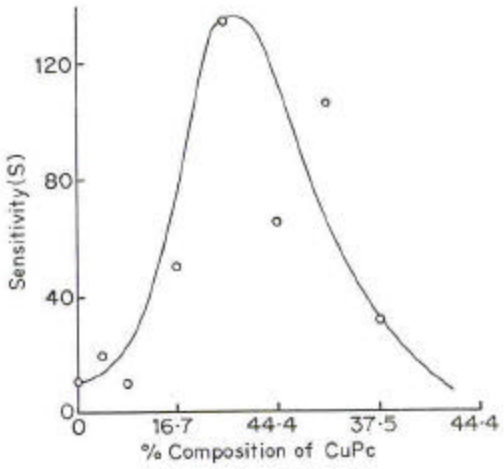

Fig.6.46 Sensitivity of PANI/CuPc composites with PVAc-$CuCl_2$ towards NO_2

A conclusion can be drawn in the present context that CuPc plays the active role in detecting the presence of NO_2. Also an optimum CuPc is required for obtaining a reversible sensor.

6.4 Conclusions:

Charge transport analysis of the PANI/PEO-$CuCl_2$ blends brings out the presence of Schottky barrier at the interface of the materials. The blend shows a remarkable sensitivity towards methanol that was characterized in terms of the response time, the decay time and the composition. The electron transfer involved during the process of methanol sensing influences the modulation of the PANI/PEO-$CuCl_2$ barriers.

The charge transport studies in the present case revealed that no barriers exist at the PANI/PVAc interface. The conduction takes place by SCLC mechanism that occurs by the filling up of the traps in PANI and PVAc. Introduction of $CuCl_2$ in PVAc gives rise to formation of a complex between the impurity PVA and $CuCl_2$ that is responsible for photoconductivity of the blend. In case of the composite with PVAc, the charge transport occurs by SCLC type of mechanism.

The chemical sensitivity of the PANI/PVAc blends towards methanol increased by the addition of $CuCl_2$ as it plays an important role in trapping the electrons donated by methanol, thus increasing the conductivity. On the other hand, the composite exhibits more sensitivity towards NO_2 than methanol by the virtue of the filler-CuPc. Also the sensitivity of the blend towards NO_2 increases by the addition of CuPc. Hence CuPc not only enhances the response but also imparts specificity to the composite.

6.5 References:

1. Surville R, Josefowicz M, Yu L T, Perichon J, Buvet R, Electrochim Acta, 13 (1968) 1451
2. Huang W S, Humphery B D, MacDiarmid A G, J Chem Soc Faraday Trans 82 (1986) 2385
3. Travers J P, Chroboczeck J, Devreux F, Genoud F, Nechtschein M, Syed A, Genies E M, Tsintavis C, Mol Cyst Liq Cryst 121 (1985) 195
4. MacDiarmid A G, Chiang J, Richter A F, Epstein A J, Synth Metals, 18 (1987) 285
5. Heeger A J, Synth Metals, 55 (1993) 3471
6. Yin K H, Yoshino K, Hashizume K, Isa I, Jpn J Appl Phys 36 (1997) 3537
7. Lacroix J C, Diaz A F, Makromol Chem Makromol Symp 8 (1987) 17
8. Byun S W, Im S S, Synth Metals 69 (1995) 219
9. Granstrom M, Inganas O, Synth Metals, 55 (1993) 460
10. (a)Martin C R, Parthasarthy P, Menon V, Synth Metals 55-57 (1993) 1165
    (b)Penner R M, Martin C R, J Electrochem Soc 133 (1986) 2206
    ©Martin C R, Dyke L S V, Cai Z, Liang W, J Am Chem Soc 112 (1990) 8976
11. Yang J, Hou J, Zhu W, Xu M, Wan M, Synth Metals 80 (1996) 283 12.
12. Nakajima T, Kawagoe T, Synth Metals 28 (1989) 629
13. Duek EAR, De Paoli M A, Adv Mater 5 (1993) 650
14. Jelle B P, Hagen G, Nodland S, Electrochim Acta, 38 (1993) 1497
15. Akhtar M, Weakliem H A, Paiste R M, Gaughan K, Synth Metals 26 (1988) 203
16. Linford R G, Applications of Electroactive Polymers, Edt. B Scrosati, Chapter 1, Chapman and Hall, 1993
17. Hasan, Erlandsson, MacDiarmid A G, Somasiri NLDS, Spring Series Solid State Sciences Vol 63, Springer-Verlag , Berlin (1985) 218
18. Sariciftci N S, Kuzmay H, Neugebauer H, Neckel A, J Chem Phys 92 (1990) 4530
19. Asturias G E, MacDiarmid A G, Synth Metals, 29 (1989) E-157
20. Hazda I, Furukawa, Ueda F, Synth Metals 29 (1989) 303

21. (a) Bredas J L, Themans B, Andre J M, Silbey R, Boudreaux D S, Chance R R, Bull Soc Chim Belg 95(7) (1986) 511
(b) Monkmon A P, Bloor D, Stevens J C H, Wilsan P, Synth Metals 29(1) (1989) E2277

22. Strella (1970,1971) quoted by Seanor D A, Electrical properties of polymers (Eds. Frisch K C, Patsis A, Ch.3p.37-51, Technomic Publ. Co Westport, Conn (1972)

23. Duke C B, Paton A, Conwell E M, Salaneck W R, Lundstroem I, Synth Metals 21(2) (1987) 163

24. Bailey F E, Koleske J V, Poly(ethylene oxide), Academic, 1976

25. (a) Seanor D A, Electrical properties of polymers, Polymer Science Vol 2, Ch.17 1229 Edt Jenkins A D, North Holland Publishing Co.1972
(b) Scrosati B, Applications of electroactive polymers, Chapman and Hall, London (1993) 144

26. Fox L P, Carbon-Black Polymer Composites, Edt E K Sichel, Plastics Engineering, Marcel Dekker, 1982

27. Charlesworth J M, Patridge A C, Garrard N, J Phys Chem 97 (1993) 5418

28. Alcacer L, Conducting polymers-special applications, Riedel, Dordrecht 1989, 189

29. Blackwood D, Josowicz M, J Phys Chem 95 (1991) 493

30. (a)Middlehock S, Audet S A, Silicon Sensors, Academic, London 1989

31. (a) Radhakrishnan S, Polym Commun 26 (1985) 153
(b) Radhakrishnan S, Saini D R, J Mater Sci, 26 (1991) 5950

32. Moore W J, Basic Physical Chemistry, Prentice-Hall, Englewood Cliffs ,NJ, 1986, 365

33. Seanor D A, Electrical properties of polymers, Frisch K C,Patsis A, Technomic Publishing Co, Conn 1977

34. Rodriguez F, Principles of polymer systems, Tata McGraw Hill Publishing Co., New Delhi, 1974

35. (a) Smith W M, Manufacture of Plastocs VI, New York : Van Nostrad Reinhold Co 1964
(b) Mahmood M H, Ghani R A, Dunn A S, Makromol Chem Rapid Commun 2 (1) (1981) 75

36. A K St Clair, Taylor L T, Advance in Organometallic and Inorganic Polymer Science Edt. Carraher C E Jr, Sheats J E, Pittman C U Jr, Marcel Dekker 1982

37. Sumita O, Fakuda A, Kuze E, J Polym Sci Polym Phys Ed 18 (1980) 877

38. Hogo N, Shirai H, Hayashi S, J Polym Sci Symp No. 47 (1974) 299

39. Okada M, Makuuchi K, Kogyo Kagaku Zasshi, 73 (1970) 1211

40. (a) Sussman A, J Appl Phys 38 (1967) 2738
(b) Hamman Phys Status Solidi 4 (1964) K97

41. Saji T, in: Leznoff C C, A.B.P.Lever (Eds.) ; Phthalocyanine Properties and Applications,2, VCH New York 1993, p.163

42. Loufty R O, Sharp J H, Hsiao C K, Ho R, J Appl Phys 52(8) (1981) 5218

43. Minami N, Sasaki K, Tsuda K, J Appl Phys 54(11) (1983) 6764

44. Saito T, Kawanishi T, Kakuta A, Jpn J Appl Phys 30(7) (1991) L1182

45. Heilmeier G H, Harrison , Phys Rev 132 (1963) 2010

46. Sczczurek A, Lorenz, Int J Environ Anal Chem 23 (1986) 161

47. Chadwick W, Wright J D, Ewky R L, J Chem Soc, Faraday Trans I, 76 (1980) 2194

48. (a) Honeyborne C L, Ewen R J, J Phys Chem Solids 44 (1983) 833
(b) Honeyborne C L, Ewen R J, J Phys Chem Solids 44 (1983) 215

49. (a) Kaufhold J, Hauffe K, Ber Bunsenges, Phys Chem 69 (1965) 168
(b) Oirschot G J, Leeuwen D, Madema J, J Electroanal Chem 37 (1992) 373

List of Publications

1. Conducting polymer-based chemical sensor : characteristics and evaluation of polyaniline composite films, **Swati Unde**, J.Ganu, and S. Radhakrishnan , *Advanced Materials for optics and electronics*, 6, (1996) 151-157

2. Effect of dopant ion on the conductivity behaviour of polypyrrole, **Swati Unde** and S. Radhkrishnan , *Polymers, Synthesis and applications*, Edt. Paramjit Singh, D.K Vohra and Daljit Singh, Allied Publishers, New Delhi (1997) 26

3. Source of instability in solid state polymeric electrochromic cells:the deterioration of indium tin oxide electrodes , S. Radhakrishnan, **Swati Unde** , A. B. Mandale, *Materials Chemistry and Physics*, 48 (1997) 268-271

4. Current – Voltage characteristics of conducting polypyrrole in solid polyethylene oxide electrolytes, S. Radhakrishnan, **Swati Unde**, *Journal of Applied Polymer Science*, 71, (1999) 2059-2067

5. Effect of substrate preconditioning on charge transport at the phthalocyanine-conducting polymer film interface, S. Radhakrishnan , **Swati Unde** , *Thin Solid Films*, 347 (1999) 229-232

Patents:

1. An improved process for rapid deposition of conducting polymer films on insulating substrates.
   S. Radhakrishnan and Swati Unde
   Ind.Pat. 264/DEL/97 Appl. dt. 31-1-97

2. An improved process for depositing conducting polymer films for use in electrochromic devices
   S. Radhakrishnan and Swati Unde
   Ind.Pat. 32/DEL/97 Appl. dt. 8-12-97

3. An improved process for the promotion of adhesion of the films to glass substrates especially for ECD applications
   S. Radhakrishnan and Swati Unde
   Ind. Pat. NF/87/97 Appl.dt. 2-4-97